University of Fort Hare

Faculty of Science and Agriculture

SYNTHESIS, CHARACTERIZATION & APPLICATION OF VISIBLE LIGHT RESPONSIVE NITROGEN DOPED TiO_2 AND COPOLYMER-GRAFTED ASYMMETRIC MEMBRANES WITH OZONOLYSIS FOR WATER TREATMENT

A thesis submitted in fulfillment of the requirements for the Doctoral Degree in Chemistry

By

Henry H. Mungondori

(Student number: 201004161)

Supervisors: Prof. L. Tichagwa

: Dr. D.M. Katwire

: Dr. E. Green

University of Fort Hare
Together in Excellence

January 2015

Declaration

I declare that this thesis entitled "Synthesis, characterization and application of visible light responsive N-TiO_2 and copolymer grafted asymmetric membranes with ozonolysis for water treatment," is the result of my own research except where cited in the references. The dissertation has not been accepted for any degree and is not concurrently submitted in candidature of any other degree.

Signature : ……

Name : HENRY HEROE MUNGONDORI…….……

Date : 10-04-2015….……

Dedication

This work is dedicated to the Mungondori family and my fiancé Tawanda Mataruse for their unconditional love and support.

Acknowledgements

I thank the Lord for the gift of life and keeping me in good health throughout my studies.

I thank my supervisors Professor L. Tichagwa, Dr D.M. Katwire, and Dr E. Green for their support and guidance. May the dear Lord bless them abundantly for their help and kindness during the duration of my studies.

I am very grateful for the advice and help from other members of the Department of Chemistry. I give special thanks to Mr K. Tshapu for his assistance with XRD analysis, and Mr T. Mcako for assistance with AAS, UV-Vis, and FT-IR analyses.

I appreciate the financial support provided by Govan Mbeki Research and Development Centre (GMRDC) and the National Research Foundation (NRF South Africa).

Finally, I would like to express the utmost thanks to my parents (Henry Senior and Susan) and my siblings (Aglin, Onward, Enos, Amanda, and Angela) for their love and support throughout the entire tenure of my studies. I also thank Mkwasha wangu Alfred Madzara and all my friends (Lavern Nyamutswa, Raymond Taziwa, Farai Makombe, Pardon Nyamukamba, Dr Tavengwa Bunhu, Innocent Mutize, Dr Raymond Chiruka, Dr Calistus Bvenura, Donnovan Mafukidze, Tinashe Mutema, Tafadzwa Chikwanha, Tafadzwa Machirori, Bither Kaela, Xoliswa Gxumisa, and Sivuyisiwe Jikele) for their support throughout my studies. To all of them, I extend my gratitude and thanks.

Abstract

The use of titanium dioxide for the photo-catalytic removal of organic, inorganic, and microbial pollutants from natural water and wastewater has been considered a very promising technique. The aim of this study was to prepare nitrogen doped titanium dioxide, immobilize it on asymmetric polymeric membranes of poly (methacrylic acid) grafted onto poly (vinylidene difluoride) (PVDF) blended with poly (acrylonitrile) (PAN), and evaluate the photo-catalytic, antimicrobial, and antifouling properties of the membranes.

Nitrogen doped titanium dioxide (N-TiO_2) nano-particles were prepared by a low temperature sol gel synthesis technique. The modification of TiO_2 with nitrogen allows photo-sensitization of the photo-catalyst towards visible light utilization. The N-TiO_2 nano-particles were characterized by fourier transform infrared spectroscopy (FT-IR), scanning x-ray photoelectron spectroscopy (SXPS), X-ray diffraction analysis (XRD), diffuse reflectance spectroscopy (DRS), Brunauer Emmett Teller (BET) surface area analysis, and transmission electron microscopy (TEM). The characterizations revealed the presence of the expected functional groups and confirmed successful doping and that the product was visible light responsive.

Novel poly (methacrylic acid) grafted onto poly (vinylidene difluoride)/ poly (acrylonitrile) (PMAA-g-PVDF/ PAN) asymmetric membranes were prepared by the dry-wet phase inversion technique. The poly (methacrylic acid) (PMAA) side chains where grafted onto an activated PVDF backbone by reversible addition fragmentation chain transfer (RAFT) polymerization. The photo-catalytic membranes were generated by blending N-TiO_2 with the polymer solution before casting the membranes. The membranes were characterized by FT-

IR, nuclear magnetic resonance spectroscopy (NMR), scanning electron microscopy (SEM), and thermo-gravimetric analysis (TGA). FT-IR and NMR analyses confirmed successful grafting of MAA chains onto PVDF while SEM confirmed the successful preparation of membranes with asymmetric structure.

The efficacy of the photo-catalytic asymmetric membranes was evaluated on the removal of herbicides from synthetic water. Bentazon was easily degraded while atrazine and paraquat were recalcitrant and proved difficult to degrade. The best results were observed with 3 % N-TiO_2-PMAA-g-PVDF/ PAN asymmetric membranes on the photo-degradation of bentazon, atrazine and paraquat in water. Significant enhancement in the photo-degradation of the three herbicides was observed when photo-catalytic degradation was coupled with ozonation. Liquid chromatography-mass spectrometry (LC-MS) analysis confirmed the presence of a degradation by-product during the photo-catalytic degradation of bentazon. The photo-catalytic membranes were also evaluated on the photo-catalytic reduction of heavy metals Pb^{2+} and Fe^{3+} in water, and the best results were obtained using 1 % N-TiO_2-PMAA-g-PVDF/ PAN and 1 % N-TiO_2-PAN asymmetric membranes.

All prepared photo-catalytic membranes where capable of completely inactivating *E. coli* ATCC 8739 within 120 minutes of exposure and inactivation rate increased with increasing N-TiO_2 photo-catalyst loading. However, there was an indication from the results obtained that N-TiO_2 supported on PMAA-g-PVDF/ PAN showed a higher inactivation rate of *E. coli* ATCC 8739 compared to N-TiO_2-PAN and N-TiO_2-PVDF membranes.

The 1 % N-TiO_2-PMAA-g-PVDF/ PAN membranes gave the highest pure water flux (421.83 L/m^2h). This increase (PVDF = 30.50 L/m^2h, PAN = 73.85 L/m^2h) in pure water flux is owed

to PMAA grafting as well as addition of N-TiO_2. These modifications resulted in an increased membrane surface hydrophilicity, which promoted permeation of pure water through the membrane structure. A high bovine serum albumin (BSA) rejection (76.5 %) was noted and can be attributed to steric hindrance brought about by PMAA side chains which prevented the bulky BSA molecules from attaching to the membrane surface for PMAA-g-PVDF/ PAN membranes. However, the supporting porous sub-layer of an asymmetric membrane seemed to play a very important role in the overall permeability of a membrane. PVDF membranes are highly hydrophobic hence they gave a very low pure water flux.

Table of contents

List of tables

List of figures

List of abbreviations

AD	Alzheimer's disease
AOP	Advanced oxidation process
AOT	Advanced oxidation technology
BET	Brunauer Emmet Teller surface area analysis
C.B	Conduction band
CBPs	Chlorination by-products
CFU	Colony forming units
COD	Chemical oxygen demand
CTC	5-cyano-2, 3-ditolyl tetrazolium
DBP	Disinfection by-products
DCAA	Dichloroacetic acid
DCM	Dichloromethane
DMAC	Dimethyl acetamide
DMDC	Dimethyl dicarbonate
DOC	Dissolved organic carbon
DRS	Diffuse reflectance spectroscopy
EHA	Environmental health agency
ENR	Enrofloxacin
EOM	Effluent organic matter
FAO	Food and Agriculture Organization of the United Nations
FT-IR	Fourier transform infrared spectroscopy
GO	Graphene oxide
HAA	Haloacetic acid
HEMA	2-hydroxyethyl methacrylate
HOMO	Highest occupied molecular orbital

IRP	Iron regulatory protein
IUPAC	International union of pure and applied chemistry
LC-MS	Liquid chromatography-mass spectrometry
LUMO	Lowest unoccupied molecular orbitals
MAR	Marbofloxacin
MF	Microfiltration
MMT	Montmorillonite
MO	Methyl orange
MPD	M-phenylenediamine
NDMA	N-nitrosodimethylamine
NMR	Nuclear magnetic resonance spectroscopy
NOx	Nitric oxide
NOM	Natural organic matter
OMB	Ozone microbubbles
OMM	Ozone millibubbles
PAA	Poly (acrylic acid)
PAH	Polycyclic aromatic hydrocarbon
PAN	Poly (acrylonitrile)
PCB	Polychlorinated biphenyl
PCDD	Polychlorinated dibenzodioxin
PCDF	Polychlorinated dibenzofuran
PCP	Pentachlorophenol
PD	Parkinson’s disease
PDA	Poly (dopamine)
PMAA	Poly (methacrylic acid)
PVDF	Poly (vinylidene difluoride)
RAFT	Reversible addition fragmentation chain transfer

RB5	Reactive black 5
ROS	Reactive oxygen species
SEM	Scanning electron microscopy
SMPs	Soluble microbial products
SSF	Stainless steel filter
SXPS	Scanning X-ray photoelectron spectroscopy
TCAA	Trichloroacetic acid
TCE	Trichloroethylene
TEM	Transmission electron microscopy
TGA	Thermo-gravimetric analysis
THM	Trihalomethane
TMC	Trimesoyl chloride
TMS	Tetramethyl silane
TOC	Total organic carbon
TOrC	Trace organic contaminants
UF	Ultrafiltration
UNICEF	United Nations Children's Fund
UV/VIS	Ultraviolet/ visible light spectroscopy
V.B	Valence band
VOC	Volatile organic compound
WHO	World health organization
XRD	X-ray diffraction analysis

CHAPTER 1

1. Introduction

1.1. Study introduction and motivation

Water is one of the elements responsible for life on planet earth. It has been treated as a cheap and abundant resource by mankind until a few decades back. The philosophy towards water has changed dramatically, it is at present considered a valuable resource, which can easily be polluted and is difficult to decontaminate (Philippopoulos and Nikolaki, 2010). Due to population growth, rapid urbanization, rising farming, and changes in climate, the world is facing a drastic shortage of potable water especially in developing economies. According to the Blue planet network, 1.2 billion people in the world do not have access to safe drinking water, and about 2.2 million people in developing countries, most of them children, die every year from preventable diseases related to lack of access to safe drinking water, inadequate sanitation, and poor hygiene. Unfortunately, despite a growing recognition that more must be done to help those without clean water or adequate sanitation, a report by the Pacific Institute estimates that over 34 million people might perish in the next 20 years from water-related diseases even if the United Nations "Millennium Development Goals," which aim to cut the proportion of those without safe access by half, are met (WHO/UNICEF, 2005).

1.1.1. Water pollution

Water pollution can be defined as the contamination of water bodies (surface water e.g. lakes, rivers, oceans, aquifers; and groundwater), mostly by human activities. Water pollution transpires when pollutants such as particles, chemicals or substances that contaminate water

are discharged directly or indirectly into water bodies without sufficient treatment to get rid of harmful compounds (Water pollution guide, 2003-2013).

1.1.2. Risks posed by organic and heavy metal pollutants in water

The bulk of natural organic matter (NOM) found in water do not pose a direct threat to humans. However methods like chlorination necessary in the disinfection of drinking water to curb water-borne illnesses, result in the formation of various chlorination by-products (CBPs) when chlorine reacts with dissolved organic compounds. Some examples of these chlorination by-products include trihalomethanes (THMs), halo-acetic acids (HAAs), etc. Disinfection of organic by-products can cause great threat to natural ecosystems and human health, owing to their chronic toxicity, persistence, and bioaccumulation (Maeng *et al.,* 2011; Lu *et al.,* 2009; Siddiqui *et al.,* 2000). Trihalomethane species like chloroform have been suggested to be potential carcinogens from toxicological studies that have been carried out since the 1970s. There are various toxicological and epidemiological studies that have been carried out to establish relationships between levels of CBPs in drinking water and numerous carcinogenic and other adverse health effects (Legay *et al.,* 2011; Richardson *et al.,* 2007; Villanueva *et al.*, 2007).

Synthetic chemicals like pentachlorophenol (PCP) widely used in agriculture and industry for their bactericidal and fungicidal properties have a stable structure and are known to be highly carcinogenic posing risks to human health. Studies by other researchers have proven that PCP exposed in the environment can be transformed into polychlorinated dibenzo-p-dioxins and polychlorinated dibenzofurans (PCDD/Fs) that are toxic to organisms in the ecosystem (Black *et al.,* 2012; Jin *et al.,* 2012; Harnly *et al.,* 2000).

Chlorination significantly diminishes the risk of pathogenic infections, but in the presence of bromine in water hypochlorous acid (HOCl) can oxidize the bromide to hypobromous acid (HOBr), a much stronger halogenating agent than HOCl. Brominated disinfection by-products pose more significant health risks to humans than their chlorinated analogues (Uyak and Toroz, 2007). Studies conducted on drinking and natural water demonstrated that the yields of THMs and HAAs increased as the initial bromide concentration increased during chlorination (Yang and Shang, 2004; Duong *et al.,* 2003; Chang *et al.,* 2001; Luong *et al.,* 1982).

Mining operations, metal plating facilities, battery manufacturing processes, and many other industries lead to the discharge of heavy metal pollutants into the environment through their waste-water (Leinonen and Letho, 2001). Gradual accumulation of toxic heavy metals may occur in human bodies either by direct intake or via food chains (Abdel Salam *et al.,* 2011). Heavy metal contaminants such as Cu^{2+}, Fe^{3+}, Mn^{2+}, Zn^{2+}, Cd^{2+} and Pb^{2+} are non-biodegradable and thus tend to accumulate in living organisms, causing various diseases and disorders (Myroslav *et al.,* 2006; Moreno *et al.,* 2001; Bailey *et al.,* 1999). There is evidence that toxic metals can interact with deoxyribonucleic acid (DNA) and proteins causing oxidative deterioration of biological macromolecules. Thus the homeostatic breakdown of metal-ions has been involved in a plethora of diseases (Halliwell and Gutteridge, 1990, 2007; Valko *et al.,* 2005; Mates, 2000; Mates *et al.,* 1999; Stohs and Bagchi, 1995).

1.1.3. Removal of organics from potable water

Biological treatment of low concentration of highly chlorinated aromatic compounds in aqueous waste streams often leaves the chlorinated compounds untreated or requires longer periods, e.g. several days (Susarla *et al.,* 1998; Bryant *et al.,* 1991). Bio-filtration has

successfully been used in water treatment plants for degradation of organics and ammonia removal, however, bio-filtration has drawbacks that include complex water and air distribution systems, backwash requirements, periodic massive biofilm removal and a high nitrite residue in the effluent (Carlson and Amy, 2000; Zhang *et al.,* 2000). The electrochemical reductive approach is a method that ensures the selective removal of chlorine atoms under mild conditions without use of highly reactive reducing agents. It is a promising method for detoxification of chlorine-containing aromatic hydrocarbons; however, non-aqueous reaction media such as aprotic solvents are required for effective performance (Cui *et al.,* 2005; Cheng *et al.,* 2003).

Nano-filtration membranes are capable of removing natural organic matter although the rejection is lower than reverse osmosis membranes. Nano-filtration is rather seen as a combinatory technique capable of eliminating hardness and a broad spectrum of other components such as pollutants in a single step (Van der Bruggen and Vandecasteele, 2003). Reverse osmosis is capable of removing most of the organic pollutants but not in sufficient quantities. Modern dyes are highly stable, rendering conventional physicochemical and biological treatment techniques ineffective for their removal. Coagulation and flocculation, electro-floatation, precipitation, ion exchange, membrane filtration, electrochemical destruction, irradiation, biological (Khehra *et al.,* 2005) and ozonation (Garg *et al.,* 2004) are the conventional methods used in the removal of dyes from water. Currently there is a lot of on-going research on membrane technologies to come up with better and more efficient and cost effective membranes.

1.1.4. Removal of heavy metals from potable water

There are many techniques that can be employed in the treatment of water polluted with inorganic pollutants (heavy metals), and these include; chemical precipitation, flocculation, solvent extraction, ion exchange, reverse osmosis, etc. (Arief *et al.*, 2008).

Heavy metal adsorption on conventional adsorbents like activated carbon have been used as an effective adsorption process in many applications, and the activated carbon produced by carbonizing organic materials is the most widely used adsorbent. The high cost of the activation process, however limits its use in wastewater treatment applications (Amarasinghe and Williams, 2007). The regeneration of activated carbon for reuse is also known to result in rapid loss of its adsorption capacity (Garg *et al.*, 2004).

Reverse osmosis is a very efficient way of treating polluted water, but owing to membrane fouling it becomes a cost prohibitive technique (Bruning, 2012). Electro-dialysis is a suitable method to keep the concentration of dissolved salts to acceptable levels compared to reverse osmosis, however, it is cost effective only for concentrated solutions and does not remove uncharged molecules. Ion exchange regarded as some kind of adsorption technique is an effective but expensive treatment process (Nomanbhay and Palanisamy, 2005).

Advanced oxidation technologies have been employed quite extensively in the removal of organic, inorganic and elimination of microbial pollutants from water. The use of semi-conductors in the photo-catalytic breakdown of organic pollutants is a very promising method of water treatment. The most researched semi-conductor photo-catalyst is titanium dioxide, however, its use is limited due several drawbacks which include; its large band gap energy, tendency to agglomerate at high concentration and post-recovery of the catalyst particles after

water treatment (Chong *et al.*, 2010). Hence there is on-going research to improve the photo-catalytic properties of titanium dioxide for commercial purposes.

With the emergence of new and recalcitrant pollutants in water systems due to industrialization, there is need to develop new, efficient and cost effective water treatment technologies. Several researchers have investigated the efficacy of TiO_2, and modified TiO_2 photo-catalyst on the removal of various pollutants from water, and they established that it was a potential alternative treatment technique. However, there are still issues associated with the use of slurry type TiO_2 photo-reactors and also to establish if it does not produce toxic disinfection by-products during the treatment process. The issue of TiO_2 post recovery has prompted many researchers to explore many potential support materials for this photo-catalyst to avoid potential secondary pollution of the treated water which is likely to cause adverse health problems to humans and other species which depend on those water sources.

No single method manages to remove all contaminants and often a combination of treatment processes are required to effectively treat water. Regardless of which method of treatment is considered, water is generally tested first to determine what substances are present. It is very important to know what contaminants are present and their quantities prior to selecting the method of treatment because this helps to choose the best and most effective method. In this study the main focus is photo-catalysis as a way to effect water treatment. Titanium dioxide offers great potential as an industrial technology material for detoxification or remediation of waste water due to several factors: photo-catalysis can occur under ambient conditions very slowly, and direct UV light exposure increases the rate of reaction; there is complete oxidation of substrates to CO_2 and H_2O; titanium dioxide has relatively high chemical

stability and photo-stability; it can also be supported on many suitable reactor substrates; and it is relatively cheap.

Ozonation is another widely used industrial technology for detoxification or remediation of water and waste water. Despite the high oxidation potential of ozone, the presence of refractory pollutants and formation of by-products (Rice and Cotruvo, 1978) that are not further oxidized necessitates the combination of ozonation with other AOPs. The hydroxyl radical is generally more thorough. The simplest and cost effective way to convert a conventional ozonation process into AOP is the addition of hydrogen peroxide (H_2O_2) (Von Gunten, 2003; Glaze *et al.,* 1992; Duguet *et al.,* 1985). Several researchers have observed improved removal of organic pollutants from water through the synergistic effects of ozone and hydrogen peroxide (Pisarenko *et al.,* 2012, Chelme-Ayala *et al.,* 2011, Matilainen and Sillanpää, 2010). The current study focuses on investigating the synergistic effects of N-TiO_2 photo-catalysis and ozonation. Ozonation was also used as a comparative study to N-TiO_2 photo-catalysis.

1.2. Problem statement

The most commonly utilized photo-catalyst material for research and industrial purposes is titanium dioxide (TiO_2). The capability of this advanced oxidation technology has been widely reported in the depollution of water contaminated with persistent organic compounds and microorganisms. Currently, the main technical challenges hindering its commercialisation are centred on the post-recovery of the catalyst particles after water treatment (Chong *et al.,* 2010). Several researchers have conducted work on the immobilization of titanium dioxide on different support material, for example natural clays (Kun *et al.*, 2006), glass fibre (Pugh *et al.,* 1995), stainless steel (Murabayashi *et al.,* 1993),

and micro-porous cellulose membranes (Bellobono *et al.*, 1992). Most of these techniques encounter problems such as membrane structure deterioration, low photo-catalytic activity and loss of deposited TiO_2 layer over time. This current work seeks to address the problems of catalyst post-recovery through the use of PMAA-g-PVDF (poly (vinylidene difluoride))/ PAN (poly (acrylonitrile)) membranes as matrix for the photo-catalyst. The study seeks to develop a membrane with improved, antifouling, antimicrobial, and high photo-catalytic activity.

1.3. Aims and objectives

1.3.1. Main aim

The major aim is to develop visible light responsive N-TiO_2 supported on PMAA-g-PVDF/ PAN asymmetric membrane for water-treatment.

1.3.2. Specific objectives

- To synthesize and characterize nitrogen doped titanium dioxide (N-TiO_2) nanoparticles.
- To incorporate nitrogen doped titanium dioxide nanoparticles into PVDF, PAN, and PMAA-g-PVDF/ PAN asymmetric membrane matrices.
- To characterize the prepared N-TiO_2 nanoparticles and PVDF, PAN, and PMAA-g-PVDF/ PAN asymmetric membranes.
- To establish the filtration capacity of the N-TiO_2-PMAA-g-PVDF/ PAN asymmetric membranes.

- To evaluate the photo-catalytic properties of the N-TiO_2-PVDF, N-TiO_2-PMAA-g-PVDF/ PAN, and N-TiO_2-PAN membranes alone and in tandem with ozone (O_3) technique on water depollution.
- To evaluate the antimicrobial and antifouling properties of the N-TiO_2/ PMAA-g-PVDF/ PAN membranes.
- To establish the degradation products of a bentazon.

1.4. Scope of study

This study focuses on the preparation of nitrogen doped titanium dioxide nano-particles via the sol gel method, using optimum conditions that had been established in the research group (Mungondori and Tichagwa, 2013; Nyamukamba *et al.,* 2012). The main focus of the study was to establish suitable conditions for the immobilization of the photo-catalytic material on asymmetric polymer membrane support to allow easy removal of spent titanium dioxide photo-catalyst from water.

1.5. Thesis outline

This thesis comprises of three main sections and is made up of nine chapters. The first section includes chapters one and two, which present the introduction and the literature review. Chapter one gives a general introduction to the thesis. The problem statement, aims and objectives, scope of study as well as thesis outline are presented in this chapter. Chapter two is the literature review, giving detailed information on advanced oxidation technologies. Of particular interest is the photo-catalytic applications of the semi-conductor TiO_2, modifications to improve its performance, immobilization to avert post-recovery problems. The chapter also presents studies on polymeric membranes as highlighting their use as both

filtration media and photo-catalytic membranes capable of degrading organic pollutants as well as reducing heavy metal ions to allow their removal from water.

The second section is made up of Chapters three, four and five which present the experimental work executed to achieve the aims and objectives of this thesis. This section deals with the preparation of the photo-catalytic semi-conductor material as well as the support materials for the photo-catalyst. Chapter three presents the materials and chemical reagents used in this study. The last section of chapter three gives the main characterization techniques used in this study. Chapter four is on the preparation and characterization of nitrogen doped titanium dioxide (N-TiO_2). Chapter five gives detailed information on the preparation of three types of polymeric asymmetric membranes; that is PAN, PMAA-g-PVDF/ PAN, and PVDF asymmetric membranes. The last section of this chapter presents the results on the characterization of these membranes.

The last section is made up of chapters six, seven, and eight which cover the evaluation of the prepared photo-catalytic membranes on the removal of organics, heavy metals and microbial pollutants. Chapter six presents results on the removal of the herbicides bentazon, paraquat and atrazine from water using N-TiO_2 entrapped PAN, PMAA-g-PVDF/ PAN and PVDF membranes. The findings on the removal of bentazon, paraquat, and atrazine by ozonolysis as well as O_3/ 3 % N-TiO_2 system are presented. The last section of this chapter gives results on the N-TiO_2 assisted reduction of Pb^{2+} and Fe^{3+} heavy metal ions from synthetic water. Chapter seven is on the evaluation of the antimicrobial properties of N-TiO_2 entrapped PAN, PMAA-g-PVDF/ PAN, and PVDF membranes. The membranes were evaluated on the inactivation of *Escherichia coli* ATCC 8739 in water. Chapter eight presents findings on the

filtration of 1 mg/ mL BSA solution and static protein adsorption studies to assess the antifouling properties of the prepared membranes.

Chapter nine gives general conclusions on this study and recommendations for future work.

1.6. Bibliography

Abdel Salam O.E., Reiad N.A., and ElShafei M.M. *Journal of Advanced Research*: 2 **(2011)** 297-303.

Amarasinghe B.M.W.P.K., and Williams R.A. *Chemical Engineering Journal*: 132 (1-3) **(2007)** 299-309.

Amy G., and Drewes J. *Environmental Monitoring and Assessment*: 129 **(2007)** 1-3, 19-26.

Arief V.O., Trilestari K., Sunarso J., Indraswati N., and Ismadji S. *Clean*: 36 (12) **(2008)** 937-962.

Arlington Institute report, **(2005)**, Global water crisis. www.arlingtoninstitute.org/global-water-crisis (Accessed, **20-05-2011**).

Bailey S.E., Trudy J., Olin T.J., Bricka M.R., and Adrian D.D. *Water Research*: 33 (11) **(1999)** 2469-2479.

Barker D.J., and Stuckey, D.C. *Water Research*: 33 (14) **(1999)** 3063-3082.

Bellobono, I.R., Morazzoni, F., Tozzi, P.M. *International Journal of Photo-energy*: 7 **(2005)** 109-113.

Black R.R., Meyer C.P., Yates A., Van Zwieten L., Chittim B.G., Gaus C., and Mueller J.F. *Environmental Pollution*: 166 **(2012)** 10-16.

Blue Planet Network report, **(2006)**, The Facts about the Global Drinking Water Crisis. www.blueplanetnetwork.org/water/facts (Accessed, **20-05-2011**).

Bruning H. Advanced Water Treatment and Re-use Manual, Wageningen University, **(2012)**.

Bryant F.O., Hale D.D., and Rogers J.E. *Applied Environmental Microbiology*: 57 (8) **(1991)** 2293-2301.

Carlson K.H., and Amy G.L. *Water Research*: 34 (4) **(2000)** 1386-96.

Chang, E.E., Lin, Y.P., Chiang, P.C. *Chemosphere*: 43 (8) **(2001)** 1029-1034.

Chelme-Ayala P., El-Din M.G., Smith D.W, Adams C.D. *Water Research*: 45 **(2011)** 2517-2526.

Cheng H., Scott K., and Christensen P.A. *J. Electrochemical Society*: 150 **(2003)** 17-24.

Chong M.N., Jin B., Chow C.W.K., and Saint C. *Water Research*: 44 **(2010)** 2997-3027.

Cui C., Quan X., Chen S., and Zhao H. *Separation and Purification Technology*: 47 **(2005)** 73-79.

Dalton T.P., He L., Wang B., Miller M.L., Jin L., Stringer K.F., Chang X.Q., Baxter C.S., and Nebert D.W. *Proceedings of the National Academy of Sciences of U.S.A*: 102 **(2005)** 3401-3406.

Duguet J.P., Brodard E., Dussert B. and Mallevialle J. *Ozone Science and Engineering*: 7, **(1985)** 241-253.

Duong H.A., Berg M., Hang H.M., Pham H.V., Gallard H., Giger W., and Gunten U. *Water Research*: 37 (13) **(2003)** 3242-3252.

Eisenstein R.S., and Blemings K.P. *Journal of Nutrition*: 128 **(1998)** 2295-2298.

El Goresy A., Chen M., Dubrovinsky L., Gillet P., Graup G. *Science*: 293 **(2001)** 1467-1470.

Environmental Health Agency (EHA) report, **(2011)**, Diseases acquired via recreational bathing. www.ehagroup.com. (Accessed, **21-11-2011**).

Flora S.J.S., Mittal M., and Mehta A. *Indian Journal of Medical Research*: 128 **(2008)** 501-523.

Flora S.J.S., and Pachauri V. *International Journal of Environmental Research: Public Health*: 7 **(2010)** 2745-2788.

Fujishima A., Honda K. *Nature*: 238 (**1972**) 37-38.

Garg V.K., Kumar R., and Gupta R. *Dyes and Pigments*: 63 (3) **(2004)** 243-250.

Glaze W.H., Beltran F., Tuhkanen T., Kang J.-W. *Water Pollution Research Journal of Canada*: 27 (1) **(1992)** 23-42.

Halliwell B., and Gutteridge J.M.C. *Methods in Enzymology*: 186 **(1990)** 1–85.

Halliwell B., and Gutteridge J.M.C. Free Radicals in Biology and Medicine, 4th ed, Oxford University Press, **(2007)**.

Harnly M.E., Petreas M.X., Flattery J., and Goldman L.R. *Environmental Science and Technology*: 34 **(2000)** 1143-1149.

Hunter P.R. *Journal of Water and Health*: **(2003)** 65.

Jiang Z., Greenberg D., Narato J.P., Steffen R., and Dupont H.L. *Journal of Clinical Microbiology*. 40 **(2002)** 4185-4190.

Jin X.W., Zha J.M., Xu Y.P., Giesy J.P., and Wang Z.J. *Environmental Science and Pollution Research*: 19 **(2012)** 609-618.

Jomovaa K., and Valko M. *Toxicology*: 283 **(2011)** 65-87.

Khehra M.S., Saini H.S., Sharma D.K., Chadha B.S., and Chimi S.S. *Dyes and Pigments*: 67 **(2005)** 55-61.

Kumar A. and Clark C.S. Lead loadings in household dust in Delhi, India: Indoor

Air: 19 **(2009)** 414-420.

Kun R., Mogyorosi K., and Dekany L. *Applied Clay Science*: 32 **(2006)** 99-110.

Lee D.W., Andersen J.K., and Kaur D. *Molecular Interventions*: 6 **(2006)** 89-97.

Legay C., Rodriguez M.J., Sadiq R., Sérodes J.B., Levallois P., and Proulx F. *Journal of Environmental Management*. 92 **(2011)** 892-901.

Leinonen H., and Letho J. *Waste Management Research*: 19 **(2001)** 45-57.

Liochev S.I., and Fridovich I. *Redox Rep*ort: 7 **(2002)** 55-57.

Lu J., Zhang T., Ma J., and Chen Z. *Journal of Hazardous Materials*: 162 (1) **(2009)** 140-145.

Luong T.V., Peters C.J., Perry R. *Environmental Science and Technol*ogy: 16 (8) **(1982)** 473-479.

Maeng S.K., Sharma S.K., Lekkerkerker-Teunissen K., and Amy G.L. *Water Research*: 4 (5) **(2011)** 3015-3033.

Mates J.M. *Toxicology*: 153 **(2000)** 83-104.

Matilainen A., and Sillanpää M. *Chemosphere*: 80 **(2010)** 351-365.

Mattesini M., Almeida J.S., Dubrovinsky L., Dubrovinskaia N., Johansson B., and Ahuja R. *Physical Review B*: 212101 **(2004)** 70.

Moreno N., Querol X., and Ayora C. *Environmental Science and Technology*: 35 **(2001)** 3526-3534.

Mungondori H., and Tichagwa L. *Materials Science Forum*: Vol. 734 **(2013)** 226-236.

Murabayashi M., Itoh K., Kawashima K., Masuda R., Susuki S. *Trace Metalsin the Environment:* 3 **(1993)** 783.

Myroslav S., Boguslaw B., Artur T.P., and Jacek N. *Journal of Colloid and Interface Science*: 304 **(2006)** 21-28.

Nomanbhay S.M. and Palanisamy K. *Electronic Journal of Biotechnology*: 8 (1) **(2005)** 43-53.

Nyamukamba P., Tichagwa L., and Greying C. *Materials Science Forum*: 712 **(2012)** 49-63.

Pacific Institute report, **(2011)**, Global water crisis. www.pacinst.org/global_water_crisis/ (Accessed, **21-11-2011**).

Patrick L. *Alternative Medicine Review*: 11 **(2006)** 2-22.

Philippopoulos C.J., and Nikolaki M.D. Photo-catalytic Processes on the Oxidation of Organic Compounds in Water, New Trends in Technologies, Blandna ramov (Ed.). InTech Publishers, Croatia, **(2010)** 89-107.

Pisarenko A.N., Stanford B.D., Yan D., Gerrity D, and Snyder S.A. *Water Research*: 46 **(2012)** 316-326.

Prousek J. *Pure and Applied Chem*istry: 79 **(2007)** 2325-2338.

Pugh K., Kiserov D., Sullivan J., and Grinstead J.H. Jr. *ACS Symposium Series:* 607 **(1995)** 174.

Rice R.G. and Cotruvo J.A. Ozone/Chlorine Dioxide, Oxidation Products of Organic Materials. Ozone Press International, Cleveland, OH, **(1978)** 490.

Richardson S.D., Plewa M.J., Wagner E.D., Schoeny R., and DeMarini D.M. *Mutation Research*: 636 **(2007)** 178-242.

Siddiqui M., Amy G., Ryan J., and Odem W. *Water Research*: 34 (13) **(2000)** 3355-3370.

Speisky H., Gomez M., Carrasco-Pozo C., Pastene E., Lopez-Alarcon C., and Olea-Azar C. *Bioorganic Medicinal Chemistry Letters*: 16 **(2008)** 6568-6574.

Stohs, S., Bagchi, D. *Free Radical Biology and Medicine*: 18 **(1995)** 321-336.

Susarla S., Yonezawa Y., and Masunaga S. *Water Research*: 32 **(1998)** 639-648.

United States Environmental Protection Agency, 2013. http://www.epa.gov/agriculture/lcwa.html. **(**Accessed **09-07-2013)**.

Uyak, V., Toroz, I. *Journal of Hazardous Materials*; 149 (2) **(2007)** 445-451.

Valko M., Morris H., and Cronin M.T.D. *Current Medicinal Chemistry*: 12 **(2005)** 1161-1208.

Van der Bruggen B., and Vandecasteele C. *Environmental Pollution*: 122 **(2003)** 435-445.

Villanueva C.M., Cantor K.P., Grimalt, J.O., Malats N., Silverman D., Tardon A., Garcia-Closas R., Serra C., Carrato A., Castano-Vinyals G., Marcos R., Rothman N., Real F.X., Dosemeci M., and Kogevinas M. *American Journal of Epidemiology*: 165 (2) **(2007)** 148-156.

Von Gunten U. *Water Research*: 37 **(2003)**1443-1467.

Waalkes M.P., Liu J., Ward J.M., and Diwan L.A. *Toxicology*: 198 **(2004)** 31-38.

Waalkes M.P. *Journal of Inorganic Biochemistry*: 79 **(2000)** 241-244.

Wang, Z., Rossman, T.G. The carcinogenicity of arsenic. In: Chang, T. (Ed.),

Toxicology of Metals. CRC Press, Boca Raton, FL, **(1996)** 221-229.

Water Education report, **(2011)**, www.freedrinkingwater.com/water-education/quality-water-filtration-method.htm (Accessed, 22-05-2011).

Water pollution guide, 2003-2013. http://www.water-pollution.org.uk/. **(**Accessed **09-07-2013)**.

WHO/ UNICEF Joint Monitoring Programme for Water Supply and Sanitation, **(2006)**, http://www.wateraid.org/documents/plugin_documents/global_cause_and_effect__mdg_midway_paper.pdf. (Accessed, **21-11-2011**).

Yang J.M., Arnush M., Chen Q.Y., Wu X.D., Pang B., and Jiang X.Z. *Reproduction Toxicology*: 17 **(2003)** 553-560.

Yang X., and Shang C. *Environmental Science and Technology*: 38 (19) **(2004)** 4995-5001.

Zhang S.Y., Wang J.S., Jiang Z.C., and Chen M.X. *Bioresource Technology*: 73 (1) **(2000)** 91-93.

CHAPTER 2

2. Literature Review

2.1. Introduction

Water covers more than 70 % of the earth's crust, yet billions of people lack access to clean water supply. Humans use water for drinking and bathing to agricultural activities, as well transportation and power generation. Most urban communities harvest water from natural water bodies which include; streams, rivers and aquifers. The water undergoes various treatment processes that remove any chemicals, organic substances or pathogenic organisms that could be harmful to human health, before it can be delivered to the community.

Waste water is usually treated via: chemical precipitation, evaporation, reverse osmosis, electro-dialysis, phytoextraction and ultrafiltration (Mobasherpour *et al.,* 2011; Sprynskyy *et al.,* 2006; Li *et al.,* 2003). These technologies are practical and applicable solely to concentrated wastewaters, but are ineffective when applied to lowly concentrated wastewaters (Pavasant *et al.,* 2006; Muhammad *et al.,* 1998). Waste waters polluted with organics like chlorophenols and dyes can be treated using advanced oxidation technology, electrochemical methods, microbiological decomposition, ozonation, coagulation and membrane filtration (Zhang *et al.,* 2011; Lata *et al.,* 2008; Lin *et al.,* 2008).

2.2. Advanced oxidation technology in water treatment

Advanced oxidation technologies (AOTs) or processes (AOPs) are a set of chemical treatment techniques designed to eliminate organic (and sometimes inorganic) materials in

water and waste water by oxidation through reactions involving hydroxyl radicals (·OH). The oxidation of organic pollutants occurring primarily through reactions with the hydroxyl radical is termed advanced oxidation (Goi, 2005; Glaze *et al.,* 1987), however in water treatment applications, AOPs usually refer to a particular subset of processes that include ozonolysis (O_3), hydrogen peroxidation (H_2O_2), and/or ultra-violet (UV) light radiation (Grote, 2012). Advanced oxidation processes can be split into two categories, which are established and emerging technologies. Table 1 gives details on the above mentioned AOP categories.

Table 1: Established and emerging advanced oxidation processes (AOPs)

Established technologies	Emerging technologies
Hydrogen peroxidation/ ozonolysis (H_2O_2/ O_3)	TiO_2-catalyzed UV oxidation
Hydrogen peroxidation/ Ultra-violet light radiation (H_2O_2/ UV)	High energy electron beam irradiation (E-beam)
Ozonation/ ultraviolet light radiation (O_3/ UV)	Cavitation (Sonication & hydrodynamic)
	Fenton's reaction

2.2.1. Oxidation

The oxidation process is defined as the transfer of one or more electrons from an electron donor (reductant) to an electron acceptor (oxidant). In an oxidation reaction the oxidant has a higher affinity for electrons. The transfer of electrons induces chemical transformation of

both the oxidant and the reductant, in some instances generating radicals. These are unstable and highly reactive; leading to further oxidation of organic or inorganic species present in the system until thermodynamically favourable products are generated. Table 2 gives the oxidation potentials of some known oxidizing agents.

Table 2: Relative oxidation power for some oxidizing species

Species	Oxidation potential (eV)
Fluorine	3.06
Hydroxyl radical	2.80
Nascent oxygen	2.40
Ozone	2.07
Hydrogen peroxide	1.77
Perhydroxyl radical	1.70
Hypochlorous acid	1.49
Chlorine	1.36

Fluorine has the highest oxidation although it is not used in water treatment. The hydroxyl radical (·OH) is a non-selective powerful oxidizing agent that acts rapidly on organic pollutants (Mohapatra *et al.*, 2014; Parsons and Williams, 2004; Trapido *et al.*, 2000; Langlais *et al.*, 1991). AOPs incorporate two stages (a) generation of strong oxidants (b) and the subsequent reaction with organic or inorganic pollutants in water. The generation of ·OH

radicals is commonly accelerated by combining the following AOPs as necessary: (ozone (O_3), hydrogen peroxide (H_2O_2), titanium dioxide (TiO_2), heterogeneous photo-catalysis, UV radiation, ultrasound, and (or) high electron beam irradiation). The end products of complete mineralization of organic compounds are carbon dioxide (CO_2) and water (H_2O).

2.2.2. Advantages of AOPs

Some of the advantages of AOPs are:

- Fast reaction rates
- Potential to reduce organic compounds toxicity
- Capability to mineralize organics, i.e. conversion to CO_2 and water
- Do not accumulate waste for further treatment, like in the case of membranes
- Do not produce "spent carbon" such as activated carbon adsorption
- Can easily be automated and controlled
- Reduced Labour Input
- Do not create sludge as with physical chemical process or biological processes (wasted biological sludge)

2.2.3. Disadvantages of AOPs

Some of the disadvantages of AOPs are:

- They are capital intensive
- Complex chemistry must be tailored to specific application
- For some applications quenching of excess peroxide is necessary

(Mohapatra *et al.,* 2014; Parsons and Williams, 2004; Trapido *et al.,* 2000; Langlais *et al.,* 1991)

2.3. Established technologies

2.3.1. Ozone (O_3) treatment

2.3.1.1. Ozonation-reaction mechanisms

Ozone is a very powerful and selective oxidizing agent (Khan *et al.,* 2010 and Dalmazio *et al.,* 2007), only second to the hydroxyl radical. This renders it capable of oxidizing many organic and inorganic compounds in water. It is highly reactive, and as soon as it is dissolved in water, it undergoes a series of very complex self-decomposition and oxidation reactions (Zhou and Smith, 2002). The Staehelin, Bühler, and Hoignè (SBH) model (Staehelin and Hoignè, 1982) and the Tomiyasu, Fukutomi, and Gordon (TFG) model (Tomiyasu *et al.*, 1985) are the two most widely accepted mechanisms for ozone decomposition and oxidation.

However the mechanisms postulate that ozone decomposition in water is a radical chain process whereby decomposition intermediates will further catalyse removal of molecular ozone. Ozone can react either by direct oxidation of substrate or via ozone decomposition to generate hydroxyl radicals that oxidise substrate (Wang *et al.,* 2012; Ben *et al.,* 2012; Kim *et al.,* 2012; Gomez-Pacheco *et al.,* 2011; Khan *et al.,* 2010; Uslu and Balcioglu, 2008; Zhou and Smith, 2002; EPA, 1999). Findings from several research investigations revealed that: (1) ozone can react directly with organic pollutants that have high electron density sites or (2) through oxidation of compounds by hydroxide free radicals generated upon decomposition of ozone (Fig. 2.1).

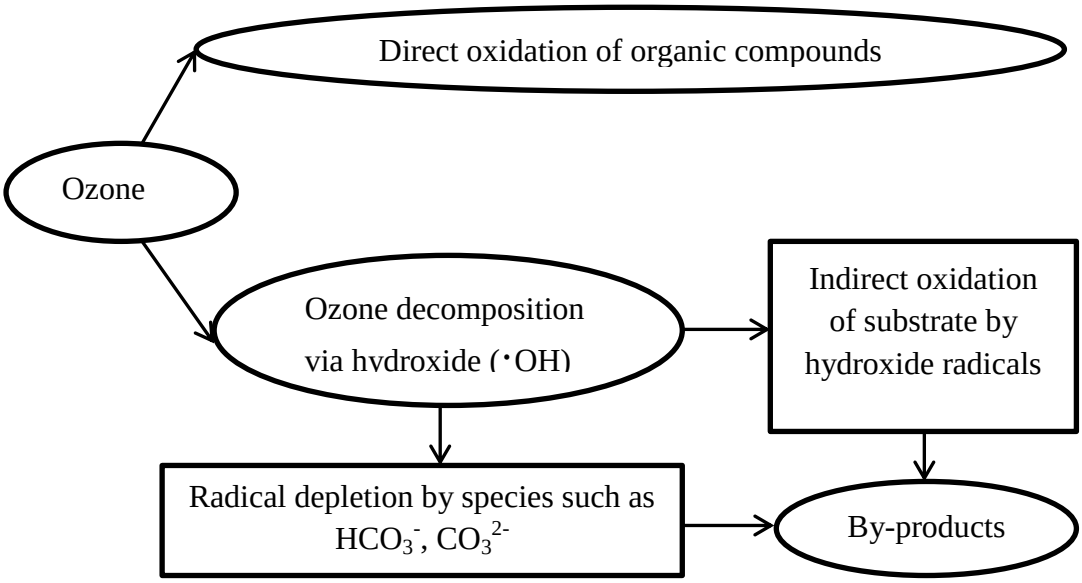

Figure 2.1: Oxidation reactions of compounds in water during ozonation (Wang *et al.*, 2012)

The direct oxidation pathway is relatively slow compared to indirect oxidation by hydroxyl radicals. Hydroxyl radical reactions are non-selective virtually reacting with nearly all the organic compounds through hydrogen atom abstraction, direct electron transfer, or insertion, however the hydroxyl radical concentration is relatively small under normal ozonation conditions (Zhou and Smith, 2002; Hoigné and Bader 1977). Figure 2.2 shows the mechanism of alkene ozonolysis. The initial step of the reaction is a 1,3-dipolar cycloaddition of ozone to the alkene producing a primary ozonide (molozonide, 1,2,3-trioxolane) which decomposes leading to a carbonyl oxide and a carbonyl compound. The carbonyl oxides resemble ozone in being 1,3-dipolar compounds, and undergo 1,3-dipolar cycloaddition to the carbonyl compounds with the reverse regiochemistry, resulting in a mixture of three possible secondary ozonides (1,2,4-trioxolanes).

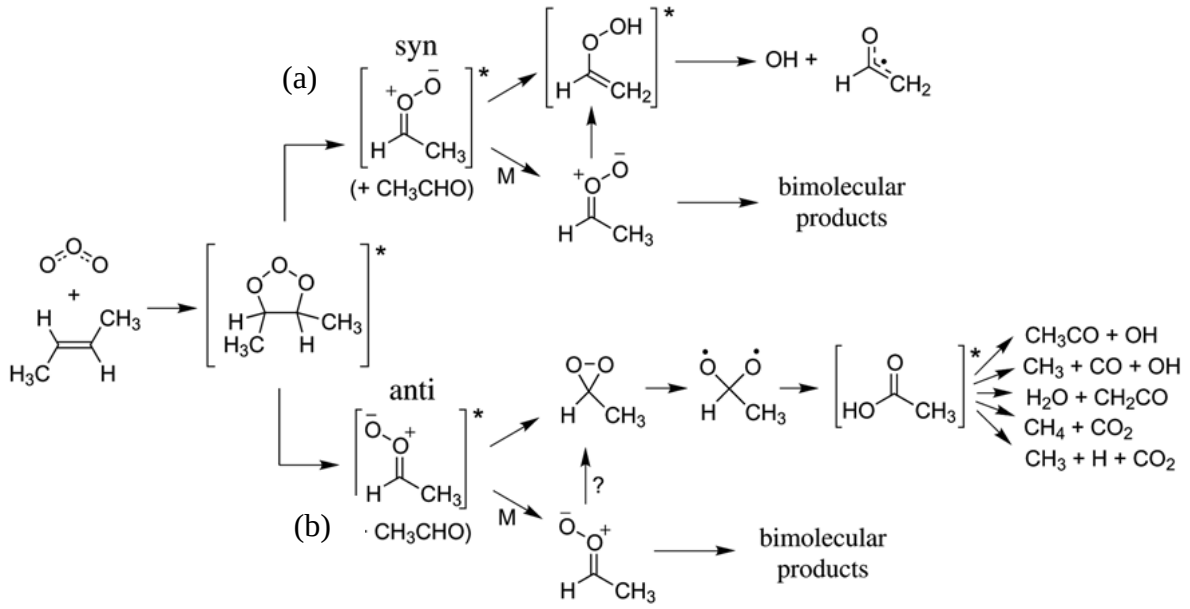

Figure 2.2: Mechanism of alkene Ozonolysis (a) syn (same side or face) oxidative cleavage (b) anti (opposite sides or faces) oxidative cleavage resulting in the formation of intermediate M in either reaction path (http://ent.arp.harvard.edu/kinetics/)

2.3.1.2. Ozone microbial inactivation mechanism

Ozone is a powerful antimicrobial agent that is capable of inactivating bacteria, fungi, viruses, protozoa, and bacterial and fungal spores (Khadre *et al.*, 2001). The manner in which biocides impact on microorganisms is dependent on their chemical structure, however it is not the only factor limiting antibacterial/ antifungal effectiveness. Most of the biocidal agents interfere with metabolic pathways after penetrating into the cell, which in turn leads to the necrosis of the microorganism (Turkiewicz *et al.*, 2013; Turkiewicz, 2011; Van Hamme *et al.*, 2003; Viera, 1999; Sunde *et al.*, 1990). Upon dissolution of molecular ozone in water, the molecule can remain as O_3 or decompose via a variety of mechanisms, ultimately producing the hydroxyl free radical (·OH) which is a stronger oxidizing agent than ozone. The hydroxyl radical targets membrane components such as proteins, lipids, and polysaccharides leading to cell lysis with further oxidation (Fig. 2.3). Ozone inactivation is a

complex process that encompasses oxidation of certain membrane and wall constituents such as unsaturated fatty acids and cell constituents such as enzymes and nucleic acids. Both ozone and its breakdown components (•OH) play a role in the inactivation mechanism of microbes. The microbes are killed due to cell membrane disruption or disintegration leading to cell content leakage. Micro-organisms cannot develop resistance against ozone due to its mode of inactivation which is cell lysis, unlike other disinfectant agents that have to permeate the cell to have any effect on the microbe (Ruiz *et al.,* 2007; Blanc, 2005; Thanomsub *et al.,* 2002).

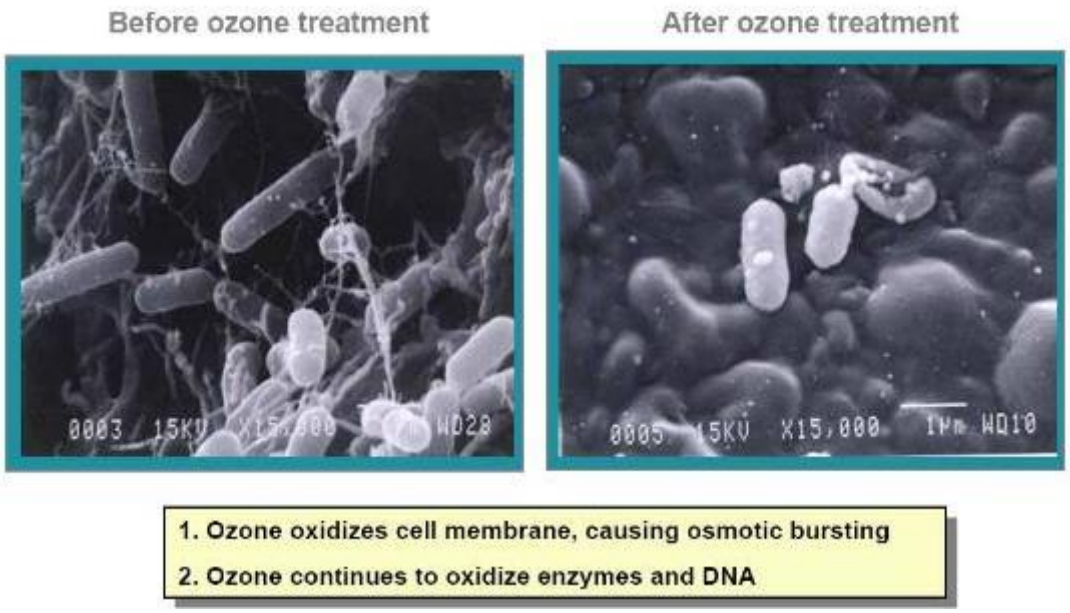

Figure 2.3: Biocidal action of ozone on bacterial cells (Juan, 2000)

2.3.1.3. Primary uses of ozone

Ozone is used at various stages in drinking water treatment and these include:

- Disinfection;
- Oxidation of inorganic pollutants, such as iron, manganese, and sulfide;

- Oxidation of organic micro-pollutant, including pesticides, phenolic pollutants, taste and odour compounds; and
- Oxidation of organic macro-pollutant, including removal of colour, increasing organic compound biodegradability, and chlorine demand reduction.

2.3.1.4. Disinfection

Ozone technology is one of the most widely researched AOPs due to its use in a number of water and waste water treatment facilities as a disinfecting and clarifying agent (Mohapatra *et al.,* 2014). Ternes and co-workers, 2003, reported that ozonation is an appropriate technique for the treatment of wastewater and wastewater sludge. It was found that ozone possesses strong cell lytic activity and can exterminate microorganisms found in activated sludge and also further oxidize the organic substances released from the cells. Ozone is a good disinfectant and is capable of inactivating even more resistant pathogenic microorganisms such as protozoa (e.g. *Cryptosporidium parvum* oocysts) where conventional disinfectants (chlorine, chlorine dioxide) fail. Orr and co-workers, 2004, discovered that ozone alone, or in combination with hydrogen peroxide was incapable of destroying the highly toxic STX and GTX-2/3, and only partially destroyed dc-STX, and the low-toxicity C-toxins and GTX-5 from water contaminated with cell free extracts of *Anabaena circinalis*. Ramseier *et al.,* 2011 treated drinking water with ozone and other oxidants to investigate the kinetics of membrane damage of native drinking water bacterial cells. They measured membrane damage via flow cytometry using a combination of SYBR Green I and propidium iodide (SGI+PI) staining as indicator for cells with permeabilized membranes and SGI alone to measure total cell concentration. They discovered that only ozonation resulted in a decrease of the total cell concentrations for the investigated reaction times. Chand *et al.,* 2007, achieved 75 % elimination of *Escherichia coli* (*E. coli*) from water in about 3 hours of treatment time using

an optimized combination of hydrodynamic cavitation and ozonation. In another study coliform inactivation effectiveness was carried on wastewater from a wastewater treatment plant (University of Sao Paulo-Brazil) using varying doses of ozone (5, 8, & 10 mg O_3 L^{-1}). The total coliform inactivation range was 2.00-4.06 log_{10}, and the inactivation range for *Escherichia coli* was 2.41-4.65 log_{10} (Silva *et al.,* 2010).

2.3.1.5. Removal of organics and pharmaceutically active compounds (PhACs)

Carballa *et al.,* 2007, observed that an ozone dose of 20 mg O_3 /g total suspended solids (TSS) was able to remove up to 60% of carbamazepine, when they studied the influence of ozone pre-treatment on sludge anaerobic digestion and simultaneous removal of pharmaceutical and personal care products. Nakada *et al.,* 2007, observed varied removal efficiency (8.3-81 %) when they studied removal of carbamazepine during sand filtration and ozonation at a municipal sewage treatment plant. Rosal and co-workers, 2010, achieved 100 % removal of carbamazepine with ozonation doses lower than 130 μM, after biological pre-treatment. A study by Lee *et al.,* 2012, on the feasibility of ozone and bio-filtration as an alternative to reverse osmosis (RO) for the elimination of pharmaceutical and personal care products (PPCPs), including carbamazepine from treated wastewater revealed that ozone doses of 4-8 mg L^{-1} were nearly as effective as RO.

2.3.2. Disinfection parameters of ozone

The section below describes the relation between ozone decomposition with variations in pH, temperature and concentration of organic & inorganic constituents. A high aqueous ozone concentration is necessary for efficient inactivation of microbes, thus factors accelerating ozone decomposition are not desirable.

2.3.2.1. Influence of pH on ozonolysis

Studies by Farooq, 1976, indicated that changes in pH have little or no effect on ozone inactivation of acid-fast bacteria such as *mycobacteria* and *actinomycetes*. Roy 1979, observed a slight decrease in the virucidal efficacy of ozone residuals with decrease in pH. However, Vaughn and co-worker, 1987, observed an opposite effect. The decomposition rate of ozone with changes in pH appears to be the main factor controlling its disinfection efficiency (Ding *et al.,* 2013; Dow *et al.,* 2006). Langlais *et al.,* 1991, reported that ozone decomposition occurs faster in aqueous solutions with higher pH and forms a variety of oxidants with differing reactivities. Studies by Harakeh and Butler, 1984, and Vaughn *et al.,* 1987, revealed a decrease in virus inactivation by ozone at alkaline pH (pH 8 to 9) for poliovirus 1 and rotaviruses SA-11 and Wa. Studies by Wickramanayake, 1984a, indicated an improvement in *Giardia muris* cyst inactivation when the pH was increased from 7-9.

2.3.2.2. Influence of temperature on ozonolysis

The solubility and stability of ozone is reduced when temperature increases, however chemical oxidation and disinfection rates remain stable (Ran *et al.,* 2010; Li *et al.,* 2001; Katzenelson *et al.,* 1974). Studies have shown that a temperature increase from 0-30 ˚C significantly reduces the solubility of ozone in water and rapidly increases its decomposition. Nevertheless, this phenomenon has no effect on the disinfection rate of bacteria (Ding *et al.,* 2013; Larson and Mariñas, 2003; Kinman, 1975). Ding and co-workers, 2013 studied ozone inactivation of prions, and they discovered that the rate of inactivation increased with increasing temperature.

2.3.2.3. Influence of suspended matter on ozonolysis

Studies by Walsh and co-workers in 1980 revealed that ozone inactivation rates of microbes found in minute flocs of aluminium was not reduced at floc turbidity levels of 1 and 5 NTU (nephelometric turbidity unit). They clearly indicated that the floc offered no protection at all to the microbes. In waters heavily polluted with organics increased slime growth is observed due to an abundance of ozonation by-products (easily metabolized) that promote growth since ozonation does not completely degrade organics to carbon dioxide and water (Wilczak *et al.*, 1992; Edward and Benjamin, 1991; Troyan and Hanson, 1989).

2.3.2.4. Advantages of ozonation

The use of ozonation in drinking water treatment offers the following advantages:

- Taste and odour reduction,
- Effective iron and manganese removal,
- Capability to remove colour,
- Capable of efficient disinfection over a wide range of pH and temperature,
- Capable of destroying bacteria, viruses, spores, giardia and cryptosporidium with brief contact periods,
- Reduces the formation of disinfection by-products (DBP) such as trihalomethanes (THMs) and haloacetic acids (HAAs),
- Does not require the on-site storage like other chemicals with the associated hazards and costs,
- Capable of removing hydrogen sulphide,
- Ozonation can reduce the amount of chemicals required for flocculation or flotation by 20-50 %,

- Ozonation is known to reduce turbidity and dissolved organic carbon by enhancing aerobic digestion in biologically active filters,
- Capable of removing synthetic micro-pollutants found in surface and ground water.

2.3.2.5. Disadvantages of ozonation

Disadvantages of ozonation in water treatment include:

- Low ozone doses may fail to effectively inactivate some spores, cysts and viruses,
- Ozonation is more complex compared to other disinfection methods,
- Ozone is highly reactive and corrosive, which calls for the use of corrosion-resistant material, such as stainless steel,
- Ozonation is not cost-effective for poor quality (poorly treated) wastewater,
- Ozone is extremely irritating and possibly toxic, so off-gases from the contactor must be destroyed to prevent worker exposure,
- The cost of treatment is relatively high, being both capital- and power-intensive,
- Ozonation has no measurable residual which necessitates post-chlorination
- Ozonation may generate some undesirable aldehydes and ketones when it reacts with certain organics,
- Ozone is less soluble in water than chlorine; therefore special mixing devices are required.

(Spartan environmental technologies, 2014; Chelme-Ayala *et al.,* 2011; Matilainen and Sillanpää, 2010; Irabelli *et al.,* 2008; Vilve *et al.,* 2008; Tech brief, 1999; Budd *et al.,* 1999; Cotruvo *et al.,* 1999; Langlais *et al.,* 1991)

2.3.3. Hydrogen peroxide/ Ozone (H_2O_2/ O_3)

Hydrogen peroxide (H_2O_2) is a clear, colourless liquid with a slightly pungent odour. Hydrogen peroxide is commercially produced almost exclusively according to the Anthraquinone-autoxidation process using hydrogen and atmospheric oxygen. In this process an anthraquinone derivative is used as the reaction carrier.

The process starts with the reduction of an anthraquinone (Fig. 2.4) to its corresponding anthrahydroquinone, typically through hydrogenation on a palladium catalyst. The starting anthraquinone is regenerated as the anthrahydroquinone undergoes autoxidation with hydrogen peroxide being produced as a by-product.

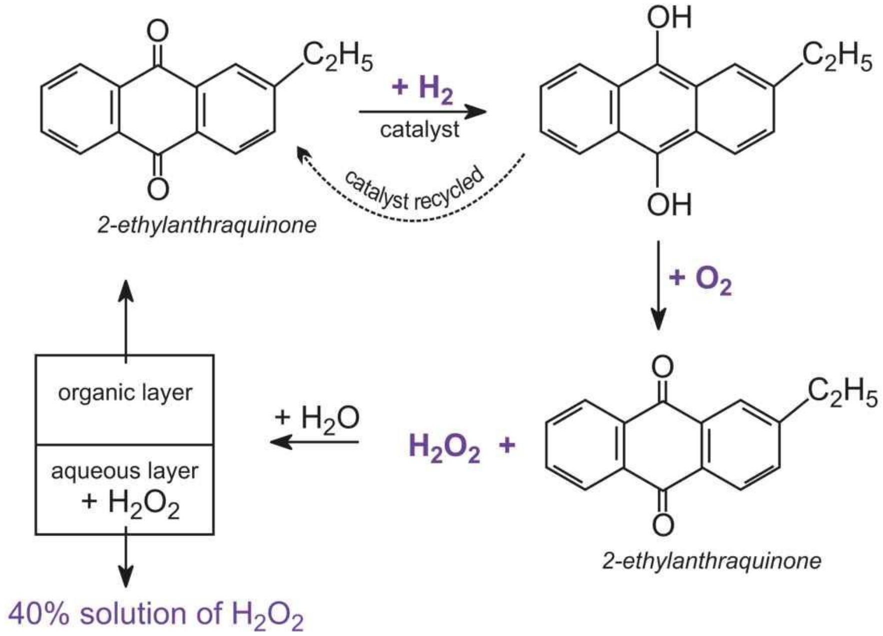

Figure 2.4: Hydrogen peroxide production process (http://h2o2.evonik.com/product/h2o2)

Equation 2.2 shows a simplified overall process for the production of hydrogen peroxide.

$$H_2 + O_2 \longrightarrow H_2O_2 \quad \text{……………………...…………. (2.2)}$$

2.3.3.1. Hydrogen peroxide/ ozone reactions

Combination of hydrogen peroxide (H_2O_2) with ozone allows the enhancement of O_3 transformation to hydroxyl radicals ($^{\cdot}OH$) in solution. Hydrogen peroxide is weekly acidic, hence dissociates into the hydro-peroxide ion (HO_2^-) in aqueous medium (Equation 2.3). The hydro-peroxide ion (Equation 2.4) rapidly reacts with ozone, unlike H_2O_2 which reacts slowly (Hoigne, 1998).

$$H_2O_2 + H_2O \longrightarrow HO_2^- + H_3O^+ \quad \text{(2.3)}$$

$$O_3 + HO_2^- \longrightarrow {}^{\cdot}OH + O_2^- + O_2 \quad \text{(2.4)}$$

The hydroxyl radical reacts further with the hydroxyl ion, hydro-peroxide ion, hydrogen peroxide and ozone (Equations 2.5-2.9 respectively).

$$^{\cdot}OH + OH^- \longrightarrow H_2O + O^- \quad \text{(2.5)}$$

$$^{\cdot}OH + HO_2^- \longrightarrow HO_2^{\cdot} + OH^- \quad \text{(2.6)}$$

$$^{\cdot}OH + H_2O_2 \longrightarrow HO_2^{\cdot} + H_2O \quad \text{(2.7)}$$

$$^{\cdot}OH + O_3 \longrightarrow HO_2^{\cdot} + O_2 \quad \text{(2.8)}$$

$$HO_2^{\cdot} \Longleftrightarrow O_2^- + H^+ \quad \text{(2.9)}$$

The reactions in equations 2.5-2.9 (Gottschalk *et al.,* 2010; Zhong *et al.,* 1999) occur simultaneously with pollutant oxidation by the hydroxyl radical.

In an H_2O_2/ O_3 system, ozone is generated on site since it decomposes rapidly. On the other hand H_2O_2 is fed from an aqueous solution, and the specific ratio depends on the disinfection

requirements, bromide concentration, contaminant concentration, and other water quality parameters (Liang, 1999).

2.3.3.2. Disinfection

Studies by Williams *et al.,* 2005 indicated that ozone and hydrogen peroxide were more effective after longer contact periods in terms *Salmonella* and *E. coli* O157:H7 inactivation in juice products. They concluded that contact and reactivity could be increased through agitation by stirrers or via bubbling of ozone. Nevertheless, mechanical stirring may lead to ozone half-life reduction (Wickramanayake, 1984). Reports by Padron, 1995, indicate that pressurizing ozone (gaseous) and hydrogen has a positive effect on Salmonella Typhimurium inactivation in egg shell products. Pressure is believed to force the sanitizer into the pores of the shell eggs hence effecting better inactivation. However, studies by Koidis and other, 2000, revealed that pressurized aqueous ozone did not have similar effects on shell eggs. An ozone/ dimethyl dicarbonate (DMDC) system was observed to possess improved inactivation capability on five strains of *Salmonella* in apple cider and orange juice compared to the ozone/ hydrogen peroxide system (Williams *et al.,* (2005).

2.3.3.3. Organic pollutants removal

Several researchers have observed improved removal of organic pollutants from water through the synergistic effects of ozone and hydrogen peroxide. Pisarenko and co-workers, 2012, investigated the effect of combining ozone and hydrogen peroxide on the removal of trace organic contaminants (TOrC) and the link to N-nitrosodimethylamine (NDMA) formation in drinking and wastewater treatment. They observed little effect on NDMA removal with ozone alone. The addition of hydrogen peroxide (3.5 mg peroxide/ L) to 10 mg

O_3/ L resulted in a 46 % removal efficiency of NDMA. Trace organic contaminant removal with ozone and ozone/ peroxide also yielded similar trends (Pisarenko *et al.,* 2012).

The ozone/ peroxide process has been observed not to provide additional removal benefits over ozone alone for compounds such as carbamazepine, trimethoprim, and diclofenac that are easily oxidized. In another investigation 50 % removal of two herbicides (bromoxynil and trifluralin) was achieved using ozone alone. An enhancement of bromoxynil and trifluralin degradation was observed using O_3/ H_2O_2 process (Chelme-Ayala *et al.,* 2011). Studies conducted by other researchers revealed that addition of hydrogen peroxide is beneficial in the reduction of the optimum ozone dose required in the removal of dissolved organic carbon (DOC) and total organic carbon (TOC) (Irabelli *et al.,* 2008; Paode *et al.,* 1995; Prados *et al.,* 1995a).

Findings by Irabelli *et al.,* 2008 indicated that post-ozonation with the O_3/ H_2O_2-system attains better removal of DOC juxtaposed to pre-ozonation. Nevertheless, the overall concentrations of trihalomethane (THM) were higher in samples post- and pre-treated with the O_3/ H_2O_2 system compared to ozonated samples (Irabelli *et al.,* 2008). In similar studies, Mosteo and co-workers, 2009, did not realise any significant improvement in THM reduction after addition of either H_2O_2 or TiO_2 to the ozone treatment. The simultaneous addition of H_2O_2 and TiO_2 to the ozonation system resulted in lower production of trihalomethanes (Matilainen and Sillanpää, 2010).

2.3.3.4. Advantages of a H_2O_2/ O_3 system

Some of the advantages include:

- The effective removal of MTBE and other natural and synthetic organics by H_2O_2/ O_3 process has been shown to be more effective than using O_3 or H_2O_2 alone. The use of a combination of O_3 and H_2O_2 to produce hydroxyl radicals, as opposed to O_3 alone, allows for a lower dosage of O_3 to be used. This in turn has a desirable effect in reducing operation costs and bromate formation potential.
- The theoretical yield of hydroxyl radicals for H_2O_2/ O_3 is less affected by water quality (i.e., turbidity, iron, and nitrates) which lowers the yield for UV processes.
- H_2O_2/O_3 systems have been thoroughly tested and applied in decontamination applications for ground-water. Therefore, the implementation of H_2O_2/ O_3 systems has a field-proven history of operation and regulatory acceptance.

2.3.3.5. Disadvantages of H_2O_2/ O_3

Some of the disadvantages include:

- Ozone (O_3) use can potentially result in bromate formation; however, bromate formation can be reduced by lowering the pH to below 6.5, and increasing the H_2O_2 to O_3 ratio, or adding another radical scavengers like ammonia that will react with hydroxyl radicals before bromide.
- Residual hydrogen peroxide (H_2O_2) can serve as an oxygen source for microorganisms and can promote biological re-growth in the distribution system.

(Chelme-Ayala *et al.*, 2011; Catalkaya and Kargi, 2009; Irabelli *et al.*, 2008; Ikehata and Gamal El-Din, 2005; Crawford, 1999)

2.3.4. Ultraviolet/ Ozone

Ultraviolet (UV), light is an invisible form of electromagnetic radiation having a shorter wavelength than the light which humans can see. UV carries more energy (shorter

wavelength) than visible light (longer wavelength) and can sometimes break bonds between atoms and molecules, changing the chemistry of materials exposed to it. UV light can also induce fluorescence in some substances.

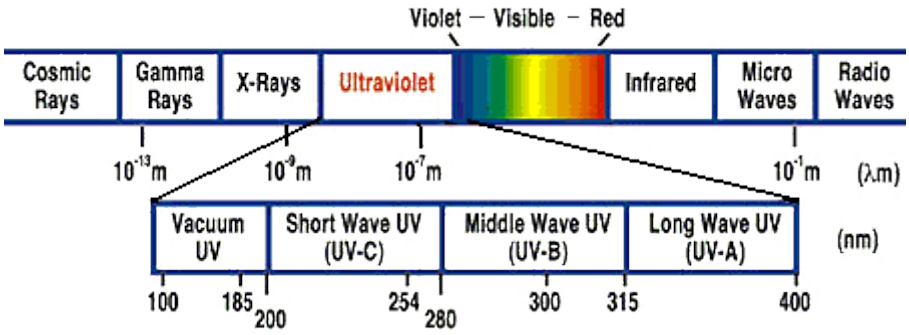

Figure 2.5: UV light spectrum

One of the ways of disinfecting water is via UV-light exposure. UV light disinfection can be used alone or in combination with other processes. It is known to be beneficial if it precedes membrane filtration since it can supress bio-fouling in the system. UV-LED light sources are commercially available. These UV-LED light sources emit monochromatic UV light at 365 nm (or 385 nm). Their low power consumption makes them an energy-saving and environmentally friendly light source.

2.3.4.1. Ultraviolet/ Ozone reactions

In the O_3/ UV oxidation process, hydroxyl radicals are produced according to the following equations:

$$O_3 \xrightarrow{h\nu} O^1(D) + O_2 \quad \text{(2.10)}$$

$$O^1 + H_2O \xrightarrow{k_{O_3}} H_2O_2 \quad \text{(2.11)}$$

$$H_2O_2 \longrightarrow HO^{\cdot} + {}^{\cdot}OH \quad \text{(2.12)}$$

The above reactions occur simultaneously with pollutant oxidation by the hydroxyl radical (Andreozzi *et al.,* 1999). The O_3/ UV system behaves similarly to the O_3/ H_2O_2 and the H_2O_2/ UV systems (Legrini *et al.,* 1993; Glaze *et al.,* 1987). The use of O_3/ UV systems requires the use of a sparging device.

2.3.4.2. Disinfection

During UV/ O_3 treatment, inactivation of microbial pollutants can transpire through direct reaction with ozone, UV photolysis, and synergistic action UV/ O_3. Studies were carried out to assess the effectiveness of O_3/ UV systems in the reduction of microbial pollutants in vegetable wash water in the fresh-cut industry. It was reported in literature that the O_3/ UV system achieved a 6.6 log CFU mL^{-1} reduction after treatment for 60 minutes. Also a very significant turbidity reduction was achieved by the O_3/ UV system. The researchers concluded that the O_3/ UV system was a suitable alternative sanitizer for the fresh-cut wash process (Selma *et al.,* 2008). In another study it was concluded that ozone activated with UV light could be a highly suitable alternative to chlorine for washing shredded lettuce, not only in reducing microbial populations, but also maintaining visual quality (Allende *et al.,* 2006). Other researcher investigated the effects of temperature and UV light on the performance of ozone in the inactivation of *Mycobacterium fortuitum* using a laboratory scale continuous flow system. They observed that when UV light was used as a catalyst in ozone disinfection no apparent increase in inactivation of *M. fortuitum* was observed. Nevertheless, UV light alone was observed to exert a huge inactivation potential (Farooq *et al.,* 1977). Dumètre and co-workers investigated the effects of UV light and ozone in the inactivation of *Toxoplasma gondii* oocysts. They achieved a 4-log inactivation of *T. gondii* with UV fluences greater above 20 mJ/ cm^2. However, ozone was not able to inactivate *T. gondii* (Dumètre *et al.,* 2008).

2.3.4.3. Organic pollutant removal

Several researchers have investigated the synergistic effect of UV/ O_3 on the degradation of organic pollutants in water. Studies were carried out to investigate the degradation of dichloroacetic acid (DCAA) and trichloroacetic acid (TCAA) using UV radiation and ozone. Their findings indicated that UV radiation or ozone alone did not attain appreciable levels of degradation of these haloacetic acids. They discovered that the UV/ O_3 system was the most suitable advanced oxidation process for the degradation of DCAA and TCAA in water (Wang *et al.*, 2009).

Vollmuth and Niessner investigated the removal of polychlorinated dibenzodioxin (PCDD), polychlorinated dibenzofuran (PCDF), polycyclic aromatic hydrocarbon (PAH), polychlorinated biphenyl (PCB) and chlorinated phenols from landfill seepage water using UV irradiation, ozone and UV/ O_3. They achieved 90 % removal efficiency for the degradation of chlorinated phenols and PAH. However, there was no significant effect on the degradation of PCDD/ PCDF (Vollmuth and Niessner, 1995). Esplugas and others investigated UV/ O_3 degradation of phenol while varying pH between 3 and 9. They achieved 80.9 % phenol removal efficiency with non-buffered solution, 92.6 % phenol removal at pH 6.9, and 91.9 % phenol removal at pH 9.4 in a period of eighty minutes. They concluded that the changes in degradation of phenol due to the synergistic effects of UV and O_3 were very marginal (Esplugas *et al.*, 2002).

2.3.4.4 Advantages of UV

Some of the advantages include the following:

- Ultraviolet light is a physical process that does not need addition of chemicals.

- UV is very effective towards inactivation of protozoa, nevertheless viruses are more resistant.
- There are no known UV disinfection by-products and it only requires short contact times.

2.3.4.5. Disadvantages of UV

Some of the disadvantages include the following:

- UV disinfection has no residual effect.
- There are variations in output among different types of UV lamps.
- It is not possible to measure lamp dose in practise.
- UV disinfection is affected by turbidity.

(Wang *et al.,* 2009; Esplugas *et al.,* 2002; Vollmuth and Niessner, 1995)

2.4. Emerging technologies

2.4.1. Cavitation

It can be described as the formation, growth, and collapse of micro-bubbles or cavities with the successive local release of large sums of energy. The energy is as a result of the fast collapse of the cavities, compressing entrapped gas and vapour leading to local hot spots. This high energy brings about excitation of dissolved gases, vaporized water and solutes which can eventually dissociate leading to the formation of ˙OH and ˙OOH radicals. Sonochemical reactors generate cavities through ultrasound irradiation while hydrodynamic reactors do so through interchange of flow energy and pressure energy. Optic cavitation is produced by high light intensity photon, which rupture the liquid continuum, while particle

cavitation is produced by elementary particles of any other type of beam (Chakinala *et al.*, 2009; Gogate and Kabadi, 2009; Torres *et al.*, 2008; Torres *et al.*, 2007; Mason and Pétrier, 2004; Mason and Lorimer, 2002; Gogate, 2002; Luche, 1999; Shah *et al.*, 1999; Crum, 1995; Suslick, 1990; Mason and Lorimer, 1988). Figure 2.6 shows an illustration of cavitation in water.

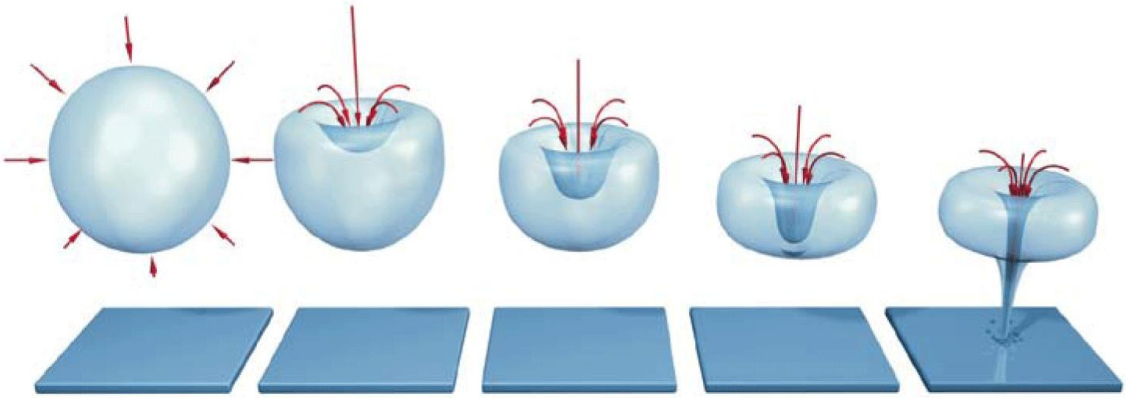

Figure 2.6: Illustration of cavitation in water (eswt.net, 2012)

2.4.1.1. Mechanism of radical formation

Hydroxyl and peroxide radicals are generated within cavities according to the following equations:

$$H_2O \xrightarrow{\text{Ultrasound}} H^{\cdot} + HO^{\cdot} \quad \text{.....} \quad (2.13)$$

$$O_2 \xrightarrow{\text{Ultrasound}} 2O^{\cdot} \quad \text{.....} \quad (2.14)$$

$$O^{\cdot} + H_2O \longrightarrow 2HO^{\cdot} \quad \text{.....} \quad (2.15)$$

$$H^{\cdot} + O_2 \longrightarrow HO^{\cdot} + O^{\cdot} \quad \text{(2.16)}$$

$$H^{\cdot} + O_2 \longrightarrow HOO^{\cdot} \quad \text{(2.17)}$$

The amount of ˙OH radicals produced during acoustic cavitation can be estimated by measuring the H_2O_2 present, since it is produced when $HO^{\cdot}$ radicals combine in the absence of organic pollutants (Chakma and Moholkar, 2013; Méndez-Arriaga *et al.,* 2008; Torres *et al.,* 2008; Torres *et al.,* 2007; Adewuyi, 2005; Chemat *et al.,* 2001; Pétrier and Francony, 1997).

2.4.1.2. Organic pollutant removal by cavitation

Sonochemical and hydrodynamic cavitation have been employed in the removal of organic pollutants from water resources and industrial waste waters. Jiang and co-workers investigated the sonolytic degradation of chlorobenzene. The degradation was described using the following equations:

$$C_6H_5Cl \xrightarrow{\text{Ultrasound}} C_6H_5^{\cdot} + Cl^{\cdot} \quad \text{(2.18)}$$

$$C_6H_5^{\cdot} \longrightarrow C_4H_3^{\cdot} + C_2H_2 \quad \text{(2.19)}$$

$$C_4H_3^{\cdot} \longrightarrow C_4H_2 + H^{\cdot} \quad \text{(2.20)}$$

$$C_4H_2 \longrightarrow C_2H_2 + C \quad \text{(2.21)}$$

After fifty minutes of degradation, they observed some brown carbonaceous particles in the sonochemical reactor. They deduced that phenyl radicals could further decompose into

$C_4H_2^{\cdot}$, C_2H_2, and C (Jiang *et al.*, 2002). Several researchers have carried out studies to investigate the effectiveness of sonochemical or hydrodynamic cavitation towards organic pollutant abatement. Torres and co-workers carried out a comparative study of ultrasonic cavitation and Fenton process on the removal of bisphenol A from water, a xenobiotic that exhibits endocrine disruption action. They conducted their experiments using deionized acidic water (pH 3) and natural water (pH 7.6). Ultrasound cavitation and Fenton reaction showed equal rates of bisphenol A elimination as well as primary intermediates in deionized water. Chemical oxygen demand (COD) and total organic carbon (TOC) analyses allowed them to deduce that the Fenton process was slightly more efficient than the ultrasound cavitation. Experiments carried out in natural waters showed that the Fenton process was inhibited whereas the cavitation process was never affected at all (Torres, 2007).

Destaillats and others investigated the sonochemical degradation of dichloromethane (DCM), trichloroethylene (TCE) and the methyl orange (MO) using a pilot scale reactor (UES 4000 C Pilot-station). They compared the observed reaction rates on the degradation of the three pollutants with those obtained using bench-scale reactors under similar conditions in order to evaluate the performance of the pilot-station. The pseudo-first-order degradation rate for TCE in the pilot-station was observed to be more than 4 times higher than the corresponding smaller values measured in lab-scale reactors. A similar trend was also observed in the degradation of DCM (Destaillats *et al.*, 2001).

Li and co-workers investigated the degradation of phenol using micro-bubble collapse technique. They achieved 60 % removal efficiency in a period of two hours when air was employed as the source of micro-bubbles. They also investigated the dependence of phenol degradation on pH of the solution and the type of gas entrapped in the micro-bubbles. There

was a linear increase in pseudo-first order rate constant *k*, with increasing H^+ in the solution. The highest *k* values were achieved with oxygen micro-bubbles (Li *et al.,* 2009). Takahashi and co-workers also observed similar trends on the degradation phenol using micro-bubbles. They achieved 30 % phenol degradation after the addition of acid (sulphuric, nitric and hydrochloric acid) and the degradation process yielded intermediates such as formic acid, oxalic acid, benzoquinone and hydroquinone (Takahashi *et al.,* 2007).

Tasaki and others investigated the degradation of methyl orange using short wavelength UV irradiation with oxygen micro-bubbles. Their findings showed that the oxygen micro-bubbles enhanced the decolourization rate of methyl orange under 185-254 nm irradiation. However, micro-bubbles under 365 and 254 nm irradiation did not cause any significant change in the decolourization of methyl orange. They also established that the pseudo-zero order reaction rate constants in micro-bubble system were 2.1 times higher than in the conventional large bubble system (Tasaki *et al.,* 2009).

An in-depth analysis conducted by González-García stated that sonochemical degradation follows a radical mechanism which produces a very wide range of chlorinated compounds in very low concentrations. They concluded in their analysis that sonochemical degradation alone was not an efficient treatment to lower the organic pollutant level in waste water (González-García *et al.,* 2010).

2.4.1.3. Microbial inactivation by cavitation

Cavitation generates highly reactive free radicals from the collapse of micro-bubbles and these have great potential to disinfect water (Agarwal *et al.,* 2011; Takahashi *et al.,* 2009; Li *et al.,* 2009; Jyoti and Pandit, 2004). Acoustic cavitation is generally a more expensive

disinfection measure compared to hydrodynamic cavitation. Some bacterial species generate colonies and spores which agglomerate in clusters protecting them from attack by biocides. In some cases flocs of fine particles can also trap bacterial cells leading to their protection from biocidal action, whilst some bacteria develop resistance towards conventional biocides such as chlorine. Power ultrasound is known to disrupt these bacterial aggregations enhancing biocide efficiency (Kesari *et al.*, 2011; Joyce and Mason, 2009). Figure 2.7 gives a schematic of sonochemical inactivation of bacteria in water.

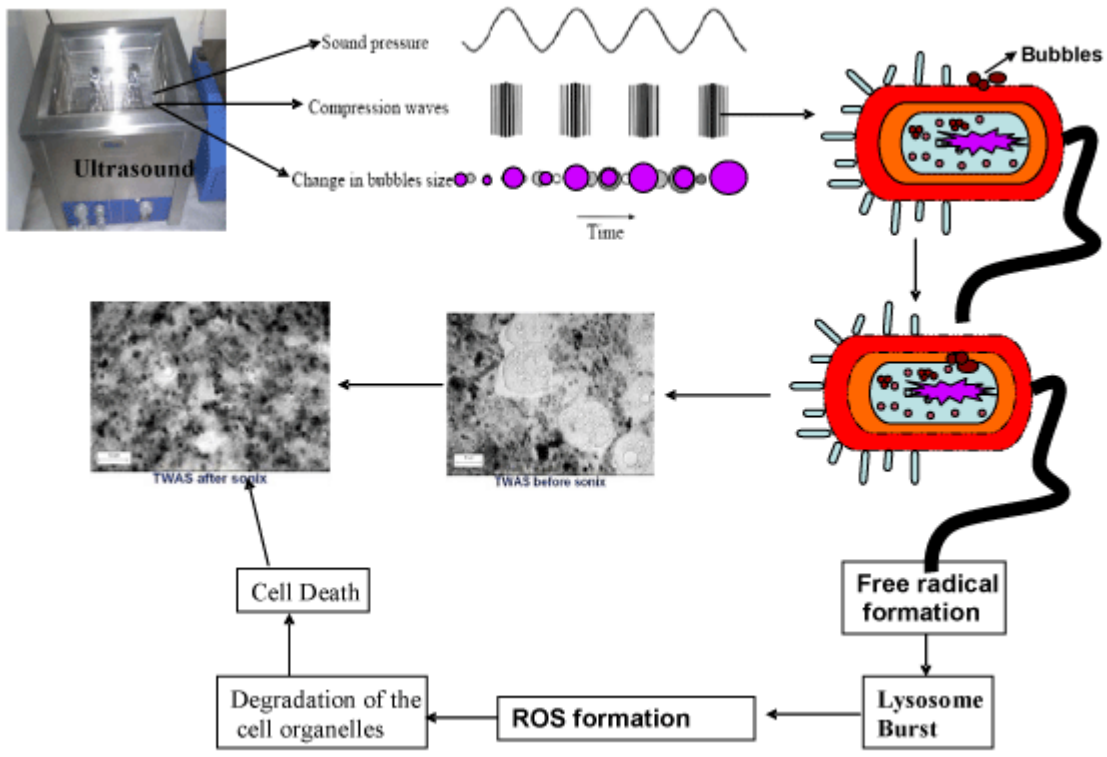

Figure 2.7: Sonochemical inactivation of bacterial cells in water (Kesari *et al.*, 2011)

During ultrasound water disinfection, the imploding bubbles produce high shear forces and liquid jets which may have sufficient energy to physically damage bacterial cell walls. The radicals produced ($HO^{\cdot}$, $H^{\cdot}$) oxidise cell wall components leading to leakage of intracellular components and eventually cell death. Small amounts of hydrogen peroxide are also

produced which contribute to the biocidal action (Agarwal *et al.*, 2011; Gogate and Kabadi, 2009; Joyce and Mason, 2009; Earnshaw *et al.*, 1995).

Several studies have been carried out to evaluate the effectiveness of cavitation on the inactivation of microbial pollutants in water. Kobayashi and co-workers investigated the inactivation of *Escherichia coli* using carbon dioxide micro-bubbles at a low pressure and near room temperature. They achieved a 6 log reduction in *E. coli* population in 60 minutes using CO_2 micro-bubbles at 40 ˚C and a pressure of 2.0 MPa. They also established that N_2-micro-bubbles were not capable of inactivating *E. coli*. An increase in the amount of CO_2 used was observed to increase the *E. coli* population reduction rate (Kobayashi *et al.*, 2009). Mezule and others also investigated the effectiveness of hydrodynamic cavitation on the inactivation of *E. coli*. Their study measured respiratory activity using the 5-cyano-2, 3-ditolyl tetrazolium chloride (CTC) method. Their findings showed that 75 % of the *E. coli* cells had been inactivated within 3 minutes of exposure (Mezule, 2009). Several other studies have been conducted showing high inactivation efficiencies for E. coli using hydrodynamic cavitation (Arrojo *et al.*, 2008; Jyoti and Pandit, 2004, 2003, 2001).

In another study the effectiveness of ozone micro-bubbles was investigated on the inactivation of *Fusarium oxysporum* f. sp. *melonis* and *Pectobacterium carotovorum* subsp. *carotovorum* in hydroponic cultures. Their investigation focused on the comparison of the performance of ozone micro-bubbles (OMB) and ozone milli-bubbles (OMM). OMB gave a higher inactivation rates against *F. oxysporum* f. sp. *melonis* and *P. carotovorum* subsp. *carotovorum* compared to OMM. They concluded that OMB may be used as a disinfecting method for the inactivation of phytopathogens in hydroponic culture solutions (Kobayashi *et al.*, 2011).

2.4.1.4. Advantages of cavitation

- It can effectively inactivate various microbial agents in water
- Cavitation is capable of converting chemical substrates like chlorinated hydrocarbons, aromatic compounds, textile dyes, phenolic compounds and esters into short chain organic acids, carbon dioxide and inorganic ions as final products.

2.4.1.5. Disadvantages of cavitation

- Comparatively higher cost of water treatment
- Ultrasonic treatment of water is highly energy intensive.
- There are problems associated with efficient operation at levels of power dissipation required for treatment.
- Ultrasonication is not economically feasible alone, hence requires coupling with other techniques.
- It is a degradative technique which may produce potentially toxic by-products.

(Agarwal *et al.*, 2011; Takahashi *et al.*, 2009; Li *et al.*, 2009; Jyoti and Pandit, 2004)

2.4.2. Fenton process

The Fenton process is an advanced oxidation technique that employs hydrogen peroxide (H_2O_2) and ferrous sulphate ($FeSO_4$) to generate hydroxyl radicals. The Fenton reagent was discovered by Henry John Horstman Fenton in the 1890s.

2.4.2.1. Mechanism of Fenton process

During the Fenton process Fe^{2+} ions are oxidized by H_2O_2 to Fe^{3+} with the subsequent production of one equivalent of hydroxyl radicals and hydroxide ions. The Fe^{3+} ions are reduced to Fe^{2+} ions by H_2O_2 producing a hydroperoxyl radical and a proton. The process is summarized by the following equations (Jiang *et al.,* 2010; Liu *et al.,* 2007; Guivarch *et al.,* 2003; Chamarro *et al.,* 2001):

$$Fe^{2+} + H_2O_2 \longrightarrow Fe^{3+} + HO^{\cdot} + HO^{-} \quad \text{(2.22)}$$

$$Fe^{3+} + H_2O_2 \longrightarrow Fe^{2+} + HOO^{\cdot} + H^{+} \quad \text{(2.23)}$$

In the photo-Fenton reaction, the Fe^{3+} ions produced or its complexes act as the light absorbing species resulting in the production of hydroxyl radicals and the regeneration of Fe^{2+} ions (Fallmann *et al.,* 1999):

$$Fe^{3+} + H_2O \xrightarrow{h\nu} Fe^{2+} + HO^{\cdot} + H^{+} \quad \text{(2.24)}$$

$$[Fe^{3+}L_n] \xrightarrow{h\nu} [Fe^{2+}L_{n-1}] + L^{\cdot} \quad \text{(2.25)}$$

The above reactions occur simultaneously with pollutant oxidation by the hydroxyl radical in aqueous solution.

2.4.2.2. Disinfection

The Fenton process has been evaluated on the inactivation of microbial pollutants in water by several researchers. Teodoro and co-workers investigated the efficacy of the Fenton process on *Pseudomonas aeruginosa* inactivation in grey-water pre-treated by constructed wetlands. The investigation was carried out at pH 3 and neutral pH, keeping the Fe^{2+} constant and varying hydrogen peroxide concentration between 150 and 25 mgL^{-1}. The most efficient disinfection and clarification of grey-water was observed in the system maintained at pH 3. Nevertheless, the H_2O_2/ UV system with concentration of 150 mgL^{-1} hydrogen peroxide gave results similar to systems adjusted to pH 3. They concluded that the high H_2O_2 concentration was the main factor contributing to the efficient inactivation of *Pseudomonas aeruginosa* and clarification of grey-water (Teodoro *et al.*, 2014).

In another study, the efficacy of solar photo-Fenton at neutral pH was investigated in the inactivation of natural enteric bacteria (*Escherichia coli*) in real municipal wastewater. They carried out control experiments to establish the individual effects of mechanical stress, pH, reactants concentration, and UVA radiation as well as the combined effects of UVA-Fe and UVA-H_2O_2. The synergistic bactericidal effect of solar-UVA with 50 mgL^{-1} of H_2O_2 resulted in complete disinfection of total coliforms within 120 min. The photo-Fenton process accelerated the disinfection process, attaining total inactivation within 60 minutes. Optimization studies indicated that the best conditions were 50 mgL^{-1} of hydrogen peroxide and 20 mgL^{-1} of Fe^{2+} (Ortega-Gómez *et al.*, 2014).

Several other studies have been conducted to investigate the efficacy of the Fenton process: *Salmonella* spp. Inactivation (Ndounla and Pulgarin, 2014), *E. coli* inactivation (Rubio *et al.*,

2013; Rodríguez-Chueca *et al.,* 2012; Spuhler *et al.,* 2010; Diao *et al.,* 2004), and *Phytophthora capsici* inactivation (Polo-Lopez *et al.,* 2013).

2.4.2.3. Organic pollutant removal

The efficacy of the Fenton reagent (Fe^{2+}, H_2O_2) was investigated by many researchers on the degradation of organic pollutants in water. Oxidation of organic pollutants by Fenton reagent may proceed according to the following equations (Zang *et al.,* 2005; Neyens and Baeyens, 2003; Kang and Hwang, 2000):

$$RH + HO^{\cdot} \longrightarrow H_2O + R^{\cdot} \quad \text{..... (2.26)}$$

$$R^{\cdot} + Fe^{3+} \longrightarrow Fe^{2+} + R^{+} \quad \text{..... (2.27)}$$

Lin and others investigated the degradation efficiency of the Fenton reagent on surfactant waters (alkyl-benzene sulphonate (ABS) and linear alkyl-benzene sulphonate (LAS)). These surfactants are commonly used in household and industrial detergents. The focus of the study was on the effects of pH, amounts of ferrous sulphate and hydrogen peroxide, and temperature on the surfactant degradation. Residual H_2O_2 interferes with COD measurements; hence the findings indicated that for every 1 mgL^{-1} residual H_2O_2 an additional 0.26 mgL^{-1} COD is generated. An optimum pH of 3 was maintained to avoid precipitation of Fe^{3+}. They also established that 50 minutes of Fenton treatment with 90 mgL^{-1} $[FeSO4]_O$ was sufficient to achieve more than 95 % ABS and LAS removal (Lin *et al.,* 1999).

Chamarro and co-workers investigated the efficacy of the Fenton reagent on the degradation of formic acid, phenol, 4-chlorophenol, 2,4-dichlorophenol and nitrobenzene in aqueous

solution. They established a stoichiometric coefficient of 0.5 mol of organic compound per mol of hydrogen peroxide in the Fenton reaction. However, for formic acid the coefficient was approximately one owing to the direct formation of CO_2. The treatment was capable of removing the toxic compounds (Chamarro *et al.*, 2001). Several other studies were conducted on the degradation of pesticides (Huston and Pignatello, 1999; Fallman *et al.*, 1999), azo dyes (Guivarch, 2003), phenolic compound (Gernjak *et al.*, 2003), landfill leachate (Zhang *et al.*, 2005), dimethyl phthalate (Liu *et al.*, 2007), and phenol degradation (Jiang *et al.*, 2010).

2.4.2.4. Advantages of the Fenton process

Some of the advantages include:

- The main advantage of the Photo-Fenton process is the light sensitivity up to a wavelength of 600 nm
- The depth of light penetration is high
- The use of a homogenous solution allows high contact between oxidising agent and pollutant

2.4.2.5. Disadvantages of the Fenton process

Some of the disadvantages include:

- Operation requires low pH values (below pH 4) to avoid Fe^{3+} precipitation.
- There is need for iron removal after reaction.
- The high H_2O_2 consumption is major drawback in the photo-Fenton reaction if total degradation is to be achieved.

(Jiang *et al.*, 2010; Liu *et al.*, 2007; Guivarch *et al.*, 2003; Chamarro *et al.*, 2001)

2.4.3. Photo-catalysis

Photo-catalysis is the acceleration of a photoreaction in the presence of a catalyst. There are two types of photo-catalysis: homogeneous photo-catalysis where the reactants and the photo-catalysts exist in the same phase and heterogeneous photo-catalysis where the reactants and the photo-catalysts are in different phases. Transition metal oxides and semiconductors (TiO_2, ZnO, ZrO_2, ZnS, CdS, etc) are the most common heterogeneous photo-catalysts. They are mostly employed in water and wastewater treatment, air treatment, and energy generation (Yousefzadeh *et al.*, 2014; Zhang *et al.*, 2014, Quan *et al.*, 2014, Khan and Berk, 2014, Cao *et al.*, 2014; Zhang *et al.*, 2014, Castro *et al.*, 2009; Mills and Hunte, 1997; Hoffmann *et al.*, 1995; Fox and Dulay, 1993). In a semiconductor, the valence band (HOMO) and the conduction band (LUMO) are separated by a band gap which when exposed to a photon of light of equal or higher energy an electron is promoted to the conduction band leaving a positive hole which is highly oxidizing (Silva and Faria, 2009). The electron-hole pair can recombine or react with donor (D) or acceptor (A) species adsorbed on or close to the surface of the particle (Litter, 1999; Herrmann, 1999). Conduction band electrons can photo-catalytically reduce adsorbed species if their redox potential is more positive than the flatband potential and the valence band positive holes can oxidize adsorbed species if they have redox potentials greater than the flatband of the valence band.

Titanium dioxide (TiO_2) is the most extensively studied semiconductor photo-catalyst. It is the most suitable catalyst for heterogeneous photo-catalysis owing to its various attributes, which include: photo-stability, chemical and biological inertness, photo-activity, relative non-toxicity, adsorption properties, superhydrophilicity, and antimicrobial action (Quan *et al.*, 2014; Konstantinou and Albanis, 2003; Anpo, 2000; Linsebigler *et al.*, 1995). Titanium dioxide crystallizes in two main phases, which are anatase and rutile (Kabra *et al.*, 2004;

Linsebigler *et al.,* 1995). Anatase is stable at low temperatures (T≤550 ˚C) while rutile starts appearing beyond 600 ˚C (Grabowska *et al.,* 2012; Alonso *et al.,* 2009, Reddy *et al.,* 2002; Zhang *et al.,* 2000; Murray *et al.,* 1993). Titanium dioxide has band gap energy of 3.2 eV for the anatase phase and 3.0 eV for the rutile phase (Zhang *et al.,* 2014; Quan *et al.,* 2014; Alonso *et al.,* 2009; Chen *et al.,* 2008; Li *et al.,* 2005).

2.4.3.1. Mechanism of TiO_2 photo-catalysis

Titanium dioxide is a very strong UV light absorber (λ > 385 nm) due its large band gap (Grabowska *et al.,* 2012; Ren *et al.,* 2007). Upon irradiation of TiO_2 with photons of light with energy equal or greater than the band gap, an electron is promoted from the valence band to the conduction band. The heterogeneous photo-catalytic process can be expressed by the following equations:

$$TiO_2 \longrightarrow TiO_2\,(e^-_{cb}, h^+_{vb}) \longrightarrow \text{Recombination} \quad \text{...(2.28)}$$

$$TiO_2\,(h^+_{vb}) + H_2O \longrightarrow TiO_2 + HO^{\cdot}_{ads} + H^+ \quad \text{(2.29)}$$

$$TiO_2\,(h^+_{vb}) + HO^-_{ads} \longrightarrow TiO_2 + HO^{\cdot}_{ads} \quad \text{(2.30)}$$

$$TiO_2\,(h^+_{vb}) + D_{ads} \longrightarrow TiO_2 + D^+_{ads} \quad \text{(2.31)}$$

$$HO^{\cdot} + D_{ads} \longrightarrow D_{ox} \quad \text{(2.32)}$$

$$TiO_2\,(e^-_{cb}) + A_{ads} \longrightarrow TiO_2 + A^-_{ads} \quad \text{(2.33)}$$

(D_{ads}, A_{ads}) species adsorbed on the surface of TiO_2

The oxidation of organic pollutants in water may transpire through hydroxyl radical oxidation or the oxidative power of the positive hole of the valence band. In the presence of adsorbed oxygen, superoxide radicals ($O_2^{\cdot -}$) are generated and these lead to the formation of more hydroxyl radicals in the system (Grabowska *et al.,* 2012; Litter, 1999). The superoxide radical may undergo protonation leading to the formation of the hydroperoxyl radical ($HO_2^{\cdot}$) (Silva and Faria, 2009). Total mineralization of organic pollutants results in the formation of CO_2 and H_2O as end products. Titanium dioxide photo-catalysis may also induce reduction of cationic species in water. Figure 2.8 shows the simplified diagram of the heterogeneous photo-catalytic process.

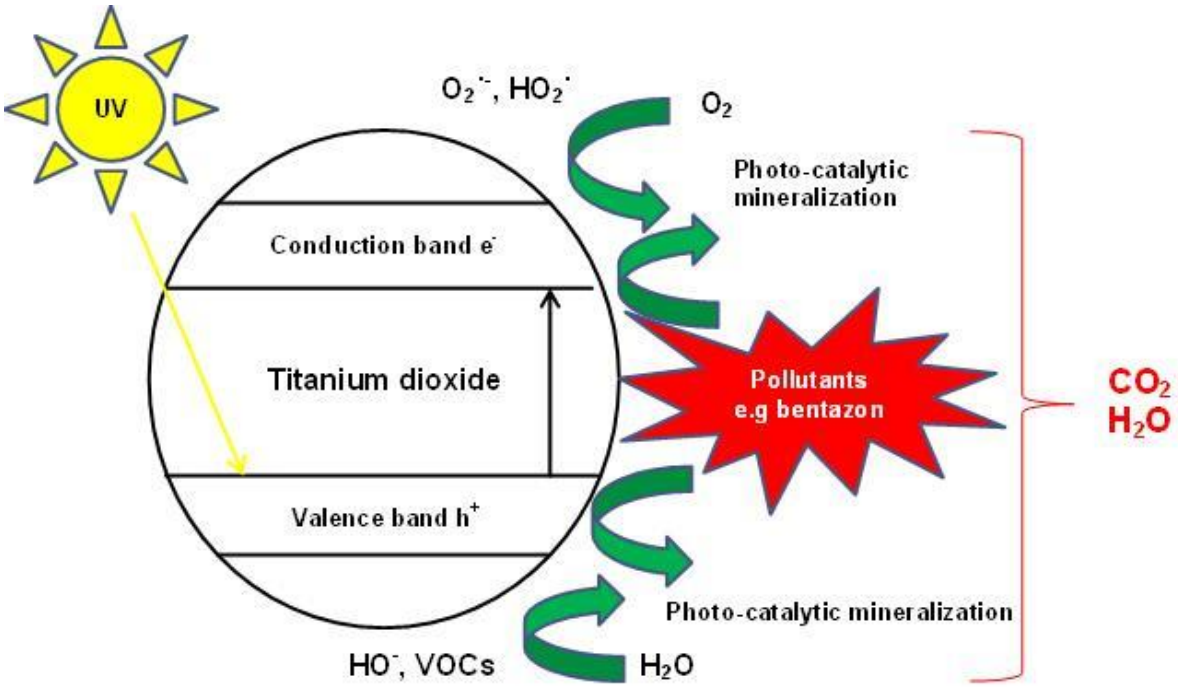

Figure 2.8: Simplified diagram of TiO_2 heterogeneous photo-catalysis showing positive holes (h^+) created in the valence band and electrons (e^-) promoted to the conduction band

2.4.3.2. Preparation of titanium dioxide

There are several techniques that can be employed in the preparation of TiO_2 nano-particles. Some of them include; sol-gel, microwave assisted methods, hydro/ solvo-thermal methods, deposition methods and oxidation methods. The method of choice for this study is sol-gel technique because it is simple and does not require sophisticated equipment.

The sol-gel method involves the evolution of inorganic networks through the formation of a colloidal suspension (**sol**) and gelation of the sol to form a network in a continuous liquid phase (**gel**). The starting material for synthesizing these colloids comprise of a metal or metalloid element surrounded by several reactive ligands. The starting material is processed to form a dispersible oxide and forms a sol in contact with water or dilute acid. Elimination of the liquid part from the sol produces the gel, and the sol/ gel transition regulates the particle size and shape. The oxide is produced through calcination of the gel.

A sol can be described as a stable dispersion of colloidal particles or polymers in a solvent with amorphous or crystalline particles. A gel is composed of a three dimensional continuous network, which encloses a liquid phase. In a colloidal gel, the network is built from aggregation of colloidal particles. In a polymer gel the particles have a polymeric sub-structure made up of agglomerates of sub-colloidal particles. The forces of attraction between sol particles may be van der Waals forces or hydrogen bonds. A gel may also be produced through linking polymer chains. In most gel systems used for materials synthesis, the interactions are of a covalent nature and the gelation process is irreversible. If other interactions are involved, the gelation process may be reversible. The technique behind sol-gel synthesis is to “dissolve” the compound in a liquid in order to bring it back as a solid in a regulated way. The advantage of sol-gel method is the elimination of co-precipitation

problems, which may cause inhomogeneity and enables mixing at an atomic level and results in minute particles, which are easy to sinter.

2.4.3.3. Titanium dioxide modifications

Titanium dioxide can only be activated by UV light, UV light only accounts for about 3-5 % of the solar spectrum. This necessitates the modification of TiO_2 to allow utilization of visible light, which constitutes a much wider spectrum (Ren *et al.,* 2007; Yang *et al.,* 2006). Several researchers have explored different methods to shift the spectral response of TiO_2 towards the visible region to improve its photo-catalytic efficiency. Titanium dioxide photo-catalyst has been doped with some transition metals (Anpo and Takeuchi, 2003; Klosek and Raftery, 2001; Wang *et al.,* 2000; Yamashita *et al.,* 1999; Choi *et al.,* 1994; Ghosh and Maruska, 1977), non-metals (Mungondori and Tichagwa, 2013; Nyamukamba *et al.,* 2012; Ren *et al.,* 2007; Yang *et al.,* 2006; Asahi *et al.,* 2001), and ionic species to allow utilization of visible or solar light, and reduce recombination of electron-hole pairs (Ahmed *et al.,* 2010). Other researchers have explored plasmonic photo-sensitization through successive ionic layer adsorption and reaction (SILAR) technique preceded by photo-reduction (Wang *et al.,* 2014). Ionic species incorporated into the TiO_2 lattice structure can act as charge traps hence reducing electron-hole recombination which improves photo-catalytic efficiency. The influence of doping on photo-catalytic activity is determined by several factors which include; amount and type of dopant, synthesis technique, physic-chemical properties of the catalyst, and the structure and concentration of pollutant (Ahmed *et al.,* 2010).

2.4.3.4. Transition metal ion doping

Several researchers have investigated the use of transition metal dopants to sensitize TiO_2 towards visible light utilization. Doping with transition metal ions was observed to increase

formation of Ti^{3+} states which cause more oxygen defects hence allowing adsorption of oxygen on the surface of TiO_2 which results in increased rate of photo-catalysis (Kumar and Devi, 2011). Choi and co-workers investigated the photo-reactivities of 21 metal ion doped colloids. They established that doping TiO_2 with between 0.1-0.5 % metal ion (Fe^{3+}, Ru^{3+}, Mo^{5+}, Re^{5+}, V^{4+}, Os^{3+}, and Rh^{3+}) significantly increased its photo-activity for both oxidation and reduction while Co^{3+} (partially filled electronic configuration) and Al^{3+} lowered the photo-activity (Choi *et al.,* 1994). When Fe^{3+} traps electron and hole pairs, its oxidation state changes to 2+ and 4+, which are relatively unstable leading to the release of the electron and hole to adsorbed surface oxygen and hydroxyl ions respectively. This prevents electron-hole pair recombination hence increasing the rate of photo-activity of TiO_2 (Kumar and Devi, 2011). Nevertheless, the photo-catalytic activity of transition metal ion doped TiO_2 is low due to the fact that transition metals may act as recombination centres for charge carriers (Quan *et al.,* 2014; Choi *et al.,* 1994) and they were observed to cause thermal instability of anatase TiO_2 (Ren *et al.,* 2007; Kang, 2005).

2.4.3.5. Non-metal doping

Non-metal doping has been explored by several researchers and is a promising modification that allows TiO_2 to maintain thermal stability. Yang and others prepared nitrogen doped TiO_2 thin films using ion-assisted electron-beam evaporation. The TiO_xN_y thin films had a red shifted absorption band edge (500 nm) and exhibited visible light induced photo-catalytic properties. The thin films were capable of photo-degrading methylene blue under visible light irradiation and the best N substitutional loading in the thin films was 5.6 weight % (Yang *et al.,* 2006). Investigations conducted by Batzill and co-workers indicated that no band gap narrowing occurs in nitrogen doped TiO_2. However, nitrogen doping induces localized N 2p states within the band gap just above the valence band, and these facilitate the formation of

oxygen vacancies at elevated temperatures. Dopant-induced energy levels within the band gap may increase the yield for electron-hole pair formation under visible light irradiation (Batzill *et al.,* 2006). Ren and co-workers also prepared carbon doped TiO_2 via low temperature hydrothermal synthesis. They observed that the carbon doped TiO_2 was able to absorb visible light in the range 400-450 nm, and possessed very high photo-activity towards the degradation of rhodamine B compared to undoped TiO_2 as well as commercial Degussa P25 TiO_2 (Ren *et al.,* 2007). Nevertheless, nitrogen doping is the most promising dopant although it requires co-doping to further enhance the photo-catalytic performance of TiO_2 (Nasir *et al.,* 2014; Quan *et al.,* 2014; Songkhum and Tantirungrotechai, 2013; Cong *et al.,* 2011; Fujishima *et al.,* 2008; Emeline *et al.,* 2007).

2.4.3.6. Other TiO_2 modifications

Titanium dioxide may also be modified through several other ways. It was reported in literature that TiO_2 can be combined with other semiconductors to achieve better charge separation in a light energy conversion system. Charge can be transferred from one semiconductor to another with suitable band edge positions that are thermodynamically favourable increasing the lifespan of charge carriers hence enhancing photo-catalytic activity (Kumar and Devi, 2011; Serpone *et al.,* 1995). When a wide band gap energy semiconductor like tin dioxide (SnO_2) is coupled to TiO_2, an improvement in the photo-catalytic activity is observed (Zhou *et al.,* 2008; Hattori *et al.,* 2000).

Noble metals can also be deposited on the surface of TiO_2 to extend the lifespan of the electron-hole pairs and also to extend the absorption band edge into the visible light region. It was reported in literature that semiconductor-metal composites act as passive sinks for electrons reducing recombination rate (Xiang *et al.,* 2010; Yu *et al.,* 2009; Kamat, 2007).

Photo-generated electrons are distributed between the semiconductor and metal nanoparticles when they are in contact until equilibrium is attained. The photo-catalytic performance of the semiconductor-metal heterojunction is to a larger extent influenced by the size and shape of metal nano-particles (Subramanian *et al.,* 2004). Anpo and Takeuchi reported that addition of small amounts of noble metal like platinum (Pt) and rhodium (Rh) greatly enhanced the photo-catalytic activity of TiO_2 (Anpo and Takeuchi, 2003). Li and Li also studied the performance of Au/ Au^{3+}-TiO_2. UV-Vis diffuse reflectance spectra (DRS) and optical absorption spectra indicated that a new energy level had been created below 3.2 eV in the Au/ Au^{3+}-TiO_2 which allowed optical absorption in the visible region and enabled excitation by visible light (E < 3.2 eV) (Li and Li, 2001).

2.4.3.7. Disinfection

The research into titanium dioxide disinfection potential was sparked by Matsunaga and co-workers in 1985 when they reported that UV-light irradiated TiO_2-Pt thin films were able to inactivate bacterial cultures in water within 60-120 minutes of exposure (Matsunaga *et al.,* 1985). Ever since their report on TiO_2 water disinfection, several studies have been conducted to establish the disinfection potential of this photo-catalyst on various microorganisms. Earlier research findings could show that TiO_2 really possessed antimicrobial activity against bacteria (Huang *et al.,* 2000; Maness *et al.,* 1999; Jacoby *et al.,* 1998; Horie *et al.,* 1996; Matsunaga and Okochi, 1995), viruses (Hajkova *et al.,* 2007; Zan *et al.,* 2007; Lee *et al.,* 1997; Watts *et al.,* 1995), and tumour cells (Sakai *et al.,* 1994; Cai *et al.,* 1992), but, the bactericidal function was never understood well. Several studies on water treatment employed fine TiO_2 powder suspended in the water to be treated and illuminated with a strong light, such as a mercury lamp. These systems, nonetheless, had two major problems; the recovery of TiO_2 powder and the high cost of providing light from a lamp. In

this study the focus is on the use of N-TiO_2 photo-catalytic asymmetric polymeric membranes.

2.4.3.8. TiO_2 mode of microbial inactivation

Illumination of TiO_2 with the right wavelength of light triggers a series of reactions that result in the production of the hydroxyl radical which has been suggested to be the most toxic for microorganisms owing to its capability to degrade substrates like proteins, lipids, carbohydrates, nucleic acids, and many others. It was reported in literature that the $HO^{\cdot}$ radical promotes peroxidation of polyunsaturated phospholipid components of the lipid membrane causing disorder in the cell membrane (Li *et al.,* 2008; Srinivasan *et al.,* 2003; Maness *et al.,* 1999). Matsunaga and others made the first attempt to elucidate the mechanism of TiO_2 photo-cytotoxicity. They demonstrated that oxidation of coenzyme A (CoA) may be a possible mechanism of photo-induced microbial cell inactivation. By then, the reactivity of ROS was thought to be non-selective. A possible role of ROS was oxidation of the cell membrane prior to the oxidation of CoA (Matsunaga *et al.,* 1985; Dadjour *et al.,* 2005). The small TiO_2 particles may also enter the already damaged cell membranes and cause further damage (McCullagh *et al.,* 2007). A study by Gelover and co-workers indicated that faecal coliforms treated TiO_2 photo-catalysis could not self-repair (Gelover *et al.,* 2006). However, Adams and co-workers observed that bacterial death also occurred in the dark indicating that other unknown mechanisms may be involved (Adams *et al.,* 2006). Several researchers have demonstrated that doping TiO_2 with silver significantly improves photo-catalytic inactivation of bacteria (Page *et al.,* 2007; Reddy *et al.,* 2007) and viruses (Kim *et al.,* 2006). The general trend in the mechanism of microbial cell death observed by many researchers was initial cell membrane damage followed by destruction of intracellular components (Fig. 2.9).

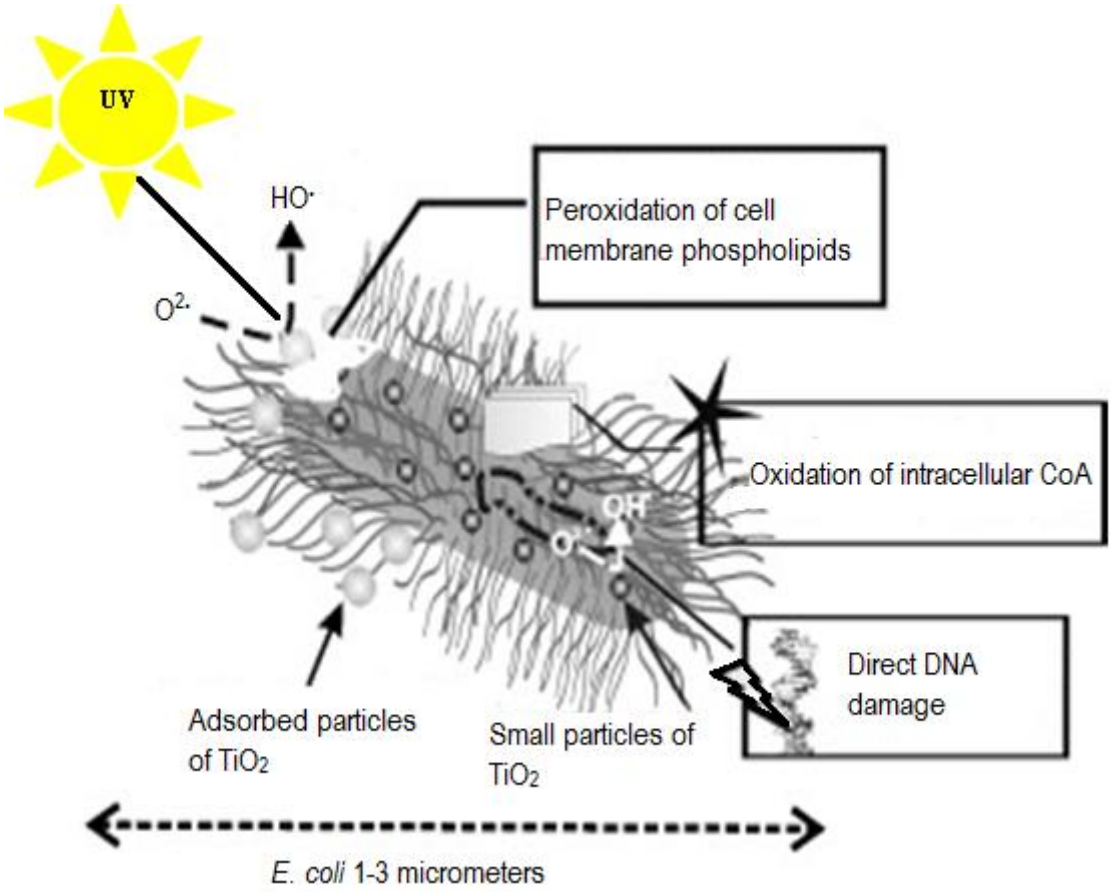

Figure 2.9: Schematic diagram of TiO_2 mechanisms of microbial cell inactivation (Matsunaga *et al.*, 1985)

The retention of nano-TiO_2 is critical not only because of the cost associated with loss of the photo-catalyst, but also, and more importantly, owing to its potential impacts on human health and ecosystems. In light of this problem, several researchers have focused on studying the efficacy of immobilized TiO_2 on the inactivation of microbial pollutants in water. Baram and co-workers investigated efficacy of immobilized TiO_2 nanotube electrodes on the inactivation of *E. coli* through photo-electrocatalysis. Their use of the high surface area TiO_2 nanotubes enabled them to attain high photocurrent and an extremely fast *E. coli* inactivation rate ($\sim 10^6$ CFU/ ml bacteria within 10 min) (Baram *et al.,* 2009). In another study, they also investigated nano-tubular TiO_2 layer with high surface area on the photo-catalytic inactivation of *Escherichia coli* bacteria and other microorganisms. They achieved *E. coli*

inactivation under direct sunlight and also over several cycles (Baram *et al.*, 2011). Hayden and co-workers also reported cadmium sulphide coated TiO_2 nanotubes with increased visible light activity. They achieved total inactivation of *E. coli* in a short time using a small applied potential (Hayden *et al.*, 2010).

2.4.3.9. Organic pollutant removal

The presence of organic pollutants in water and wastewater is of great concern since most of them have been known to cause adverse health effects especially to humans. TiO_2 photo-catalytic oxidation has been perceived as the most successful advanced oxidation process for the elimination of toxic water pollutants. Although slurry type TiO_2 provides the largest surface area for photo-catalytic reactions, there are problems associated with post-recovery of the fine particles which may result in secondary pollution (Pozzo *et al.*, 1997). Hence most researchers are currently focused on utilizing immobilized TiO_2 for removal of organic pollutants and other harmful products.

The oxidation of cimetidine was investigated under continuous flow using UV light illuminated TiO_2 nano-fibres immobilized on a stainless steel filter (SSF). They employed PVDF as the coupling agent and carried out an oxidation experiment while varying the thickness of the TiO_2-PVDF layer. They achieved 40-90 % oxidation of cimetidine at a flow rate of 10 L/ m^2h with a thickness of 10 μm for the TiO_2 nano-fibres. No further increase in oxidation rate of cimetidine was observed when thickness of the TiO_2 nano-fibre layer was increased to 29 μm (Ramasundaram *et al.*, 2013). In another study, TiO_2-modified zeolites with adsorption and photo-catalytic properties were used in the removal of some antibiotics (marbofloxacin (MAR), and enrofloxacin (ENR)) from water. The derivatization with TiO_2 improved the adsorption capacity of the zeolite and allowed solar induced degradation of the

fluoroquinolones. They achieved complete removal of fluoroquinolones from the outlet of a wastewater treatment plant after spiking with MAR and ENR at the micrograms per litre levels, with the best performing modified zeolite (Maraschi *et al.,* 2014).

Glass immobilized TiO_2/ CNT composites were investigated on the removal of methylene blue from water. A 62 % removal efficiency was achieved for methylene blue with sol gel prepared TiO_2/ CNT composites as opposed to 46 % removal efficiency using bare TiO_2 (Sampaio *et al.,* 2013). Shinde and co-workers investigated the efficacy of conductive glass immobilized N-TiO_2 photo-catalyst on the degradation of salicylic acid, 4-chlorophenol, benzoic acid and oxalic acid. Their photo-catalytic system under solar light irradiation proved to be another suitable approach for the oxidative removal of non-biodegradable organic pollutants in water (Shinde *et al.,* 2014). Mendret and co-workers studied the degradation of acid orange under UV light irradiation using TiO_2/ Al_2O_3 composite membranes. The rate of photo-degradation was quite low under continuous flow, however, photo-degradation helped to enhance composite membrane flux and to prevent membrane fouling (Mendret *et al.,* 2013). Several other studies have been conducted on the organic pollutant efficacy of immobilized titanium dioxide photo-catalyst (Saggioro *et al.,* 2015; Vaiano *et al.,* 2015; Rathinavelu and Palanivelu, 2014; Sampaio *et al.,* 2013; Yun *et al.,* 2013; Naeem and Ouyang, 2013; Avisara *et al.,* 2013). Photo-catalytic membranes (PMs) have shown great potential for use in energy-efficient water purification and wastewater treatment owing to their ability to combine the physical separation of membrane filtration, organic pollutant degradation and anti-microbial property achieved by photo-catalysis in one unit (Leong *et al.,* 2014).

2.4.3.10. Support material for TiO_2

Although titanium dioxide at nano-level has many advantages, it is very difficult to isolate from treated water, which hinders its practical application. Several support material have been explored as matrix for TiO_2 photo-catalyst and these include glass (Mungondori and Tichagwa, 2013; Daneshvar *et al.,* 2005; Hofstadler *et al.,* 1994), polymer films (Dhananjeyan *et al.,* 2001; Uchida *et al.,* 1995), sand (Haarstrick *et al.,* 1996; Matthews, 1991), activated carbon (Ao and Lee, 2003) and clay (Meng *et al.,* 2008). Many attempts were made to recover TiO_2 nano-particles from its suspension by membrane filtration; however, a lot of problems are encountered in the process (Thiruvenkatachari *et al.,* 2005). In this study, the use of novel N-TiO_2-PMAA-g-PVDF/ PAN asymmetric polymeric photo-catalytic membranes is proposed. They will combine ultrafiltration, photo-catalytic and antimicrobial properties.

2.4.3.11. Membranes

A membrane is a layer of material which serves as a selective barrier between two phases and remains impermeable to specific particles, molecules, or substances when exposed to the action of a driving force. Some components are allowed passage by the membrane into a permeate stream, whereas others are retained by it and accumulate in the retentate stream. Figure 2.10 shows a schematic diagram of a cross-flow membrane.

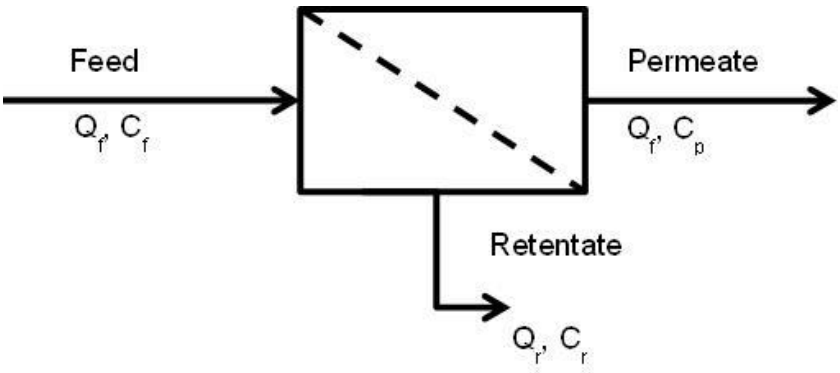

Figure 2.10: Schematic diagram of a cross-flow membrane (Where Q_f, Q_p, and Q_r are the feed, permeate and retentate flux and C_f, C_p, and C_r are the concentrations of pollutant in the feed, permeate and retentate respectively)

Membranes can be of various thicknesses, with homogeneous or heterogeneous structure. According to IUPAC, there are three different types of pore size classifications: micro-porous ($dp < 2$ nm), meso-porous (2 nm $< dp < 50$ nm), and macro-porous ($dp > 50$ nm). Membranes can be neutral or charged, and particles transport can be active or passive. The latter can be facilitated by pressure, concentration, chemical or electrical gradients of the membrane process (Scott and Hughes, 1996). Membranes can be generally classified into synthetic membranes and biological membranes.

Synthetic membranes are fabricated in two main geometries: Flat sheet, utilized the in construction of flat sheet, and frame modules etc., and cylindrical, utilized in tubular and capillary modules. Although the most practically useful membranes are asymmetric, some membranes are symmetric. Symmetric membranes are of a uniform structure, and are of three general types: with approximate cylindrical pores, porous, and non-porous (homogeneous). Symmetric membranes are prepared via track etching or precipitation from the vapour phase (Khulbe *et al.,* 2008; Strathmann, 1986).

Asymmetric membranes are characterized by a non-uniform structure, comprising an active top layer or skin supported by a porous sub-layer. An integrally skinned asymmetric membrane has the same material for the top dense layer and the porous sub-layer, while a composite one has different material. Asymmetric membranes are prepared via dry-wet phase inversion technique (Loeb-Sourirajan method), or thermally induced phase separation method (Khulbe *et al.,* 2008; Kesting, 1990).

In this study asymmetric photo-catalytic membranes were prepared through the dry-wet phase inversion technique. The polymer material of choice is dissolved in a suitable solvent, and homogenized through continuous stirring. The polymer solution is then cast on a flat sheet of glass and partial evaporation of solvent allowed. The sheet of glass with cast polymer solution is then placed in a coagulation bath that carries the non-solvent. The solvent used is compatible with the non-solvent but is not able to dissolve the polymer. The movement of solvent from polymer solution into the non-solvent allows the solidification of the membrane. To produce photo-catalytic membranes, TiO_2 powders are blended with the polymer solution and then placed in the coagulation bath.

To be effective for separation, membrane materials should ideally possess the following properties:

- Chemical resistance (to both feed and cleaning fluids),
- Mechanical stability,
- High permeability,
- High selectivity,
- Stable operation

Khulbe *et al.,* 2008; Scott and Hughes, 1996; Kesting, 1990; Strathmann, 1986)

2.4.3.12. Poly (vinylidene difluoride) PVDF

PVDF is a highly non-reactive & pure thermoplastic fluoropolymer (Fig. 2.11). It has a low melting point (177 ˚C) and a density of 1.78 gcm^{-3}. PVDF is the material of choice when the porous structure will be exposed to ozone or chlorine (Sencadas *et al.,* 2004; Nalwa, 1991).

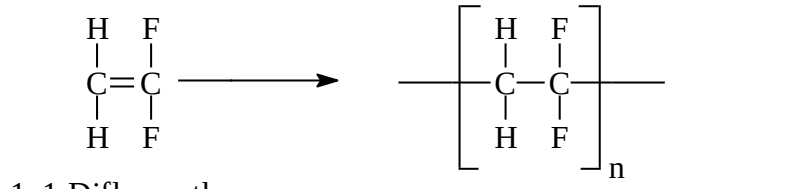

1, 1-Difluoroethene — Poly (vinylidene difluoride)

Figure 2.11: Polymerization of 1, 1-Difluoromethane

Poly (vinylidene difluoride) has the following attributes:

- Resistance to most chemicals and solvents (e.g. acids and alkalis),
- Unaffected by long-term exposure to UV radiation,
- Withstands exposure to harsh thermal and chemical conditions,
- Low permeability to most gases and liquids,
- Low weight,
- Mechanical strength and toughness,
- High abrasion resistance.

(Sencadas *et al.,* 2004; Hester *et al.,* 2002; Kong and Lee, 1999; Nalwa, 1991)

PVDF membranes have been used in water filtration by many researchers. Kong and Lee reported a hydrophobic flat sheet PVDF membrane prepared by immersion precipitation technique. The micro-porous hydrophobic membrane allowed the permeation of an oil phase at almost zero pressure and retained the water. It was reported that oil removal can be as high

as 77 % under normal experimental conditions (Kong and Lee, 1999). Wang and others fabricated PVDF hydrophobic asymmetric hollow fibre membranes with narrow pore size and ultra-thin skin. The PVDF hollow fibres produced a water permeation flux of 41.5 Kg/ m^2/ h during direct contact membrane distillation with a 99.99 % sodium chloride salt rejection (Wang *et al.,* 2008). PVDF is hydrophobic; hence modification is necessary to allow high water flux during filtration. Hester and co-workers reported pH responsive self-organizing blends of poly (vinylidene difluoride) (PVDF) and an amphiphilic comb polymer with a PVDF backbone and poly (methacrylic acid) (PMAA) side chains. Their findings indicated that membranes containing PVDF-g-PMAA exhibited rapid and reversible pH-dependent flux variations of over an order of magnitude as the feed solution pH was varied between 2 and 8 (Hester *et al.,* 2002).

Recently researchers have also focused on the preparation of PVDF membranes with inorganic fillers to improve on hydrophilicity of the membranes to achieve high water flux. Cruz and co-workers prepared PVDF/ TiO_2 membranes by grafting acrylic acid onto PVDF then coated the surface with TiO_2 sols. A 98.77 % reactive black 5 (RB5) dye colour removal was achieved in 5 hours with PDVF/ poly (acrylic acid (PAA)/ TiO_2 at pH 1.25. The study also showed that the modified membranes have lower total filtration resistance compared to unmodified PVDF membranes (Cruz *et al.,* 2014). Safarpour and co-workers prepared PVDF membranes loaded with 0.05 weight % inorganic filler (graphene oxide/ TiO_2). Their findings indicated that the blended membranes with 0.05 weight % rGO/ TiO_2 nano-composite with GO to TiO_2 ratio of 70/ 30 had improved permeability and antifouling performance (Safapour *et al.,* 2014). In this current study N-TiO_2-PMAA-g-PVDF/ PAN photo-catalytic membranes were prepared and evaluated for their photo-catalytic, antimicrobial and antifouling properties.

2.4.3.13. Poly (acrylonitrile) PAN

PAN is a synthetic, semi-crystalline organic polymer prepared by the polymerization of acrylonitrile (Fig. 2.12). It has none of the hazardous properties of its monomer. Owing to the formation of strong chemical bonds between the nitrile groups, the polymer molecules resist most organic solvents and do not melt without decomposing. PAN only melts above 300 ˚C.

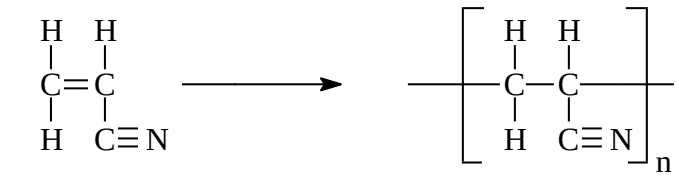

Acrylonitrile Poly (acrylonitrile)

Figure 2.12: Polymerization of acrylonitrile

Poly (acrylonitrile has the following attributes:

- Resistant to most chemicals and solvents (e.g. acids and alkalis),
- Low permeability to gases,
- Slow to burn/ thermal stability,
- Mechanical strength and toughness,
- Unaffected by long-term exposure to UV radiation.

PAN only membranes have not found extensive use in water filtration experiments. Scharnagl and Buschatz reported on ultrafiltration and microfiltration fabricated through phase inversion technique. They showed that morphology of membrane was dependent on concentration of polymer solution and temperature of coagulation bath. The findings of their study revealed that flux of the membranes could be adjusted between 100 and 2000 L/ m^2h with high rejection (Scharnagl and Buschatz, 2001). Most applications of PAN membranes

are in conjunction with other polymers to enhance performance. Ulbricht and Belfort studied poly (acrylonitrile) (PAN) and poly (sulfone) (PSf) ultrafiltration (UF) membranes modified by low temperature plasma. Hydrophilic PAN membranes modified by plasma treatment showed high fouling resistance during static protein adsorption studies, and improved protein UF performance (fluxes up to 150 %) (Ulbricht and Belfort, 1996). Low and co-workers reported M-phenylenediamine (MPD) and trimesoyl chloride (TMC) nano-filtration membranes coated on both sides with poly (acrylonitrile) (PAN) for the purpose of water softening. Experiments carried out revealed that thick monomer solutions and denser PAN structure lead to membranes with better solutes rejection (Low *et al.,* 2008). Currently researchers are working on improving the mechanical strength of PAN nano-fibre membranes. Chemical modification of PAN with poly (dopamine) (PDA), to strengthen the fibres and improve on hydrophilicity, has been reported (Huang *et al.,* 2014).

Bibliography

Adewuyi Y.G. *Environmental Science and Technology*: 39 (10) **(2005)** 3409-3420.

Agarwal A., Ng W.J., and Liu Y. *Chemosphere*: 84 **(2011)** 1175-1180.

Ahmed S., Rasul M.G., Martens W.N., Brown R., and Hashib M.A. *Desalination*: 261 **(2010)** 3-18.

Allende A., Tomás-Barberán F.A., and Gil M.I. *Trends in Food Science & Technology*: 17 (9) **(2006)** 513-519.

Alonso E., Montequi I., and Cocero M.J. *Journal of Supercritical Fluids*: 49 **(2009)** 233-238.

Anderson group. HOx Production: Ozonolysis of Alkenes. http://ent.arp.harvard.edu/kinetics/sciobj/freerad/hoxprod.html. Accessed (28-04-2014).

Andreozzi R., Caprio V., Insola A., and Marotta R. *Catalysis Today*: 53 (1999) 51-59.

Anpo M. *Pure and Applied Chemistry*: 72 **(2000)** 1265-1270.

Anpo M., and Takeuchi M. *Journal of Catalysis*: 216 **(2003)** 505-516.

Ao C.H., and Lee S.C. *Applied Catalysis B*: *Environmental*: 44 **(2003)** 191-205.

Asahi R., Morikawa T., Ohwaki T., Aoki K., and Taga Y. *Science*: 293 **(2001)** 269.

Avisara D., Horovitza I., Lozzi L., Ruggieri F., Baker M., Abel M.-L., and Maman H. *Journal of Hazardous Materials*: 244-245 **(2013)** 463-471.

Baram N., Starosvetsky D., Starosvetsky J., Epshtein M., Armon R., Ein-Eli Y. *Electrochimica Acta*: 54 **(2009)** 3381-3386.

Baram N., Starosvetsky D., Starosvetsky J., Epshtein M., Armon R., and Ein-Eli Y. *Applied Catalysis B*: *Environmental*: 101 (3-4) **(2011)** 212-219.

Barlow P. *An Introduction to Ozone Generation*: **(1994)** 1-5.

Batzill M., Morales E.H., and Diebold U. *Physical Review Letters*: 96 **(2006)** 1-4.

Ben W., Qiang Z., Pan X., and Nie Y. *Journal of Environmental Engineering*: 138 **(2012)** 272-277.

Blanc D. *Journal of Hospital Infections*: 60 (1) **(2005)** 69-72.

Budd G.C., Logdson G.S. and Long B.W. "Overview of Chlorine Dioxide, Ozone and Ultraviolet Irradiation.'' Cotruvo J.A., Craun G.F. and Hearne N., eds. Providing

Safe Drinking Water in Small Systems: Technology, Operations, and Economics. Boca Raton: CRC Press LLC, **(1999)**.

Cai R., Kubota Y., Shuin T., Sakai H., Hashimoto K., and Fujishima A. *Cancer Research*: 52 **(1992)** 2346-2348.

Cao L., Wang R., Wang D., Xu L., and Li X. *Chemical Physics Letters*: **(2014)** 1-19.

Castro A.L., Nunes M.R., Carvalho M.D., Ferreira L.P., Jumas J.-C., Costa F.M., and Florencio M.H. *Journal of Solid State Chemistry*:182 **(2009)** 1838-1845.

Chakinala A.G., Gogate P.R., Burgess A.E., and Bremner D.H. *Chemical Engineering Journal*: 152 **(2009)** 498-502.

Chakma S., and Moholkar V.S. *American Institute of Chemical Engineers*: **(2013)** 1-11.

Chamarro E., Marco A., and Esplugas S. *Water Research*: 35 (4) **(2001)** 1047-1051.

Chand R., Bremner D.H., Namkung K.C., Collier P.J., and Gogate P.R. *Biochemical Engineering Journal*: 35 (3) **(2007)** 357-364.

Chelme-Ayala P., Gamal El-Din M., Smith D.W. and Adams C.D. *Water Research*: 45 **(2011)** 2517-2526.

Chelme-Ayala P., El-Din M.G., Smith D.W, Adams C.D. *Water Research*: 45 **(2011)** 2517-2526.

Chemat F., Teunissen P.G.M., Chemat S., and Bartels P.V. *Ultrasonics Sonochemistry*: 8 **(2001)** 247-250.

Chen X., Wang X., Hou Y., Huang J., Wu L., and Fu X. *Journal of Catalysis*: 255 **(2008)** 59-67.

Choi W.Y., Termin A., and Hoffmann M.R. *Journal of Physical Chemistry*: 98 **(1994)** 13669-13679.

Crum L.A. *Ultrasonics Sonochemistry*: 2 (**1995)** S147-S152.

Cong Y., Tian B., and Zhang J. *Applied Catalysis B*: *Environmental*: 101 **(2011)** 376-381.

Daneshvar N., Salari D., Niaei A., Rasoulifard M.H., and Khataee A.R. *Journal of Environmental Science and Health Part A*: 40 **(2005)** 1605-1617.

Dalmazio I., Almeida M.O., Augusti R., and Alves T.M.A. *Journal of the American Society for Mass Spectrometry*: 18 **(2007)** 679-687.

Destaillats H., Lesko T.M., Knowlton M., Wallace H., and Hoffmann M.R. *Industrial and Engineering Chemistry Research*: 40 **(2001)** 3855-3860.

Dhananjeyan M.R., Mielczarski E., Thampi K.R., Buffat P., Bensimon M., Kulik A., Mielczarski J., Kiwi J. *Journal of Physical Chemistry B*: 105 **(2001)** 12046-12055.

Diao H.F., Li X.Y., Guc J.D., Shi H.C., and Xie Z.M. *Process Biochemistry*: 39 **(2004)** 1421-1426.

Dimitriou M.A. Design guidance manual for ozone systems-IOA Pan American Committee: **(1990)** 2-5.

Ding N., Neumann N.F., Price L.M., Braithwaite S.L., Balachandran A., Mitchell G., Belosevic M., and Gamal El-Dina M. *Applied Environmental Microbiology*: 79 **(2013)** 2721-370.

Dow S.M., Barbeau B., von Gunten U., Chandrakanth M., Amy G. and Hernandez M. *Water Research*: 40 **(2006)** 373-382.

Duguet J.P., Brodard E., Dussert B. and Mallevialle J. *Ozone Science and Engineering*: 7, **(1985)** 241-253.

Dumètre A., Le Bras C., Baffet M., Meneceur P., Dubey J.P., Derouin F., and Duguet J.-P. *Veterinary Parasitology*: 153 **(2008)** 209-213.

Earnshaw R.G., Appleyard J., and Hurst R.M. *International Journal of Food Microbiology*: 28 (2) **(1995)** 197-219.

Edwards M. and Benjamin M.M. *Journal of American Water Works Association*: 83 (6) **(1991)** 96-105.

Emeline A.V., Kuznetsov V.N., Rybchuk V.K., and Serpone N. *International Journal of Photoenergy*: 2008 **(2007)** 1-19.

Esplugas S., Giménez J., Contreras S., Pascual E., and Rodríguez M. *Water Research*: 36, (4) **(2002)** 1034-1042.

Fallmann H., Krutzler T., Bauer R., Malato S., and Blanco J. *Catalysis Today*: 54 **(1999)** 309-319.

Farooq S. 1976. *Kinetics of Inactivation of Yeasts and Acid-Fast Organisms with Ozone.* Ph.D. Thesis, University of Illinois at Urbana-Champaign, IL, **(1976)**.

Farooq S., Engelbrecht R.S., and. Chian E.S.K. *Water Research*: 11 (8) **(1977)** 737-741.

Fox M.A., and Dulay M.T. *Chemical Reviews*: 93 **(1993)** 341-357.

Fujishima A., Zhang X., and Tryk D.A. *Surface Science Reports*: 63 **(2008)** 515-582.

Gelover S., Gomez L.A., Reyes K., and Leal M.T. *Water Research*: 40 **(2006)** 3274-3280.

Gernjak W., Krutzler T., Glaser A., Malato S., Caceres J., Bauer R., and Fernández-Alba A.R. *Chemosphere*: 50 **(2003)** 71-78.

Ghosh A.K., and Maruska H.P. *Journal of the Electrochemical Society*: 124 **(1977)** 1516-1522.

Glaze W.H. *Environmental Science and Technology*: 21(3) **(1987)** 224-230.

Glaze W.H., Beltran F., Tuhkanen T., Kang J.-W. *Water Pollution Research Journal of Canada*: 27 (1) **(1992)** 23-42.

Glaze W.H., Kang J.W., and Chapin D.H. *Ozone: Science and Engineering*: 9 **(1987)** 335.

Gogate P.R. *Advances in Environmental Research*: 6 **(2002)** 335-358.

Gogate P.R., and Kabadi A.M. *Biochemical Engineering Journal*: 44 **(2009)** 60-72.

Goi A. *Thesis on Chemistry and Chemical Engineering*: **(2005)** 15.

Gomez-Pacheco C.V., Sanchez-Polo M., Rivera-Utrilla J., and Lopez-Penalver J. *Journal of Chemical Engineering*: 178 **(2011)** 115-121.

González-García J., Sáez V., Tudela I., Díez-Garcia M.I., Esclapez M.D., and Louisnard O. *Water*: 2 **(2010)** 28-74.

Gottschalk C., Libra J. A. and Saupe A. Ozonation of Water and Waste Water: A Practical Guide to Understanding Ozone and its Applications, 2nd Edition. Germany: John Wiley & Sons, **(2010)**.

Grabowska E., Reszczynska J., and Zaleska A. *Water Research*: 46 **(2012)** 5453-5471.

Grote B. *37th Annual Qld Water Industry Operations Workshop Parklands, Gold Coast*: **(2012)** 17-23.

Guivarch E., Trevin S., Lahitte C., and Oturan M.A. *Environmental Chemistry Letters*: 1 **(2003)** 38-44.

Haarstrick A., Kut O.M., and Heinzle E. *Environmental Science and Technology*: 30 **(1996)** 817-824.

Hajkova P., Spatenka P., Horsky J., Horska I., and Kolouch A. *Plasma Processes and Polymers*: 4 **(2007)** 397-401.

Harakeh M.S. and Butler M. *Ozone Science and Engineering*: 6 **(1984)** 235-243.

Hattori A., Yokihisa Y., Tada H., and Ito S. *Journal of the Electrochemical Society*: 147 **(2000)** 2279-2283.

Hayden S.C., Allam N.K., and El-Sayed M.A. *Journal of the American Chemical Society*: 132 **(2010)** 14406-14408.

Herrmann J.M. *Catalysis Today*: 53 **(1999)** 115-129.

Hester J.F., Olugebefola S.C., and Mayes A.M. *Journal of Membrane Science*: 208 **(2002)** 375-388.

Hoffmann M.R., Martin S.T., Choi W., and Bahnemann D.W. *Chemical Reviews*: 95 **(1995)** 69-96.

Hofstadler K., Bauer R., Novalic S., and Heisler G. *Environmental Science and Technology*: 28 **(1994)** 670-674.

Hoigné J., and Bader H. *Water Research*: 10 **(1977)** 377-386.

Horie Y, David D.A., Taya M., and Tone S. *Industrial and Engineering Chemistry Research*: 35 **(1996)** 3920-3926.

Huang Z., Maness P.C., Blake D.M., Wolfrum E.J., Smolinski S.L., and Jacoby W.A. *Journal of Photochemistry and Photobiology A*: *Chemistry*: 130 **(2000)** 163-170.

Huston P.L., and Pignatello J.J. *Water Research*: 33 (5) **(1999)** 1238-1246.

Irabelli A., Jasim S. and Biswas N. *Ozone Science and Engineering Journal*: 30 **(2008)** 356-366.

Jacoby W.A., Maness P.C., Wolfrum E.J., Blake D.M., and Fennell J.A. *Environmental Science Technology*: 32 **(1998)** 2650-2653.

Jiang C., Pang S., Ouyang F., Mac J., and Jiang J. *Journal of Hazardous Materials*: 174 **(2010)** 813-817.

Jiang Y., Pétrier C., and Waite D.T. *Ultrasonics Sonochemistry*: 9 **(2002)** 317-323.

Joyce E.M., and Mason T.J. International Green Process Engineering Congress and the European Process Intensification Conference, Venice, Italy, **(2009)**.

Jyoti K.K., and Pandit A.B. *Biochemical Engineering Journal*: 18 **(2004)** 9-19.

Jyoti K.K., and Pandit A.B. *Biochemical Engineering Journal*: 7 **(2001)** 201-212.

Jyoti K.K., and Pandit A.B. *Ultrasonics Sonochemistry*: 10 **(2003)** 255-264.

Kabra K., Chaudhary R., R.L. and Sawhney R.L. *Industrial and Engineering Chemical Research*: 43 **(2004)** 7683-7696.

Kamat P.V. *Journal of Physical Chemistry C*: 111 **(2007)** 2834-2860.

Kang M. *Materials Letters*: 59 **(2005)** 3122-3127.

Kang Y.W., and Hwang K.-Y. *Water Research*: 34 **(2000)** 2786-2790.

Katzenelson E., Kletter B., and Shuval H.I. *Journal of American Water Works Association*: 66 **(1974)** 725-729.

Kesari K.K., Kumar S., Verma H.N., and Behari J. *Hydrology*: *Current Research*: 2 (115) **(2011)**.

Kesting R.E. *Journal of Applied Polymer Science*: 41 **(1990)** 2739-2752.

Khadre M.A., Yousef A.E. and Kim J.-G. *Journal of Food Science*: 66 (9) **(2001)** 1242-1252.

Khan H., and Berk D. *Journal of Photochemistry and Photobiology A*: *Chemistry*: **(2014)** 1-44.

Khan M.H., Bae H., and Jung J.-Y. *Journal of Hazardous Materials*: 181 **(2010)** 659-665.

Khulbe K.C., Feng C.Y., and Matswura T. Synthetic polymeric membranes. Springer, 1st edition, **(2008)** 5-8.

Kim J.P., Cho I.H., Kim I.T., Kim C.U., Heo N.H., and Suh S.H. *Romanian Journal of Chemistry*: 51 (11) **(2006)** 1121-1129.

Kim T-H., Kim S.D., Kim H.Y., Lim S.J., Lee M., and Yu S. *Journal of Hazardous Materials*: 227-228 **(2012)** 237-242.

Kinman R.N. *Critical Reviews in Environmental Control*: 5 **(1975)** 141-152.

Klosek S., and Raftery D. *Journal of Physical Chemistry B*: 105 **(2001)** 2815-2819.

Kobayashi F., Hayata Y., Ikeura H., Tamaki M., Muto N., and Osajima Y. *Journal of Agricultural Safety and Health and Biological Engineering Transactions*: 52 **(2009)** 1621-1626.

Kobayashi F., Ikeura H., Ohsato S., Goto T., and Tamaki M. *Crop Protection*: 30 (11) **(2011)** 1514-1518.

Koidis P., Bori M., and Vareltzis K. *Arch. Lebensmittelhygiene*: 51 **(2000)** 4-6.

Kong J., and Lee K. *Separation and Purification Technology*: 16 **(1999)** 83-93.

Konstantinou I.K., and Albanis T.A. *Applied Catalysis B*: *Environmental*: 42 **(2003)** 319-335.

Kumar S.G., and Devi L.G. *Journal of Physical Chemistry A*: 115 **(2011)** 13211-13241.

Langlais B., Reckhow D.A. and Brink D.R. Ozone in Water Treatment: Application and Engineering. Lewis Publishers Inc., Chelsea, Michigan, USA **(1991)**.

Larson M.A. and Mariñas B.J. *Water Research*: 37 **(2003)** 833-844.

Lata H., Garg V.K., and Gupta R.K. *Desalination*: 219 **(2008)** 250-261.

Lee S., Nishida K., Otaki M., and Ohgaki S. *Water Science and Technology*: 35 **(1997)** 101-106.

Legrini O., Oliveros E., and Braun A.M. *Chemical Reviews*: 93 **(1993)** 671.

Leong S., Razmjou A., Wang K., Hapgood K., Zhang X., and Wang H. *Journal of Membrane Science*: 472 **(2014)** 167-184.

Li H., Gyurek L.L., Finch G.R., Smith D.W., and Belosevic M. *Journal of Environmental Engineering ASCE*: 127 **(2001)** 456-467.

Li P., Takahashi M., and Chiba K. *Chemosphere*: 75 **(2009)** 1371-1375.

Li Q., Mahendra S., Lyon D.Y., Brunet L., Liga M.V., Li D., and Alvarez P.J.J. *Water Research*: 42 (18) **(2008)** 4591-4602.

Li X.Z., and Li F.B. *Environmental Science and Technology Letters*: 35 (11) **(2001)** 2381-2387.

Li Y., Hwang D.-S., Lee N.H., and Kim S.-J. *Chemical Physics Letters*: 404 **(2005)** 25-29.

Li Y.H., Ding J., Luan Z., Di Z., Zhu Y., Xu C., Wu D., and Wei B. *Carbon*: 41 **(2003)** 2787-2792.

Li Y.H., Wang S., Luan Z., Ding J., Xu C., and Wu D. *Carbon*: 41 **(2003)** 1057-1062.

Liang S., Palencia S.L., Yates R.S., Davis M.K., Bruno J.M., and Wolfe R.L. *Journal of American Water Works Association*: Vol. 91 (6) (1999) 104-114.

Lin J.X., Zhan S.L., Fang M.H., Qian X.Q., and Yang H. *Journal of Environmental Management*. 87 **(2008)** 193-200.

Lin S.H., Lin C.H., and Leu H.G. *Water Research*: 33 (7) **(1999)** 1735-1741.

Liu H., Wang C., Li X., Xuan X., Jiang C., and Cui H. *Environmental Science and Technology*: 41 **(2007)** 2937-2942.

Linsebigler A.L., Lu G., and Yates J.T. *Chemical Reviews*: 95 **(1995)** 735-758.

Litter M.I. *Applied Catalysis B*: *Environmental*: 23 **(1999)** 89-114.

Low S.C., Liping C., and Hee L.S. *Desalination*: 221 **(2008)** 168-173.

Luche J.L. *Synthetic Organic Sonochemistry*, Plenum Press, New York, **(1999)**.

Maness P.C., Smolinski S., Blake D., Huang Z., Wolfrum A.J., and Jacoby W.A. *Applied Environmental Microbiology*: **(1999)** 4094-4098.

Maraschi F., Sturini M., Speltini A., Pretali L., Profumo A., Pastorello A., Kumar V., Ferretti M., and Caratto V. *Journal of Environmental Chemical Engineering*: 2 **(2014)** 2170-2176.

Mason T.J., and Lorimer J.P. *Applied Sonochemistry*: The Uses of Power Ultrasound in Chemistry and Processing, Wiley-VCH Verlag GmbH,Weinheim, **(2002)**.

Mason T.J., and Lorimer J.P. *Sonochemistry*: Theory, Applications and Uses of ultrasound in Chemistry, John Wiley & Sons, New York, **(1988)**.

Mason T.J., and Pétrier C. Advanced oxidation processes for water and wastewater treatment, in: Parson S., (Ed.), *Ultrasound Processes*, IWA Publishing, London, **(2004)** 185-208.

Matilainen A., and Sillanpää M. *Chemosphere*: 80 **(2010)** 351-365.

Matsunaga T.R., Nakajima T.T., and Wake H. *Microbiology Letters*: 29 **(1985)** 211-214.

Matsunaga T.R., and Okochi M. *Environmental Science and Technology*: 29 **(1995)** 501-505.

Matthews R.W. *Water Research*: 25 **(1991)** 1169-1176.

McCullagh C., Robertson J.M.C., Bahnemann D.W., and Robertson P.K.J. *Research on Chemical Intermediates*: 33 (3-5) **(2007)** 359-375.

Mendret J., Hatat-Fraile M., Rivallin M., and Brosillon S. *Separation and Purification Technology*: 111 **(2013)** 9-19.

Méndez-Arriaga F., Torres-Palma R.A., Pétrier C., Esplugas S., Gimenez J., and Pulgarin C. *Water Research*: 42 **(2008)** 4243-4248.

Meng X., Qian Z., Wang H., Gao X., Zhang S., and Yang M. *Journal of Sol-Gel Science and Technology*: 46 **(2008)** 195-200.

Mezule L., Tsyfansky S., Yakushevich V., and Juhna T. *Desalination*: 248 (1–3) **(2009)** 152-159.

Mills A., and Hunte S.L. *Journal of Photochemistry and Photobiology A*: *Chemistry*: 108 **(1997)** 1-35.

Mobasherpour I., Salahi E., and Pazouki M. *Arabian Journal of Chemistry*: **(2011)** http://dx.doi.org/10.1016/j.arabjc.2010.12.022.

Mohapatra D.P., Brar S.K., Tyagi R.D., Picard P., and Surampalli R.Y. *Science of the Total Environment*: 470-471 **(2014)** 58-75.

Moras D., Uhlig P., Petitinbert J.F., Henery C.H., and Ayad L. High Concentration Ozone Generation, Proceedings of 11th World Ozone Congress - San Francisco, **(1993)** S-8-1 to S-8-15.

Muhammad N., Parr J., Smith M.D., and Wheatley A.D. Adsorption of heavy metals in slow sand filters. *24th WEDC Conference*, Islamabad, Pakistan, **(1998)**.

Mungondori H., and Tichagwa L. *Materials Science Forum*: Vol. 734 **(2013)** 226-236.

Murray C.B., Norris D.J., and Bawendi M.G. *Journal of the American Chemical Society*: 115 **(1993)** 8706.

Naeem k., and Ouyang F. *Journal of Environmental Sciences*: 25 (2) **(2013)** 399-404.

Nakada N., Shinohara H., Murata A., Kiri K., Managaji S., and Sato N. *Water Research*: 41 **(2007)** 4373-4382.

Nalwa H.S. *Journal of Macromolecular Science Part C*: 31 **(1991)** 341-432.

Nasir M., Bagwasi S., Jiao Y., Chen F., Tian B., and Zhang J. *Chemical Engineering Journal*: 236 **(2014)** 388-397.

Ndounla J., and Pulgarin C. *Science of the Total Environment*: 493 **(2014)** 229-238.

Neyens E., and Baeyens J. *Journal of Hazardous Material B*: 98 **(2003)** 33-50.

Nyamukamba P., Tichagwa L., and Greying C. *Materials Science Forum*: 712 **(2012)** 49-63.

Orr P.T., Jones G.J., and Hamilton G.R. *Water Research*: 38 (20) **(2004)** 4455-4461.

Ortega-Gómeza E., García B.E., Martín B.M.M., Ibáñez P.F., and Pérez J.A.S. *Water Research*: 63 **(2014)** 316-324.

Padron M. *Avian Diseases*: 39 **(1995)** 627-630.

Page K., Palgrave R.G., Parkin I.P., Wilson M., Savin S.L.P., and Chadwick A.V. *Journal of Materials Chemistry*: 17 **(2007)** (1) 95-104.

Paode R.D., Chandrakanth M.S., Amy G.L., Gramith J.T., and Ferguson D.W. *Ozone Science and Engineering*: 17 **(1995)** 25-51.

Parsons S.A., and Williams M. Advanced oxidation processes for water and wastewater treatment. London, UK: IWA Publishing; **(2004)**.

Pavasant P., Apiratikul R., Sungkhum V., Suthiparinyanont P., Wattanachira S., and Marhaba, T. F. *Bioresource Technology*: 97 **(2006)** 2321-2329.

Pétrier C., and Francony A. *Ultrasonics Sonochemistry*: 4 **(1997)** 295-300.

Pisarenko A.N., Stanford B.D., Yan D., Gerrity D, and Snyder S.A. *Water Research*: 46 **(2012)** 316-326.

Polo-López M.I., Oller I., P. Fernández-Ibánez P. *Catalysis Today*: 209 **(2013)** 181-187.

Pozzo R.L., Baltanas M.A., and Cassano A.E. *Catalysis Today*: 39 **(1997)** 219-231.

Prados M., Paillard H., and Roche P. *Ozone Science and Engineering*: 17 **(1995a)** 183-194.

Quan F., Hu Y., Zhang X., and Wei C. *Applied Surface Science*: **(2014)** 1-37.

Ramasundaram S., Yoo H.N., Song K.G., Lee J., Choi K.J., and Hong S.W. *Journal of Hazardous Materials*: 258-259 **(2013)** 124-132.

Ramseier M.K., Von Gunten U., Freihofer P., and Hammes F. *Water Research*: 45 (3) **(2011)** 1490-1500.

Ran Z.L., Li S.F., Huang J.L., Yuan Y.X., Cui C.W., and Williams C.D. *Journal of Environmental Sciences China*: 22 **(2010)** 1954-1959.

Rathinavelu J.R, and Palanivelu K. *Journal of Environmental Chemical Engineering*: 2 **(2014)** 1804-1812.

Reddy K.M., Manorama S.V., and Reddy A.R. *Materials Chemistry and Physics*: 78 **(2002)** 239-245.

Reddy M.P., Venugopal A., and Subrahmanyam M. *Water Research*: 41 **(2007)** 379-386.

Ren W., Ai Z., Jia F., Zhang L., Fan X., and Zou Z. *Applied Catalysis B*: *Environmental*: 69 **(2007)** 138-144.

Rice R.G. and Cotruvo J.A. Ozone/Chlorine Dioxide, Oxidation Products of Organic Materials. Ozone Press International, Cleveland, OH, **(1978)** 490.

Rice R.G. and Netzwer A. Handbook of ozone technology and applications, Volume 1- Ann Arbor Science Publishers, **(1982)** 1-15.

Rodríguez-Chueca J., Mosteo R., Ormad M.P., and Ovelleiro J.L. *Solar Energy*: 86 **(2012)** 3260-3267.

Rosal R., Rodriguez A., Perdigon-Melon J.A., Petre A., Garcia-Calvo E., and Gomez M.J. *Water Research*: 44 **(2010)** 578-588.

Roy D. *Inactivation of Enteroviruses by Ozone.* Ph.D. Thesis, University of Illinois at Urbana-Champaign, **(1979)**.

Roy D., Engelbrecht R.S. and Chian E.S.K. *Journal of American Water Works Association*: 74 (12) **(1982)** 660.

Rubio D., Nebot E., Casanueva J.F., and Pulgarin C. *Water Research*: 47 **(2013)** 6367-6379.

Ruiz B., Bauzá J., Benito J. and Pascual A. IOA Conference and Exhibition Valencia, Spain, **(2007)** 6.4-1 – 6.4-7.

Saggioro E.M., Oliveira A.S., Buss D.F., Magalhaes D.P., Pavesi T., Jimenez M., Maldonado M.I., Ferreira L.F.V., and Moreira J.C. *Dyes and Pigments*: 113 **(2015)** 571-580.

Safarpour M., Khataee A., and Vatanpour V. *Separation and Purification Technology*: **(2014)**.

Sakai H., Baba R., Hashimoto K., Kubota Y., and Fujishima A. *Biochimica et Biophysica Acta*: 1201 **(1994)** 259-265.

Sampaio M.J., Marques R.R.N., Tavares P.B., Faria J.L., Silva A.M.T., and Silva C.G. *Journal of Environmental Chemical Engineering*: **(2013)** 945-953.

Sampaio M.J., Silva C.G., Silva A.M.T., Vilar V.J.P., Boaventura R.A.R., and Faria J.L. *Chemical Engineering Journal*: 224 **(2013)** 32-38.

Scharnagl N., and Buschatz H. *Desalination*: 139 (1-3) **(2001)** 191-198.

Scott K.S., and Hughes R. Industrial membrane separation technology, Blackie Academic and Professional, 1st edition, **(1996)** 3-7.

Selma M.V., Allende A., López-Gálvez F., Conesa M.A., and Gil M.I. *Food Microbiology*: 25 **(2008)** 809-814.

Sencadas V., Lanceros-Méndez S., and Mano J.F. *Thermochimica Acta*: 424 **(2004)** 201-207.

Serpone N., Maruthamuthu P., Pichat P., Pelizzetti E., and Hidaka H. *Journal of Photochemistry and Photobiology A*: *Chemistry*: 85 **(1995)** 247-255.

Shah Y.T., Pandit A.B., and Moholkar V.S. Cavitation Reaction Engineering, Plenum Publishers, NY, USA, **(1999)**.

Shinde S.S., Bhosale C.H., and Rajpure K.Y. *Journal of Photochemistry and Photobiology B*: *Biology*: 141 **(2014)** 186-191.

Silva C.G., and Faria J.L. *Journal of Molecular Catalysis A*: *Chemical*: 305 **(2009)** 147-154.

Silver G.H.R., Daniel L.A., Bruning H., and Rulkens W.H. *Bioresource Technology*: 101 (18) **(2010)** 6981-6986.

Songkhum P., and Tantirungrotechai J. *Research on Chemical Intermediates*: 39 **(2013)** 1555-1561.

Spartan Environmental technologies. Advanced oxidation technologies, "Applications of Ozone Water Treatment for Drinking (Potable) Water", http://www.spartanwatertreatment.com/drinking-water-ozone.html. (**Accessed 05-05-2014**).

Sprynskyy M., Buszewski B., Terzyk A.P., and Namieśnik J. *Journal of Colloid and Interface Science*: 304 **(2006)** 21-28.

Spuhler D., Rengifo-Herrera J.A., and Pulgarin C. *Applied Catalysis B: Environmental*: 96 **(2010)** 126-141.

Staehelin J., and Hoigné J. *Environmental Science and Technology*: 16 (10) **(1982)** 676-681.

Strathmann H. Synthetic Membranes: Science, Engineering and Application, Springer, **(1986)** 1-37.

Subramanian V., Wolf E.E., and Kamat P.V. *Journal of the American Chemical Society*: 126 **(2004)** 4943-4950.

Sunde E., Thorstenson T. and Torsvik T. Growth of bacteria on water injection additives. *65th Conf. SPE ATCE*, New Orleans, Los Angeles, USA, **(1990)** 727.

Suslick K.S. *Science*: 247 **(1990)** 1439.

Takahashi M., Chiba K., and Li P. *Journal of Physical Chemistry B*: 111 **(2007)** 11443-11446.

Tasaki T., Wada T., Fujimoto K., Kai S., Ohe K., Oshima T., Baba Y., and Kukizaki M. *Journal of Hazardous Materials*: 162 **(2009)** 1103-1110.

Tech Brief. A national drinking water clearing house fact sheet, 1999. http://www.nesc.wvu.edu. (**Accessed 05-05-2014**).

Teodoro A., Boncz M.A., Júnior A.M., and Paulo P.L. *Journal of Environmental Chemical Engineering*: 2 **(2014)** 958-962.

Ternes T.A., Stuber J., Herrmann N., McDowell D., Ried A., and Kampmann M. *Water Research*: 37 **(2003)** 1976-1982.

Thanomsub B., Anupunpisit V., Chanphetch S., Watcharachaipong T., Poonkhum R. and Srisukonth C. *J. Gen. Appl. Microbiol*: 48 **(2002)** 193-199.

Thiruvenkatachari R., Kwon T.O., and Moon I.S. *Separation and Purification Technology*: 40 **(2005)** 2871-2888.

Tomiyasu H., Fukutomi H., and Gordon G. *Inorganic Chemistry*: 24 **(1985)** 2962-2966.

Torres R.A., Pétrier C., Combet E., Carrier M., and Pulgarin C. *Ultrasonics Sonochemistry*: 15 **(2008)** 605-611.

Torres R.A., Abdelmalek F., Combet E., Pétrier C., and Pulgarin C. *Journal of Hazardous Materials*: 146 **(2007)** 546-551.

Trapido M., Munter R., Veressinina Y., and Goi A. *Proceedings of International Conference EcoBalt*: 1 **(2000)** 36-41.

Troyan J.J. and Hansen S.P. *Treatment of Microbial Contaminants in Potable Water Supplies Technologies and Costs*. Noyes Data Corporation, Park Ridge, New Jersey, **(1989)**.

Turkiewicz A., Brzeszcz J. and Kapusta P. The application of biocides in the oil and gas industry; *Oil & Gas Institute, Krakow*, **(2013)**.

Turkiewicz A. The role of microorganisms in the oil and gas industry. *Rocznik Ochrona Środowiska*, tom: 13 **(2011)** 227-239.

Uchida H., Hirao S., Torimoto T., Kuwabata S., Sakata T., Mori H., and Yoneyama H. *Langmuir*: 11 **(1995)** 3725-3729.

Ulbricht M., and Belfort G. *Journal of Membrane Science*: 111 (2) **(1996)** 193-215.

Uslu M.O., and Balcioglu I.A. *Ozone Science and Engineering*: 30 **(2008)** 290-299.

Vaiano V., Sacco O., Sannino D., and Ciambelli P. *Chemical Engineering Journal*: 261 **(2015)** 3-8.

Van Hamme J.D., Singh A. and Ward O.P. *Microbiology and Molecular Biology Reviews*: 67 (4) **(2003)** 503-549.

Vaughn J.M. *Applied Environmental Microbiology*: 53 (1987) 2218-2221.

Viera M. *International Biodeterioration and Biodegradation*: 44 **(1999)** 201-207.

Vilve, M., Törönen, T., Sillanpää, M. *Ozone Science and Engineering*: 30 **(2008)** 256-262.

Vollmuth S., and Niessner R. *Chemosphere*: 30 (12) **(1995)** 2317-2331.

Von Gunten U. *Water Research*: 37 **(2003)**1443-1467.

Wang K., Guo J., Yang M., Junji H., and Deng R. *Journal of Hazardous Materials*: 162 **(2009)** 1243-1248.

Wang K.Y., Chung T.-S., and Gryta M. *Chemical Engineering Science*: 63 (9) **(2008)** 2587-2594.

Wang Q., Qiao J., Jin R., Xu X., and Gao S. *Journal of Power Sources*: **(2014)** 1-28.

Wang Y.Q., Zhang L., Cheng H.M., and Ma J.M. *Chemical Journal of Chinese Universities*: 21 **(2000)** 958-960.

Watts R.J., Kong S., Orr M.P., Miller G.C., and Henry B.E. *Water Research*: 29 **(1995)** 95-100.

Wickramanayake G.B. Kinetics and mechanism of ozone inactivation of protozoan cysts (PhD dissertation). Columbus, Ohio: The Ohio State University, **(1984)**.

Wilczak A., Howe E.W, Aieta E.M., and Lee R.G. *Journal of American Water Works Association*: 84 (12) **(1992)** 85-94.

Williams R.C., Sumner S.S., and Golden D.A. *Journal of Food Science*: 70 (4) **(2005)** 197-201.

Xiang Q., Yu J., Cheng B., and Ong H.C. *Chemistry-An Asian Journal*: 5 **(2010)** 1466-1474.

Yamashita H., Ichihashi Y., Takeuchi M., Kishiguchi S., and Anpo M. *Journal of Synchrotron Radiation*: 6 **(1999)** 451-452.

Yang T.-S., Yang M.-C., Shiu C.-B., Chang W.-K., and Wong M.-S. *Applied Surface Science*: 252 **(2006)** 3729-3736.

Yousefzadeh S., Faraji M., Nien Y.T., and Moshfegh A.Z. *Applied Surface Science*: 320 **(2014)** 772-779.

Yu J., Yue L., Liu S., Huang B., and Zhang H. *Journal of Colloid and Interface Science*: 334 **(2009)** 58-64.

Yun D.-M., Cho H.-H., Jang J.-W., and Park J.-W. *Water Research*: 47 **(2013)** 1858-1866.

Zan L., Fa W., Peng T.P., and Gong Z.K. *Journal of Photochemistry and Photobiology B*: *Biology*: 86 (2) **(2007)** 165-169.

Zhang G., Li X., Li Y., Wu T., Sun D., and Lu F. *Desalination*: 274 (1-3) **(2011)** 255-261.

Zhang H., Choi H.J., and Huang C.-P. *Journal of Hazardous Materials B*: 125 **(2005)** 166-174.

Zhang Q., Gao L., and Guo J. *Applied Catalysis B*: *Environmental*: 26 **(2000)** 207-215.

Zhang X., Xie Y., Chen H., Guo J., Meng A., and Li C. *Applied Surface Science*: **(2014)** 1-30.

Zhong L., Guo J., Lu Y., Li X., and Gao G. *Chinese Journal of Chemical Engineering*: 7 (2) **(1999)** 110-115.

Zhou H. and Smith D.W. *Journal of Environmental and Engineering Science*: 1 **(2002)** 247-264.

Zhou M., Yu J., Liu S., Zhai P., and Jiang L. *Journal of Hazardous Materials*: 154 **(2008)** 1141-1148.

CHAPTER 3

3. Experimental Procedures

3.1 Introduction

This chapter gives details of the materials and reagents used in the study and the methodology followed.

3.2 Materials and chemical reagents

Titanium tetrachloride ($TiCl_4$) (99 % Merck) was used as the precursor material in the preparation of nitrogen doped titanium dioxide (N-TiO_2). Ammonia (25 % MET –U-ED Chemical Co.) was used as the nitrogen source in the preparation of N-TiO_2. Potassium hydroxide (KOH) was used to adjust pH in the preparation of N-TiO_2. Phenol (99.5 % Sigma-Aldrich) and phenol red (Searle Co.) were used as model organic contaminants in the photo-degradation analysis. Poly (acrylonitrile) (PAN) (Sigma-Aldrich, M_w 150 000) powder, poly (vinylidene difluoride) (PVDF), and methacrylic acid (99 % Sigma-Aldrich) were used as the precursor material in the preparation of PMAA-g-PVDF/ PAN membranes used as matrix for the N-TiO_2 photo-catalyst. Dimethylacetamide (DMAC) (99 % Merck), Absolute ethanol (99.9 % Merck), acetone (99 % Merck) and deionized water were used as solvents. For microbial evaluation the following materials were used; sterile inoculating loops, agar gel, nutrient broth, normal saline, plates for incubation and *E. coli* ATCC 8739 bacteria. Table 3 gives the chemical names, formulae, molecular structures and molecular masses of reagents.

Table 3: Chemicals and reagents used

Chemical name	Molecular mass/ $gmol^{-1}$	Molecular formula	Chemical structure
Titanium tetrachloride	189.71	$TiCl_4$	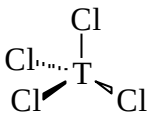
Bentazon	240.28	$C_{10}H_{12}N_2O_3S$	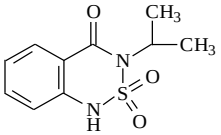
Paraquat	257.16	$C_{12}H_{14}Cl_2N_2$	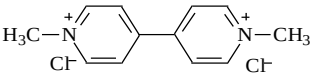
Dimethylacetamide	87.12	C_4H_9NO	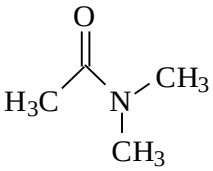
Acetone	58.08	C_3H_6O	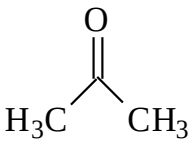
Atrazine	215.68	$C_8H_{14}ClN_5$	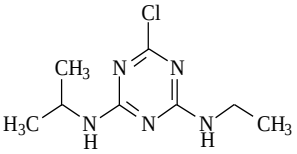
Ethanol	46.07	C_2H_6O	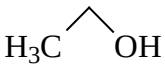
Methacrylic acid	86.06	$C_4H_6O_2$	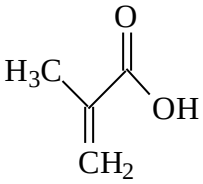

3.3. General procedures

3.3.1. Preparation of TiO_2 and N-TiO_2

Titanium dioxide was prepared by slow addition of titanium tetrachloride into deionized water in a beaker over an ice-bath under stirring. The resulting sol was heated at 90 ˚C for 10 minutes while stirring to allow the gelation process. The resulting white solution was adjusted to pH 8.0 by the addition of 0.01 M KOH solution drop-wise. The product was collected via centrifugation and washed three times with deionized water to get rid of excess chloride ions. The amorphous TiO_2 was dried in an oven at 60 ˚C. To allow phase transformation, the amorphous TiO_2 powder was heated at 550˚ C for 3 hours. Nitrogen doped TiO_2 was prepared in a similar fashion except for the addition of ammonia as a nitrogen source during the gelation stage.

3.3.2. Preparation of polymer membranes

All the polymer membranes were prepared by dissolving the polymer (PVDF, PAN and PMAA-g-PVDF) in dimethylacetamide (DMAC). The polymer solutions were homogenized through stirring, and then sonicated for 10 minutes to remove air bubbles trapped in the polymers. Each of the polymer solutions (5 mL) was uniformly spread on 6.5 × 11.5 cm flat glass plate. Partial evaporation of solvent was allowed before placing the glass plate into a coagulation bath. The coagulation bath for PAN membranes had deionized water and was maintained at 30 ˚C. The coagulation bath for PVDF and PMAA-g-PVDF/ PAN membranes was ethanol: water (3: 1 ratio) maintained at 30 ˚C. The membranes that contained different N-TiO_2 photo-catalyst loadings were prepared by blending the polymer solutions with varying amounts of the photo-catalyst before casting onto the glass plates.

3.4. Characterization techniques

This section describes the analytical techniques that were used for the characterization of the nitrogen doped titanium dioxide photo-catalyst as well as the membranes (PMAA-g-PVDF/ PAN) that had been prepared. Samples were characterized using the following techniques: Fourier transform infrared spectroscopy (FT-IR), Nuclear magnetic resonance (NMR), Brunauer-Emmet-Teller (BET) surface area analysis, X-ray diffraction (XRD) analysis, Transmission electron microscopy (TEM), Diffuse reflectance spectroscopy (DRS), tensile strength and elongation measurements, Scanning electron microscopy (SEM), Thermo-gravimetric analysis (TGA). Ultraviolet-visible spectroscopy (UV-VIS) was used for the quantitative analysis of the organic model pollutants during photo-degradation studies. Total organic carbon (TOC) analysis was used to assess the organic load of synthetic water. Liquid chromatography-mass spectrometry (LC-MS) was used to follow the degradation patterns of the herbicide bentazon. Ultrafiltration (UF) experiments were carried out to establish the filtration capacity and the antifouling properties of the membranes prepared.

3.4.1. Fourier-transform infrared spectroscopy (FT-IR)

FT-IR Spectroscopy stands for "Fourier Transform Infrared Spectroscopy". This analytical technique was developed in 1970s for qualification and quantification of compounds utilizing infrared absorption of molecules. In the FT-IR technique spectra are collected based on measurements of the coherence of a radiative source, using time-domain or space-domain measurements of the electromagnetic radiation or other type of radiation. FT-IR is employed in the identification of functional groups in samples of either inorganic or organic compounds.

IR radiation is passed through a sample and in the process some of the infrared radiation is absorbed by the sample and some of it transmitted. The spectrum obtained represents the molecular absorption and transmission, creating a molecular fingerprint of the sample. Like a fingerprint, each molecular structure produces a unique infrared spectrum. This makes infrared spectroscopy useful for the determination of the functional groups present in compounds and other analyses (Abragram, 1968; Atkins, 2006; Amand and Tullin, 2013).

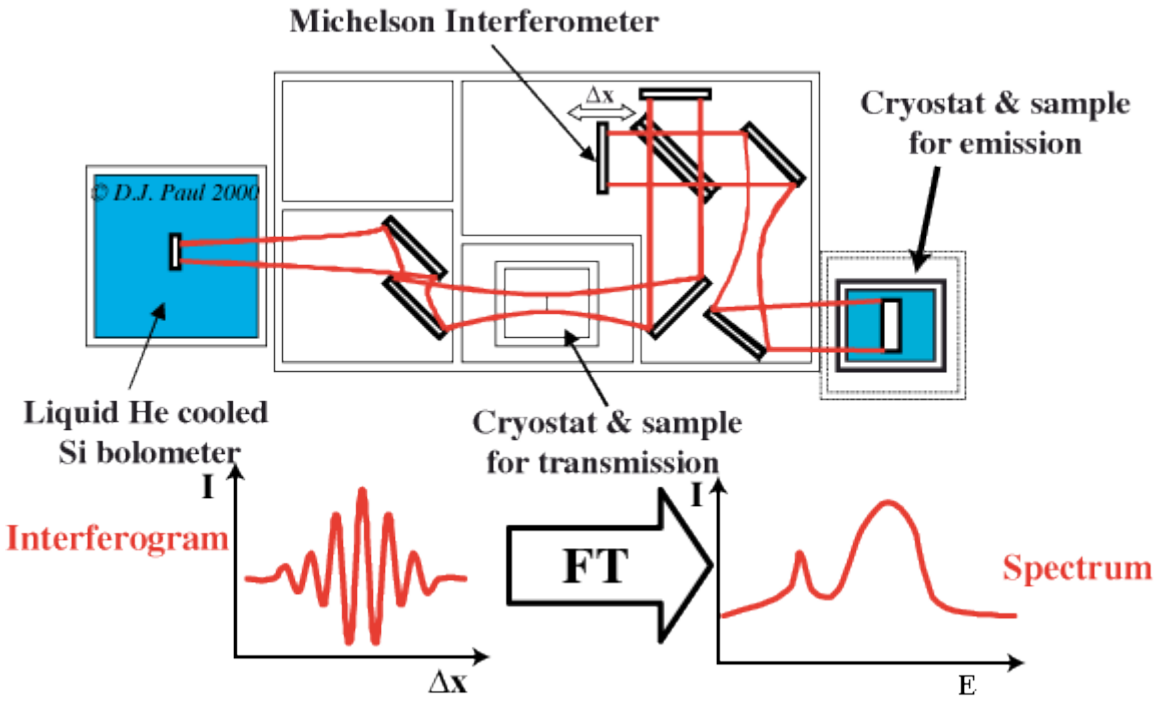

Figure 3.1: Schematic diagram of an FT-IR instrument (www.faculty.sdmiramar.edu)

3.4.2. Nuclear Magnetic Resonance spectroscopy (NMR)

Nuclear magnetic resonance spectroscopy (NMR) is an important tool for the determination of molecular structure. This technique exploits the magnetic properties of certain atomic nuclei. Some nuclei exist in discrete nuclear spin states when placed in an external magnetic field (e.g. ^{1}H, ^{13}C, ^{19}F, and ^{31}P), so NMR spectroscopy observes transitions between these spin states. The proton and carbon spectra are the most important for organic structure

determination. These spectra give information about the number of hydrogens and carbons in a molecule and how those hydrogens and carbons are connected together as well as information about functional groups (Macomber R.S, 2004; Holmes, 2012).

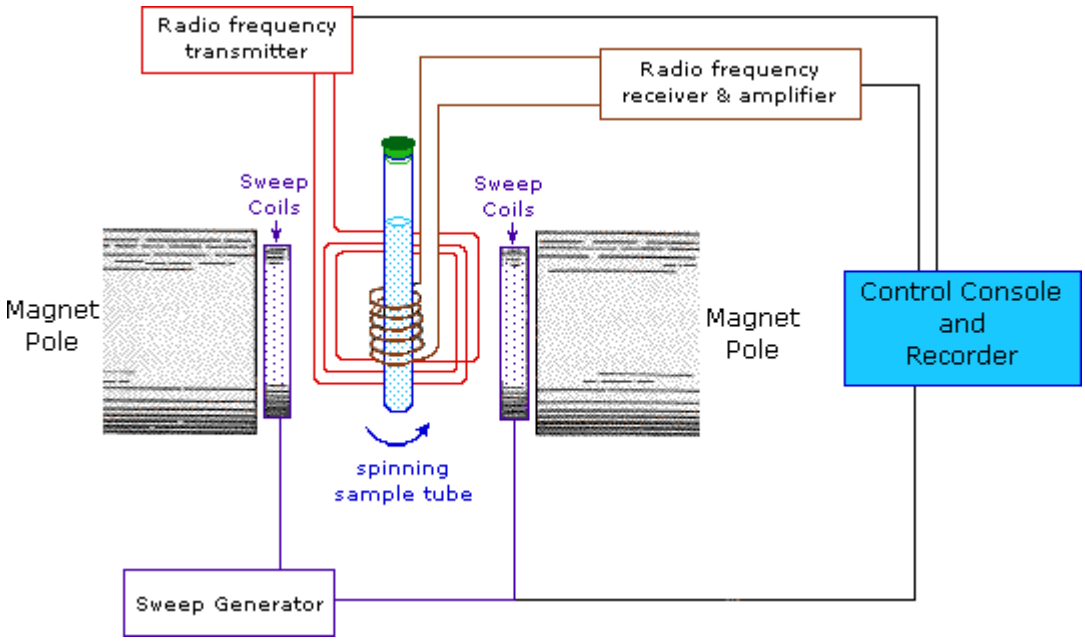

Figure 3.2: Schematic representation of NMR spectroscopy instrument (www.orgchem.colorado.edu)

3.4.3. Brunauer Emmett Teller (BET) surface area analysis

BET surface area analysis is a technique employed in the determination of the specific surface area of powders, solids and granules. The units are expressed in meter square per gram (m^2/ g). Gas molecules in the surroundings of clean solid surfaces get adsorbed and Brunauer, Emmett and Teller theory (BET) provides a mathematical model for the process of gas sorption. This process is called physisorption and is used to measure the total surface area and pore size of nano-pores, micro-pores and mesopores. The BET surface area measurement is important in understanding the behaviour of a material, as the material reacts with its

surroundings through its surface. A higher surface area material is anticipated to react faster, dissolve faster and adsorb more gas than a similar material with a lower surface area.

Surface Area is a measure of the exposed surface of a solid sample on the molecular scale. The BET (Brunauer, Emmet, and Teller) theory is the most popular model used to determine the surface area. Samples are prepared by heating while simultaneously evacuating or flowing gas over the sample to remove the released impurities. The prepared samples are then cooled with liquid nitrogen and analysed by measuring the volume of gas (typically N_2 or Kr) adsorbed at specific pressures. Krypton gas is used mostly when the measured surface is expected to be less than 2 m^2g^{-1}, which is typical for pharmaceutical samples and natural organic materials (Brunauer *et al.*, 1938; McMillan and Teller, 1951).

3.4.4. Diffuse reflectance spectroscopy (DRS)

Diffuse Reflectance Infrared Fourier Transform Spectroscopy is a technique that collects and analyses scattered IR energy. This technique is used for measurement of fine particles and powders, as well as rough surfaces (e.g., the interaction of a surfactant with the inner particle, the adsorption of molecules on the particle surface). Sampling is quick and easy because little or no sample preparation is required. As the IR beam enters the sample, it can either be reflected off the surface of a particle or be transmitted through a particle. The IR energy reflecting off the surface is typically lost. The IR beam that passes through a particle can either reflect off the next particle or be transmitted through the next particle. This transmission-reflectance event can occur many times in the sample increasing the path length. Finally, such scattered IR energy is collected by a spherical mirror that is focused onto a detector. The detected IR light is partially absorbed by particles of the sample, resulting in sample information (Scott, 1988; Workman, 1998; Jensen, 2001).

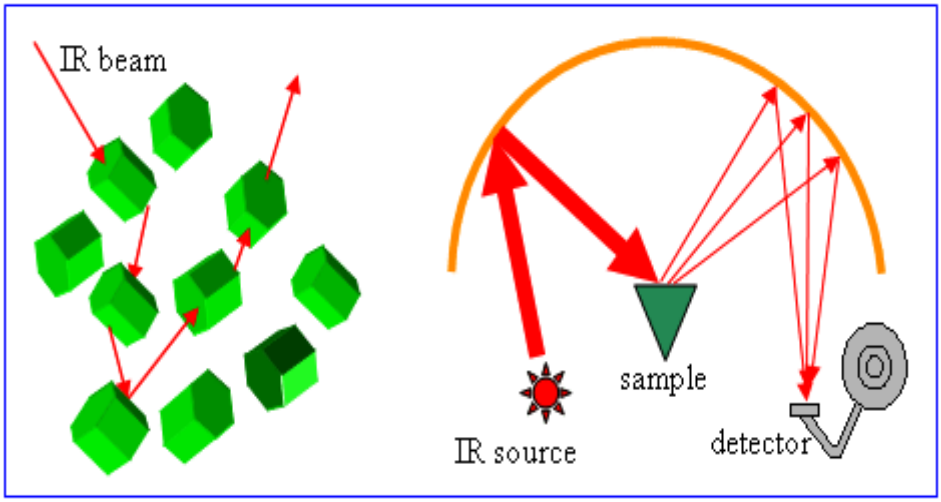

Figure 3.3: Schematic diagram of DRS instrument (Jensen, 2001)

3.4.5. X-ray diffraction (XRD)

In this technique X-rays are diffracted from the planes of a crystal (diffraction analysis), which depends on the wave character of the X-rays and the regular spacing of the planes in a crystal. Although diffraction techniques are normally used for quantitative analysis, they are most widely used for qualitative identification of crystalline phases (Durward, 1992).

X-ray powder diffraction analysis is a powerful technique by which X-rays of a known wavelength are passed through a sample. These X-ray diffraction techniques are based on the elastic scattering of X-rays from structures that have long-range order. The wave nature of the X-rays means that they are diffracted by the lattice of the crystal to give a unique pattern of peaks of 'reflections' at different angles and intensity, just as light can be diffracted by a grating of suitably spaced lines (André Authier, 2001**)**.

The diffracted beams from atoms in successive planes cancel out unless they are in phase, and the condition for this is given by the Bragg relationship (Equation 3.1):

$$n\lambda = 2dSin\Theta \qquad (3.1)$$

where, λ is the wavelength of the X-rays, d is the distance between different plane of atoms in the crystal lattice and θ is the angle of diffraction. The X-ray detector moves around the sample and measures the intensity of these peaks and the position of these peaks (diffraction angle 2θ). The highest peak is defined as the 100 % peak and the intensity of all the other peaks are measured as a percentage of the 100 % peak (www.plasma-biotal.com/xraydif1.html, Accessed 02-07-2013).

3.4.6. Scanning electron microscopy (SEM)

In scanning electron microscope (SEM) the electron microscope images a sample surface by scanning it with a high-energy beam of electrons in a raster scan pattern. Electrons interact with the atoms that constitute the sample producing signals that contain information about the sample's surface topography, composition and other properties such as electrical conductivity (Pergamon, 1962; Wells, 1974).

Electron Microscopes (EMs) basically operate exactly as their optical counterparts except that they utilize a focused beam of electrons instead of light to "image" the specimen and gain information about its structure and composition. The basic steps involved in all EMs are as follows: A stream of electrons is generated in high vacuum (by electron guns). This stream is accelerated towards the specimen (with a positive electrical potential) while confined and focused using metal apertures and magnetic lenses into a thin, focused, monochromatic beam (Voutou and Stefanaki, 2008; http://ncnc.engineering.ucdavis.edu, accessed 03-07-2013).

3.4.7. X-ray photo-electron spectroscopy (XPS)

X-ray photoelectron spectroscopy (XPS) is a quantitative spectroscopic method used for measuring the elemental composition, empirical formula, chemical state and electronic state

of the elements that exist within a material. XPS is also referred to as ESCA (Electron Spectroscopy for Chemical Analysis), an abbreviation introduced by Kai Siegbahn's research group. XPS is a surface analysis technique with a sampling volume that extends from the surface to a depth of approximately 50-70 Angstroms. XPS analysis can also be utilized for sputter depth profiling in the characterization of thin films by quantifying matrix-level elements as a function of depth (Fadley, 2010; Hofmann, 2013).

The surface of a sample (Fig. 3.4) is irradiated with photons of characteristic energy (usually Mg-Kα radiation or Al-Kα), which directly interact with core electrons of the sample atoms. As a result, ionized states are generated, and a photoelectron is emitted with a kinetic energy given approximately by the difference between the photon energy and the binding energy. The measured photoelectron spectrum is a direct indication of the binding energies of the different atomic electron levels and is often calibrated in eV of binding energy: The lower the kinetic energy, the higher the binding energy (McNaught and Wilkinson, 1997; Wagner, 2011).

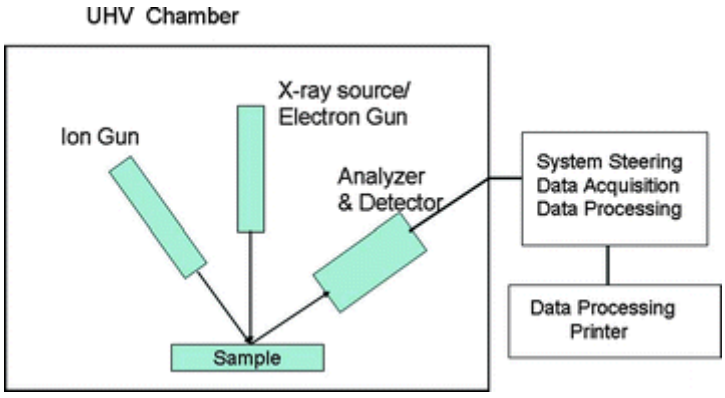

Figure 3.4: Components of a typical XPS instrument (Hofmann, 2013)

3.4.8. Thermo gravimetric analysis (TGA)

Thermo gravimetric Analysis (TGA) is a technique used to measure the amount and rate of change in the weight of a material as a function of temperature or time in a controlled atmosphere. Materials that can be characterized via TGA are those that exhibit weight loss or gain due to decomposition, oxidation, or dehydration. TGA measurements are used primarily to determine the composition of materials and to predict their thermal stability at temperatures up to 1000°C. A TGA machine comprises of a sample pan which hangs off a hook and is connected by a microgram balance arm to a tare pan. A TGA instrument continuously weighs a sample as it is heated to temperatures of up 1000 ˚C. As the temperature elevates, various components of the sample are decomposed and the weight percentage of each resulting mass change can be measured. Results are plotted with temperature on the X-axis and mass loss on the Y-axis (Coats and Redfern, 1963; Skoog *et al.*, 2007).

3.4.9. Ultra-violet/ visible spectroscopy (UV/ Vis)

Ultraviolet and visible (UV-Vis) absorption spectroscopy is a technique used in the measurement of the attenuation of a beam of light after it passes through a sample or after reflection from a sample surface. Absorption measurements can be at a single wavelength or over an extended spectral range. Ultraviolet and visible light are energetic enough to promote outer electrons to higher energy levels, and UV-Vis spectroscopy is usually applied to molecules or inorganic complexes in solution. The UV-Vis spectra have broad features that are of limited use for sample identification but are very useful for quantitative measurements. The concentration of an analyte in solution can be determined by measuring the absorbance at some wavelength and by applying the Beer-Lambert Law (Owen, 1996).

Since the UV-Vis range spans the range of human visual acuity of approximately 400 - 750 nm, UV-Vis spectroscopy is useful in characterizing the absorption, transmission, and reflectivity of a variety of technologically important materials, such as pigments, coatings, windows, and filters. This more qualitative application usually requires recording at least a portion of the UV-Vis spectrum for characterization of the optical or electronic properties of materials (Reusch, 2013; Owen, 1996).

The light source is usually a deuterium discharge lamp for UV measurements and a tungsten-halogen lamp for visible and near infrared measurements. The instruments automatically swap lamps when scanning between the UV and visible regions. The wavelengths of these continuous light sources are typically dispersed by a holographic grating in a single or double monochromator or spectrograph. The spectral band-pass is then determined by the monochromator slit width or by the array-element width in array-detector spectrometers. Spectrometer designs and optical components are optimized to reject stray light, which is one of the limiting factors in quantitative absorbance measurements (Pavia *et al.,* 2001).

3.4.10. Total organic carbon analysis (TOC)

Total Organic Carbon (TOC) is a summation of the concentration of all organic carbon atoms covalently bonded in the organic molecules of any given sample of water. The units of measure for TOC are in parts per million (ppm or mg/L). The specific organic contaminants present in a water sample cannot be determined from total organic carbon. Nevertheless, all carbon-bearing molecules present in a water sample can be detected, thus signifying the presence of any organic contaminants, irrespective of molecular make-up. TOC is determined by subtracting the Total Inorganic Carbon from the Total Carbon yields TC. (TC-TIC=TOC). This is termed the difference method, and is commonly used for volatile organic compounds.

Thermal or wet chemical oxidation of organic carbon to carbon dioxide (CO_2) is the basis of all TOC measuring methods. The carbon dioxide is detected and quantitatively evaluated. The expulsion method entails direct determination of TOC after complete expulsion of total inorganic carbon through acidification and purging with carbon-free air prior to measurement.

3.4.11. Liquid chromatography-mass spectrometry (LC-MS)

Liquid chromatography-mass spectrometry (LC-MS, or alternatively HPLC-MS) is a separation method that combines the physical separation capabilities of liquid chromatography (or HPLC) with the mass analysis capabilities of mass spectrometry. Liquid chromatography (LC) in simpler terms can be defined as the separation of components of a mixture based upon the rates at which they elute from a stationary phase over a mobile phase gradient. Separation results from the differing affinities of the mixtures components for the stationary and mobile phases, since particular components will have a greater attraction to the mobile phase and will elute quickly whilst others will be retained by the stationary phase for longer and hence elute much slower (Agilent technologies, 2013; Thurman and Ferrer, 2003). Mass spectrometers can be used as liquid chromatography detectors. Mass spectrometers generate three-dimensional data, and in addition to signal strength, they generate mass spectral data that can provide valuable information about the molecular weight, structure, identity, quantity, and purity of a sample. Mass spectral data add specificity that increases confidence in the results of both qualitative and quantitative analyses (Allwood and Goodacre, 2010; Murray, 1997).

3.5. Evaluation procedures and instrument set-up

3.5.1. Photo-degradation experiments

Photo-degradation experiments were carried out under strict UV_{366} and sunlight. Figure 3.5 shows the experimental set-up used for strict UV_{366} light experiments carried out in a darkroom.

Figure 3.5: Photo-degradation set-up under strict UV light at 25 ˚C and natural pH

All the photo-degradation experiments consisted of a control which contained a membrane disk (A = 28.3 cm^2) without N-TiO_2. The control was exposed to similar conditions as other reaction vessels. To each reaction vessel, 100 mL of organic pollutant with a concentration of 10 ppm were added. Two sets of experiments were carried out in triplicate, one under strict

UV_{366} light and the other sunlight for each of the three herbicides (bentazon, atrazine and paraquat). All experiments were carried out at natural pH and a temperature of 25 ˚C except in the cases where the effect of pH was investigated. Aliquots were collected at 20 minute intervals for a period of 2hrs 20 minutes. Changes in concentration of were followed by UV/ Vis spectroscopy. The effect of N-TiO_2 photo-catalyst loading was investigated using PAN, PVDF and PMAA-g-PVDF/ PAN membranes blended with 1 to 5 % N-TiO_2 during preparation. Table 4 shows the actual photo-catalyst loadings for each membrane type used.

Table 4: membrane type and photo-catalyst loading

Membrane type	Photo-catalyst loading (g/ L)
PAN, PVDF, and PMAA-g-PVDF/ PAN	0
1%N-TiO_2-(PAN, PVDF, PMAA-g-PVDF/ PAN)	0.6
3%N-TiO_2-(PAN, PVDF, PMAA-g-PVDF/ PAN)	1.8
5%N-TiO_2-(PAN, PVDF, PMAA-g-PVDF/ PAN)	3.0

3.5.2. Ozonolysis

Ozonolysis experiments were carried out on the degradation of the three herbicides bentazon, atrazine and paraquat. The experimental set-up is shown in Figure 3.6. Ozone was supplied at a flow rate of 25 L/ min and concentration of 4 g/ hr for all ozonolysis experiments. All the experiments were carried out in triplicate. Aliquots were collected every 5 minutes for a

period of 35 minutes. The changes in concentration of herbicides over time were followed by UV-VIS spectroscopy. The control of the experiment was kept in darkness and without ozone supply. All experiments for non-determination of the effect of pH were carried out at natural pH and a temperature of 25 ˚C.

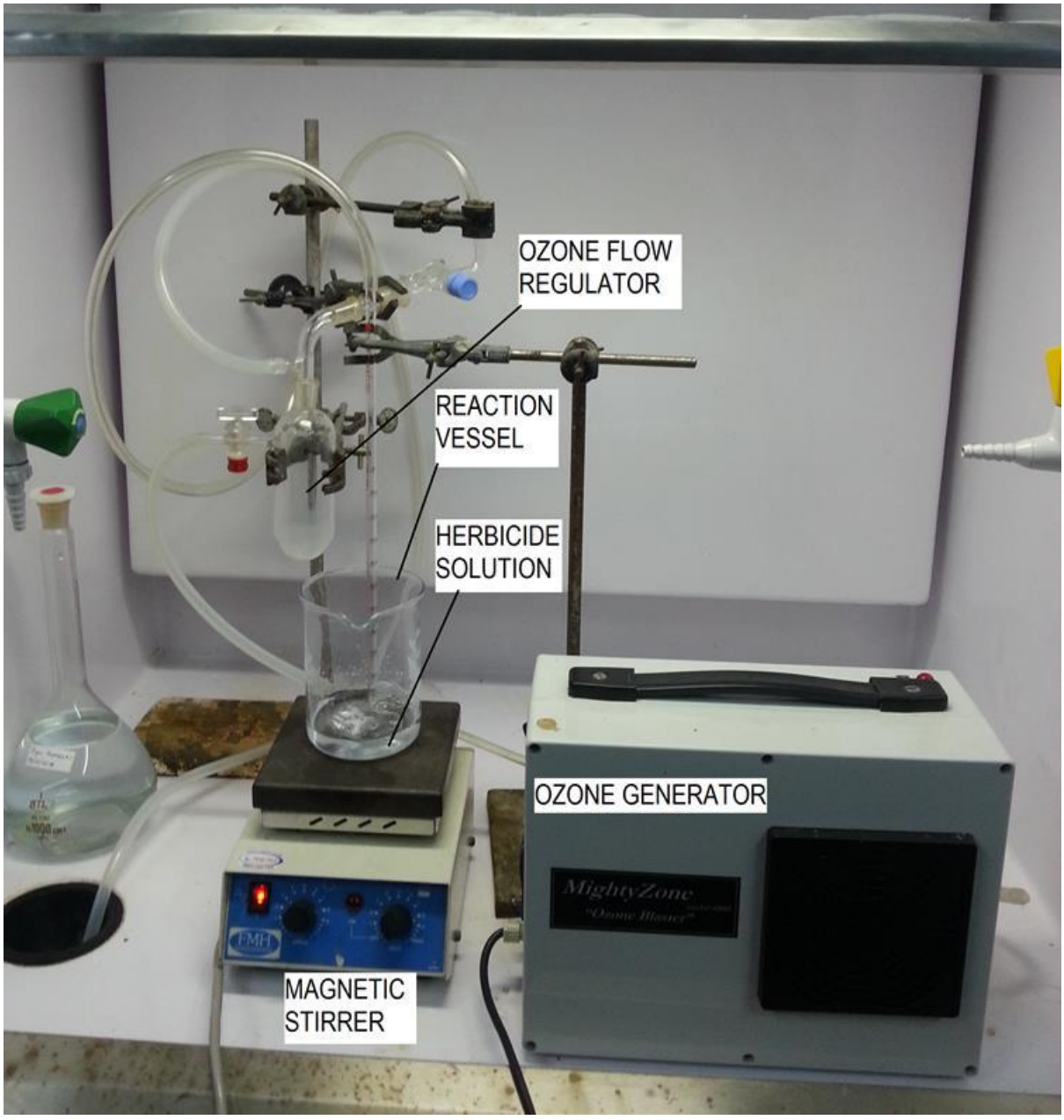

Figure 3.6: Experimental set-up for ozonolysis of herbicides at 25 ˚C and natural pH

Another set of experiments were carried out using all the prepared photo-catalytic membranes in combination with ozone under sunlight. The experimental set-up in figure 3.6 was used except that the experiments were carried out under solar irradiation.

3.5.3. Removal of heavy metals

The experimental set-up for heavy metal (Pb^{2+} and Fe^{3+}) removal was similar to the one used for organic pollutant degradation (sub-section 3.5.1). After establishing the optimum amount of N-TiO_2 photo-catalyst (sub-section 6.2.2) that can be loaded onto the membranes, heavy metal removal experiments were only carried out with PAN, PVDF, and PMAA-g-PVDF/ PAN membranes blended with 1 and 3 % N-TiO_2 photo-catalyst. The heavy metal removal experiments were carried out under sunlight using 100 mL of 10 ppm Pb^{2+} or Fe^{3+} solutions. Aliquots were collected at 60 minutes intervals for a period of 6 hours and changes in heavy metal concentration were followed by AAS spectroscopy. The control of the experiment utilized a membrane (PAN, PVDF and PMAA-g-PVDF/ PAN) disk without N-TiO_2, but exposed to similar conditions with other reaction vessels. All experiments for non-determination of the effects of pH were carried out at natural pH.

3.5.4. Antimicrobial experiments

All antimicrobial experiments were carried out under visible light irradiation. The evaluation of antimicrobial activity was carried out using sterilized 90 mm petri dishes. Evaluation was carried out on (1 % and 3 % N-TiO_2) nitrogen doped titanium dioxide supported on PVDF, PMAA-g-PVDF/ PAN and PAN membranes. A total of six membranes were evaluated. Each membrane was cut into a disc (Area = 28.3 cm^2) and placed into a sterilized 90 mm petri dish. Twenty millilitres of autoclaved nutrient broth were added to each of the petri dishes holding the membranes. *E. coli* ATCC 8739 (0.1 mL) were then inoculated into each petri dish while

stirring to homogenize. All the petri dishes were covered and then exposed to sunlight to allow activation of the nitrogen doped titanium dioxide (N-TiO_2). The control of the experiment involved the use of the three membranes without any N-TiO_2 on them. These three vessels were also inoculated with 0.1 mL of *E. coli* ATCC 8739 and exposed to the same conditions as the other petri dishes. Every 30 minutes swabs were taken from each reaction vessel and placed on the freshly prepared nutrient agar plates. The set up was left for 3 hours and results collected in duplicate. All the plates were labelled and then placed in a Cocono incubator operating at 37 ˚C for 24 hours. The experimental set-up is shown in figure 3.7.

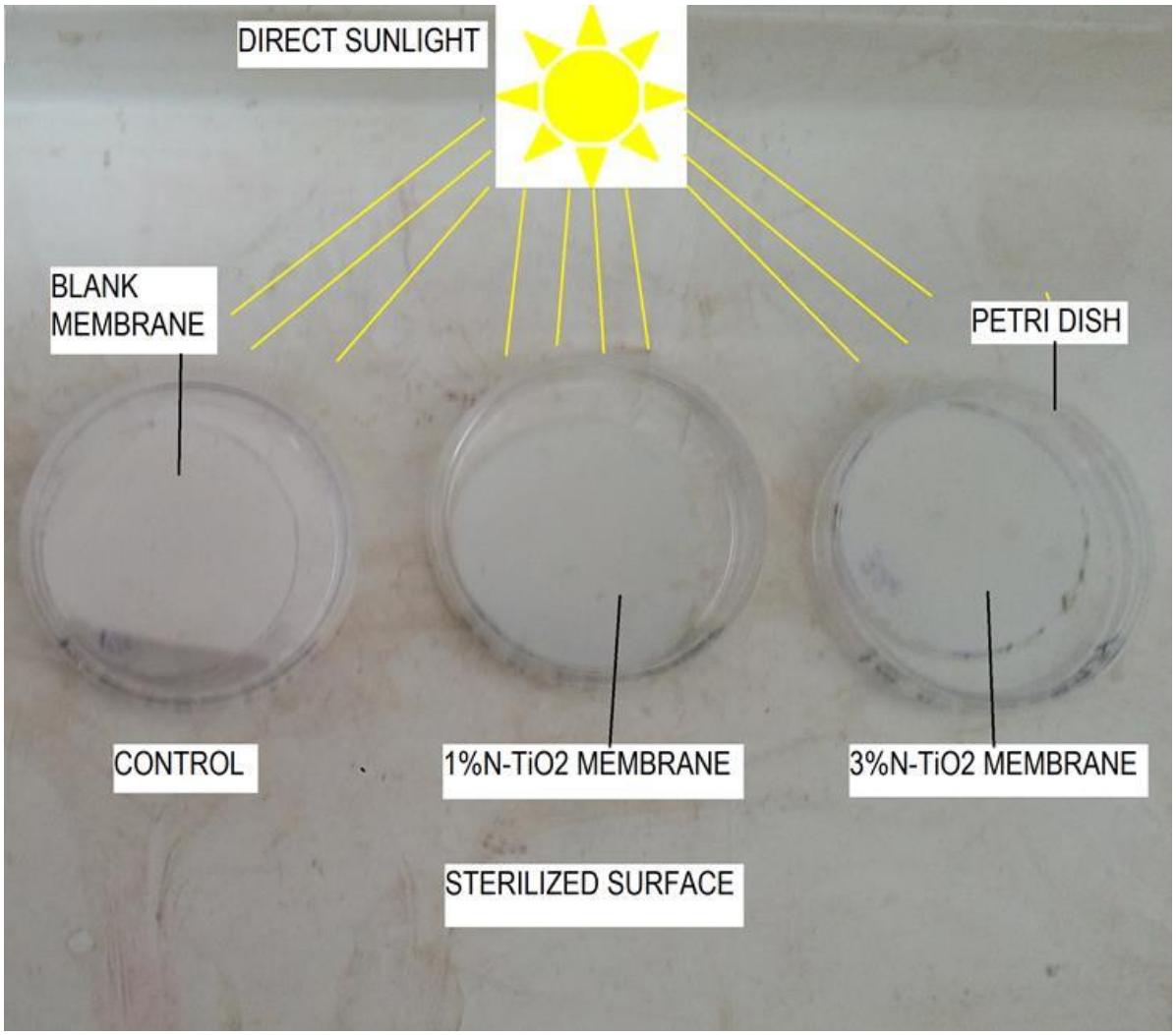

Figure 3.7: Experimental set-up for antimicrobial tests at ambient temperature

3.5.5. Antifouling experiments

The protein adsorption resistance of the N-TiO_2 modified asymmetric membranes of PAN, PVDF, and PMAA-g-PVDF/ PAN was investigated by carrying out pure water filtration tests as well BSA filtration tests. The filtration experiments were carried out using a home-made set-up consisting of a filtration cell with a perforated surface that supports a disk shaped membrane (6 cm diameter) with area 28.3 cm^2, a pressure gauge, and a vacuum pump. The filtration cell used was a dead end filtration cell, with graduations to allow measurement of permeate volume. The feed solution was continuously stirred, with a constant temperature of 25 ˚C. The filtration pressure was maintained at 96 KPa for all the experiments carried out. The membrane was fixed in place and reservoir filled with deionized water. Figure 3.8 shows the experimental set-up used.

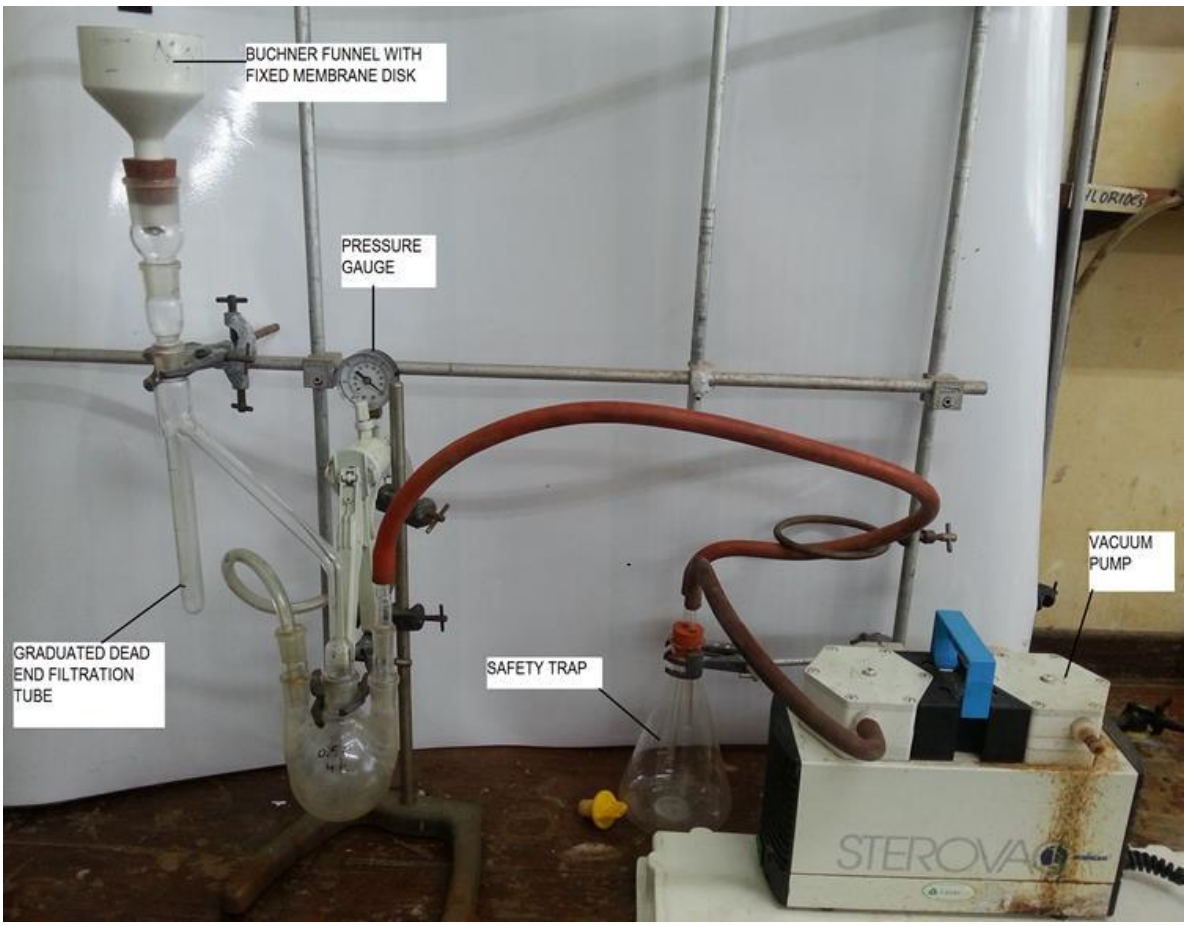

Figure 3.8: Filtration experiments set-up at a pressure of 96 KPa

Bibliography

Abragam A. Principles of Nuclear Magnetic Resonance: Cambridge University Press: Cambridge, UK **(1968)**.

Agilent technologies, Basics of LC/ MS, 2001. http://ccc.chem.pitt.edu. Accessed **(08-07-2013)**.

Allwood J.W., and Goodacre R. *Phytochemical Analysis*: 21 **(2010)** 33-47.

Amand L.E., Tullin C.J. The theory behind FT-IR analysis: Chalmers University of Technology, Sweden, **(2013)** 2-14.

An Introduction to SEMs, Northern California Nanotechnology Centre, UC Davies, http://ncnc.engineering.ucdavis.edu/pages/equipment/Introduction_to_SEM.pdf. Accessed **(03-07-2013)**.

Atkins P., and De Paula J. Physical Chemistry, 8th ed. Oxford University Press: Oxford, UK **(2006)**.

Authier A. Dynamical Theory of X-Ray Diffraction, 1st ed. Oxford University Press: Oxford, UK (2001).

Brunauer S., Emmett P.H., and Teller E. *Journal of the American Chemical Society*: 60 **(1938)** 309-319.

Coats A.W. and Redfern J.P. "Thermo gravimetric Analysis: A Review". *Analyst*: 88 **(1963)** 906-924.

Components of an FT-IR spectrometer, Thermo Nicolet FT-IR, Miramar College http://faculty.sdmiramar.edu/fgarces/LabMatters/Instruments/FTIR/FTIR.htm. Accessed **(01-06-2013)**.

Cruichshank D.W.J., Juretschke H.J., and Kato N. Ewald P.P. and His Dynamical Theory of X-ray Diffraction, 1st ed. International Union of Crystallography, **(1992)**.

Fadley C.S. *Journal of Electron Spectroscopy and Related Phenomena*: 178-179 **(2010)** 2-32.

Hofmann S. Auger- and X-Ray Photoelectron Spectroscopy in Materials Science, *Springer Series in Surface Sciences*, Springer-Verlag Berlin Heidelberg **(2013)** 1-4.

Holmes D. Basic practical NMR concepts: A guide for the modern laboratory, **(2012)** 2-38.

Jensen H.W.*A practical model for subsurface light transport, in "Proceedings of ACM SIGGRAPH."* **(2001)** 511-518.

Macomber R.S. NMR spectroscopy, basic principles and applications, **(2004)** 10-50.

McMillan W.G., and Teller E. *Journal of Physical Chemistry*: 55 (1) **(1951)** 17-20.

McNaught A.D., and Wilkinson A. Compendium of Chemical Terminology, 2nd ed, Blackwell Scientific Publications, Oxford **(1997)**.

Murray K.K. "Coupling matrix-assisted laser desorption/ ionization to liquid separations". *Mass Spectrometry Reviews* 16 (5) **(1997)** 283.

Owen T. Fundamentals of UV-visible spectroscopy, Copyright Hewlett-Packard Company, Germany **(1996)** 9-17.

Pavia D.L., Lampman G.M., and Kriz G.S. Introduction to spectroscopy: A guide for students of organic chemistry, 3rd ed. *Thomson Learning, Inc*, **(2001)** 14-24, 353-358.

Pergamon S.W. Introduction to Electron Microscopy, 1st ed. **(1962)**.

Reusch W. Basic UV-Vis Theory, Concepts and Applications, Michigan State University, **(2013)**.

Roberts, C.A., Workman, J., and Reeves III, J.B. Near infrared spectrophotometers. In: Near-Infrared Spectroscopy in Agriculture. *American Society for Agronomy Inc*., Madison WI, **(2004)** 11-31.

Scott M.J. *Photoelectric sensors and controls: selection and application*. CRC Press. **(1988)** 29.

Skoog D.A., Holler J.F., and Crouch S.R. Principles of instrumental analysis, 6th ed, Thomson Brooks/Cole, Belmont, CA, **(2007)**.

Thurman E.M., and Ferrer I. Liquid chromatography/mass spectrometry, MS/MS and time of flight MS: Columbus, OH: *American Chemical Society* **(2003)**.

University of Colorado, Boulder, Chemistry and Biochemistry Department, 2011. http://orgchem.colorado.edu/Spectroscopy/nmrtheory/NMRtutorial.html. Accessed **(02-07-2013)**.

Voutou B., and Stefanaki E.C. *Physics of Advanced Materials Winter School*, **(2008)** 1-4.

Wagner J.M. X-Ray Photoelectron Spectroscopy, Nova Science Publishers, Incorporated, **(2011)**.

Wells O.C. Scanning Electron Microscopy, 1st ed. McGraw Hill, **(1974)**.

www.uksaf.org/tech/edx.html (Accessed **03-07-2013**).

CHAPTER 4

4. Preparation and characterization of nitrogen doped titanium dioxide

4.1. Introduction

This chapter is about the preparation of nitrogen doped titanium dioxide (N-TiO_2). In an attempt to shift the absorption band edge of titanium dioxide (TiO_2) into the visible region to enhance photo-catalytic activity, N-TiO_2 was prepared via sol gel synthesis. The sol gel process is a hydrolysis and condensation technique used in the preparation of metal oxides and other materials starting from a chemical solution (Silva and Faria, 2009; Xu *et al.,* 2006). The appropriate amount of dopant is added during the hydrolysis process.

Optimum doping conditions as used by (Mungondori and Tichagwa, 2013; Nyamukamba *et al.,* 2012), were employed in the preparation of the nitrogen doped titanium dioxide nano-particles. The type of doping is substitutional, where nitrogen atoms replace some of the lattice oxygen atoms (Ksibi *et al.,* 2008; Yuan *et al.,* 2006; Kobayakawa *et al.,* 2005). Nosaka *et al.,* 2005 carried out nitrogen doping using urea and guanidine as nitrogen sources. Nolan *et al.,* 2011 also managed to prepare N-TiO_2 via sol gel using 1, 3-diaminopropane as a nitrogen source. The problem associated with such kind of dopants is the possibility of having a co-doped product, whereby carbon may also be incorporated into the lattice structure. In the current work ammonia was used as the nitrogen source to avoid producing a co-doped product. This allows for an effective assessment of the changes in the spectral response brought about in titanium dioxide by nitrogen doping.

4.2. Methodology

4.2.1. Preparation of nitrogen doped titanium dioxide

Nitrogen modified titanium dioxide nano-particles were obtained by hydrolysis of titanium tetrachloride, followed by heating, drying and calcination after addition of an appropriate amount of dopant (Fig. 4.1). In a typical experiment, titanium tetrachloride ($TiCl_4$) (98 % Merck) was added drop wise to deionized water in a beaker on an ice-bath under rigorous stirring. Ammonia solution (25 % MET-U-ED) was added as the nitrogen source, followed by heating on a hot plate at 90 ˚C for 10 minutes under stirring. The resulting precipitate was collected via centrifugation and washed three times with deionized water before drying at 60 ˚C in an oven.

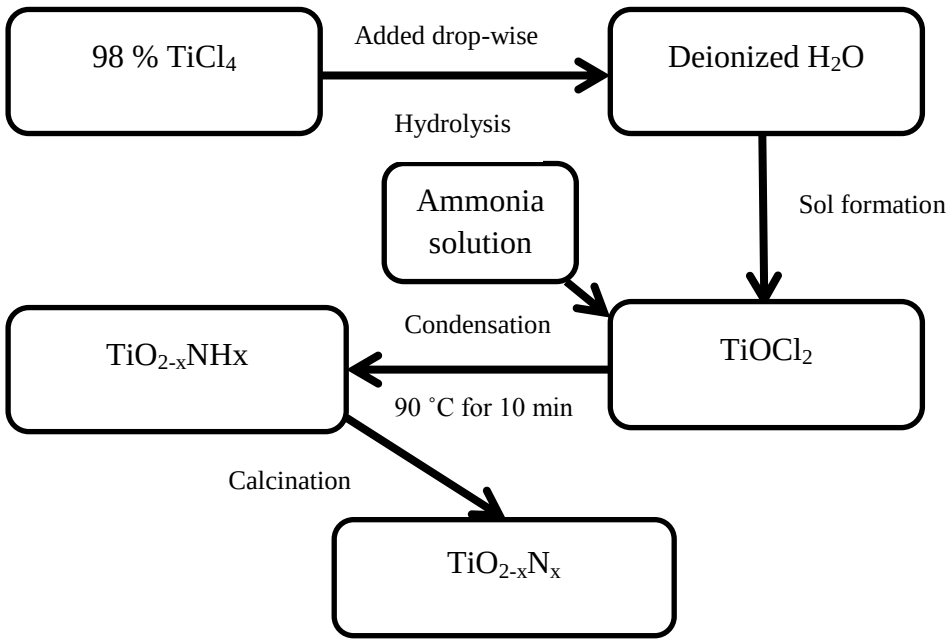

Figure 4.1: Flow diagram for the sol gel preparation of N-TiO_2

4.2.2. Calcination of nitrogen doped titanium dioxide ($TiO_{2-x}N_x$)

The dried powder was calcined at 500 ˚C under nitrogen atmosphere for 2 hours to allow the transformation from the amorphous phase of TiO_2 to predominantly anatase titanium dioxide (Nolan *et al.,* 2011; Cui *et al.,* 2010; Nosaka *et al.,* 2005) which is most photo-catalytically active. A programmable furnace shown in Fig. 4.2 was used for the calcination process. Heat was supplied at a rate of 10 ˚C/ min. Calcination also improves crystallinity which enhances photo-catalytic properties of TiO_2 (Zhang *et al.,* 2003).

Figure 4.2: Programmable furnace used in the calcination of TiO_2 and N-TiO_2

4.2.3. Preparation of undoped TiO_2

Undoped titanium dioxide nano-particles were also prepared via the sol gel synthesis method. The procedures employed were similar to those used in the preparation of N-TiO_2, except for

the exclusion of a dopant. The undoped titanium dioxide was necessary for comparison purposes with nitrogen doped titanium dioxide.

4.3. Characterization

Infrared spectra of N-TiO_2 and TiO_2 were recorded using PerkinElmer System 2000 FTIR. 1.0 mg of sample was properly mixed with 100 mg of potassium bromide (KBr) and then ground thoroughly using mortar and pestle. An adequate amount of the ground sample was pelletized using a hydraulic pelletizer to give a transparent pellet, and then the samples were run against an air background. Eight scans were carried out for each sample in the wavenumber range 4000 cm^{-1} to 370 cm^{-1} with a resolution of 4 cm^{-1}.

X-ray photo-electron spectra of N-TiO_2 were obtained using a Physical Electronics Quantum2000 spectrometer with an x-ray power of 25 W, and supplying Al Kα x-rays. The x-ray beam had a diameter of 100 μm, pass energies of 117.4 eV (wide) and 29.35 (narrow). The analyses were carried out at an ambient temperature of 20 °C ± 5 °C and a relative humidity of 50 % RH ± 25 % RH. The N-TiO_2 sample was analysed at the National Metrology Institute of South Africa (NMISA) in Pretoria by irradiating the surface of the powders with x-rays in order to extract photo-electrons. The binding energies of the extracted electrons were determined from knowing the energy of the x-ray photons and measuring the kinetic energies of the extracted electrons. This quantity is unique and can be used to identify the elements from which the electrons were extracted.

X-ray diffractograms of N-TiO_2 and TiO_2 were obtained using a Bruker-AXS D8 Advance diffractometer (Cu Kα radiation with λ = 1.5406 Å) equipped with a PSD Lynx-Eye Si-strip detector (with 196 channels), at room temperature. This technique allowed for crystal phase

identification and estimation of crystallite size. The x-ray diffraction analysis was carried out in locked couple mode with an accelerating voltage 40 kV and applied current of 40 mA. Brunaur-Emmett-Teller (BET) surface area of N-TiO_2 and TiO_2 was determined using a Micromeritics Pulse Chemisorb 2700 nitrogen adsorption apparatus. Samples were dried in a helium gas flow at 250 ˚C and the surface area of the samples determined by N_2 chemisorption. Diffuse reflectance spectra (DRS) of N-TiO_2 and TiO_2 were acquired in the 200-800 nm range using a Cary 500 UV-Vis-NIR spectrophotometer. The spectra enabled determination of the shift in the absorption band edge of N-TiO_2.

Transmission electron micrographs of N-TiO_2 and TiO_2 were recorded on a JEM 200CX transmission electron microscope (JEOL, Tokyo, Japan) at an accelerating voltage of 120 kV. The TEM microscopy allowed detailed micro-structural examination and crystal structure composition investigation of the N-TiO_2 and TiO_2 nano-particles.

4.4. Results and Discussion

4.4.1. FT-IR analysis of N-TiO_2 and TiO_2

Fourier transform infrared spectroscopy (FT-IR) was used to identify the functional groups in nitrogen doped titanium dioxide and titanium dioxide. The broad peak located between 800 cm^{-1} and 400 cm^{-1} in unmodified TiO_2 is due to Ti-O stretching vibrations as seen in Fig. 4.3. Other researchers also observed similar results (Chainarong *et al.,* 2011; Beranek and Kisch, 2008). The presence of the anatase phase of titanium dioxide was identified by the valley around 480 cm^{-1} in the FT-IR spectra obtained for N-TiO_2 and TiO_2. The other labelled peaks can be ascribed to OH stretching vibrations (around 3415 cm^{-1}), OH bending vibrations 1636 cm^{-1}, and O-Ti-N stretching vibrations around 627 cm^{-1}. Etacheri *et al.,* 2010, from their

findings reported that the spectra they obtained were highly dependent on the processing temperature. They observed a shift to higher energies for the Ti-O-Ti stretching energies for unmodified TiO_2. In nitrogen doped TiO_2 stretching and deformation vibrations of NH_x groups overlap with broad bands for OH groups located between 3700-3100 cm^{-1} and 1700-1500 cm^{-1}. FT-IR analysis managed to confirm successful preparation of N-TiO_2 and TiO_2. The formation of N-T-O was also confirmed via SXPS, and the results will be discussed in the relevant section.

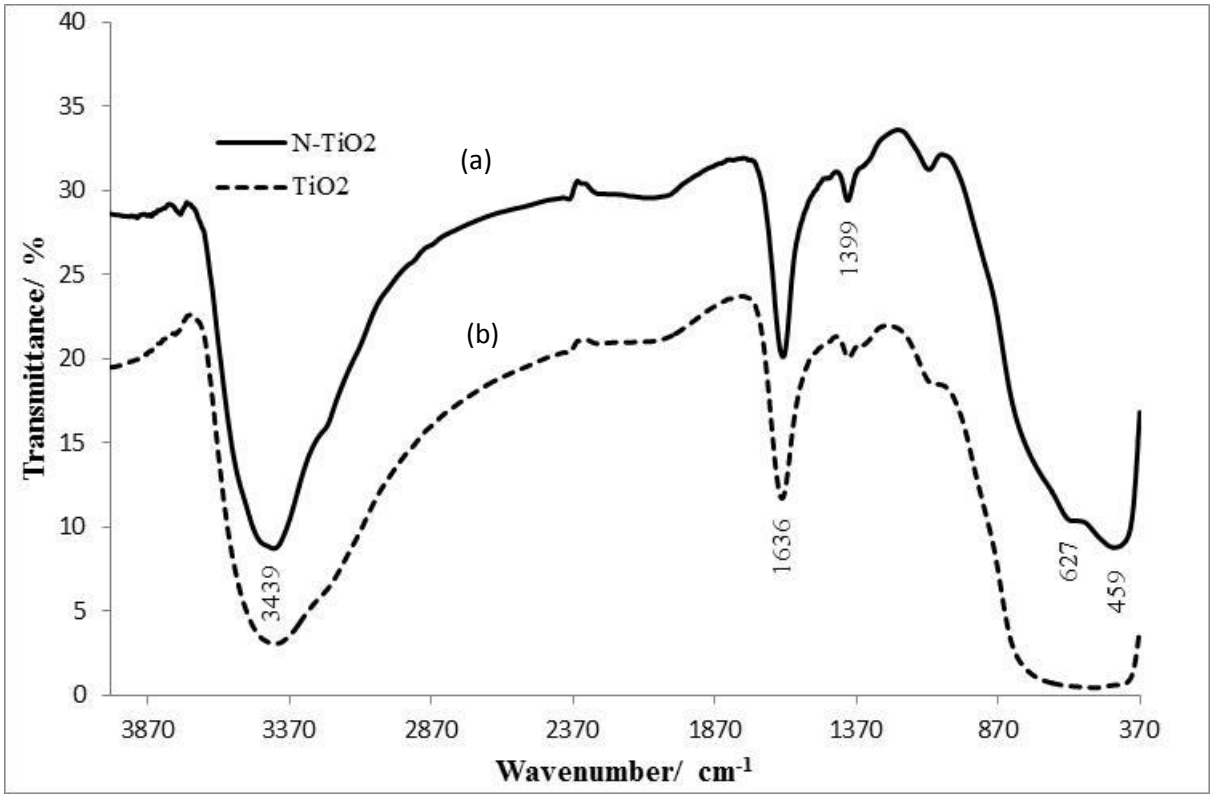

Figure 4.3: FT-IR spectra of (a) N-TiO_2 and (b) TiO_2 calcined at 550 ˚C

4.4.2. SXPS analysis of N-TiO_2

Scanning X-ray photoelectron spectroscopy (SXPS) was carried out on the N-TiO_2 to identify the elements present from their unique binding energies as shown in Fig 4.4. SXPS analysis revealed the presence of O-T-N, which is a kind of doping whereby nitrogen atoms replace

some of the lattice oxygen atoms. The N1s (Fig. 4.5) had a binding energy of 397.3 eV, which is in close agreement with the typical N1s binding energy of 397.2 eV as reported in literature (Nolan *et al.*, 2012; Guo *et al.*, 2011; Etacheri *et al.*, 2010).

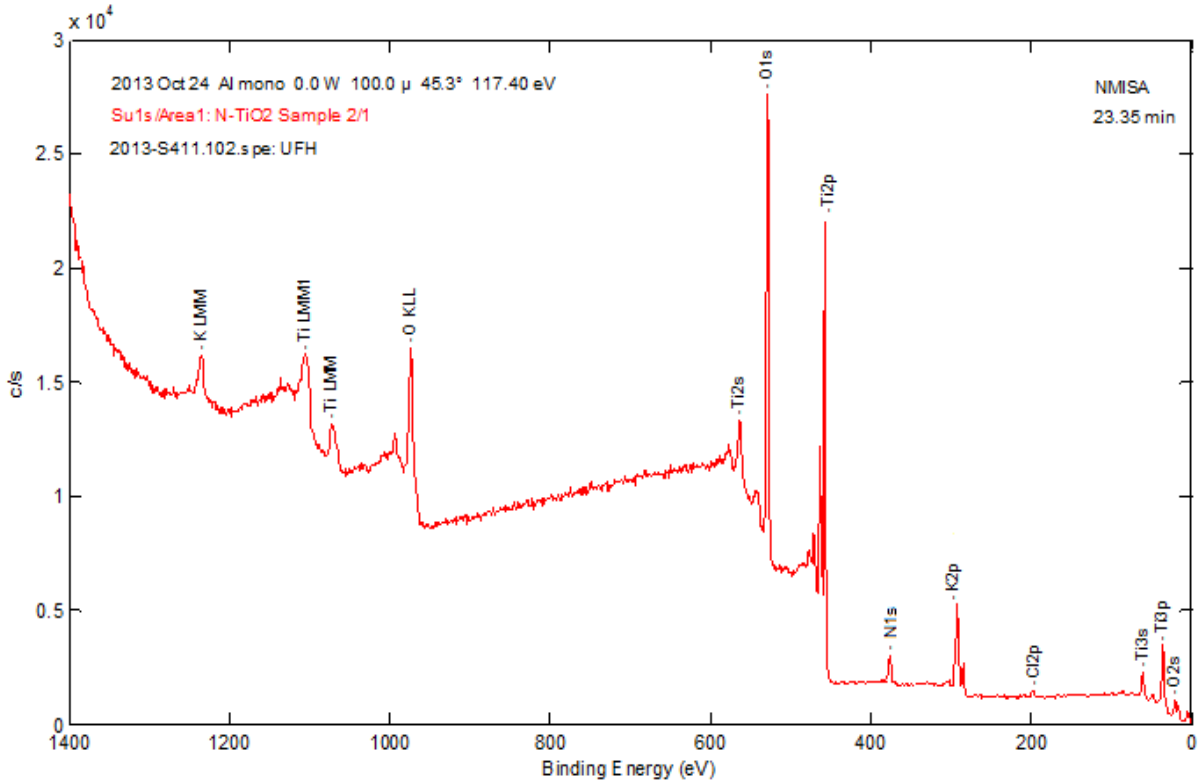

Figure 4.4: XPS spectrum of N-TiO_2 calcined at 550 ˚C

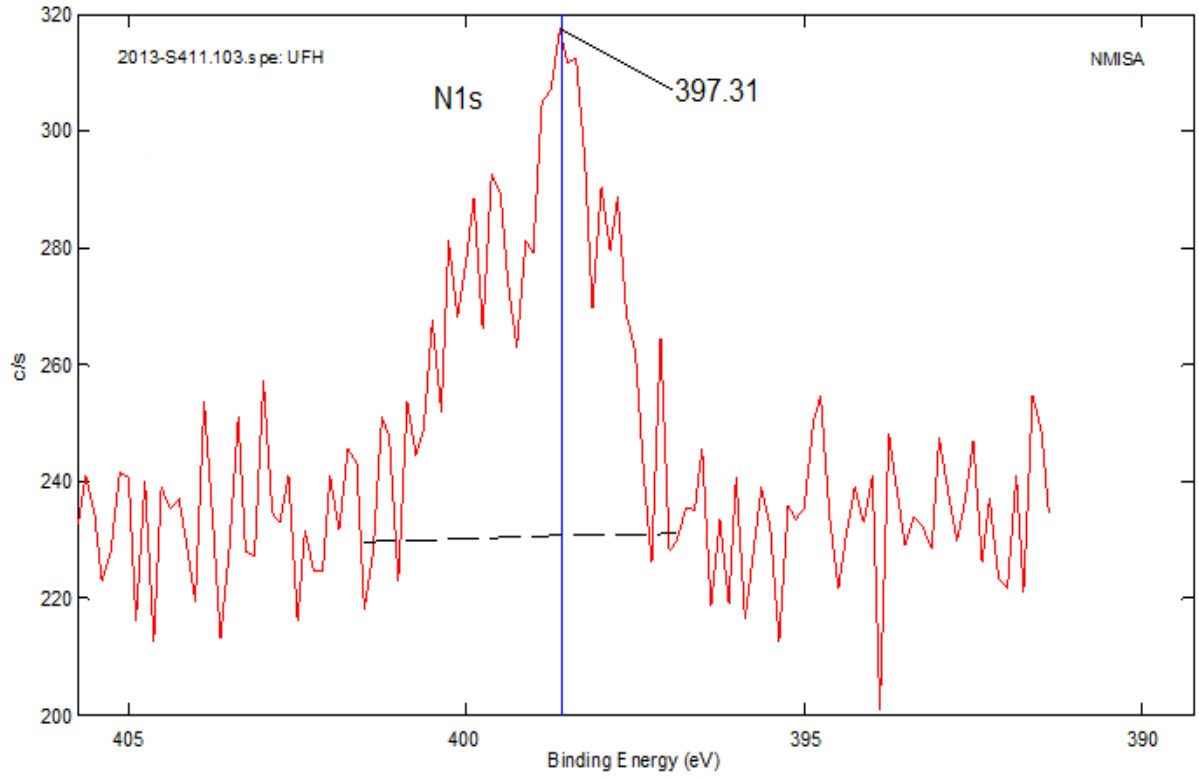

Figure 4.5: N 1s spectrum of N-TiO_2 calcined at 550 ˚C

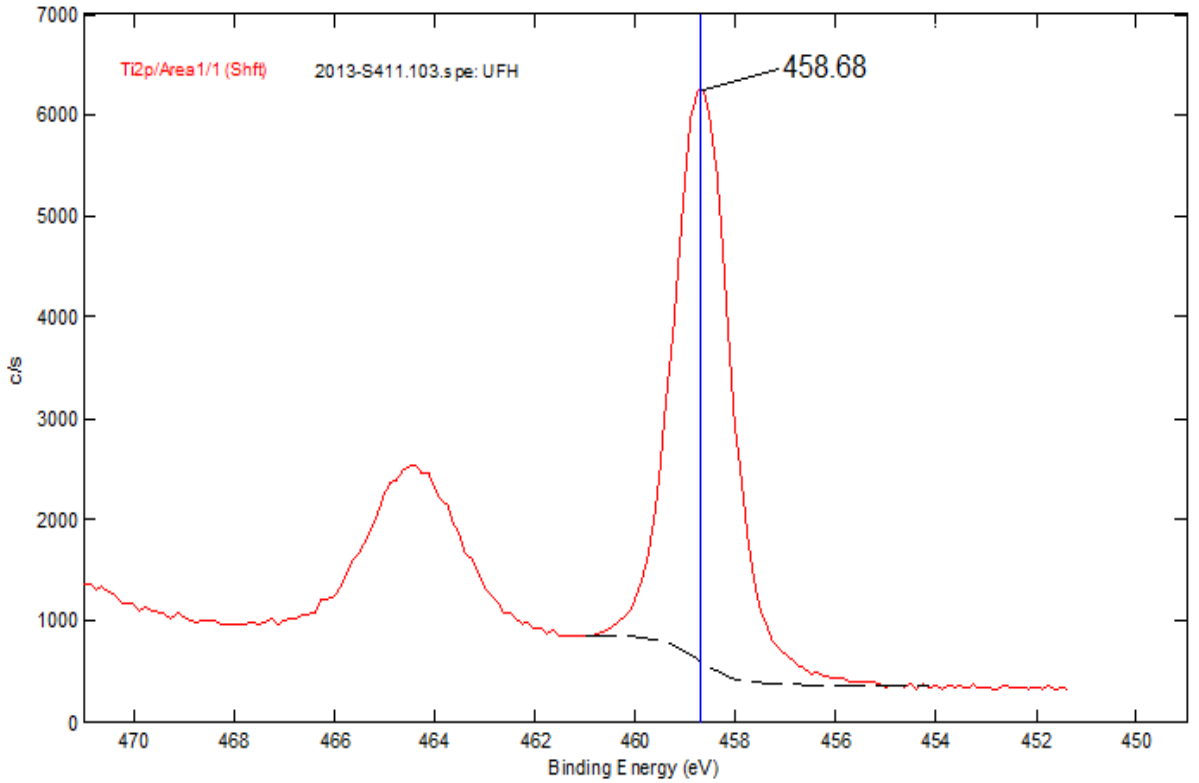

Figure 4.6: Ti2p spectrum for N-TiO_2 calcined at 550 ˚C

It was mentioned by other researchers that the N1s binding energy is highly dependent on the method of preparation, but in general most of the binding energies reported in literature range between 396 eV and 408 eV. Literature also mentions that there is still some controversy in assigning of XPS peaks for nitrogen doped titanium dioxide. Guo *et al.,* 2011 reported that a peak 396.2 eV was attributed to a chemically bound N^- species and a weak peak around 398.3 eV was derived from the presence of the O-Ti-N linkages in the crystalline TiO_2 lattice of their XPS spectra. The T2p core level peak (Fig. 4.6) had a binding energy of 458.6 eV, and this value is in agreement with values reported in literature (Guo *et al.,* 2011). SXPS and FT-IR analyses confirmed the successful preparation of N-TiO_2 nano-particles.

4.4.3. XRD analysis

X-ray diffraction analysis was carried out to identify the phase composition of N-TiO_2 and TiO_2 prepared via sol gel synthesis. Fig 4.7 shows the X-ray diffractograms of N-TiO_2, and TiO_2. The X-ray analysis revealed that the prepared TiO_2 and N-TiO_2 nano-powders were in the anatase phase. Titanium dioxide has three polymorphs; anatase and brookite, stable at low temperatures, and rutile which is stable at high temperatures. The rutile phase of titanium dioxide starts to appear if titanium dioxide powders are calcined beyond 600 ˚C (Nolan *et al.,* 2012; Guo *et al.,* 2011). Literature reports that the anatase phase is the most photo-catalytically active polymorph of titanium dioxide (Carp *et al.,* 2004; Diebold *et al.,* 2003; Hu *et al.,* 2003). Comparison of the two diffractograms clearly shows that there were changes brought about by the introduction of nitrogen into the lattice structure of titanium dioxide. The peak at a 2 theta angle of 25 ˚ is attributed to anatase phase and appears in the spectra of both TiO_2 and N-TiO_2.

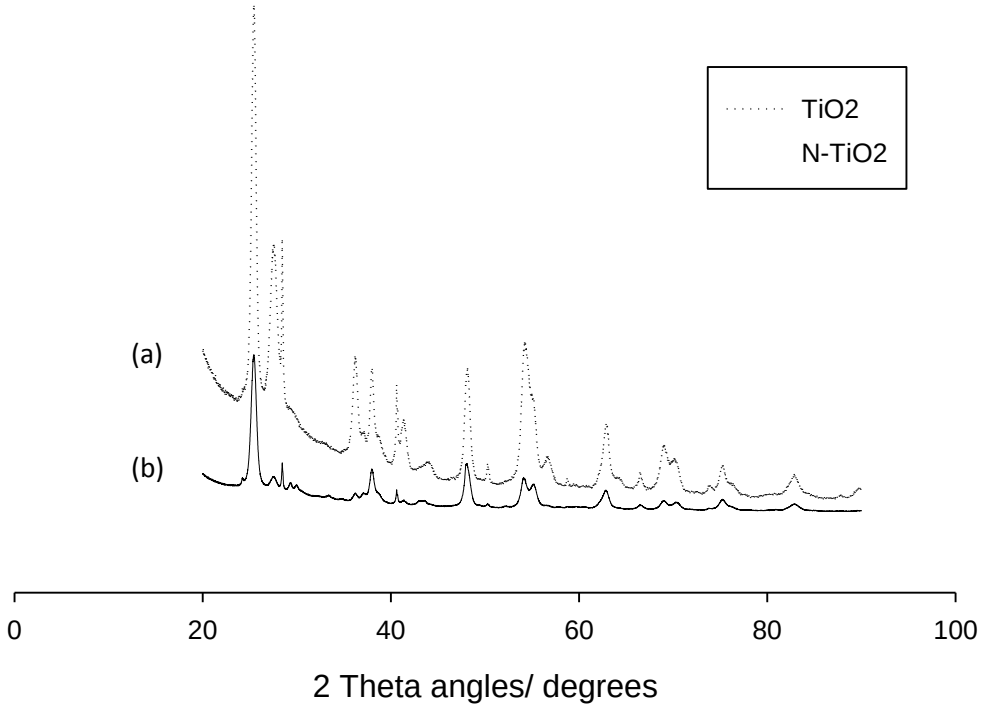

Figure 4.7: X-ray diffractograms of (a) TiO_2 and (b) N-TiO_2 calcined at 550 ˚C

The diffractogram of N-TiO_2 showed peaks at 2 theta angles of 24.2 ˚, 28.6 ˚, 29.3 ˚, and 32.8 ˚, which do not appear in the diffractogram of TiO_2 which suggest that these could be changes brought about by the introduction of nitrogen in the lattice structure of titanium dioxide. The diffractogram of titanium dioxide shows a peak at a 2 theta angle of 55.8 ˚, which has also disappeared in that of N-TiO_2 which is another indication of the changes brought about by doping TiO_2 with nitrogen.

X-ray diffraction analysis also enabled the estimation of the average particle size of TiO_2 and N-TiO_2 through the Scherrer equation. The sizes where calculated by the instrument from the anatase 101 peak which is located at a 2 theta angle of 25 ˚. Titanium dioxide had an average particle size of 16.9 nm while nitrogen doped titanium dioxide had an average particle size of

14.5 nm (Table 5). This clearly shows that replacement of some lattice oxygen atoms with nitrogen atoms allowed a reduction in the particle size of titanium dioxide nanoparticles.

Table 5: XRD particle size for TiO_2 and N-TiO_2 calcined at 550 ˚C

Sample	XRD Particle size (nm)
TiO_2	16.9
N-TiO_2	14.5

4.4.4. BET surface area analysis of TiO_2 and N-TiO_2

BET surface area analysis was used to determine the surface area and pore sizes of TiO_2 and N-TiO_2. Table 6 shows the BET surface areas obtained as well as the pore sizes.

Table 6: BET surface area and pore size of TiO_2 and N-TiO_2 calcined at 550 ˚C

Sample	BET surface area (m^2/g)	Pore size (nm)
TiO_2	283.69	5.2
N-TiO_2	309.77	8.3

The trend observed in BET surface area analysis is an increase in surface area with decrease in particle size. The prepared titanium dioxide (TiO_2) gave a surface area of (283.69 m^2g^{-1}), while nitrogen doped (N-TiO_2) had (309.77 m^2g^{-1}). These results are in agreement with the XRD particle sizes obtained for TiO_2 and N-TiO_2 (Table 5). Pore size of the nanoparticles increased with an increase in surface area. TiO_2 had a pore size of 5.2 nm, while N-TiO_2 had

a pore size of 8.3 nm. Literature reports an average BET surface area of (50 m^2g^{-1}) for commercial titanium dioxide (Degussa P25) (Guo *et al.,* 2011). The nano-powders we prepared had exceptionally high BET surface area mostly because of their small average particle sizes.

4.4.5. Diffuse reflectance spectroscopy (DRS) analysis of TiO_2 and N-TiO_2

Diffuse reflectance spectra of TiO_2 and N-TiO_2 were obtained to evaluate the shift in the absorption band edge of TiO_2 after modification with nitrogen (Fig. 4.8). The trend shown by the diffuse reflectance spectra of titanium dioxide and nitrogen doped titanium dioxide clearly show a shift in the absorption band edge of TiO_2 into the visible region with the replacement of lattice oxygen atoms by nitrogen atoms. Yuan *et al.,* 2006, reported a shift in the absorption band edge of TiO_2 from 388 nm to 600 nm with an increase in the amount of urea (which contains N in addition to C) dopant. In this study the shift in the absorption band edge of TiO_2 was from 364 nm to 402 with the addition of ammonia as the nitrogen source.

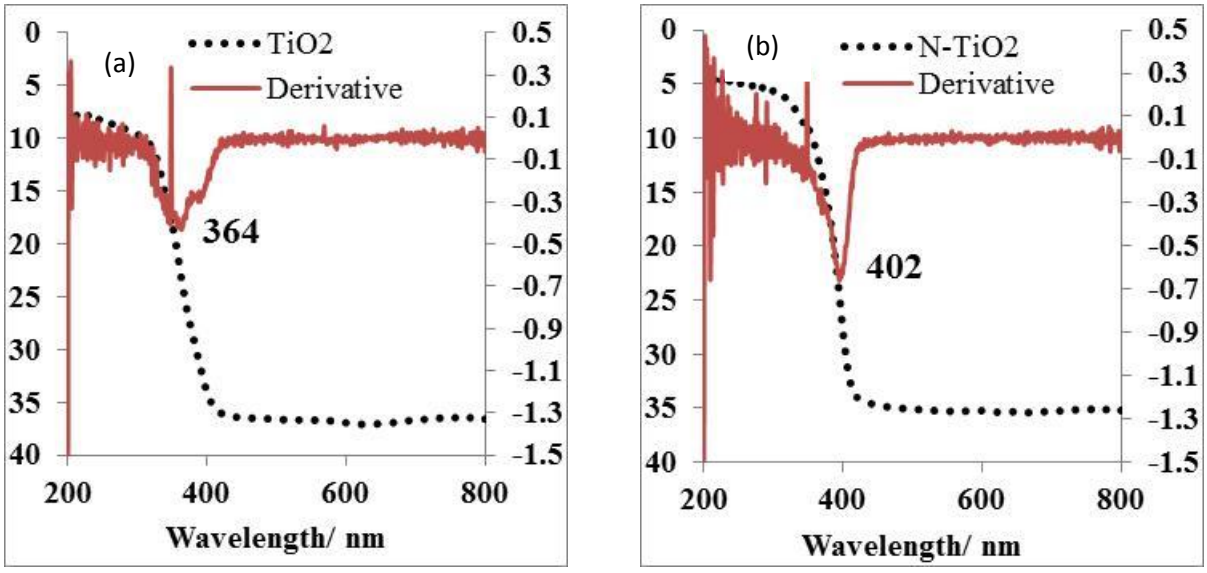

Figure 4.8: DRS (a) TiO_2 and (b) N-TiO_2 calcined at 550 ˚C

Chainarong *et al.,* 2011, also reported high visible light absorption for N-TiO_2 with an increasing amount of guanidine carbonate dopant. They mentioned that the observed shift into the visible region for N-TiO_2 was due to the introduction of new electronic states above the valence band of TiO_2, which corresponds with other literature (Wu *et al.,* 2008; Valentin *et al.,* 2007; Livraghi *et al.,* 2006; Asahi *et al.,* 2001). The extent of visible light response depends on the amount of dopant added as well as the type of dopant used, but does not necessarily translate into an increased photo-catalytic activity.

The diffuse reflectance data obtained was also used to calculate the band gap energies of TiO_2 and N-TiO_2 using Equation 4.1.

$$Eg = \frac{1239}{\lambda} \quad (4.1)$$

Where Eg is the band gap energy, 1239 is a constant and λ is the wavelength. Titanium dioxide had a band gap energy of 3.40 eV and nitrogen doped titanium dioxide had a band gap energy of 3.08 eV. Literature reports band gap energy of 3.2 eV for anatase titanium dioxide corresponding with wavelengths below 388 nm (Mungondori and Tichagwa, 2013; Nyamukamba *et al.,* 2012; Chainarong *et al.,* 2011; Yuan *et al.,* 2006). After doping titanium dioxide with nitrogen a reduction in band gap was observed (3.08 eV) which brought about the ability for N-TiO_2 to absorb visible light. The band gap energy for titanium dioxide was slightly higher than what is reported in literature, and the reason could be due to differences in the preparation conditions as well precursors.

4.4.6. Transmission electron microscopy (TEM) analysis of TiO_2 and N-TiO_2

Transmission electron microscopy images of TiO_2 and N-TiO_2 were obtained to evaluate the crystal structure composition of the prepared nano-particles. The TEM images obtained are shown in figure 4.9.

(a) 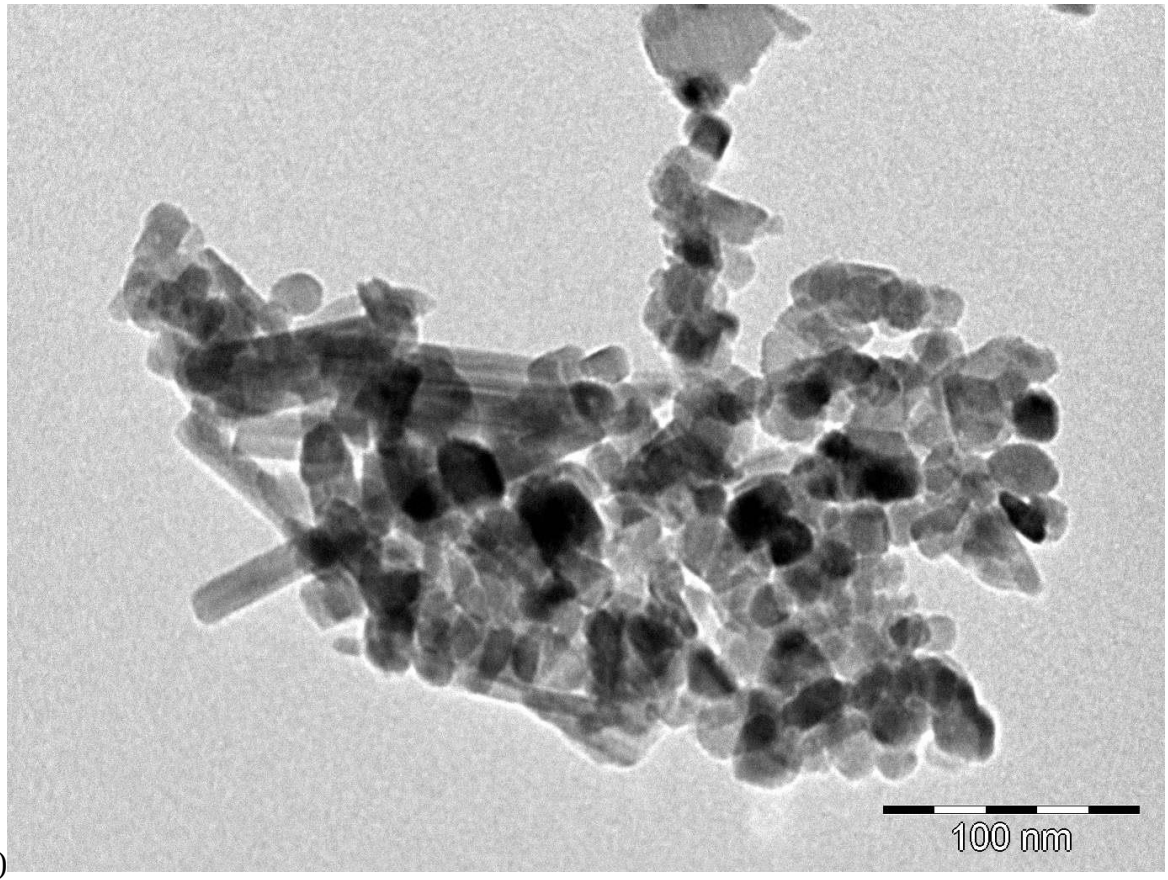

(b) 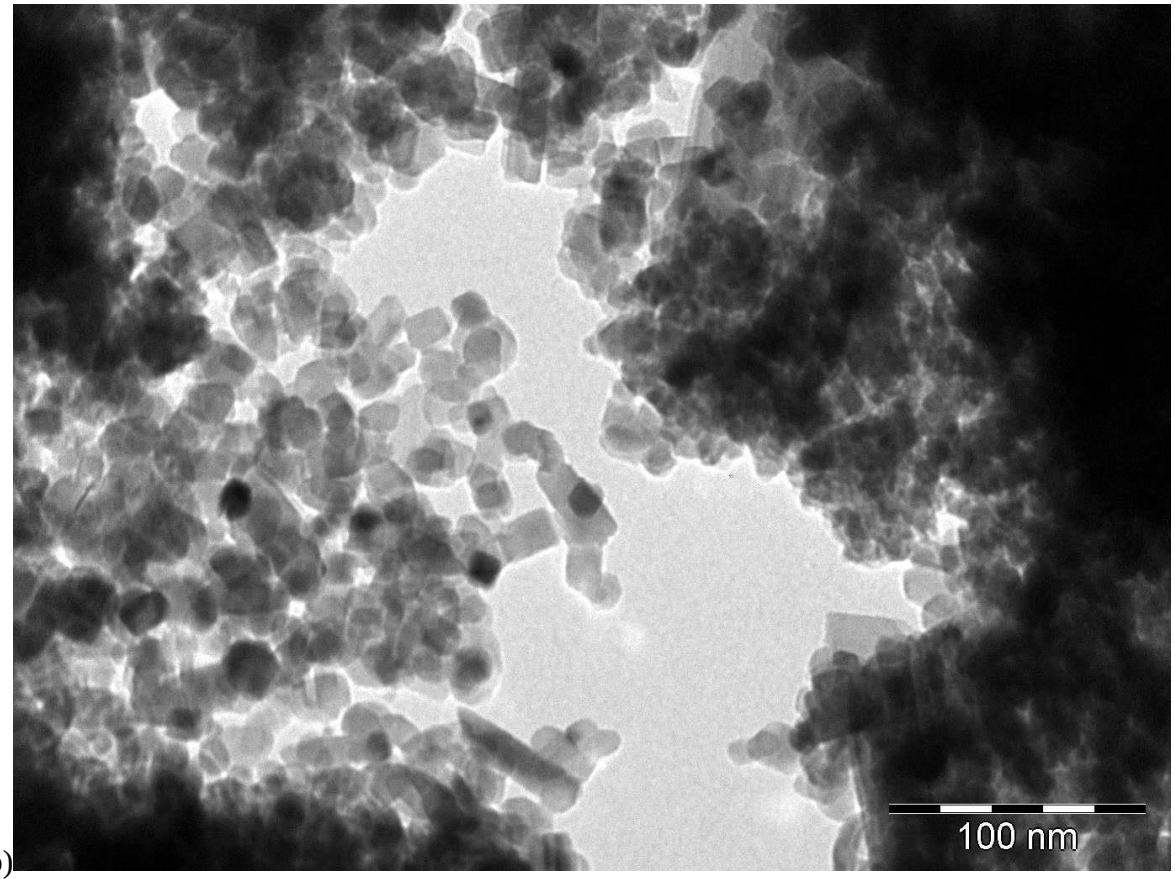

Figure 4.9: TEM images of (a) TiO_2 and (b) N-TiO_2 calcined at 550 ˚C

The images obtained for titanium dioxide nano-particles revealed the existence of some nano-rod-like structures. However the bulk of the nano-particles exhibited an ovoidal to undefined structures. Many of the nano-particles in the TEM image of titanium dioxide appear to be aggregated or in lumps. On average a particle size of 23.08 nm was obtained for the TiO_2 nano-particles. This value for average particle size is much higher than that obtained from XRD particle size estimation (16.9 nm) in section 4.4.3. Nevertheless, these differences in particle size can be expected since estimate results were acquired using different instruments.

Figure 4.9 (b) shows the TEM images obtained for nitrogen doped titanium dioxide nano-particles. The bulk of the N-TiO_2 nano-particles exhibit a rectangular conformation. However, a variation in size of these rectangular shaped nano-particles is clearly observable

from the TEM images. Measurement indicates that the average particle size of the rectangular nano-particles is 15.39 nm. This value is much closer to the XRD estimate particle size (14.5 nm) obtained for N-TiO_2 in section 4.4.3.

4.5. Conclusion

Nitrogen doped titanium dioxide was successfully prepared via sol gel technique and characterized by FT-IR, SXPS, XRD, BET, DRS, and TEM analyses. FT-IR analysis indicated the presence of the necessary functional groups. Elemental composition of the powders was confirmed via scanning x-ray photoelectron spectroscopy and it indicated the presence of Ti, O, and N. Hence the doping process was successful. The nitrogen doped titanium dioxide nano-powders were confirmed to be in the anatase phase via x-ray diffraction analysis. BET surface area analysis revealed that N-TiO_2 had a larger surface area compared to TiO_2 owing to a reduced particle size after doping. The shift in absorption band edge of N-TiO_2 was evaluated by diffuse reflectance spectroscopy which gave an absorption band edge of 402 nm for N-TiO_2 and 364 for TiO_2. The transmission electron microscopy images obtained for nitrogen doped titanium dioxide nano-particles revealed that the N-TiO_2 nano-particles exhibit a rectangular conformation. However, a variation in size of these rectangular shaped nano-particles is clearly observable from the TEM images.

Bibliography

Aguado J., Van Grieken R., Lopez-Munoz M.J., and Marugan J. *Catalysis Today*: 75 **(2002)** 95.

Asahi R., Morikawa T., Ohwaki T., Aoki K., and Tage A. *Science*: 293 (5528) **(2001)** 269-271.

Beranek R., and Kisch H. *Photochemical and Photobiological Science*: 7 **(2008)** 40-48.

Carp O., Huisman C.L., and Reller A. *Progress in Solid State Chemistry*: 32 **(2004)** 33.

Chainarong S., SikongL., Niyomwas S., and Pavasupree S. *9th Eco-Energy and Materials Science and Engineering Symposium*: Chiang Rai, Thailand 25-28 May. **2011**.

Cui L., Huang F., Niu M., Zeng L., Xu J., and Wang Y. *Journal of Molecular Catalysis A*: *Chemical*: 326 **(2010)** 1-7.

Diebold U. *Surface Science Reports*: 48 **(2003)** 53.

Etacheri V., Seery M.K., Hinder S.J., and Pillai S.C. *Chemistry of Materials*: 22 **(2010)** 3843-3853.

Guo W., Miao Q., Xin G., Wu L., and Ma T. *Key Engineering Materials*: 451 **(2011)** 21-27.

Guo W., Shen Y., Boschloo G., Hagfeldt A., and Ma T. *Electrochimica Acta*: 56 **(2011)** 4611-4617.

Hu Y., Tsai H.L., and Huang C.L. *Materials Science and Engineering*: A344 **(2003)** 209.

Kobayakawa K., Murakami Y., and Sato Y. *Journal of Photochemistry and Photobiology A*: Chemistry 170 **(2005)** 177-179.

Ksibi M., Rossignol S., Tatibouët J.M., and Trapalis C. *Materials Letters*: 62 **(2008)** 4204-4206.

Livraghi S., Paganini M.C., Giamello E., Selloni A.; Valentin, C.D., and Pacchioni G. *Journal of the American Chemical Society*: 128 (49) **(2006)** 15666-15671.

Mungondori H., and Tichagwa L. *Materials Science Forum*: Vol. 734 **(2013)** 226-236.

Nolan N.T., Synnott D.W., Seery M.K., Hinder S.J., Wassenhoven A.V., and Pillai S.C. *Journal of Hazardous Materials*: **(2012)** 88-94.

Nosaka Y., Matsushita M., Nishino J., and Nosaka A.Y. *Science and Technology of Advanced Materials*: 6 **(2005)** 143-148.

Nyamukamba P., Tichagwa L., and Greying C. *Materials Science Forum*. 712 **(2012)** 49-63.

Silva C.G., and Faria J.L. *Journal of Molecular Catalysis A*: *Chemical*: 305 **(2009)** 147-154.

Valentin C.D., Finazzi E., Pacchioni, G., Selloni A., Livraghi S., Paganini M.C., and Giamello E. *Chemical Physics*: 339 (1-3) **(2007)** 44-56.

Wu Z., Dong F., Zhao W., and Guo S. *Journal of Hazardous Materials*: 157(1) **(2008)** 57-63.

Xu C., Killmeyer R., Gray M.L., Khan S.U.M. *Applied Catalysis B*: *Environmental*: 64 **(2006)** 312-317.

Yuan J., Chen M., Shi J., and Shangguan W. *International Journal of Hydrogen Energy*: 31 **(2006)** 1326-1331.

Zhang D.B., Qi L.M., Cheng H.M., and Ma J.M. *Chinese Chemical Letters*: Vol. 14 (1) **(2003)** 100-103.

CHAPTER 5

5. Synthesis of poly (methacrylic acid) grafted onto poly (vinylidene difluoride)/ blended with poly (acrylonitrile) asymmetric membranes (PMAA-g-PVDF/ PAN)

5.1. Introduction

This chapter is about the preparation of polymeric asymmetric membranes of PMAA-g-PVDF, and PAN that will serve as both filtration membranes as well as support for N-TiO_2 photo-catalyst to avoid problems associated with the post recovery of spent photo-catalyst after the photo-degradation of pollutants in water. Asymmetric membranes are of great industrial significance. Poly (vinylidene difluoride) is the most widely employed membrane material owing to its high mechanical strength, excellent chemical resistance, and high operating temperature capabilities. Some of its important uses include processes such as pervaporation, membrane distillation, ion-exchange membranes, ultrafiltration (UF), and microfiltration (MF). Several other polymeric materials have been used as well in the manufacture of synthetic membranes.

Sui *et al.,* 2012, prepared poly (vinylidene difluoride) membranes whose surface was functionalized with 2-hydroxyethyl methacrylate (HEMA) and 2-(dimethylamino) ethyl methacrylate (DMAEMA), in a bid to improve antifouling and antibacterial properties. Hashim and co-workers, 2009, used a simplified method for preparation of hydrophilic PVDF membranes from an amphiphilic graft copolymer to try and improve water flux through the membrane. Adout *et al.,* 2010, prepared a novel poly (acrylonitrile) (PAN) ultrafiltration

membrane incorporating the amphiphilic comb copolymer additive, poly (acrylonitrile)-graft-poly (ethylene oxide) (PAN-*g*-PEO). Their membrane was capable of preventing adhesion of bacteria (*E. coli* K12) unlike unmodified commercial PAN membrane.

In this current work, asymmetric membranes of PMAA-g-PVDF/ PAN were prepared via the dry-wet phase inversion technique, also known as the Loeb-Sourirajan method (Khulbe *et al.*, 2008). This method involves the preparation of a polymer solution of a suitable viscosity, which is then cast on a suitable material and partial solvent evaporation allowed. The cast is then placed in a non-solvent bath were solidification of the membrane transpires through evaporation of solvent as well as solvent/ non-solvent interaction. Phonthammachai *et al.*, 2006, managed to prepare photo-catalytic membrane using a high surface area TiO_2 catalyst synthesized from titanium triisopropanolamine, dispersed into poly (acrylonitrile) matrix. This current work seeks to develop a novel membrane with improved photo-catalytic activity, antibacterial and antifouling properties.

5.2. Methodology

5.2.1. Pre-treatment of PVDF with ozone

The initial step in the preparation of MAA-g-PVDF is ozone pre-treatment (Fig. 5.1). A suitable amount of poly (vinylidene difluoride) (PVDF) pellets were dissolved in dimethyl acetamide (DMAC) to give a polymer solution that was 133 gL^{-1}. An ozone/ oxygen (O_3/ O_2) mixture was bubbled through the polymer solution for 10 minutes at a flow rate of 4000 mg/ hr at 25 ˚C. The activated PVDF was cooled on an ice-bath, and then precipitated in excess ethanol. The precipitate was filtered off and then dried under reduced pressure at ambient temperature. The product was stored in a sealed container for further processing.

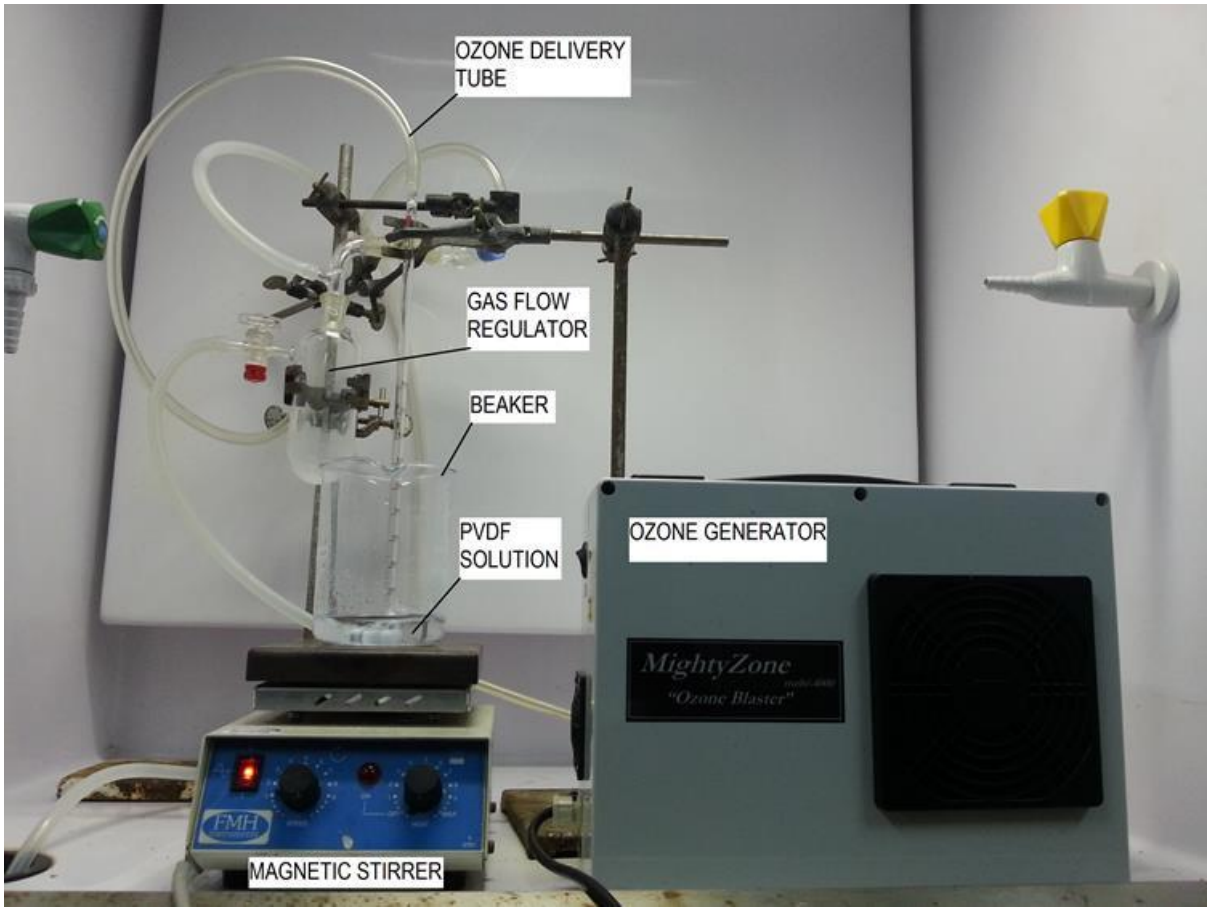

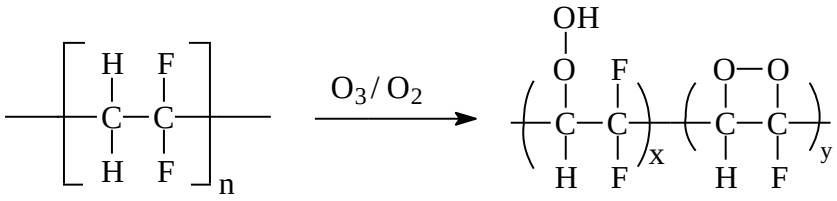

PVDF Activated PVDF

Figure 5.1: Ozone activation of poly (vinylidene difluoride) (PVDF) at a flow rate of 25 L/ min and a concentration of 4 g/ hr

5.2.2. Preparation of PMAA-g-PVDF

Methacrylic acid was grafted onto ozone pre-activated poly (vinylidene difluoride) via thermally induced reversible addition fragmentation chain transfer (RAFT) polymerization. The peroxides generated on the ozone-pre-treated PVDF facilitated the thermally initiated graft copolymerization of PMAA in the RAFT-mediated process. Ozone pre-treated PVDF

(12.7 g) were dissolved in 25 mL of dimethyl acetamide (DMAC). The polymer solution was transferred into a three necked flask with the subsequent addition of 2 mL of methacrylic acid monomer while stirring. The methacrylic acid was freed of inhibitor via vacuum distillation prior to addition. After placing a condenser and thermometer on the three necked flask, argon was saturated into the flask for 30 minutes. The reaction flask was then placed in an oil bath maintained at 60 ˚C with a steady flow of argon (Fig. 5.2). The reaction flask was cooled off after allowing ample time for the reaction to go to completion. PMAA-g-PVDF was precipitated in ethanol, filtered, re-dissolved in acetone and precipitated in ethanol. The precipitate was further purified by stirring in doubly distilled water at 55 ˚C for 24 hours to eliminate any remaining homopolymer (PMAA).

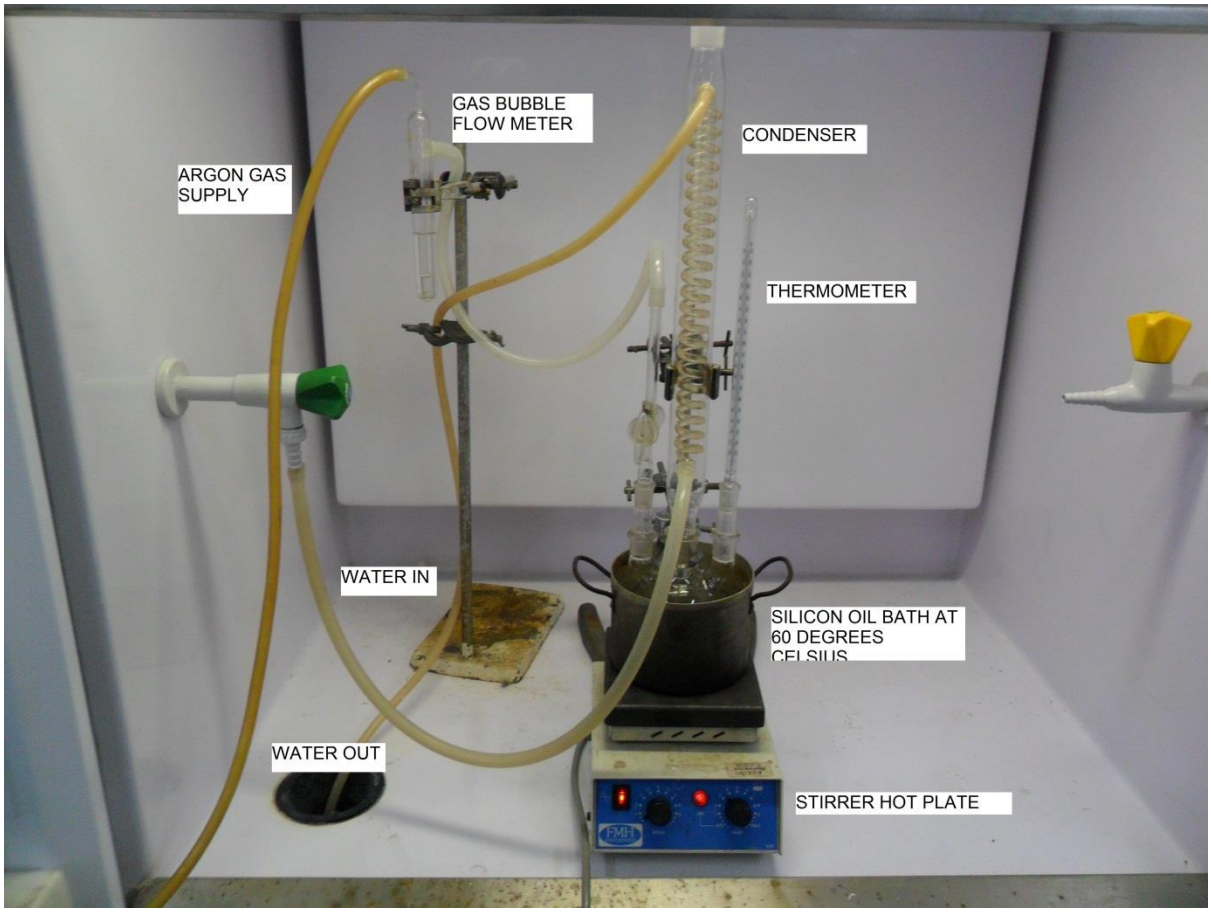

Figure 5.2: Graft copolymerization of MAA onto PVDF at 60 ˚C for 6 hrs

5.2.3. Preparation of PMAA-g-PVDF/ PAN/ N-TiO_2 membrane

A series of novel membranes impregnated with varying amounts of nitrogen doped titanium dioxide photo-catalyst were prepared via the dry-wet phase inversion technique (Loeb-Sourirajan) (Fig. 5.3). The amount of N-TiO_2 added was varied between 1-5 %.

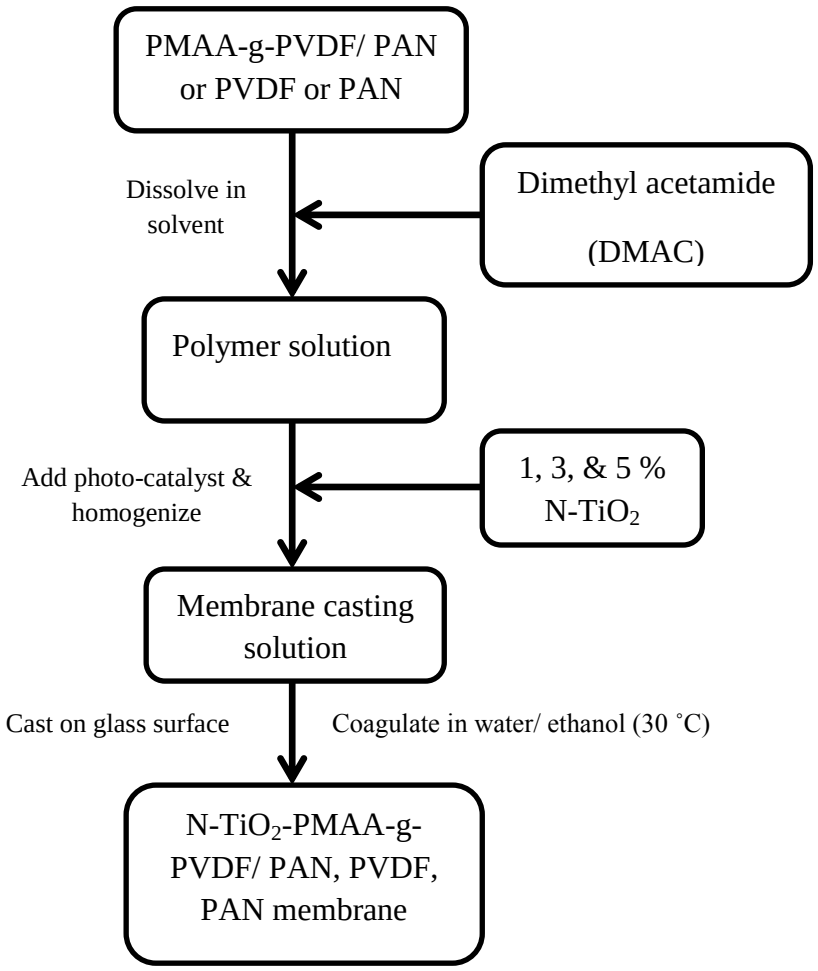

Figure 5.3: Flow diagram for the precipitation of membranes with N-TiO_2

Oh *et al.,* 2009, managed to prepare PVDF/ TiO_2 organic-inorganic composite membranes for the improvement of fouling resistance. The PVDF membrane surface was changed from hydrophobic to hydrophilic after TiO_2 addition which resulted in a reduced membrane fouling. Losito and co-workers, 2005, prepared TiO_2-poly (vinylidene difluoride) composite

films for the removal of pesticides from water in an attempt to eliminate problems associated with TiO_2 post recovery.

5.2.3.1. Preparation of N-TiO_2-PMAA-g-PVDF/ PAN membrane

A novel N-TiO_2-PMAA-g-PVDF/ PAN membrane was prepared via the Loeb-Sourirajan method. Three sets of membrane were prepared with varying amounts of N-TiO_2 photo-catalyst (1, 3, and 5 % N-TiO_2 respectively). 14.9 g of poly (acrylonitrile) (PAN) and 0.1 g PMAA-g-PVDF were dissolved in 100 mL of dimethyl acetamide (DMAC). Stirring was continued until the entire polymer was completely dissolved. A 5 mL aliquot of the polymer solution blend was added to each of the three small beakers, with the subsequent addition of N-TiO_2 photo-catalyst (1, 3, and 5 % respectively) under stirring. The beakers with polymer solution were then placed in a sonic bath for an hour to get rid of any bubbles. The polymer solutions were then cast on flat glass surface and then immersed in a coagulation bath to allow for the solidification of membrane. The coagulation bath was a mixture of ethanol and deionized water (3: 1). The membranes were then washed thoroughly with deionized water then placed in a water bath at 55 ˚C for 30 minutes to allow rearrangement of the membrane. The membranes were then stored in containers filled with deionized water to prevent them from drying up since they can become brittle if they lose water.

5.2.3.2. Preparation of N-TiO_2-PVDF and N-TiO_2-PAN membranes

For the purpose of comparison, novel N-TiO_2-PVDF and N-TiO_2-PAN series of membrane were also prepared via the dry-wet phase inversion technique. PVDF (15 g) were dissolved in 100 mL dimethyl acetamide under stirring for 3 hours to allow total dissolution and 1, 3, and 5 % of N-TiO_2 were added into 3 beakers containing 5 mL of polymer solution. The mixtures were then homogenized. After sonication for an hour to remove any air bubbles the N-TiO_2-

PVDF solutions were cast on glass plates and partial evaporation of solvent allowed. The thin membranes were then coagulated in a deionized water bath. The membranes were then treated in 55 ˚C water bath for 30 minutes and then stored under deionized water for later use. A series of N-TiO_2-PVDF solutions were also prepared in a similar fashion except for the coagulation bath which had an ethanol/ water ratio of 5:1.

5.2.3.3. Prepared membranes and conditions applied

Table 7 shows all the prepared polymeric membranes and the conditions under which they were fabricated.

Table 7: List of asymmetric membranes fabricated and the parameters used

Asymmetric membrane	Solvent used	Non solvent used in coagulation bath	Coagulation bath temperature
0, 1, 3, 5%N-TiO_2-(PAN)	DMAC	Deionized water	30 ˚C
0, 1, 3, 5%N-TiO_2-(PVDF)	DMAC	Water: Ethanol 1: 5	30 ˚C
0, 1, 3, 5%N-TiO_2-(PMAA-g-PVDF/ PAN)	DMAC	Water: Ethanol 1: 3	30 ˚C

5.3. Characterization

Infrared spectra of N-TiO_2 –PMAA-g-PVDF/ PAN/ PVDF membranes were recorded using PerkinElmer System 2000 FTIR. 1.0 mg of sample was properly mixed with 100 mg of

potassium bromide (KBr) and then ground thoroughly using mortar and pestle. An adequate amount of the ground sample was pelletized using a hydraulic pelletizer to give a transparent pellet, and then the samples were run against an air background. 8 scans were carried out for each sample in the wavenumber range 4000 cm^{-1} to 370 cm^{-1} with a resolution of 4 cm^{-1}.

Nuclear magnetic resonance spectroscopy (NMR) was used to investigate if poly (methacrylic acid) (PMAA) was successfully grafted onto poly (vinylidene difluoride) (PVDF) through structure elucidation. Proton (^{1}H) and carbon (^{13}C) spectra of PMAA-g-PVDF were acquired from a Varian ^{Unity} *Inova* 600 NMR spectrometer with a ^{1}H frequency of 300 MHz and a ^{13}C frequency of 75 MHz. A 5 mm dual channel Broad Band probe was used to collect the ^{1}H, and ^{13}C NMR spectra.

Scanning electron microscopy (SEM) was used to check the surface morphology and cross-sectional view of the N-TiO_2-PMAA-g-PVDF/ PAN/ PVDF membranes. Scanning electron microscopy (SEM) images were acquired on a JEOL JSM-6390 LV electron microscope operated at15 kV. SEM specimens were first coated with gold before acquiring images.

Thermo gravimetric analysis (TGA) was carried out on the prepared N-TiO_2-PMAA-g-PVDF/ PAN/ PVDF membranes to assess their thermal properties. A PerkinElmer TGA 7 thermo gravimetric analyser was used to acquire the thermo-grams in the temperature range 20-900 ˚C. The samples (10 mg) were run under nitrogen/ air flow with a heating rate of 15 ˚C/ min.

Tensile strength measurements were carried out using a universal electromechanical tensile tester which has a variable speed electric motor. The prepared N-TiO_2-PMAA-g-PVDF/

PAN/ PVDF membranes were cut into pieces 20 mm in length, 3.5 mm in width and 0.64 mm in thickness.

5.4. Results and discussion

5.4.1. FT-IR analysis of PMAA-g-PVDF

Fourier transform infrared spectroscopy (FT-IR) was used to identify the functional groups in PMAA-g-PVDF. Figure 5.4 shows the FT-IR spectra of methacrylic acid (MAA), poly (methacrylic acid) grafted poly (vinylidene difluoride) (PMAA-g-PVDF), and poly (vinylidene difluoride) homopolymer (PVDF).

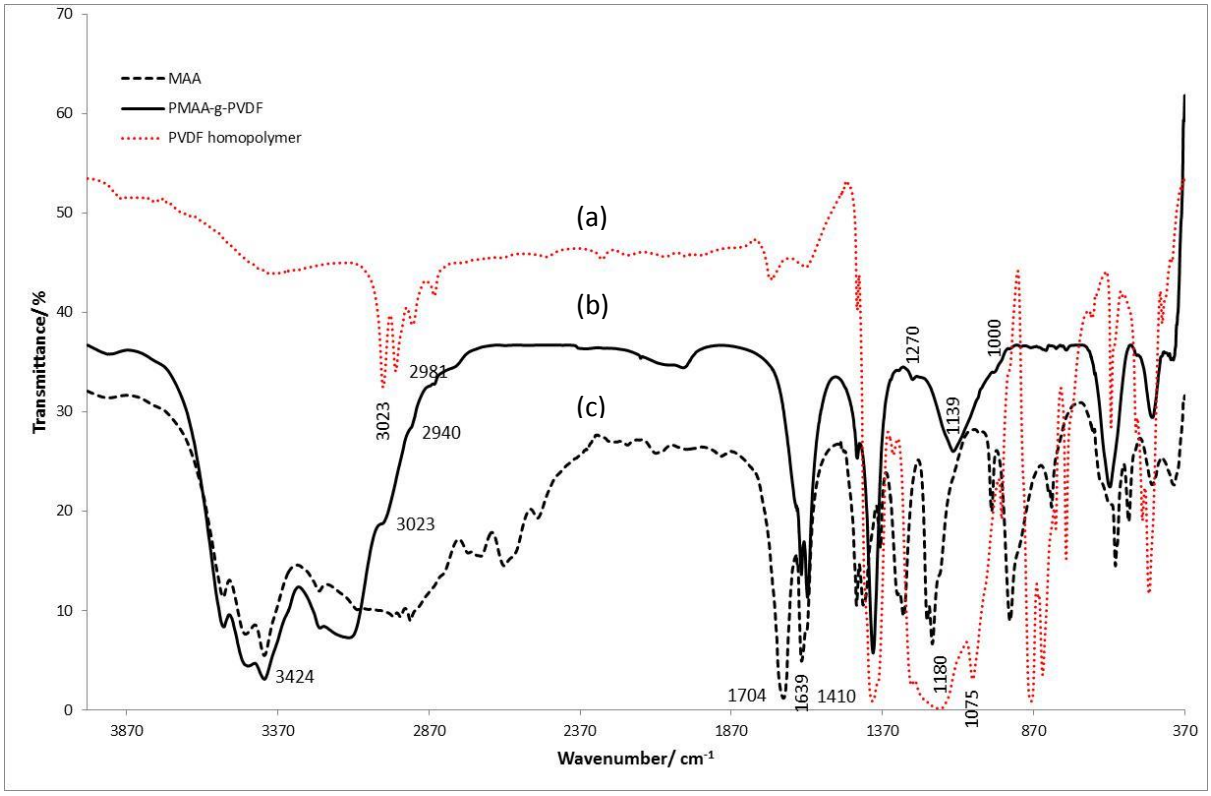

Figure 5.4: FT-IR spectra of (a) MAA, (b) PMAA-g-PVDF, and (c) PVDF prepared at 30 ˚C

The spectrum of methacrylic acid (MAA) shows peaks at 1704 cm^{-1} due to -C=O stretching vibrations of –COOH group, 1639 cm^{-1} -C-O single bond stretching vibrations, and 3424 cm^{-}

[1] owing to O-H stretching vibrations. The spectrum of PVDF homopolymer has peaks at 1410, 1180, & 1075 cm^{-1} and can be attributed to C-F deformation vibrations (Ying *et al.,* 2002). The peaks at 3023 cm^{-1} and 2981 cm^{-1} are attributed to $–CH_2$ (methylene group) anti-symmetric and symmetric stretching vibrations respectively (You *et al.,* 2012; Meng *et al.,* 2011). The peaks are superimposed with the O-H vibrations of PMAA with a band between 2500 and 3500 cm^{-1}. In the spectrum of PMAA-g-PVDF the peaks located at 1270 cm^{-1} and 1000 cm^{-1} are ascribed to the stretching vibrations of -C-O of the -COOH group and these peaks indicate the successful grafting of PMAA to PVDF. The medium peak at 1139 cm^{-1} is ascribed to C-O-C stretching vibrations consistent with the group formed with the graft reaction (Fig. 5.5) (You *et al.,* 2012; Sui *et al.,* 2012; Hashim *et al.,* 2009; Deng *et al.,* 2005; Ying *et al.,* 2002).

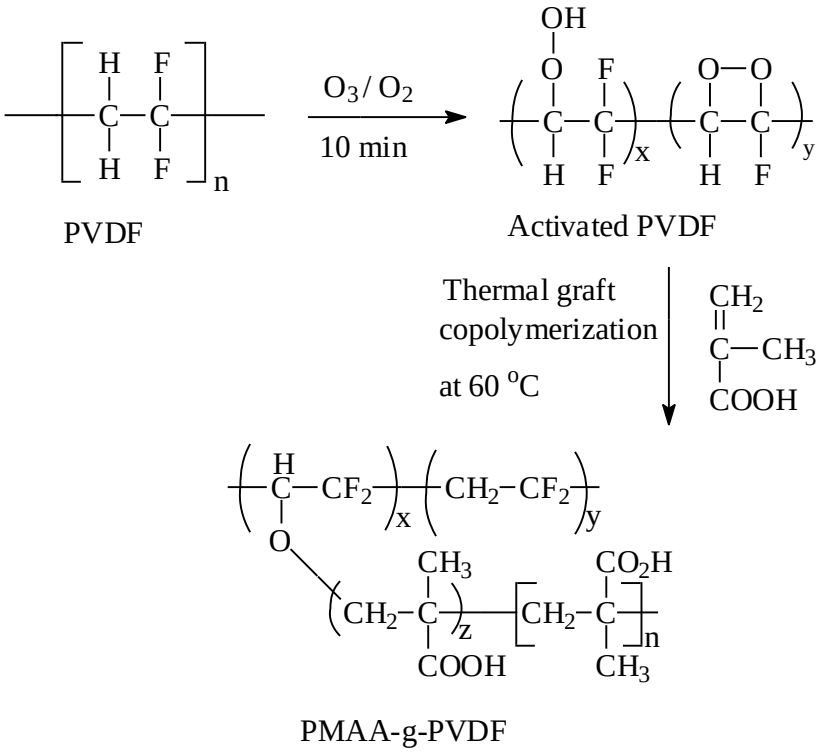

Figure 5.5: Suggested graft copolymerization of PMAA onto PVDF

5.4.2. NMR analysis of PMAA-g-PVDF

^{1}H and ^{13}C spectra were acquired to elucidate the structure of PMAA-g-PVDF and also to confirm successful grafting of PMAA onto PVDF polymer chains. Figure 5.6 and 5.7 show the proton and carbon 13 spectra of PMAA-g-PVDF respectively. The various signals appearing on the proton NMR spectrum of PMAA-g-PVDF indicate the existence of non-equivalent proton in the compound. The signal at 5.95 ppm can be ascribed to the proton of the carboxylic acid group, appears downfield of the reference tetra-methylsilane (TMS) due to deshielding.

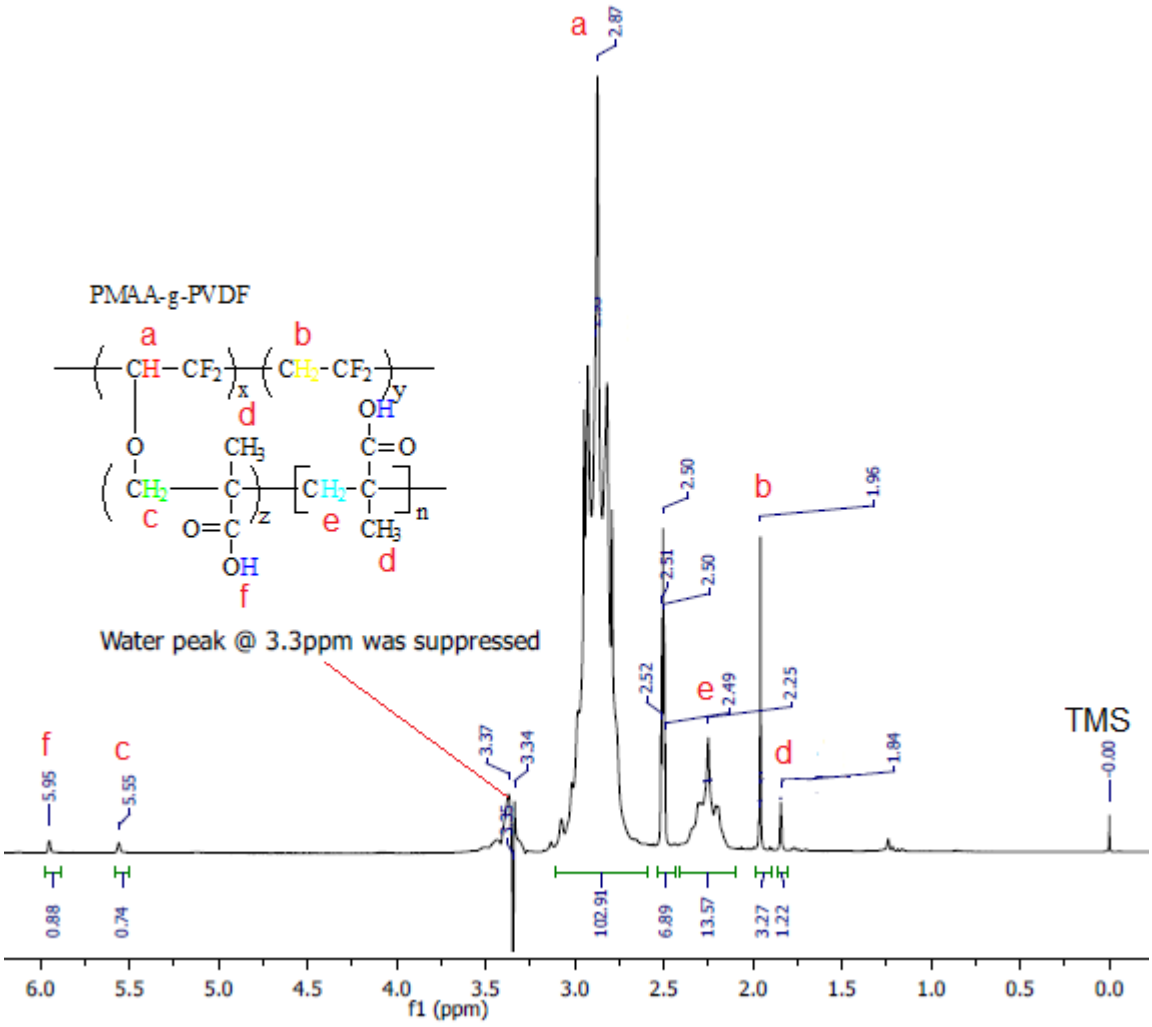

Figure 5.6: ^{1}H NMR spectrum of PMAA-g-PVDF prepared at 60 ˚C for 6 hours

The peak at a chemical shift (δ) of 5.5 ppm can be ascribed to the protons of the -O-CH_2- group which experiences some deshielding from the electronegative oxygen atoms in the vicinity. The proton of -CH-CF_2- appears at a chemical shift of 2.87 ppm; this proton experiences deshielding from the oxygen atom as we as the fluorine at the neighbouring carbon atom. The methylene and methyl groups have peaks with chemical shifts 2.49 ppm and 1.84 ppm respectively. These groups of protons appear up-field because they are more shielded than the rest of the other non-equivalent sets of protons in PMAA-g-PVDF. The chemical shifts of protons in the spectrum of PMAA-g-PVDF are in close agreement with correlation data chemical shift in various literatures (Carbajo and Neira, 2013; McMurray, 2008).

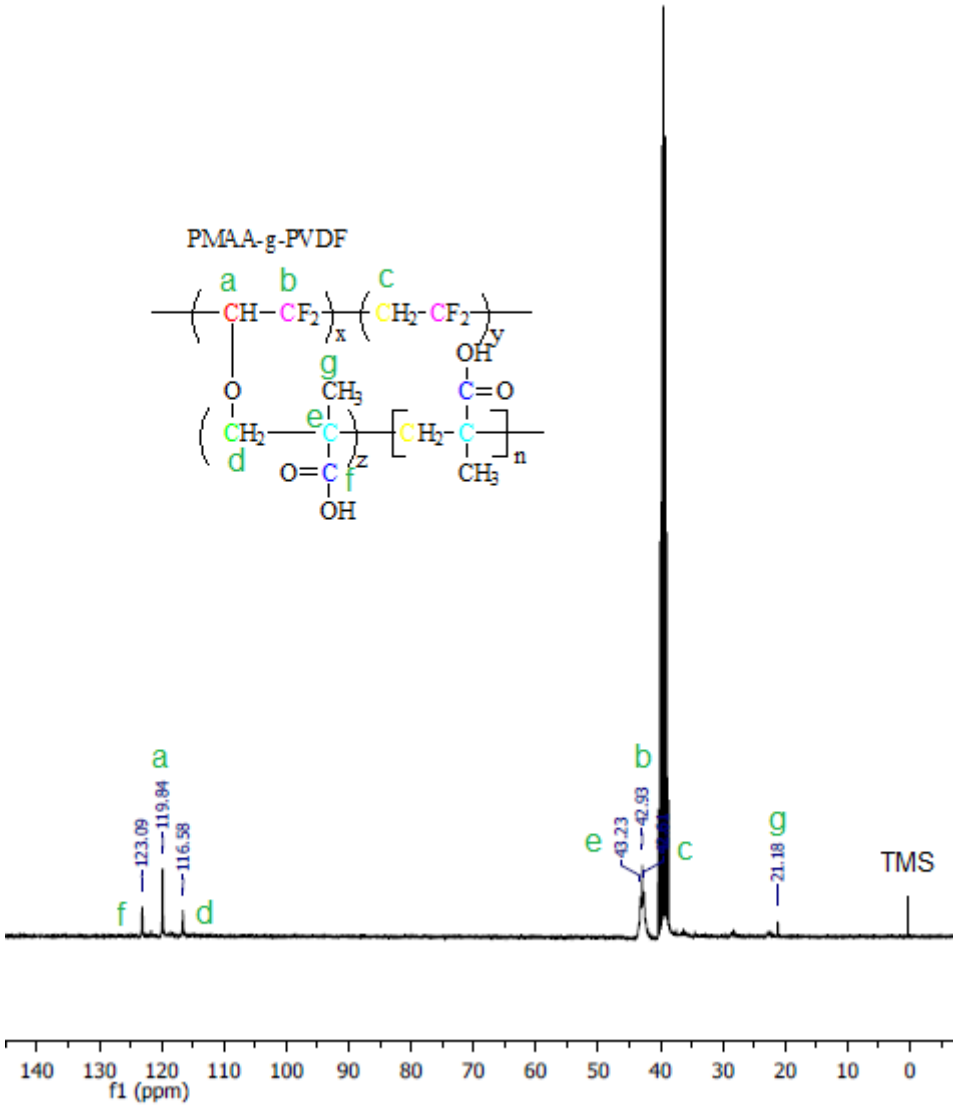

Figure 5.7: ^{13}C NMR spectrum of PMAA-g-PVDF prepared at 60 ˚C for 6 hours

The ^{13}C NMR spectrum of PMAA-g-PVDF presented seven signals representing the different carbon environments present in the structure. The ^{13}C NMR allows the mapping of the carbon skeleton of compounds. The peak at 123.09 ppm was assigned to the carbon of the carboxylic acid group. This carbon is highly deshielded since is directly attached to a highly electronegative atom of oxygen through a double bond, hence it appears downfield. The peak at 119.84 ppm was assigned to the tertiary carbon (-CH-O-) also directly bonded to an electronegative oxygen atom. The signal at 116.58 ppm was ascribed to the carbon of the

methylene group (-CH_2-O-) that is also directly bonded to a highly electronegative oxygen atom. The peak at 43.23 ppm was assigned to a quaternary carbon atom, that at 42.92 ppm to a carbon bonded to the halogen fluorine (-CF_2-). The carbon of the (-CH_2-) group had a peak at 42.61 ppm, while that of the methyl group (-CH_3) appeared up-field with a chemical shift of 21.18 ppm since it is shielded (Carbajo and Neira, 2013; McMurray, 2008). NMR spectroscopy and FT-IR spectroscopy confirmed that poly (methacrylic acid) (PMAA) was successfully grafted onto poly (vinylidene difluoride) (PVDF) via reversible addition fragmentation chain transfer (RAFT).

5.4.3. SEM analysis of N-TiO_2-(PVDF, PMAA-g-PVDF/ PAN, and PAN) membranes

5.4.3.1. SEM analysis of N-TiO_2-PAN membranes

Poly (acrylonitrile) asymmetric membranes with 1, 3, and 5 % N-TiO_2 prepared via dry-wet phase inversion technique were analyzed by scanning electron microscopy (SEM) to study their surface morphology as well as the cross-sectional view. Pristine PAN asymmetric membranes were successfully prepared. The membranes have a thin dense top layer and a porous sub-layer with fingerlike micro-voids (Fig. 5.8 (a) (Su *et al.*, 2009). The top layer of the membrane exhibits a rough surface. The morphology of the porous sub-layer of the PAN asymmetric membranes changes with the addition of N-TiO_2 (1, 3, & 5 %), from the finger-like looking micro-voids to somewhat ovoid looking smaller micro-voids. However, the surface morphology of the membranes does not change with the addition of N-TiO_2.

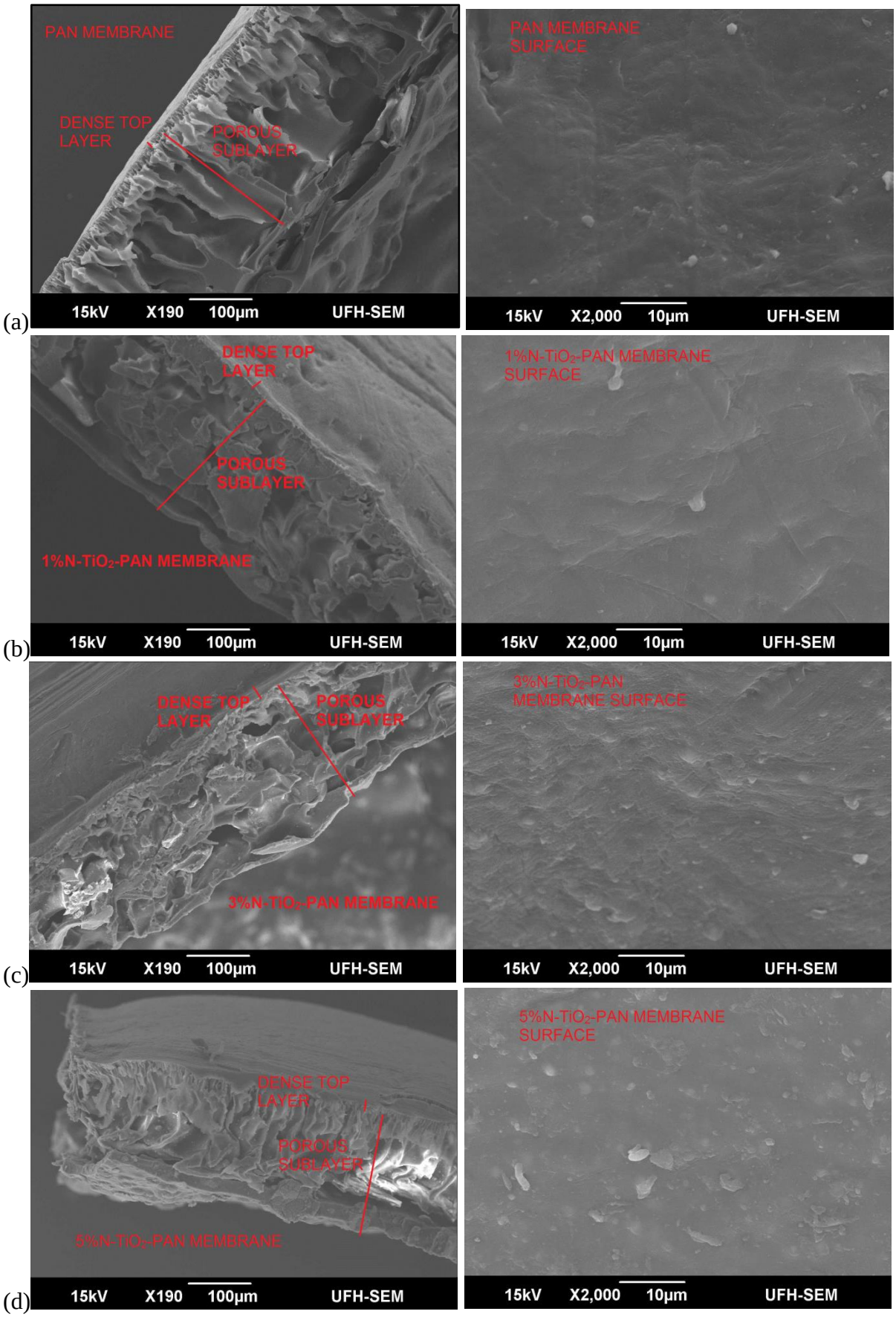

Figure 5.8: SEM images of (a) PAN, (b) 1%N-TiO_2-PAN (c) 3%N-TiO_2-PAN and (d) 5%N-TiO_2-PAN prepared at 30 ˚C, using water as non-solvent

The entire PAN asymmetric membranes produced were rough skinned (Yang and Liu, 2003). SEM confirmed the successful preparation of N-TiO_2-PAN asymmetric photo-catalytic membranes.

5.4.3.2. SEM analysis of N-TiO_2-PVDF membranes

A series of N-TiO_2-PVDF membranes prepared via the Loeb-Sourirajan method were analyzed by scanning electron microscopy (SEM) to elucidate their surface morphology as well as cross-sectional view. Fig. 5.9 shows the SEM micrographs obtained for PVDF, 1%N-TiO_2-PVDF, 3%N-TiO_2-PVDF, and 5%N-TiO_2-PVDF (a-d respectively).

(a)

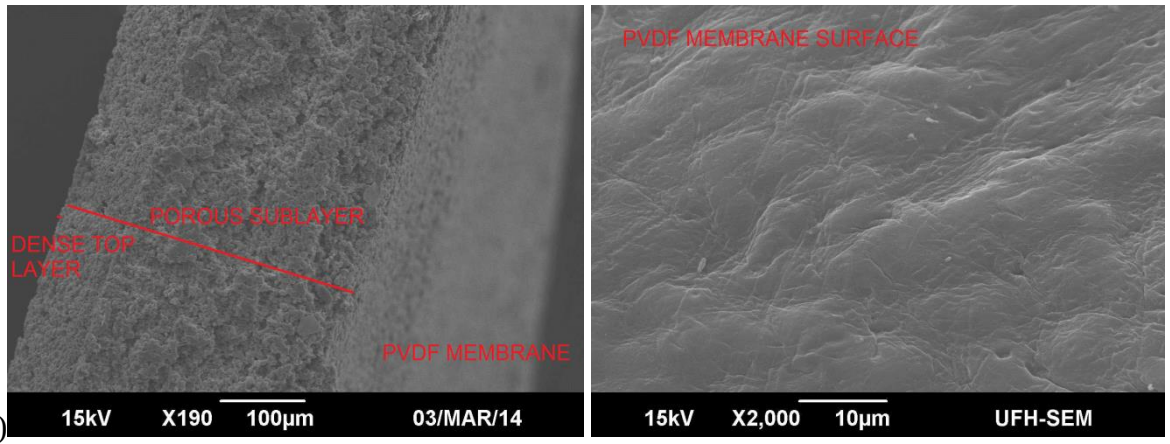

(b)

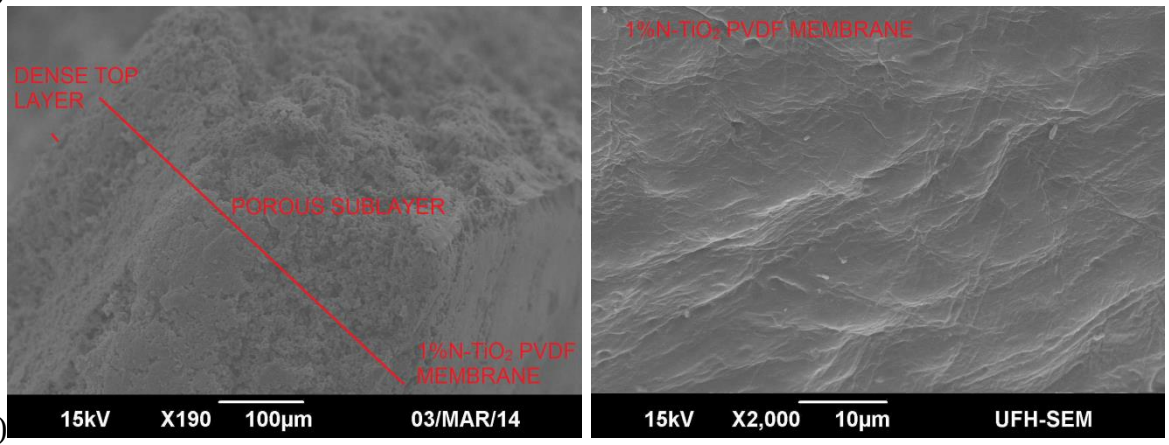

(c)

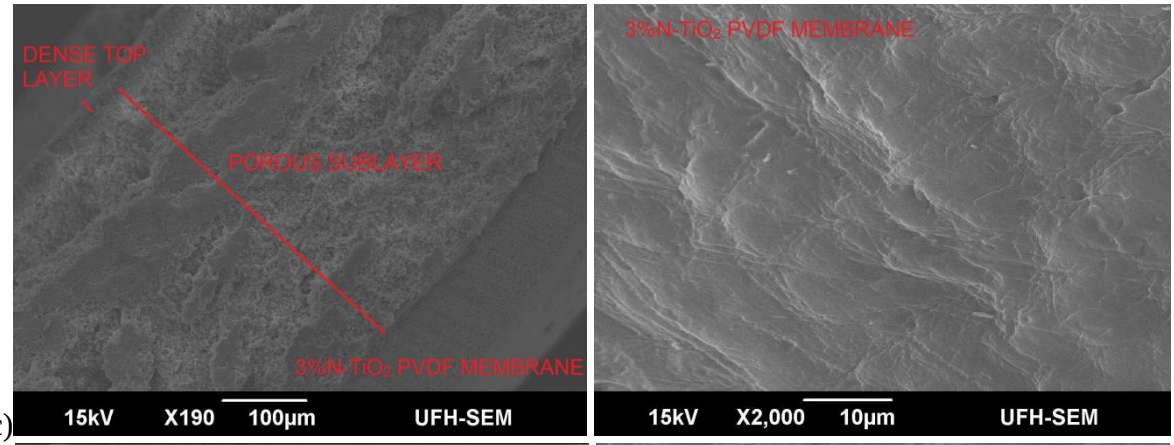

(d)

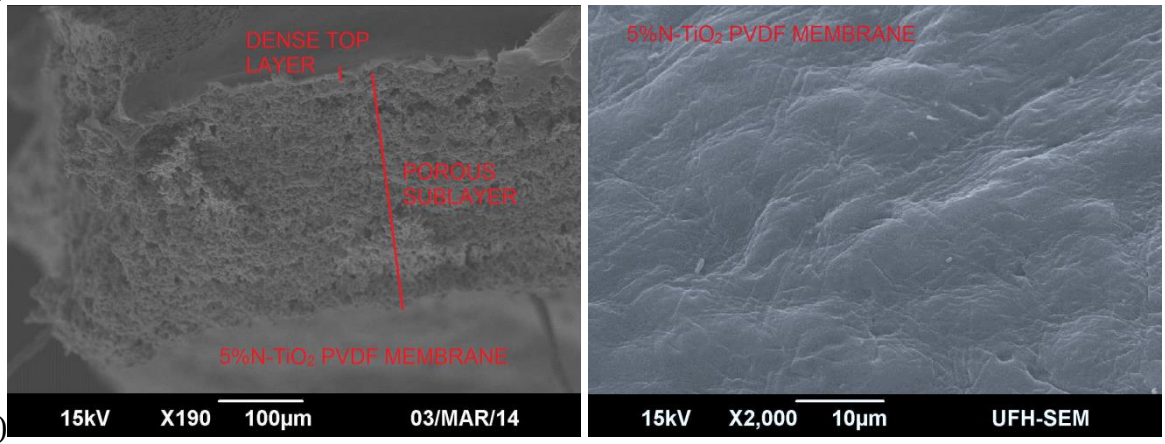

Figure 5.9: SEM images of (a) PVDF, (b) 1%N-TiO_2-PVDF (c) 3%N-TiO_2-PVDF and (d) 5%N-TiO_2-PVDF prepared at 30 ˚C, non-solvent water/ ethanol (1: 5)

Asymmetric PVDF membranes with different loadings of N-TiO_2 were successfully prepared. These membranes exhibit a thin top layer with a sponge-like (spherulite) porous sub-layer (Lai *et al.*, 2014; Liu *et al.*, 2012). The spherulites are more closely packed together just below the dense top layer of the PVDF asymmetric membrane. A transition from densely packed to sparsely packed spherulites can be observed across the membrane cross-sectional view. No significant change in the morphology of the cross-section of PVDF membranes was observed with the addition of different loadings of N-TiO_2 powder. The surface of the PVDF asymmetric membranes is rough with no visible pores. No change in surface morphology of these membranes was observed with the addition of N-TiO_2 powder.

5.4.3.3. SEM analysis of N-TiO_2-PMAA-g-PVDF/ PAN membranes

Another series of poly (methacrylic acid) grafted onto poly (vinylidene difluoride) blended with poly (acrylonitrile) membranes with different loadings of nitrogen doped titanium dioxide (1, 3, & 5 % respectively) were prepared via the Loeb-Sourirajan method. Fig. 5.10 shows the SEM images obtained for the above mentioned membranes.

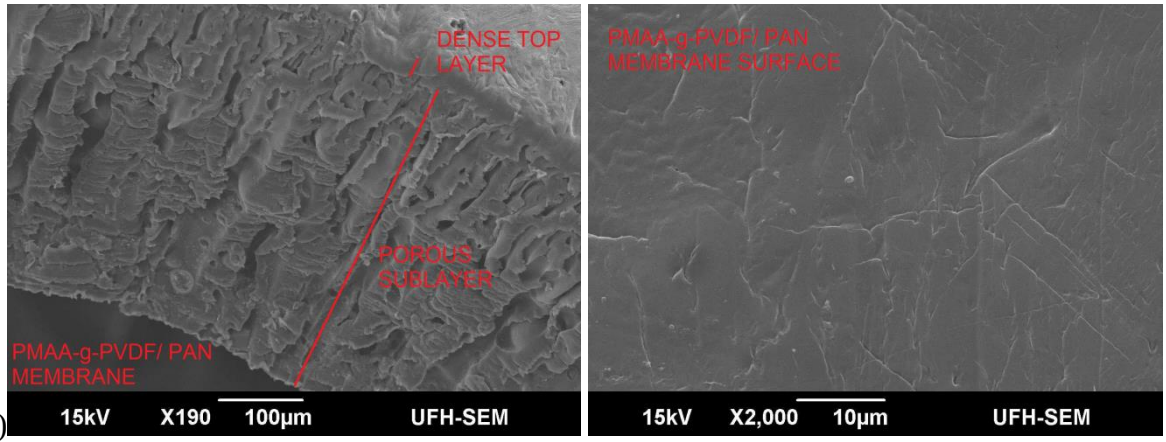

(a)

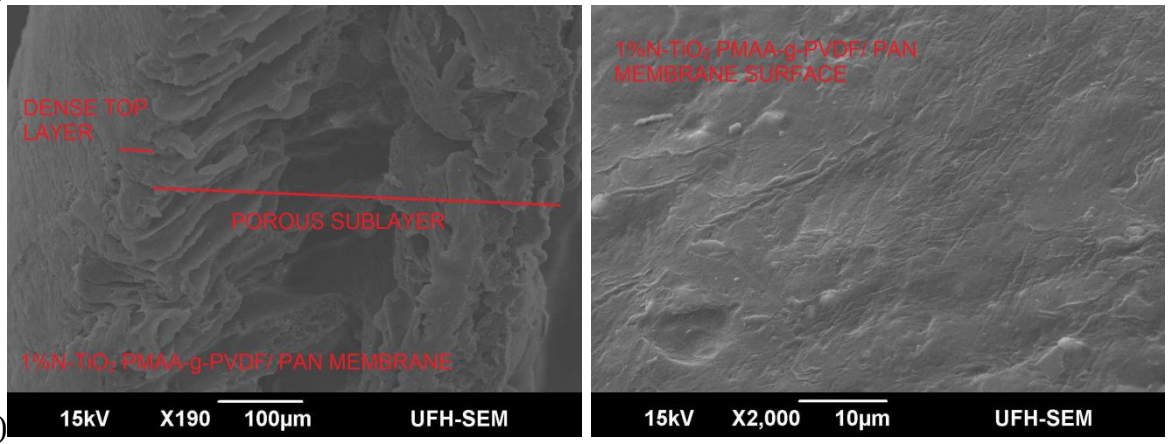

(b)

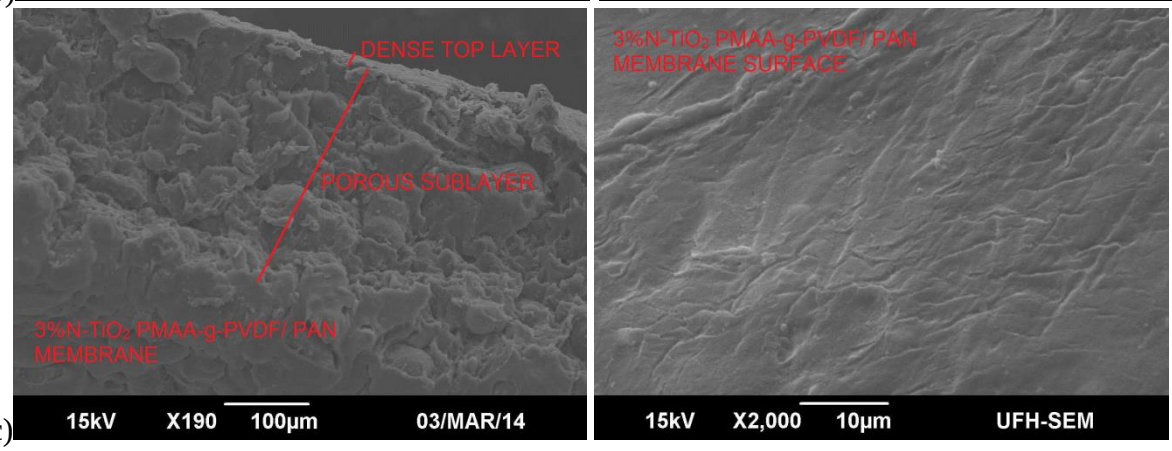

(c)

(d)

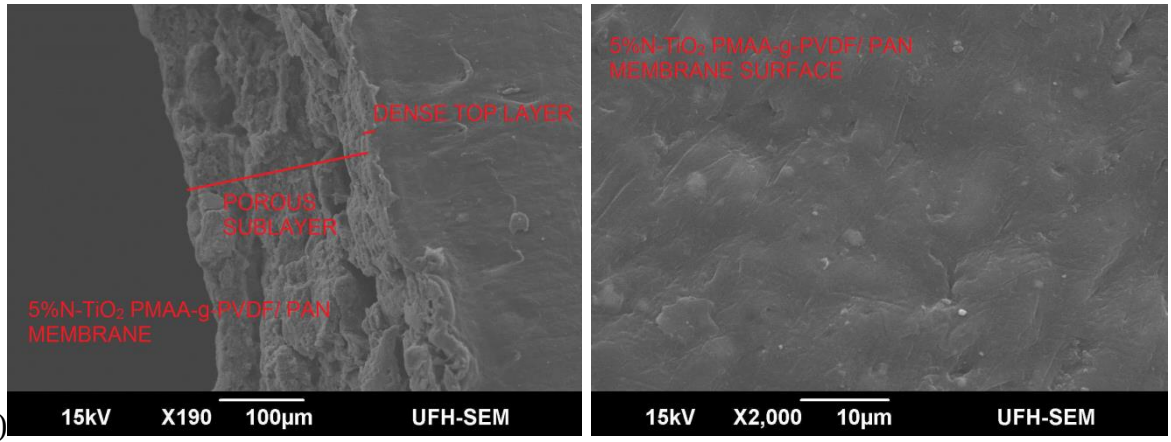

Figure 5.10: SEM (a) PMAA-g-PVDF/ PAN (b) 1%N-TiO_2 PMAA-g-PVDF/ PAN (c) 3%N-TiO_2 PMAA-g-PVDF/ PAN and (d) 5%N-TiO_2 PMAA-g-PVDF/ PAN prepared at 30 ˚C, non-solvent water/ ethanol (1: 3)

The prepared novel PMAA-g-PVDF/ PAN blend membrane exhibited a typical asymmetric structure. The cross-sectional view of the pristine PMAA-g-PVDF/ PAN blend asymmetric membranes revealed the presence of a dense top layer and a supporting porous sub-layer. The effect of addition of different loadings of nitrogen doped titanium dioxide powder could clearly be observed from the change in texture and morphology of the porous sub-layer of the membranes. The pristine PMAA-g-PVDF/ PAN blend membranes have fingerlike micro-voids in the supporting sub-layer, whereas membranes with one percent N-TiO_2 powders exhibit short fingerlike micro-voids from the top of the porous sub-layer and ovoid micro-voids towards the bottom. With further addition of (3 % and 5%) of N-TiO_2 powders, the fingerlike micro-voids disappear, and only ovoid micro-voids can be observed in the porous sub-layer of the PMAA-g-PVDF/ PAN blend asymmetric membranes.

Pristine asymmetric PMAA-g-PVDF/ PAN blend membranes have a somewhat smooth looking surface with no visible pores. However the morphology changes to a rough looking surface with the addition of different loadings of N-TiO_2 powders.

5.4.4. Tensile strength analysis of N-TiO_2-(PVDF, PMAA-g-PVDF/ PAN, and PAN) membranes

The prepared membranes were analyzed for tensile strength using a tensile tester. Fig. 5.11 show the results obtained. Pristine poly (vinylidene difluoride) membranes exhibited a high tensile strength (4.4 MPa) (Yang and Liu, 2003). A steady decrease in the tensile strength was observed with the addition of nitrogen doped titanium dioxide in the PVDF membranes (1%N-TiO_2-PVDF (4.0 MPa); 3%N-TiO_2-PVDF (3.8 MPa); and 5%N-TiO_2-PVDF (3.4 MPa)). The incremental addition of N-TiO_2 powders in PVDF membranes resulted in their gradual loss of mechanical strength. Similar trends were observed for PMAA-g-PVDF/ PAN and PAN membranes; however PMAA-g-PVDF/ PAN membranes exhibited higher tensile strength compared to PAN membranes. The highest decrease in mechanical strength was observed in PAN (25.9 %), followed by PVDF (22.7 %) and then PMAA-g-PVDF/ PAN (8.0 %).

Poly (vinylidene difluoride) (PVDF) membranes exhibited the highest elasticity compared to poly (methacrylic acid) grafted poly (vinylidene difluoride) (PMAA-g-PVDF) and poly (acrylonitrile) (PAN) membranes. A decrease in the elongation at break was observed for these membranes as more of the inorganic particles in the form of Ti were added to the membranes (Fig. 5.12). In another study Yan and co-workers 2006, observed an increase in elongation at break with the addition of alumina (Al_2O_3) up-to a certain limit, then a decrease in the elasticity of PVDF membranes with further additions. In the current work similar trends were observed with the addition of N-TiO_2 powders, where there was a decrease in the elongation at break for all the membranes prepared.

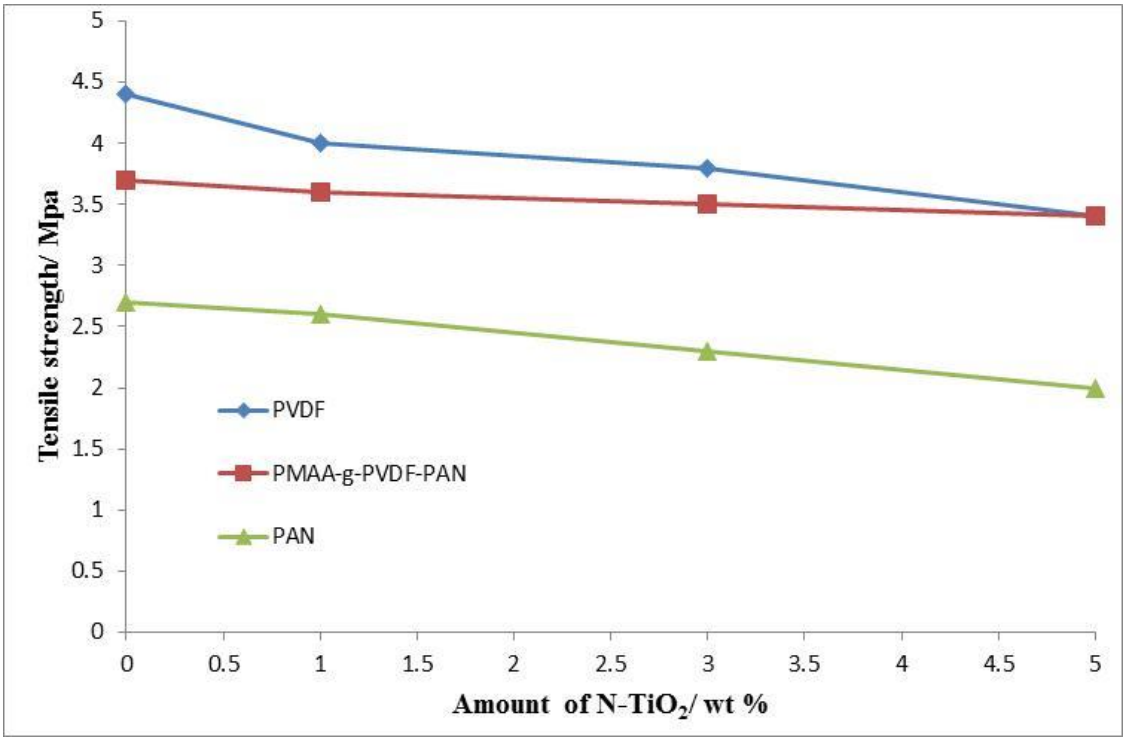

Figure 5.11: Tensile strength of (a) PVDF, (b) PAN & (c) PMAA-g-PVDF/ PAN membranes prepared at 30 ˚C

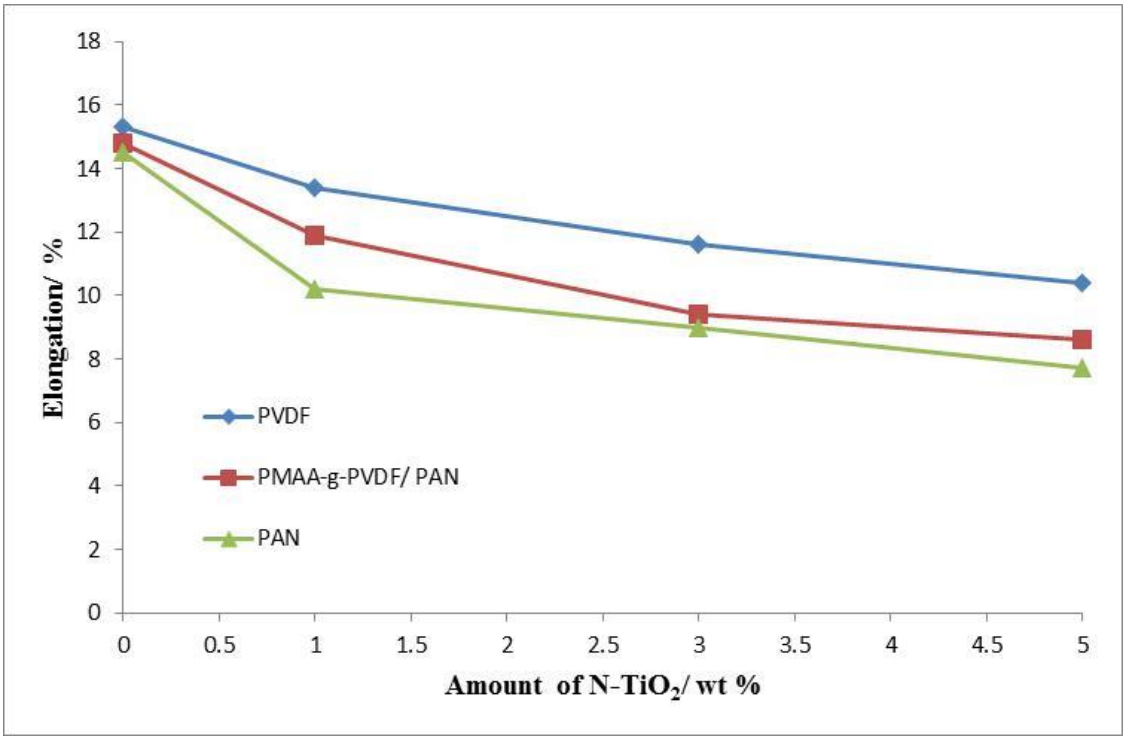

Figure 5.12: Elongation of (a) PVDF, (b) PMAA-g-PVDF/ PAN & (c) PAN membranes prepared at 30 ˚C

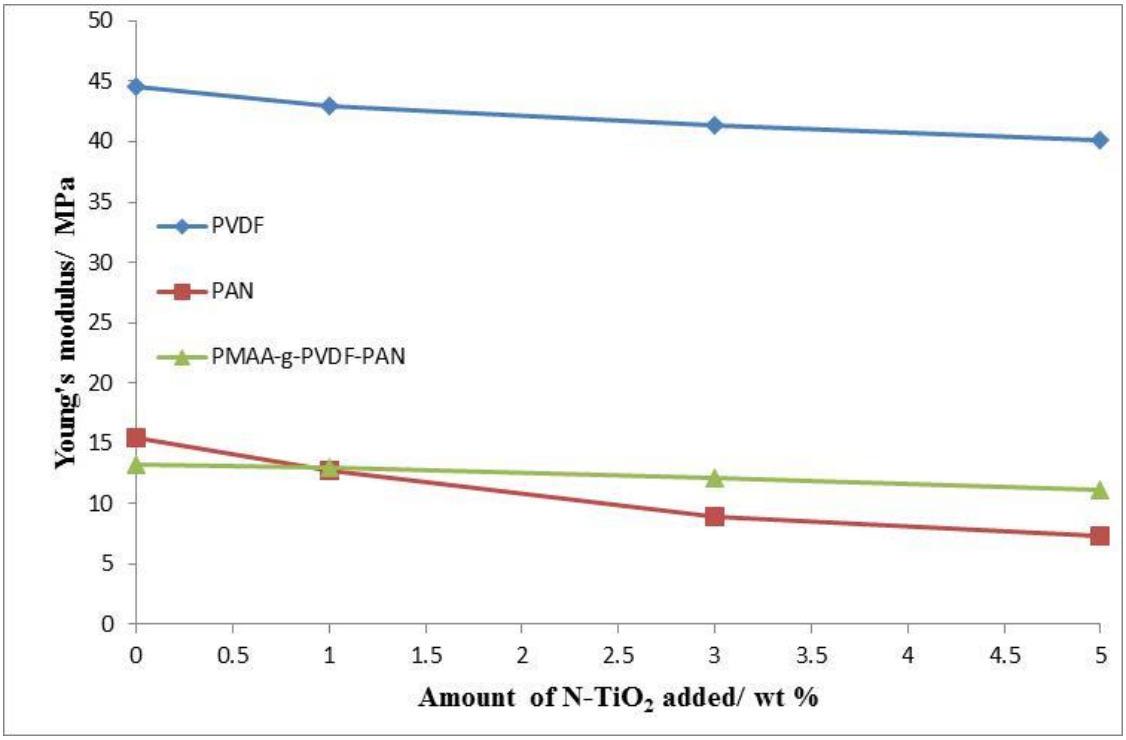

Figure 5.13: Young's modulus of (a) PVDF, (b) PAN & (c) PMAA-g-PVDF/ PAN membranes prepared at 30 ˚C

Similar trends were also observed in Young's modulus (Fig. 5.13) where there was a decrease with the addition of N-TiO_2 (44.5 to 40.1 MPa for PVDF, 13.2 to 11.2 MPa for PMAA-g-PVDF/ PAN and 15.5 to 7.3 MPa for PAN).

5.4.5. TGA analysis of N-TiO_2-(PVDF, PMAA-g-PVDF/ PAN and PAN membranes

The thermal properties of the series of asymmetric membranes prepared were analysed by thermo-gravimetric analysis.

5.4.5.1. TGA analysis of N-TiO_2-PVDF

The thermograms obtained for poly (vinylidene difluoride) membranes incorporated with different amounts of nitrogen doped titanium dioxide are shown in figure 5.14.

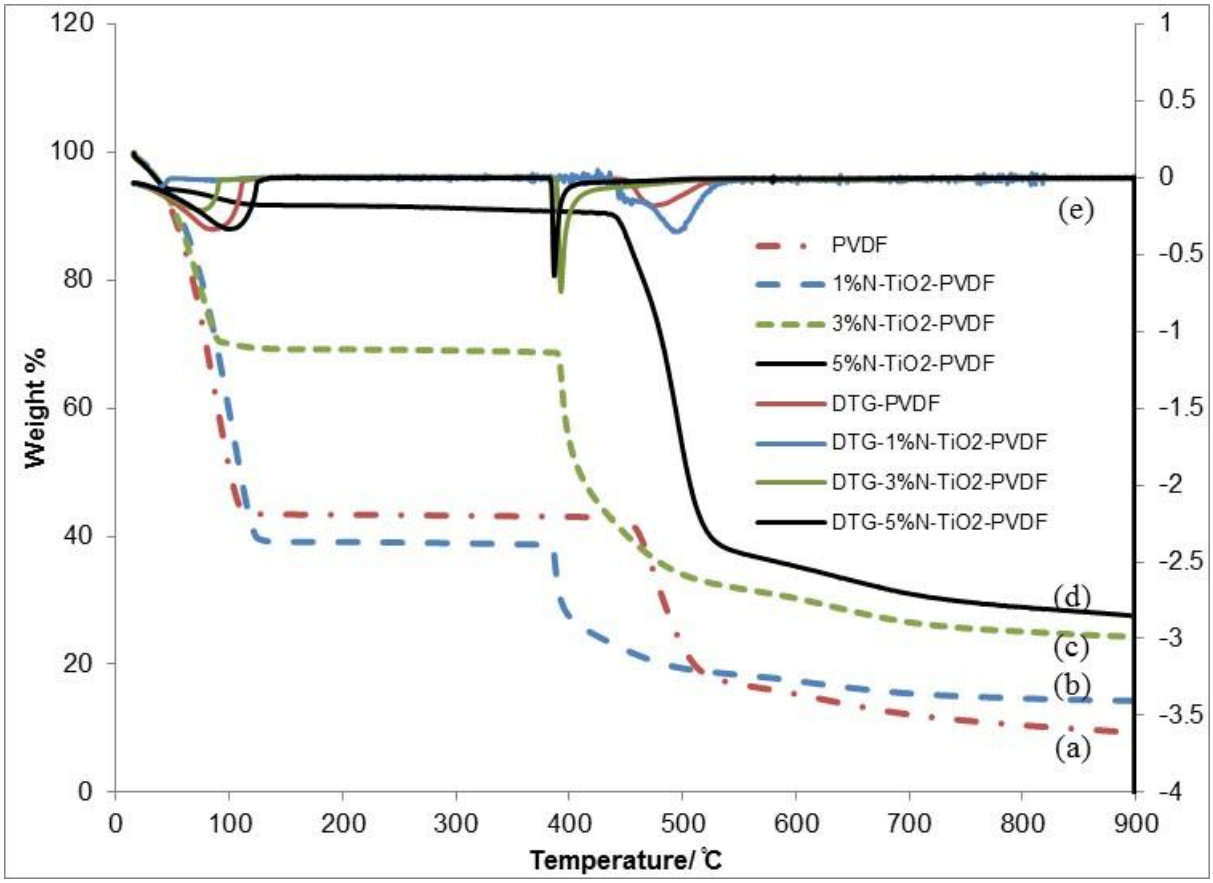

Figure 5.14: Thermograms of (a) PDVF (b) 1 % N-TiO_2-PVDF, (c) 3 % N-TiO_2-PVDF, (d) 5 % N-TiO_2-PVDF and (e) Derivatives of (a) – (d) heating rate 15 ˚C/ min

The first peak in all four thermograms denotes water loss from the membranes. As can be seen from the derivatives of the PVDF and N-TiO_2-PVDF membranes water loss is observed from around 70 ˚C. Pristine PVDF membrane {Fig. 5.14 (a)} showed stability beyond 400 ˚C as reported elsewhere (Malmonge and Mattoso, 2000; Zulfiqar *et al.,* 1994). Melting of the PVDF membrane is observed from 450 ˚C onwards. Further heating resulted in the decomposition of PVDF, with hydrogen fluoride as the major product as well the monomer and small amounts of $C_4H_3F_3$ (Zulfiqar *et al.,* 1994). Carbon-carbon fission leads to the breakdown of the polymer repeating units. The addition of N-TiO_2 to the PVDF membranes was observed to reduce stability. As observed from the thermogram of 1 % N-TiO_2-PVDF (Fig. 5.14 (b)), decomposition of the membrane begins around 420 ˚C as opposed to 450 ˚C

for pristine PVDF membranes. Increasing the amount of N-TiO_2 to 3 % and 5 % is observed to reduce the stability of the PVDF membranes further (Fig. 5.15). The thermograms indicate that decomposition starts at 400 ˚C and 410 ˚C for 3% N-TiO_2-PVDF and 5% N-TiO_2-PVDF membranes respectively. The variation of PVDF decomposition temperature as a function of inorganic filler (N-TiO_2) is shown in Figure 5.15.

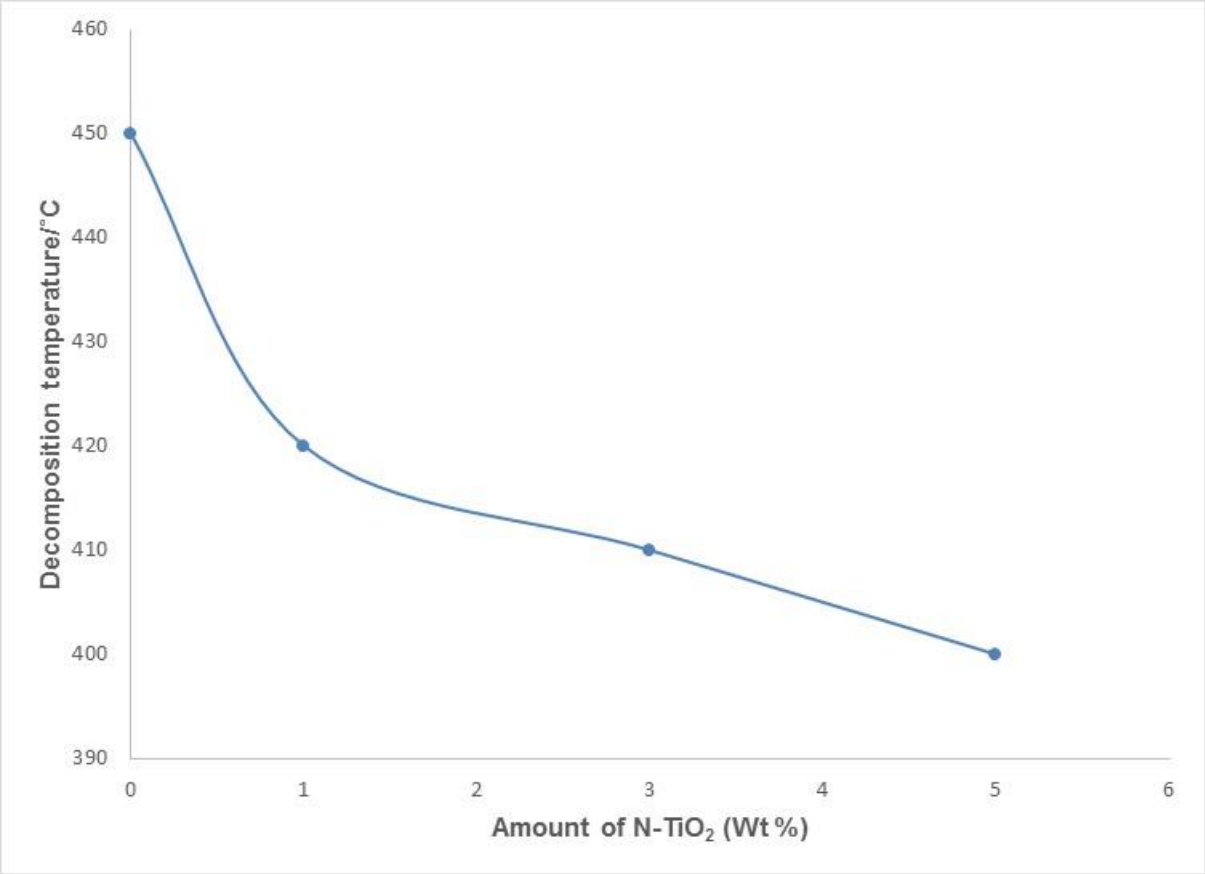

Figure 5.15: Variation of PVDF decomposition temperature as a function N-TiO_2 added

In general decomposition of PVDF membranes occurred in two stages: (i) the first stage owing to water and solvent loss occurred in the temperature range 70 ˚C to 130 ˚C, with a weight loss between 20 % and 30 % and (ii) the second stage owing to PVDF decomposition occurred in the temperature range 400 ˚C to 700 ˚C, with a weight loss of between 30 % and 50 % for PVDF and N-TiO_2-PVDF. In similar studies other researchers prepared PVDF

incorporated with different inorganic filler namely silicon dioxide (SiO_2), zeolite 4A and MCM-41. In their findings, they observed a decrease in the PVDF decomposition temperature with an increasing amount of inorganic filler in the three composites they prepared (Shen and Lua, 2012).

5.4.5.2. TGA analysis of N-TiO_2-PAN

Figure 5.16 shows the thermograms obtained for the thermal analysis of PAN membranes loaded with different amounts of N-TiO_2. It was reported elsewhere that heating poly (acrylonitrile) leads to its decomposition producing volatiles which include nitriles, the monomer, ammonia and others (Joseph and Tretsiakova-McNally, 2012; Martin *et al.,* 2001; Surinarayanan *et al.,* 1998; Xue *et al.,* 1997). The thermogram of PAN exhibits three degradation steps. The initial step observed in the temperature range 30 ˚C to 100 ˚C was due to water loss as well as solvent used in the preparation of the membrane. This initial step had a weight loss of 5 %. The PAN membrane shows stability up to 270 ˚C which marks the commencement of nitrile group decomposition. The second step of PAN membrane degradation in the temperature range 270 ˚C to 325 ˚C had a weight loss of 35 %. The third step is attributed to the degradation of the poly (acrylonitrile) chains and this is observed in the temperature range 325 ˚C to 500 ˚C with a weight loss of 25 %.

The variation of PAN membrane decomposition temperature as a function of inorganic filler (N-TiO_2) is shown in figure 5.17. The derivative thermograms of PAN membranes incorporated with N-TiO_2 clearly show that there is increased stability with the addition of the inorganic nanoparticles.

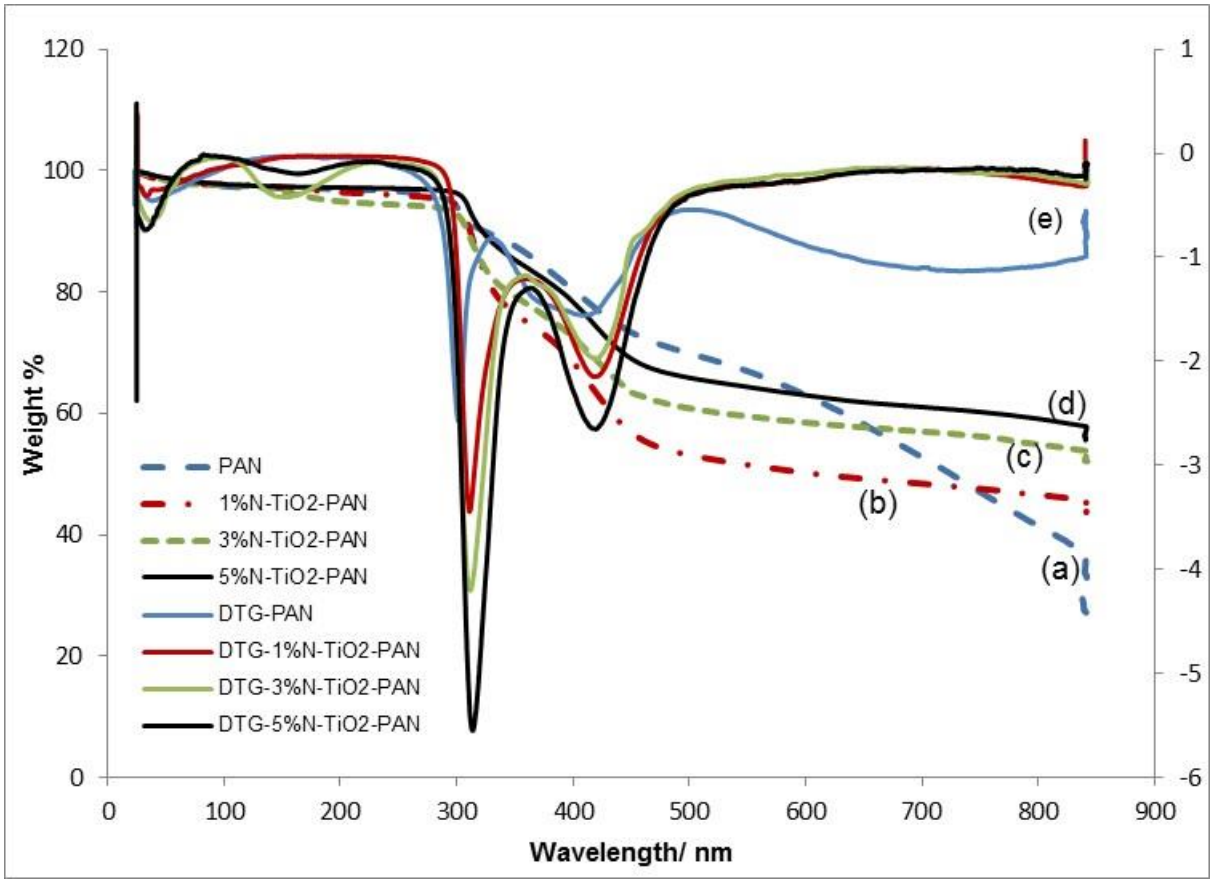

Figure 5.16: Thermograms of (a) PAN (b) 1% N-TiO_2-PAN, (c) 3% N-TiO_2-PAN, (d) 5% N-TiO_2-PAN and (e) Derivatives, heating rate of 15 ˚C/ min

When the PAN membranes were incorporated with 1 % N-TiO_2 the membranes were stable up to 310 ˚C as opposed to 270 ˚C for pristine PAN membranes. Addition of more N-TiO_2 stabilized the PAN membranes further. When the content of N-TiO_2 was increased to 3 % N-TiO_2 and 5 % N-TiO_2, the decomposition temperatures also increased to 315 ˚C and 317 ˚C respectively, entailing further stability of PAN membranes. Other researchers prepared poly (acrylonitrile)/ Na-Montmorillonite/ Silicon dioxide (PAN/ Na-MMT/ SiO_2) nano-composites. They observed similar trends whereby there was increase in thermal stability with increasing amount of either Na-Montmorillonite or Silicon dioxide (SiO_2). The highest thermal stability was observed when PAN was incorporated with both Na-MMT and SiO_2 (Yu *et al.,* 2007).

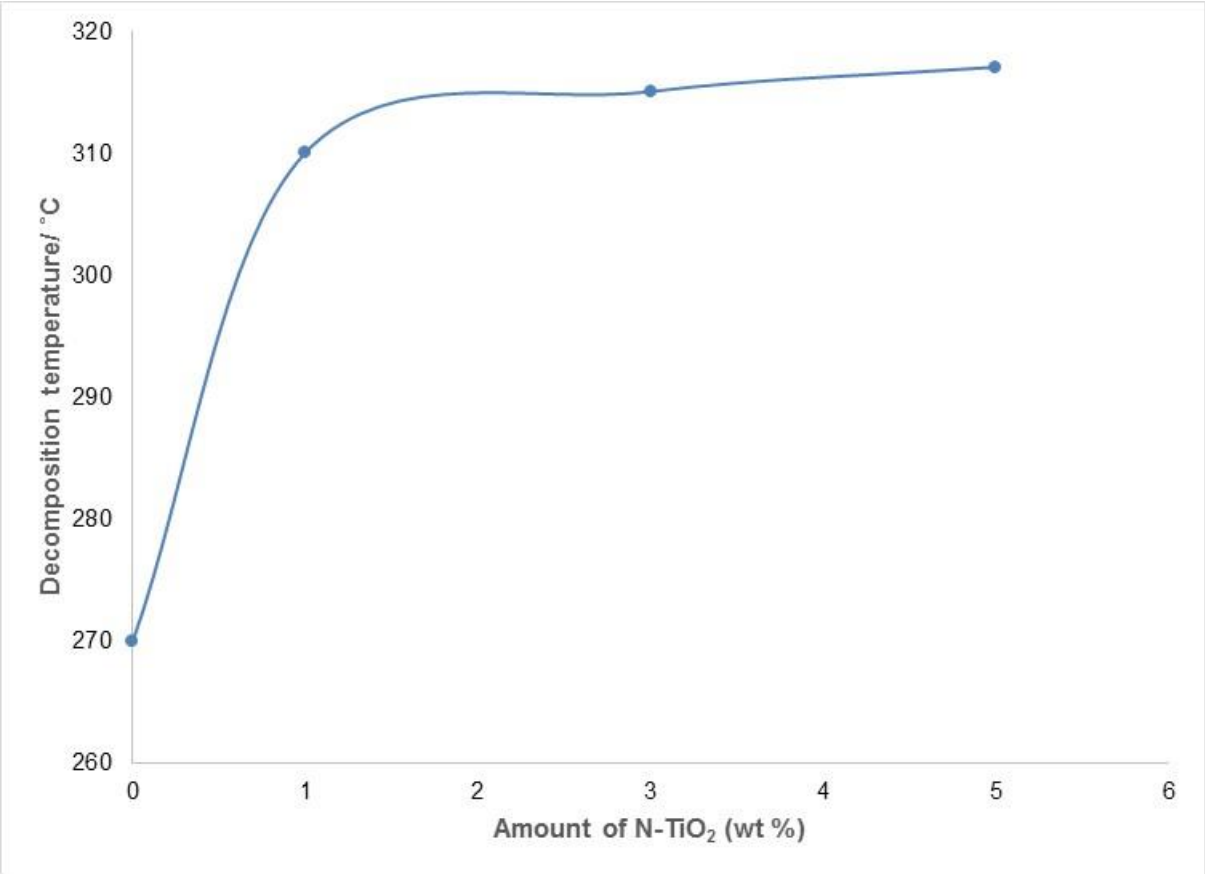

Figure 5.17: Variation of PAN decomposition temperature as a function N-TiO_2 added

5.4.5.3. TGA analysis of N-TiO_2-PMAA-g-PVDF/ PAN

The thermograms obtained for PMAA-g-PVDF/ PAN membranes incorporated with different amounts of N-TiO_2 are shown in Figure 5.18. It was reported in literature that poly (methacrylic acid) decomposes in two stages; one involving transformation in methacrylic anhydride and another decomposition from subsequent heating. These decompositions have been observed to occur at 200 ˚C and 400 ˚C (Cárdenas *et al.*, 2000; Schild, 1993; Holec and Chin, 1992). On the other hand in this study, it was observed that PAN had two major decompositions at 270 ˚C and 325 ˚C, while PVDF had decomposition beyond 450 ˚C. However, in this instance the membrane prepared was constituted of the three polymer materials, namely PMAA, PVDF and PAN.

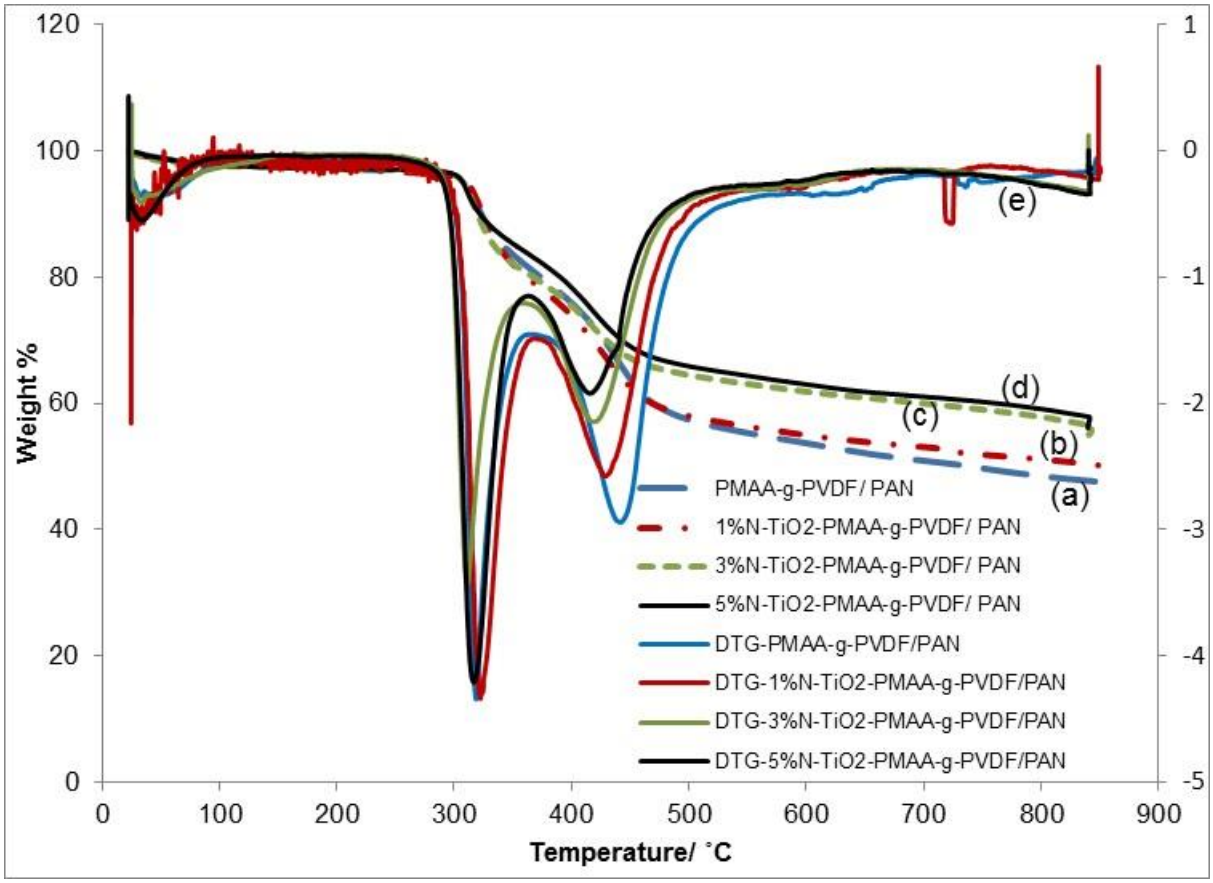

Figure 5.18: Thermo-grams of (a) PMAA-g-PVDF/ PAN, (b) 1%N-TiO_2-PMAA-g-PVDF/ PAN, (c) 3%N-TiO_2-PMAA-g-PVDF/ PAN, (d) 5%N-TiO_2-PMAA-g-PVDF/ PAN & (d) Derivative, heating rate 15 ˚C/ min

The initial step in the degradation of PMAA-g-PVDF/ PAN membrane was in the temperature range 30 ˚C up to 140 ˚C. A weight loss of 8 % was observed owing to water loss and solvents used in the preparation of the PMAA-g-PVDF/ PAN membranes. Other researchers carried out TGA-FTIR studies and observed the formation of anhydride-like structures (the majority of which involve 6-membered rings) towards the end of the first step as confirmed by the shift in the carboxyl group from 1709 cm^{-1} to 1715 cm^{-1} (Dubinsky *et al.*, 2004; McGaugh and Kottle, 1967). Also observed was the loss of residual monomer. The PMAA-g-PVDF/ PAN membrane was stable up to 320 ˚C which marked the beginning of the second step of decomposition. Here a major weight loss of 60 % was observed in the

temperature range 320 ˚C to 430 ˚C. This stage of degradation involved the decarboxylation of anhydride structures of the poly (methacrylic acid) chains releasing carbon dioxide leading to the formation of intermediates which later formed other products such as ketenes, ketones and unsaturated compounds (Cervantes-Uc *et al.,* 2006; Ho *et al.,* 1992; Maurer *et al.,* 1987); and decomposition of the nitrile groups of poly (acrylonitrile) chains with the release of ammonia and other products. The last stage of PMAA-g-PVDF/ PAN decomposition was observed in the temperature range 430 ˚C up to 510 ˚C with a weight loss of 30 %. At higher temperatures substantial decomposition of poly (methacrylic acid) chains occured resulting in the formation of a largely aromatic char with phenol functionalities as well as methyl and quaternary carbons (Fyfe and McKinnon, 1986). On the other hand, decomposition of PVDF chains occured in this temperature range with hydrogen fluoride as the major product as well the monomer and small amounts of $C_4H_3F_3$ (Zulfiqar *et al.,* 1994). Beyond 325 ˚C degradation of the poly (acrylonitrile) chains also transpired through fission of carbon bonds linking the monomers.

Figure 5.19 shows the variation of PMAA-g-PVDF/ PAN membrane decomposition temperature as a function of inorganic filler (N-TiO_2). The incorporation of nitrogen doped titanium dioxide into PMAA-g-PVDF/ PAN membranes impacted on the stability of these membranes negatively. When 1 % N-TiO_2 was added to the PMAA-g-PVDF/ PAN membrane, a decrease in the decomposition temperature was observed. PMAA-g-PVDF/ PAN membranes were stable up to 320 ˚C while 1 % N-TiO_2-PMAA-g-PVDF/ PAN was stable up to 318 ˚C. Addition of 3 % N-TiO_2 and 5 % N-TiO_2 further reduced the thermal stability of the PMAA-g-PVDF/ PAN membrane with decomposition temperatures of 315 ˚C and 310 ˚C respectively.

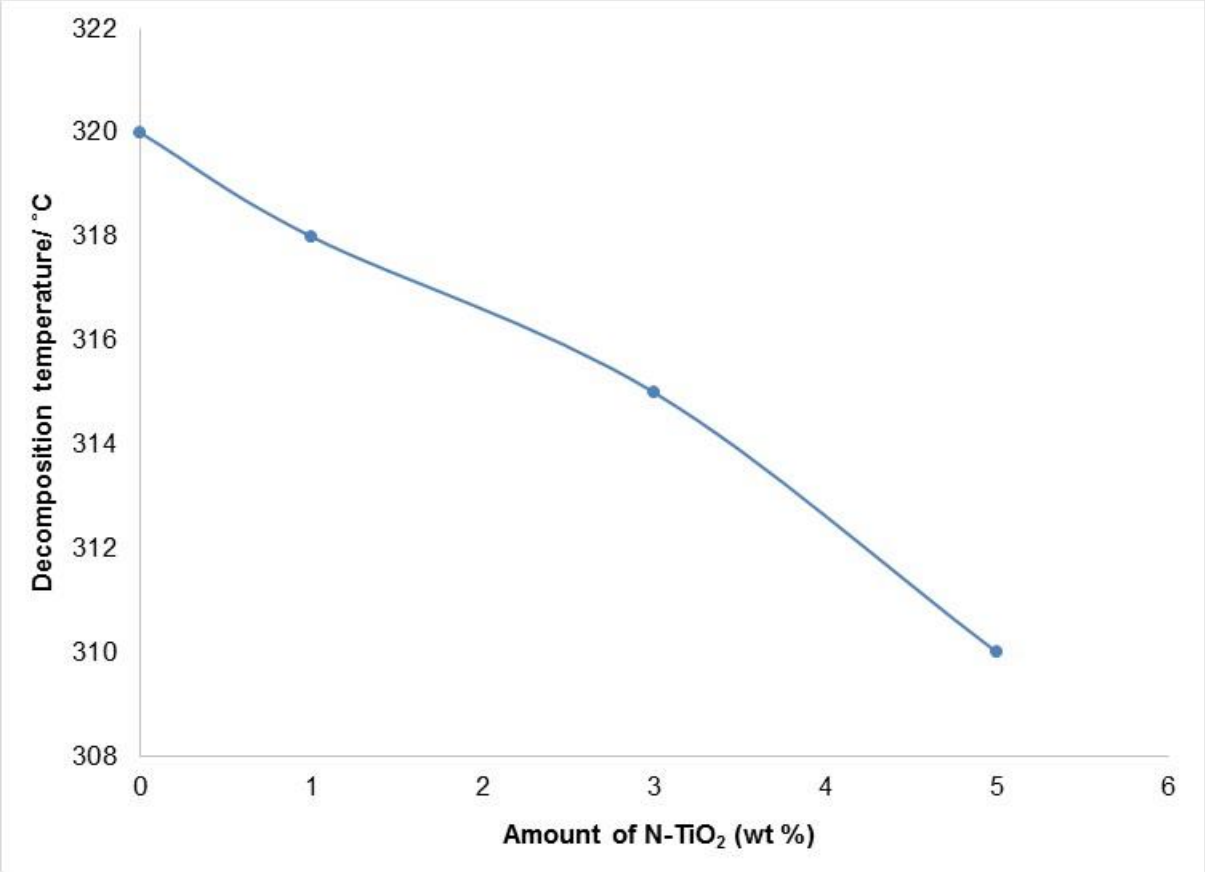

Figure 5.19: Variation of PMAA-g-PVDF/ PAN decomposition temperature as a function of added N-TiO_2

Addition of inorganic fillers such as N-TiO_2 noticeably has different effects depending on the polymer in question. In the case of poly (vinylidene difluoride) membranes (Section 5.4.5.1.) a decrease in thermal stability was observed with the addition N-TiO_2, yet in the case of poly (acrylonitrile) membranes an increase in the thermal stability was observed with the addition of N-TiO_2. However, in the present case where three polymers were combined (PMAA-g-PVDF/ PAN) a decrease in thermal stability was observed with the addition of N-TiO_2.

5.5. Conclusion

Asymmetric polymeric membranes of PAN, PVDF, and PMAA-g-PVDF/ PAN loaded with 1 %, 3 % and 5 % N-TiO_2 were prepared via the dry-wet phase inversion technique (Loeb Sourirajan method). FT-IR and NMR analyses confirmed the successful grafting of poly (methacrylic acid) chains onto poly (vinylidene difluoride). The prepared membranes all conformed to the asymmetric structure as confirmed by cross-sectional view study via scanning electron microscopy. Asymmetric membranes are characterized by a thin selective top layer supported by a porous sub-layer. Tensile strength analysis indicated that addition of incremental amounts of N-TiO_2 to the PAN, PVDF, and PMAA-g-PVDF/ PAN membranes results in a reduction in tensile strength, elongation at break and the Young's modulus. However, PMAA-g-PVDF/ PAN membranes were least affected as compared to PAN and PVDF membranes. Thermal analysis of the three different composition of membrane revealed their varying degree of stability when heated from 20 ˚C to 900 ˚C. Increasing the amount to N-TiO_2 was observed to bring about thermal stability in PAN membranes while it had an opposite effect for PVDF and PMAA-g-PVDF/ PAN membranes.

Bibliography

Adout A., Kang S., Asatekin A., Mayes A.M., and Elimelech M. *Environmental Science and Technology*: 44 **(2010)** 2406–2411.

Carbajo R.J. Neira J.L. NMR for Chemists and Biologists. *Springer*, **(2013)**, 1st edition, 36-38.

Cárdenas G., Muñoz C., and Carbacho H. *European Polymer Journal*: 36 **(2000)** 1091-1099.

Cervantes-Uc J.M., Cauich-Rodríguez J.V., Vázquez-Torres H., and Licea-Clavaríe A. *Polymer Degradation and Stability*: 91 **(2006)** 3312-3321.

Deng S., and Ting Y.P. *Langmuir*: 21 **(2005)** 5940-5948.

Dubinsky S., Grader G.S., Shter G.E., Silverstein M.S. *Polymer Degradation and Stability*: 86 **(2004)** 171-178.

Fyfe C.A., and McKinnon M.S. *Macromolecules*: 19 (7) **(1986)** 1909-1912.

Hashim N.A., Fu Liu, K. Li. *Journal of Membrane Science*: 345 **(2009)** 134-141.

Ho B.C., Lee Y.D., and Chin W.K. *Journal of Polymer Science Part A*: *Polymer Chemistry*: 30 (11) **(1992)** 2389-2397.

Holec E., and Chin W. *Journal of Polymer Science*: *Part A*: 30 **(1992)** 2389.

Khulbe K.C., Feng C.Y., and Matsuura T. Synthetic polymer membranes characterization by atomic force microscopy. *Springer*, **(2008)**, 190.

Lai C.Y., Groth A., Gray S., and Duke M. *Journal of Membrane Science*: 449 **(2014)** 146-157.

Liu F., Tao M-m., and Xue X-m. *Desalination*: 298 **(2012)** 99-105.

Losito I., Amorisco A., Palmisano F., Zambonin P.G. *Applied Surface Science*: 240 **(2005)** 180-188.

Malmonge L.F., and Mattoso L.H.C. *Polymer*: 41 **(2000)** 8387-8391.

Martin S.C., Liggat J.J., and Snape C.E. *Polymer Degradation and Stability*: 74 **(2001)** 407-412.

Maurer J.J., Eustace D.J., and Ratcliffe C.T. *Mcromolecules*: 20 (1) **(1987)** 196-202.

McGaugh M.C., and Kottle S. *Journal of Polymer Science*: Polymer Letters Ed: 5 (9) **(1967)** 817.

McMurry J. Organic Chemistry. *Thomson Learning Inc*, **(2008)**, 7th edition, 445-458.

Meng J.Q., Chen C.L., Huang L.P., Du Q.Y., and Zhang Y.F. *Applied Surface Science*: 257 **(2011)** 6282-6290.

Oh S.J., Kim N., and Lee Y.T. *Journal of Membrane Science*: 345 **(2009)** 13-20.

Phonthammachai N., Gulari E., Jamieson A.M., and Wongkasemjit S. *Applied Organometallic Chemistry*: 20 **(2006)** 499-504.

Schild H.G. *Journal of Polymer Science*: *Part A*: 31 **(1993)** 2403.

Shen Y., and Lua A.C. *Chemical Engineering Journal*: 192 **(2012)** 201-210.

Su Y.L., Cheng W., Li C., and Jiang Z. *Journal of Membrane Science*: 329 **(2009)** 246-252.

Sui T., Gao X., Wang Z., Gao C. *Journal of Membrane Science*: 394-395 **(2012)** 107-119.

Surinarayanan M., Vijayaraghavn R., and Raghavan K.V. *Journal of Polymer Science Polymer Chemistry Ed*: 36 **(1998)** 2503-2512.

Xue T.J., McKinney M.A., and Wilkie C.A. *Polymer Degradation and Stability*: 58 **(1997)** 193-202.

Yan L., Li Y.S., Xiang C.B., and Xianda S. *Journal of Membrane Science*: 276 **(2006)** 162-167.

Yang M.C., and Liu T.Y. *Journal of Membrane Science*: 226 **(2003)** 119-130.

Ying L., Wang P., Kang E.T., and Neoh K.G. *Macromolecules*: 35 (**2002)** 673-679.

You S.J., Semblante G.U., Lu S.C., Damodar R.A., and Wei T.C. *Journal of Hazardous Materials*: 237-238 **(2012)** 10-19.

Yu T., Lin J., Xu J., Chen T., Lin S., and Tian X. *Composites Science and Technology*: 67 **(2007)** 3219-3225.

Zulfiqar S., Zulfiqar M., Rizvi M., Munir A., and McNeill I.C. *Polymer Degradation and Stability*: 43 (3) **(1994)** 423-430.

CHAPTER 6

6. Evaluation of photo-catalytic properties of N-TiO_2-PMAA-g-PVDF/ PAN membranes with ozonolysis

6.1. Introduction

This chapter is on the evaluation of the photo-catalytic properties of membrane supported nitrogen doped titanium dioxide. Different photo-catalyst loadings (1 %, 3 %, and 5 % N-TiO_2) were supported on asymmetric membranes of PVDF, PMAA-g-PVDF/ PAN, and PAN. The effect of photo-catalyst loading was also investigated on the degradation of organic pollutants in water. The investigation focused on three herbicides (bentazon, paraquat and atrazine) that are commonly used in agricultural practices worldwide. The source of UV-light was a Camag lamp (50/ 60 Hz, 40 W) capable of providing UV_{254} or UV_{366}. Visible light experiments were conducted using solar irradiation. Ozonolysis was also evaluated on the degradation of the three herbicides alone, as well as in combination with membrane supported N-TiO_2. The study also focused on investigating the synergistic effect of titanium dioxide photo-catalysis and ozonation. A mighty ozone generator supplying ozone at a flow rate of 25 L/ min and concentration of 4 g/ hr was used in all ozonation experiments. The other part of the study focused on the removal of heavy metals from water using membrane supported N-TiO_2 photo-catalyst. The model heavy metal pollutants investigated were lead (Pb^{2+}) and iron (Fe^{3+}). All the experiments carried in this section utilized membrane disks 28.3 cm2 in size (diameter 6 cm), a temperature of 25 ˚C, and natural pH except in the case where effects of pH are investigated. The adjustment of pH was done by addition of an acid or a base to the experimental solutions in question.

6.2. Photo-catalytic performance of membrane supported N-TiO_2

6.2.1. Effect of support material

The effect of using different polymer support material (PVDF, PMAA-g-PVDF/ PAN and PAN) on the effectiveness of N-TiO_2 was investigated on the degradation of the herbicide bentazon in water. The essence of using different polymer materials was to investigate the robustness of each membrane material under photo-catalytic conditions, and also to establish how much it interferes with the overall photo-oxidation process. Figure 6.1 shows the degradation data of bentazon over four cycles using a fixed amount of photo-catalyst (1 % N-TiO_2) supported on PVDF, PMAA-g-PVDF/ PAN and PAN membranes. These experiments were carried out under strict UV light irradiation.

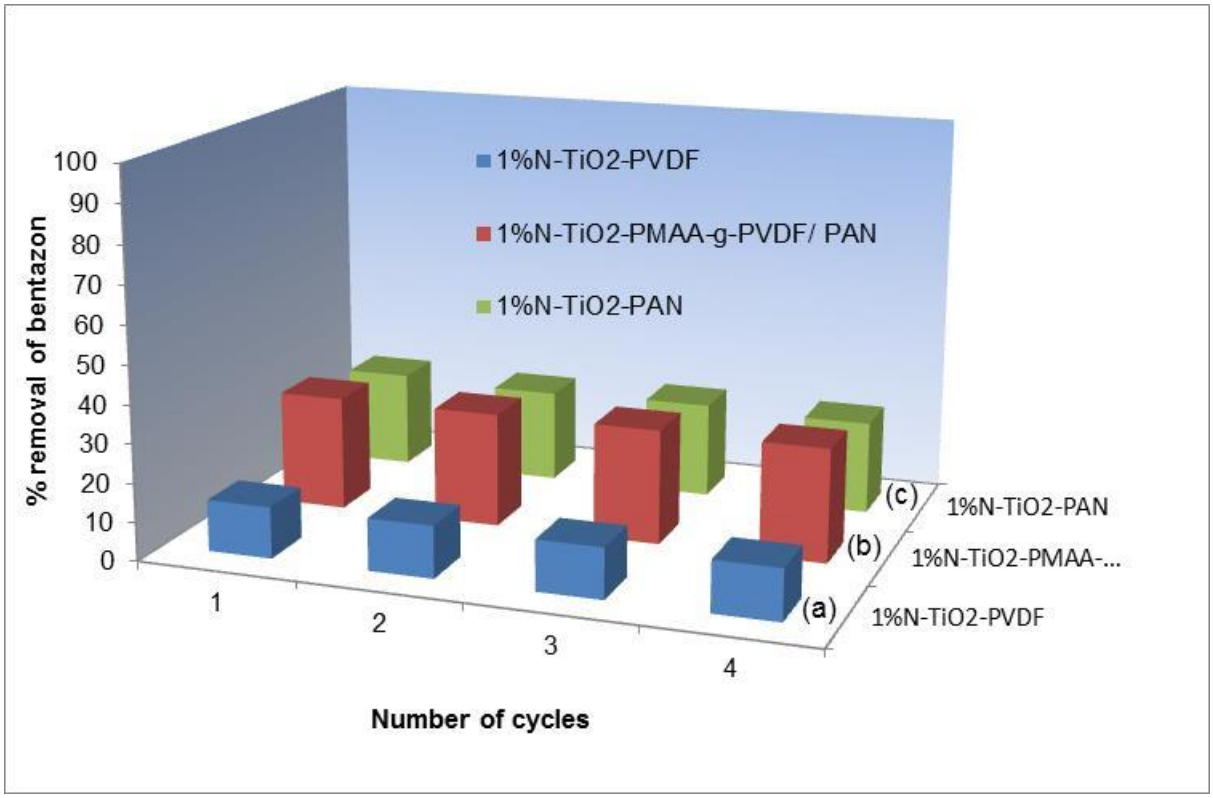

Figure 6.1: Bentazon degradation using (a) 1%N-TiO_2-PVDF, (b) 1%N-TiO_2-PMAA-g-PVDF/ PAN and (c) 1%N-TiO_2-PAN under UV_{366} light irradiation at 25 ˚C and natural pH

The rate of bentazon photo-degradation was quite low for all three photo-catalysts (1 % N-TiO_2-PVDF, 1 % N-TiO_2-PMAA-g-PVDF/ PAN, and 1 % N-TiO_2-PAN) under strict UV light irradiation. This is most probably due to the modification of titanium dioxide via doping with nitrogen to shift its absorption band edge from being a strong UV light absorber towards the visible region. Another factor that could also have contributed to low removal efficiency of the herbicide bentazon is the photo-catalyst loading. The effect of photo-catalyst loading was investigated and presented separately in another section in this chapter. The photo-catalyst (N-TiO_2) supported on PMAA-g-PVDF/ PAN membrane showed the highest rate of bentazon photo-degradation over four cycles. A 29.7 % percent removal efficiency of the herbicide bentazon was achieved using 1 % N-TiO_2-PMAA-g-PVDF/ PAN membrane, 24.5 % with 1 % N-TiO_2-PAN membrane and 13.4 % with 1 % N-TiO_2-PVDF membrane. No deterioration was observed for the three sets of membranes after four cycles of photo-degradation experiments. The findings of these experiments indicated that the most suitable photo-catalyst support material was PMAA-g-PVDF/ PAN; hence it was used in further investigations.

6.2.2. Effect of photo-catalyst loading

The effect of photo-catalyst loading was investigated on the degradation of bentazon under both UV and visible light irradiation. Asymmetric membranes of PMAA-g-PVDF/ PAN were loaded with incremental amounts of nitrogen doped titanium dioxide. Figure 6.2 shows the photo-degradation profiles obtained on the photo-degradation of the herbicide bentazon under UV light irradiation using 1 % N-TiO_2-PMAA-g-PVDF/ PAN, 3 % N-TiO_2-PMAA-g-PVDF/ PAN and 5 % N-TiO_2-PMAA-g-PVDF/ PAN. The initial concentration of herbicide bentazon in water was 10 ppm, and it is clearly visible from the control of the experiment (d) that no change in the concentration occurred when the reaction vessel was kept in the dark. This is a

clear indication that titanium dioxide modified or unmodified can only be activated by photons of light of a specific wavelength (energy equal or greater than the band gap energy); hence no photo-catalysis transpires if the reaction vessel is kept in the dark (Khan and Berk, 2014; Cao *et al.*, 2014; Castro *et al.*, 2009; Yuan *et al.*, 2006; Kobayakawa *et al.*, 2005). Photo-degradation of bentazon was observed with 1 % N-TiO_2 under UV light irradiation.

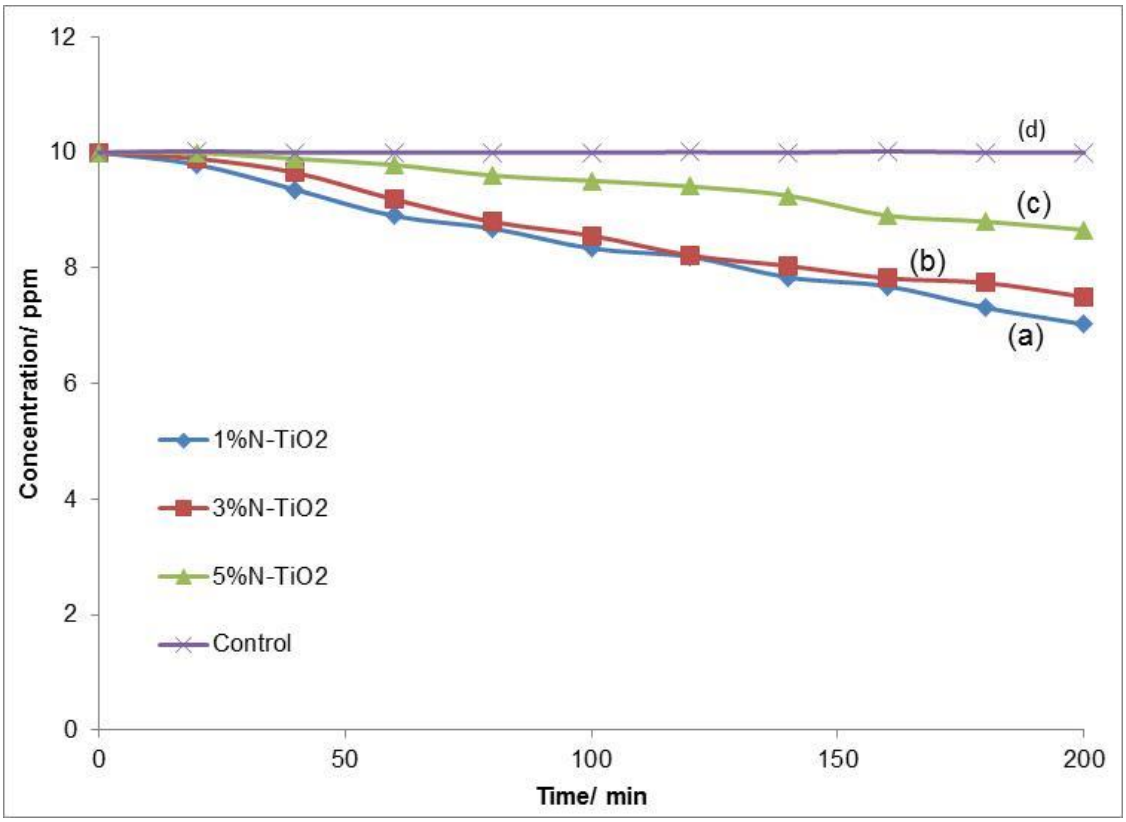

Figure 6.2: Degradation of bentazon using (a) 1%N-TiO_2 PMAA-g-PVDF/ PAN, (b) 3%N-TiO_2 PMAA-g-PVDF/ PAN, (c) 5%N-TiO_2 PMAA-g-PVDF/ PAN and (d) control at 25 ˚C, natural pH and strict UV_{366} light irradiation

About 12 % of the herbicide was removed within 3 hours of exposure to 1 % N-TiO_2 photo-catalyst. When the photo-catalyst loading was increased from 1 % N-TiO_2 to 3 N-TiO_2, the rate of bentazon photo-degradation also increased (b) and about 30 % of the herbicide bentazon was degraded. This clearly indicates that increasing the concentration of the photo-

catalyst translates to an increased rate of photo-degradation of the organic pollutant bentazon in water.

However, when the concentration of photo-catalyst was increased to 5 % N-TiO_2, no significant change in the rate of bentazon photo-degradation was observed. The most probable explanation is that this is due to loss of surface area as the N-TiO_2 nano-particles begin to form lumps or agglomerates with each increment of photo-catalyst powder. These experiments were also carried out under sunlight. Figure 6.3 shows the degradation profiles of bentazon obtained under both UV and visible light irradiation.

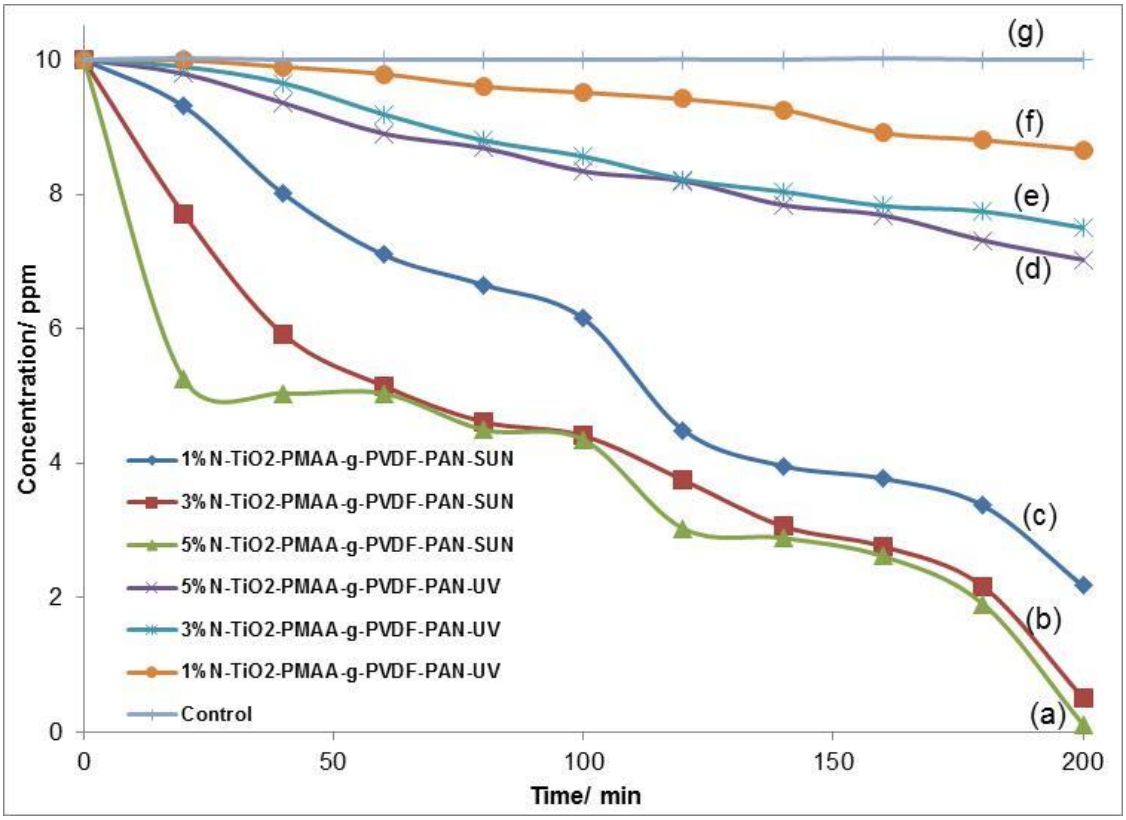

Figure 6.3: Degradation of bentazon under visible light using (a) 5%N-TiO_2, (b) 3%N-TiO_2, & (c) 1%N-TiO_2 and under strict UV light using (d) 5%N-TiO_2, (e) 3%N-TiO_2, (f) 1%N-TiO_2, & (g) control supported on PMAA-g-PVDF/ PAN at 25 ˚C, natural pH

When the photo-degradation of the herbicide bentazon was carried out under sunlight a dramatic increase in the rate of photo-degradation was observed. This huge increase in the rate of photo-degradation is owed to the effect brought about by doping TiO_2 with nitrogen (Quan *et al.,* 2014; Khan and Berk, 2014; Mungondori and Tichagwa, 2013; Nyamukamba *et al.,* 2012; Castro *et al.,* 2009). Nitrogen doping resulted in the narrowing of the band gap of TiO_2 (Ksibi *et al.,* 2008; Jiaguo *et al.,* 2006). An herbicide degradation efficiency of 78.3 % was observed within 3 hours using 1 % N-TiO_2-PMAA-g-PVDF/ PAN. Increasing the photo-catalyst loading to 3 % N-TiO_2 was observed to further increase the rate of bentazon photo-degradation, resulting in a removal efficiency of 94.9 %. Nevertheless, when the photo-catalyst loading was increased to 5 % N-TiO_2 no significant change in the rate of bentazon degradation was observed. This phenomenon was observed under both UV and visible light irradiation. The findings of this study suggested that the optimum amount of N-TiO_2 that could be incorporated into PMAA-g-PVDF/ PAN membranes was 3 % N-TiO_2. Increasing the amount of this photo-catalyst beyond 3 % N-TiO_2 appeared to be uneconomical since no significant change in the rate of bentazon photo-degradation was observed. The most sensible explanation is owed to surface area reduction caused by agglomeration of N-TiO_2 nano-particles.

In other studies Ag/ Pd-TiO_2 photo-catalyst supported on multi-walled carbon nano-tubes (MWCNT) were prepared via a modified dry-mix metal-organic chemical vapour deposition technique (MOCVD). The researchers varied the titania loading between 10 and 40 weight %. They realized a 92 % removal efficiency of 50 mg/L methylene blue with a deposition of 2% Ag on 20% TiO_2/MWCNT in 4 hours with a photo-catalyst loading of 1 g/ L (Hintsho *et al.,* 2014). You and co-workers plasma grafted poly (acrylic acid) (PAA) onto commercial poly (vinylidene difluoride) (PVDF) to introduce functional groups on the membrane surface

that could support TiO_2 nanoparticles. In their investigations, they achieved between 30 % and 42 % removal efficiency of 50 mg/ L aqueous reactive black 5 (RB5) under UV light irradiation (You *et al.,* 2012) with a photo-catalyst loading of 1.5 weight % TiO_2. Bosc and co-workers prepared asymmetric ceramic membranes coated with anatase titanium dioxide in a bid to combine membrane separation and photo-catalysed reactions. In their design, colloids and macromolecules was retained by the selective top layer whereas photo-degradation of smaller organic molecules remaining in the permeate was catered for through irradiation of the opposite side of the membrane with UV light. They observed that the side of the membrane in contact with the reception solution (methylene blue solution) (MB) remained white under continuous UV light irradiation. They noticed that for the lowest concentrations in the feed solution, MB was completely destroyed as it arrived in the reception tank (Bosc *et al.,* 2005).

6.2.3. Effect of different organic pollutants

The photo-degradation efficiency of 3 % N-TiO_2-PMAA-g-PVDF/ PAN was evaluated on the degradation of three different herbicides (bentazon, paraquat, and atrazine) in water. Figure 6.4 shows the herbicide removal efficiency profiles obtained. Removal efficiencies were calculated using the following equation:

$$RE = \frac{C}{C_0} \times 100\% \quad \text{……...….. (6.1)}$$

Where RE is the removal efficiency, C_0 is the initial concentration, and C is the concentration at any given time.

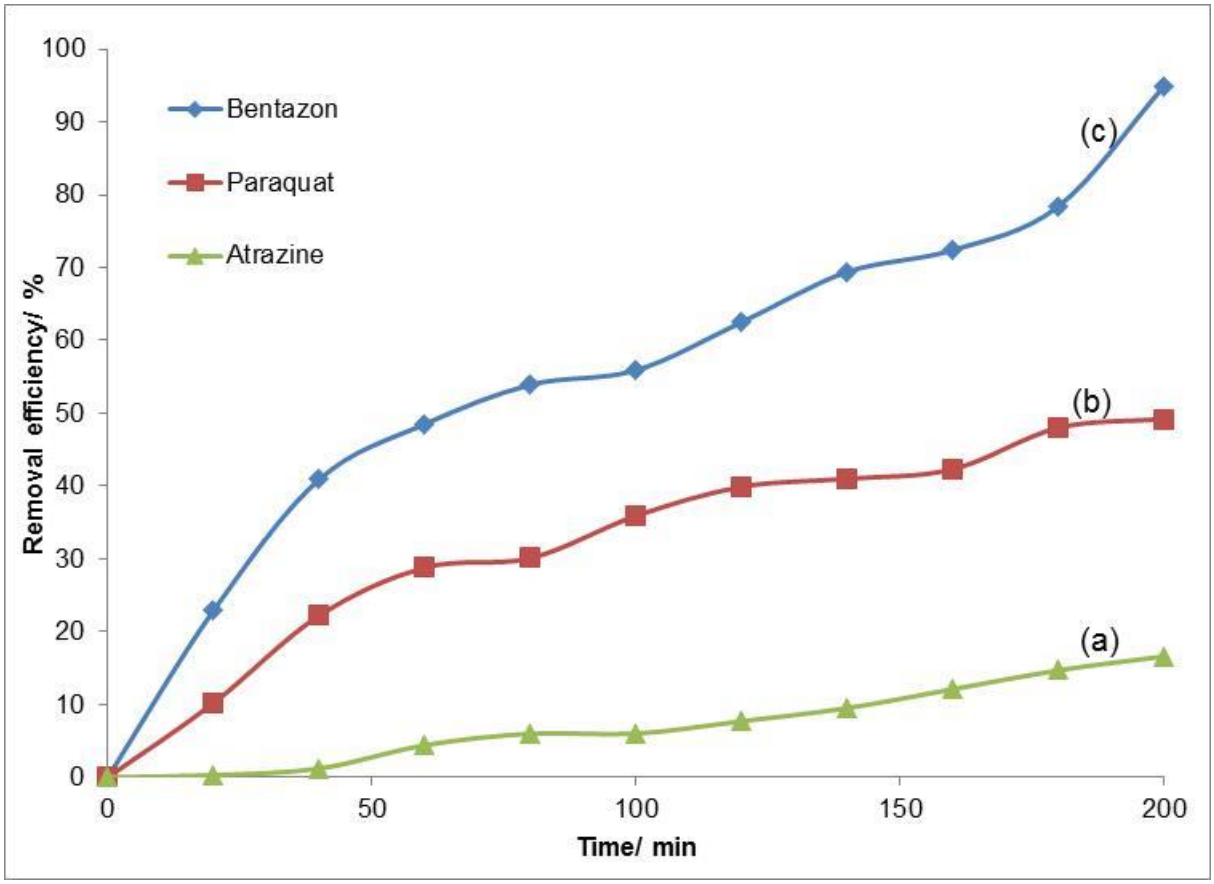

Figure 6.4: Removal efficiency of (a) atrazine, (b) paraquat, and (c) bentazon at 25 ˚C, natural pH, under solar irradiation

Experiments to evaluate the photo-degradation efficiency of three different herbicides (bentazon, paraquat, and atrazine) were carried out in triplicate. The initial concentration of all three herbicides was 10 ppm and the evaluation period was 3 hours under visible light irradiation with a photo-catalyst loading of 3 weight % (55.6 mg/ m^{-2}) N-TiO_2 supported on PMAA-g-PVDF/ PAN membranes. The photo-degradation of the herbicide bentazon was quite rapid, reaching a removal efficiency of 94.9 % in a period of 3 hours of exposure to N-TiO_2. In other studies employing slurry TiO_2 under UV light irradiation, 99 % removal efficiency of the herbicide bentazon was achieved in a period of 90 minutes (Pourata *et al.*, 2009). The difference between the two studies is the fact that slurry TiO_2 was used in the earlier studies which obviously presented a larger surface area compared to the immobilized

TiO_2 in the current study. However, one of the aims of the current study was to produce immobilized nitrogen doped TiO_2 to avert the problems associated with post-recovery of spend photo-catalyst from the aqueous environment. Seck and co-workers also conducted a comparative study on the removal efficiency of the herbicide bentazon from water using sol-gel prepared nano-crystalline TiO_2 material and Degussa P25 (commercial TiO_2) under UV light irradiation. They achieved the most efficient removal of bentazon and its toxic intermediates using nano-crystalline TiO_2 at pH 7.0 (Seck *et al.*, 2012).

A paraquat removal efficiency of 49.2 % was attained using 3 % N-TiO_2-PMAA-g-PVDF/ PAN under visible light irradiation, while that for atrazine was as low as 16.6 %. The differences in structural constitution of these three herbicides may be ascribed to the observed differences in the rate of photo-degradation. The most obvious reason deduced from the findings of this investigation may be ascribed to the differences in the mechanisms of photo-oxidation. The findings of this study (Fig. 6.4) indicated that the herbicide bentazon was more susceptible to photo-oxidation than paraquat and atrazine. Atrazine can be considered to be more recalcitrant followed by paraquat. These two herbicides proved to be more difficult to remove from water, hence more time for complete mineralization to occur. Furman and co-workers studied the photo-degradation of atrazine in surface waters of the Columbia basin, Washington. They achieved atrazine removal efficiencies of between 51 % and 80 % over two days using a xenon lamp (Furman *et al.*, 2013). Their findings also proved that atrazine is a more recalcitrant organic pollutant that required more exposure time to photo-degrade. However, Yola and co-workers achieved an atrazine removal efficiency of 94 % in 70 minutes using titanium dioxide that was prepared using boron enrichment waste (TiO_2-BEW) (Yola *et al.*, 2014). Cantavenera and co-workers investigated the photo-catalytic degradation of paraquat using polycrystalline TiO_2 Degussa P25 under near UV light irradiation. They

achieved total removal of the herbicide in 3 hours with a photo-catalyst loading of 0.4 g/ L (Cantavenera *et al.,* 2007). This is a clear indication that unimmobilized TiO_2 is more effective than immobilized TiO_2, nevertheless, the goal is to avert problems associated with photo-catalyst post-recovery. Another factor which comes into play is the limited amount of photo-catalyst that can be effectively blended or incorporated into the membrane without compromising its structure and integrity.

6.2.4. Effect of pH on the photo-degradation of organic pollutants

The effect of pH on the photo-degradation of organic pollutants was investigated. The herbicides bentazon, paraquat and atrazine were used to establish the optimum pH for the photo-degradation process. The photo-degradation experiments were carried out under both acidic and basic conditions (pH = 3, 7, 9). The pH was maintained using buffer systems. The optimum photo-catalyst loading (3 % N-TiO_2-PMAA-g-PVDF/ PAN) was used in this investigation under visible light irradiation. Figures 6.5 to 6.7 show the photo-degradation profiles obtained for the three herbicides under acidic, neutral and basic conditions respectively.

Under acidic conditions, bentazon and atrazine show fairly high rates of photo-degradation as compared to paraquat. At low pH the surface of N-TiO_2 is cationic hence favouring the adsorption of bentazon and atrazine. Removal efficiencies of 83.9 % and 62.6 % were observed for bentazon and atrazine respectively at pH 3.0. When pH was increased to 7.0, the removal efficiencies of bentazon and atrazine also increased to 90.1 % and 66.2 % respectively.

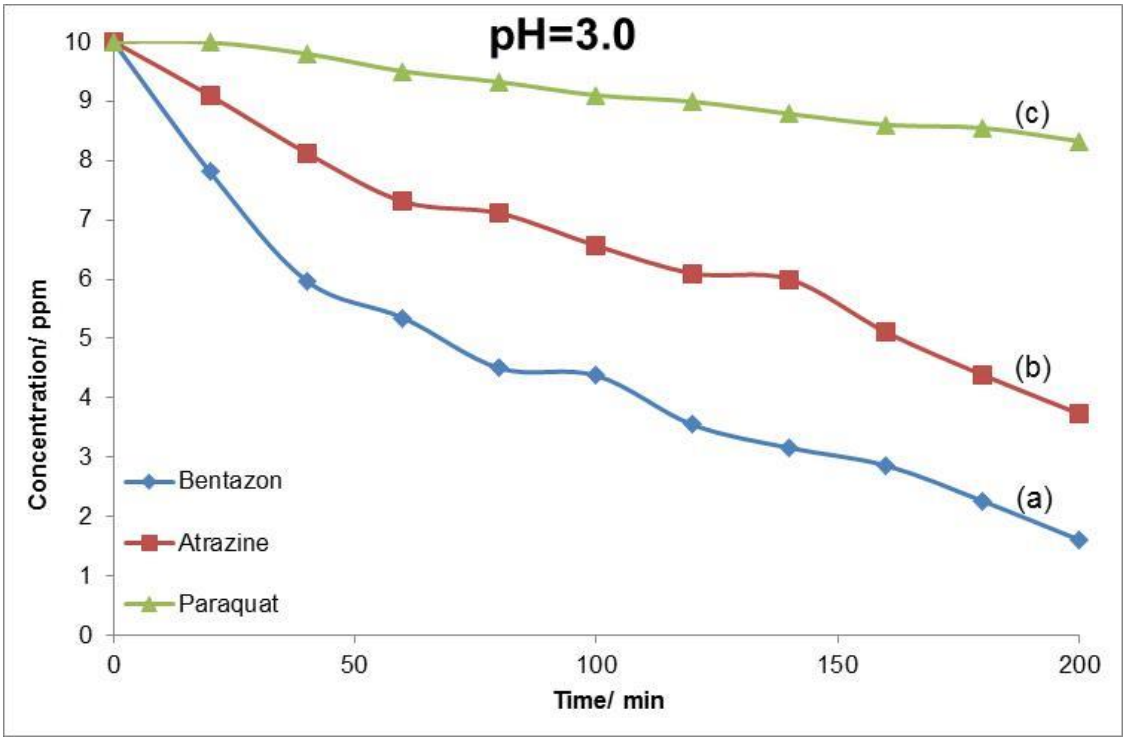

Figure 6.5: Degradation of (a) bentazon, (b) atrazine, and (c) paraquat at pH 3.0, 25 ˚C, under solar irradiation using 3 % N-TiO_2-PMAA-g-PVDF/ PAN

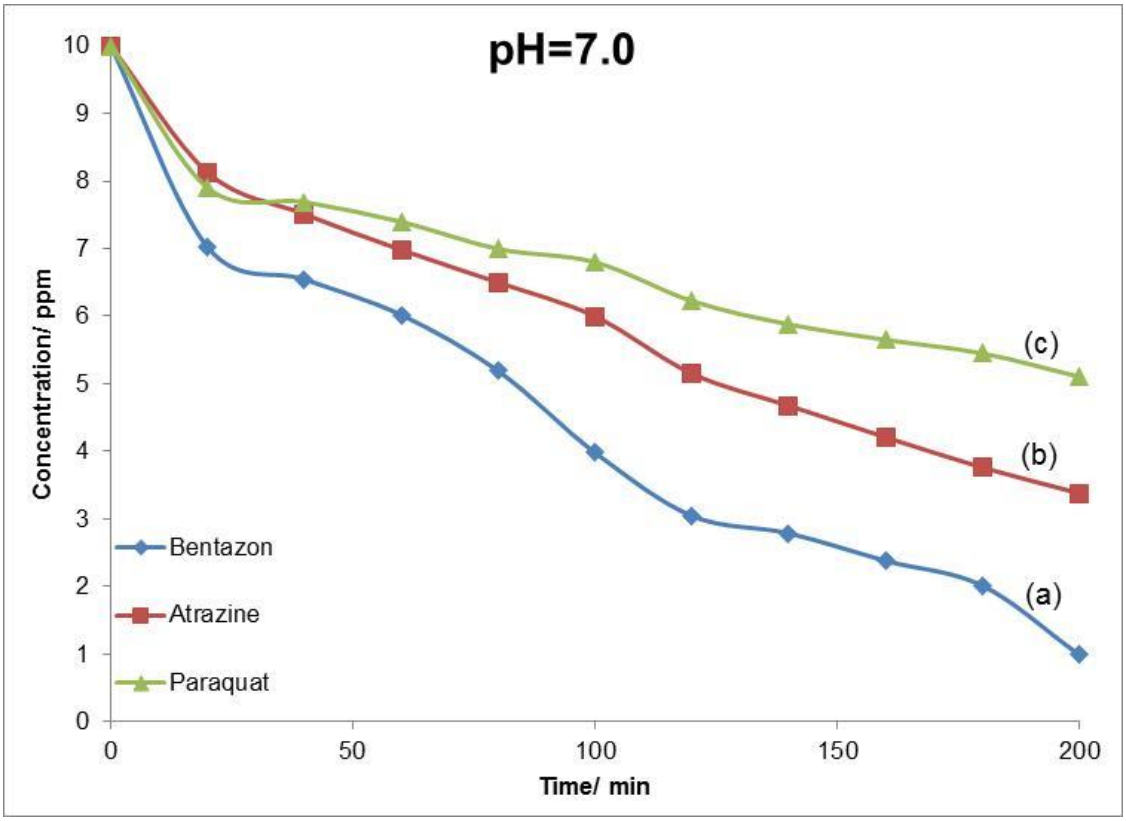

Figure 6.6: Degradation of (a) bentazon, (b) atrazine, and (c) paraquat at pH 7.0, 25 ˚C, under solar irradiation using 3 % N-TiO_2-PMAA-g-PVDF/ PAN

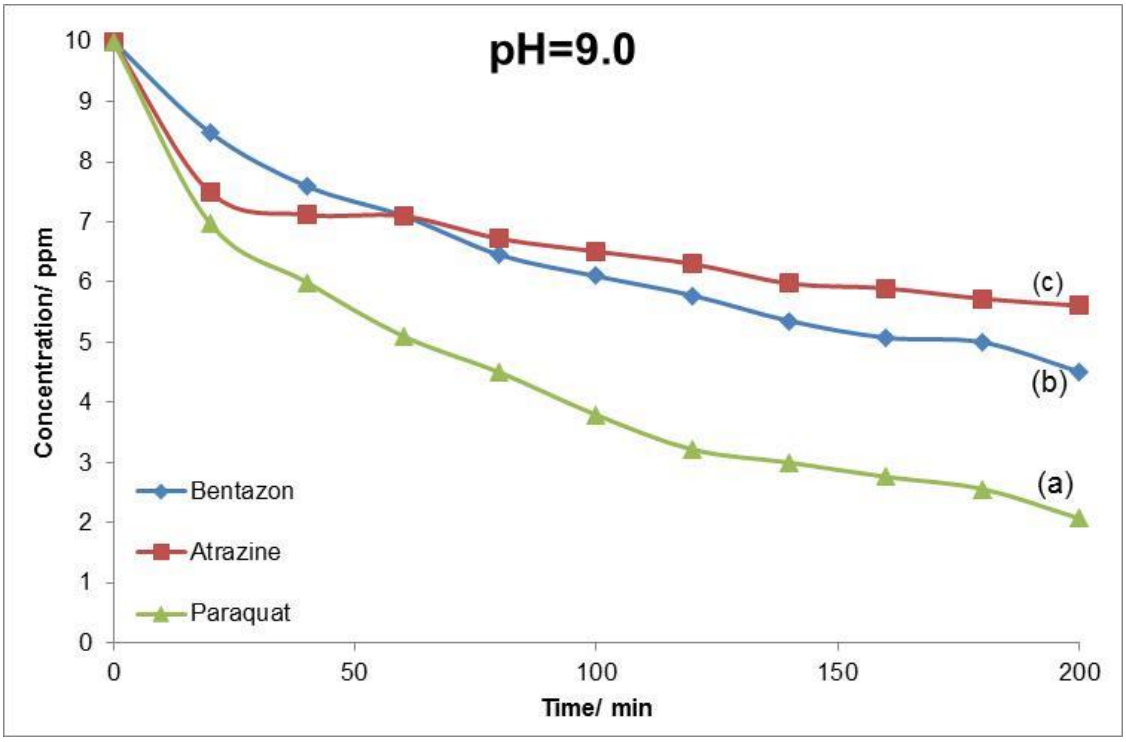

Figure 6.7: Degradation of (a) paraquat, (b) bentazon, and (c) atrazine at pH 9.0, 25 ˚C, under solar irradiation using 3 % N-TiO_2-PMAA-g-PVDF/ PAN

Studies by other researchers also indicated that the pH of an aqueous environment plays an important role in the degradation organic pollutants. Surface charge and the size of aggregates formed by the photo-catalyst are dependent on the pH of the aqueous environment (Seck *et al.*, 2012; Singh *et al.*, 2007; Haque *et al.*, 2006). At pH 3 paraquat removal efficiency was quite low (16.7 %). At low pH paraquat is cationic hence its adsorption is fairly low compared to bentazon and atrazine. When pH was increased to 9, a paraquat removal efficiency of 79.3 % was observed. Under basic conditions the photo-catalyst surface is negative, hence favouring the adsorption of cationic species like paraquat. At high pH the concentration of the hydroxyl ions is quite high, thus recombination of electron-hole pairs is minimized since hydroxyl ions act as hole-scavengers (Sorolla *et al.*, 2012). This leads to an increased rate of paraquat photo-degradation. Other researchers also investigated the photo-degradation of paraquat under acidic and basic conditions. The focus of their study was

investigating the effectiveness of commercial TiO_2 (Degussa P25), home-made TiO_2 and TiO_2/ SBA-15. They observed that paraquat removal using TiO_2/ SBA-15, which is negatively charged even at very low pH, was more advantageous since it does not call for pH adjustment of solution for efficient photo-oxidation of the herbicide (Sorolla *et al.*, 2012). Under basic conditions the rate photo-oxidation of bentazon and atrazine decreased, indicating that the optimum pH for their photo-oxidation is around pH 7.0. In other studies, high photo-degradation rates of 2-chlorophenol were observed under high pH (12.5) using a TiO_2/ UV system (Doong *et al.*, 2001). This shows that adjusting the pH of a solution is very critical in achieving high removal efficiency of organic pollutants in water.

6.2.5. TOC analysis of bentazon, atrazine and paraquat degradation

Total organic carbon (TOC) analysis (multi N/C® 3100 TOC analyzer) was carried out on the aliquots collected from the photo-degradation of the herbicides bentazon, atrazine and paraquat. The three herbicides were photo-degraded with 3 % N-TiO_2-PMAA-g-PVDF/ PAN under solar irradiation. TOC analysis was carried out to assess the organic load of synthetic water with progression of photo-degradation. Figure 6.8 shows the TOC profiles obtained for bentazon, atrazine and paraquat. The TOC was determined directly using the expulsion method, which involves initial removal of total inorganic carbon (TIC) through acidification and expulsion.

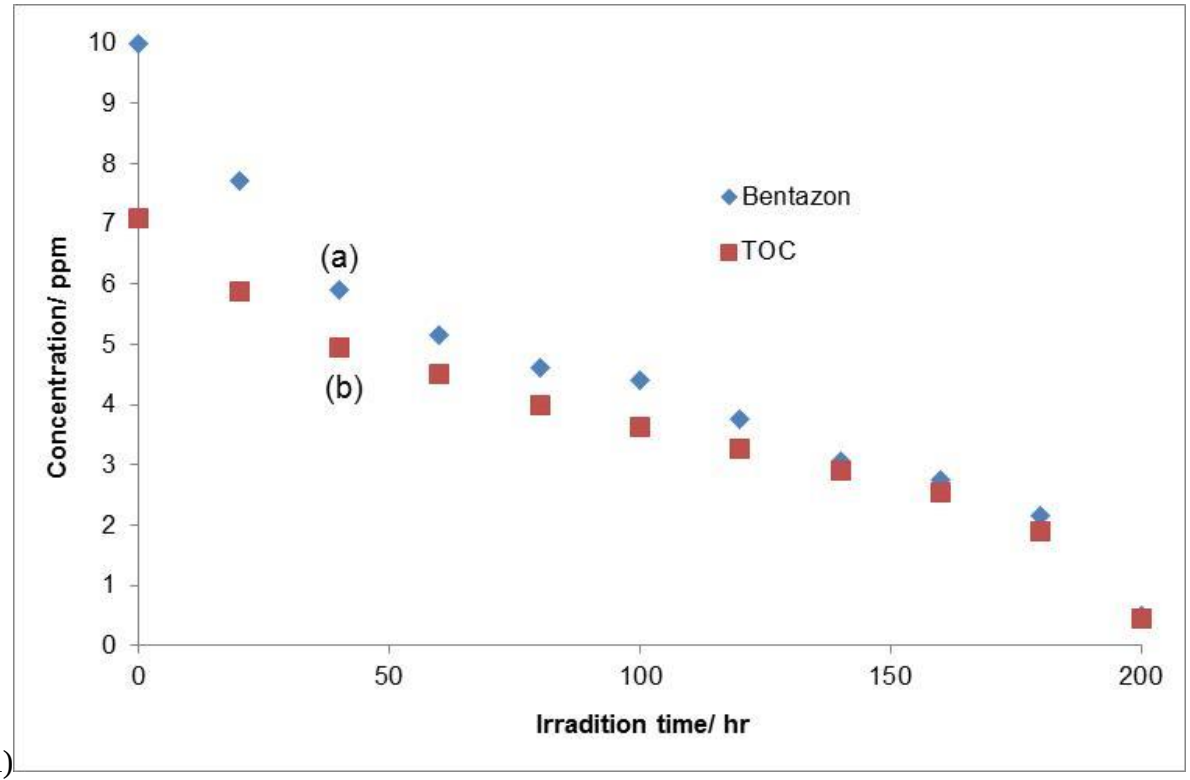
Concentration/ ppm
Irradition time/ hr
Bentazon
TOC
(a)
(b)
0
1
2
3
4
5
6
7
8
9
10
0
50
100
150
200

(i)

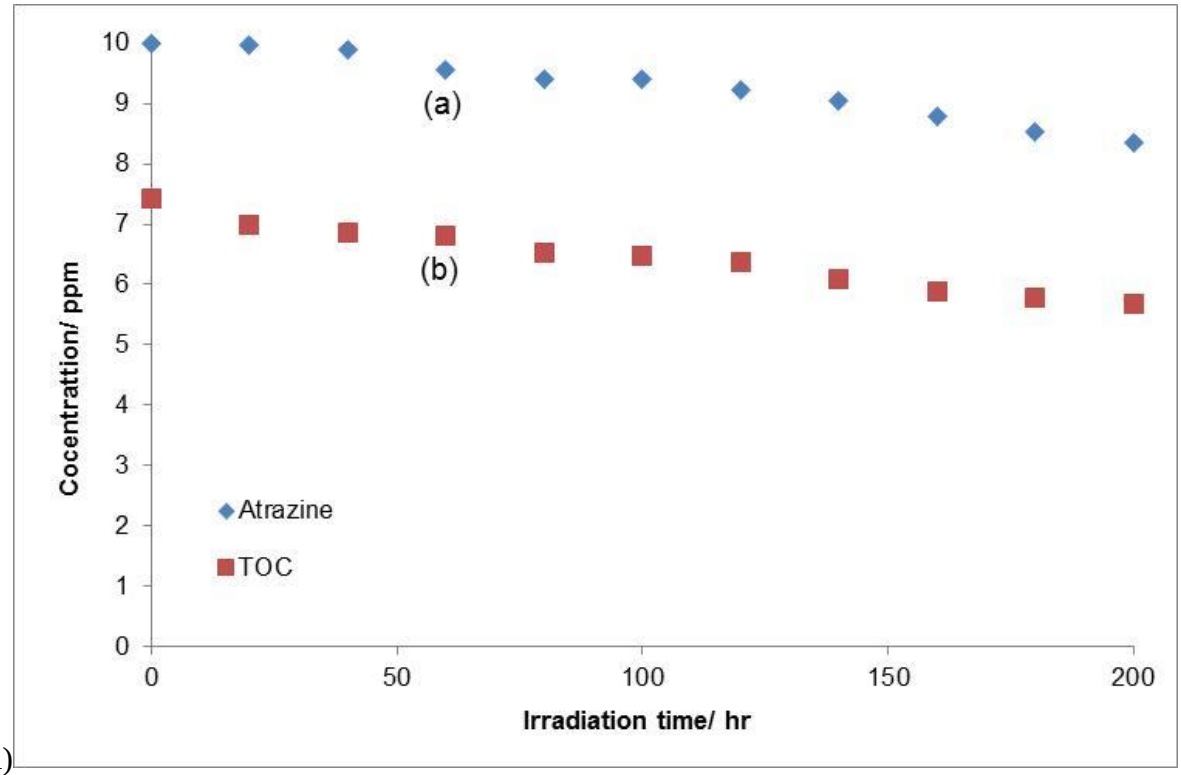
Cocentrattion/ ppm
Irradiation time/ hr
Atrazine
TOC
(a)
(b)
0
1
2
3
4
5
6
7
8
9
10
0
50
100
150
200

(ii)

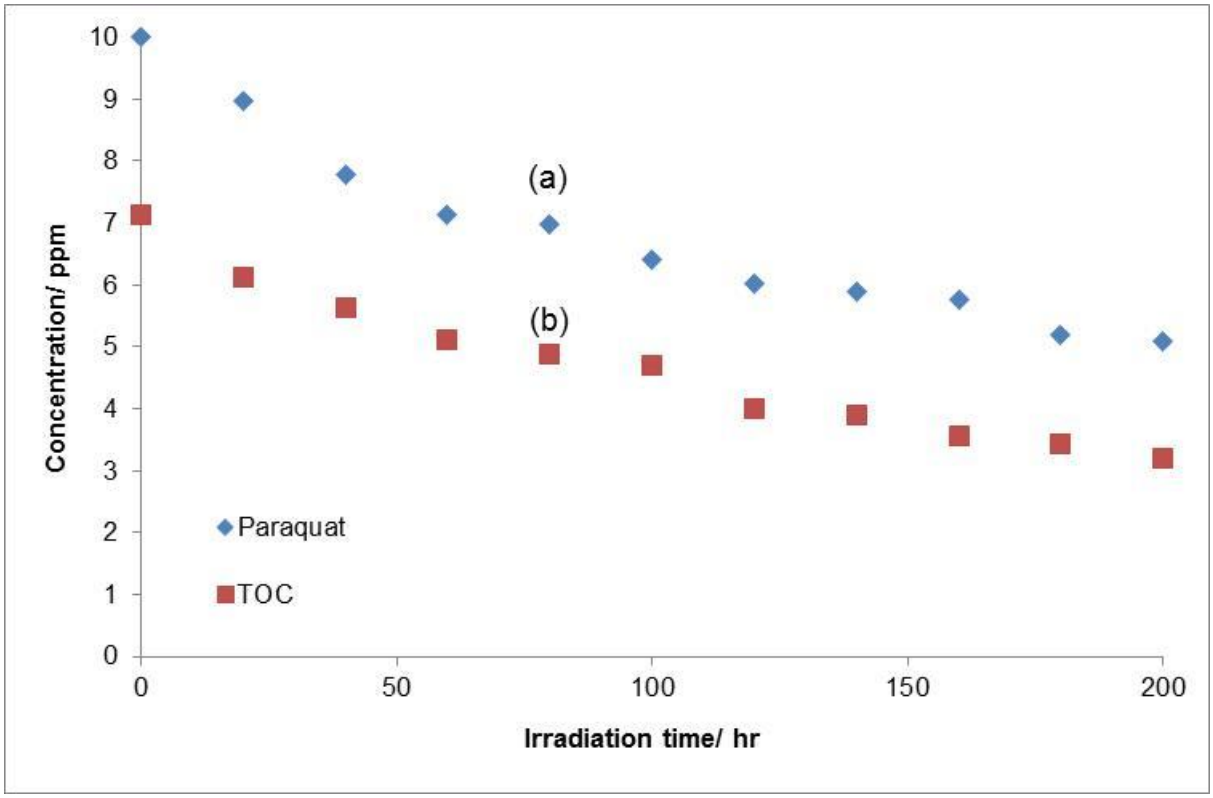

Figure 6.8: TOC analysis of the photo-degradation products of (i) bentazon, (ii) atrazine, and (iii) paraquat at 25 ˚C, natural pH, under sunlight using 3 % N-TiO_2-PMAA-g-PVDF/ PAN

The degradation of bentazon is very rapid compared to atrazine and bentazon. A decrease in the concentration of the three herbicides corresponds with the decrease in TOC over time. However, atrazine and paraquat are more recalcitrant compared to bentazon, hence a slow decrease in their concentration as well TOC was observed with the progression of the photo-degradation reaction. The TOC for the degradation of bentazon was reduced by 95.5 % while those for paraquat and atrazine were reduced by 67.9 % and 43.1 % respectively.

Cantavenera and co-workers also investigated changes in TOC for the degradation of paraquat using Degussa P25 TiO_2. They achieved an almost complete disappearance of paraquat and TOC with 0.4 g/ L TiO_2 within 3 hours of treatment. The experiments carried in the dark with TiO_2 present and also in light with TiO_2 absent showed no change in the

concentration of paraquat as well as TOC (Cantavenera *et al.*, 2007). Liu and co-workers investigated the mineralization of 2,4-dichlorophenol (2,4DCP) in water under UV illumination using a composite membrane with Fe^0, activated carbon fibre (ACF) and TiO_2 (Fe^0/ TiO_2/ ACF). They achieved 72 % TOC removal in 4 hours using Fe^0/ TiO_2/ ACF. They observed that ACF addition and its adsorption capabilities promoted 2,4DCP mineralization and TOC removal (Lui *et al.*, 2009).

6.2.6. Kinetic study of herbicide photo-degradation

It is of paramount importance to know reaction rate kinetics since it dictates how fast contaminants are degraded and whether reaction rate is pollutant dependent or pollutant independent. Reaction kinetics of membrane supported photo-catalyst are apparently dependent on the transport of pollutants and products to and fro the photo-catalyst which is entrapped in the membrane structure. The bulk of the photo-degradation reactions carried out by TiO_2 photo-catalytic membrane fit pseudo-first-order kinetics irrespective of the type of pollutant (Lin *et al.*, 2012; Romanos *et al.*, 2012; Athanasekou *et al.*, 2012; You *et al.*, 2012; Liu *et al.*, 2012; Liao *et al.*, 2012; Hu *et al.*, 2011; Morris *et al.*, 2004). This implies that reaction rate is dependent solely on the concentration of the organic matter. The kinetic studies were performed using data obtained from the photo-degradation of bentazon, atrazine and paraquat with 3 % N-TiO_2-PMAA-g-PVDF/ PAN photo-catalytic membrane at 25 ˚C, natural pH, under sunlight irradiation. The reaction kinetics plots obtained for bentazon, atrazine and paraquat are shown in Figure 6.9.

Figure 6.9 shows that the photo-catalytic degradation of the three herbicides (atrazine, paraquat, and bentazon) corresponds to pseudo-first-order reaction kinetics since it followed the following relationship:

$$\ln (C/ C_0) = kt \quad \text{.....} \quad (6.2)$$

Where C_0 is the initial concentration, C is the concentration at a given time *t*, and *k* is the apparent rate constant.

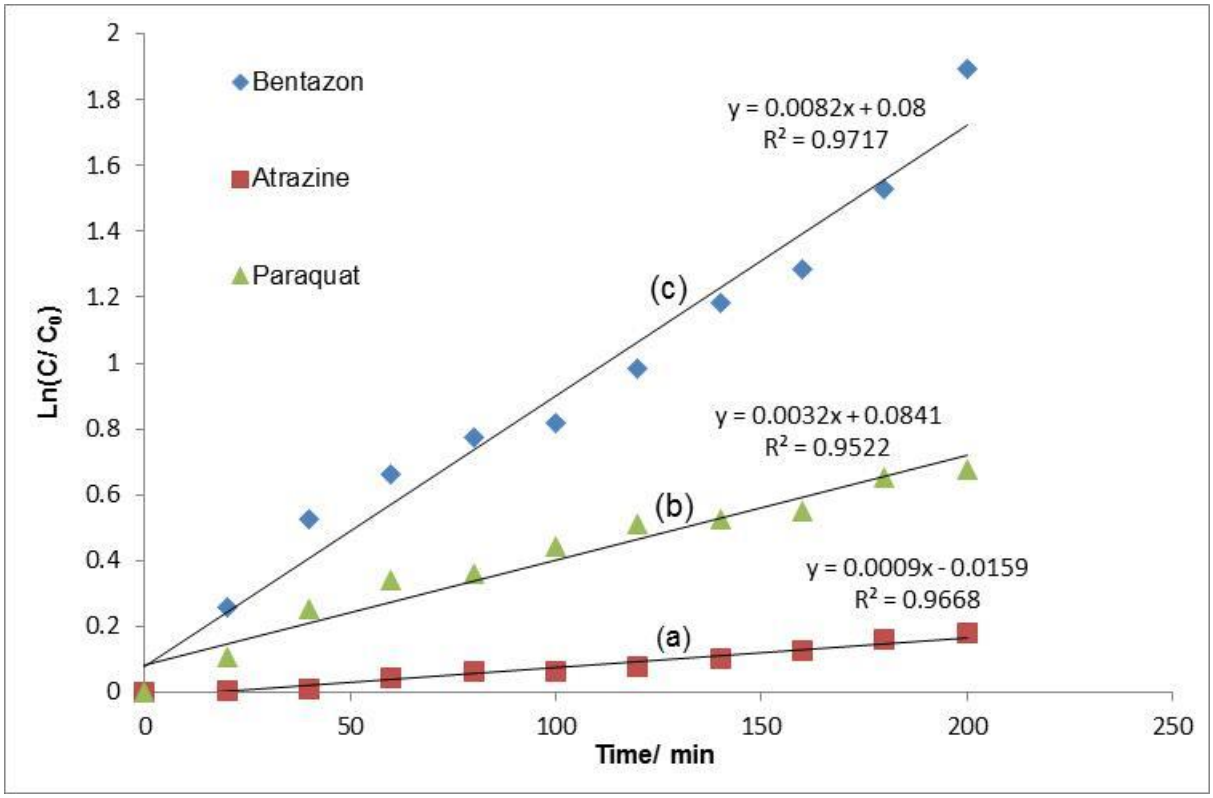

Figure 6.9: Kinetic analysis of (a) atrazine, (b) paraquat, and (c) bentazon degradation at 25 C under solar irradiation using 3 % N-TiO_2-PMAA-g-PVDF/ PAN

The photo-degradation of the three herbicides was carried out using 3 % N-TiO_2-PMAA-g-PVDF/ PAN under sunlight. The photo-degradation of bentazon had the highest rate constant (1.49×10^{-2} min^{-1}), indicating a faster rate of pollutant photo-oxidation, followed by paraquat (3.38×10^{-3} min^{-1}) and lastly atrazine had a rate constant of 9.09×10^{-4} min^{-1} indicating a much slower rate of photo-oxidation. The data obtained for apparent rate constants and linear correlation values for the three herbicides are displayed in Table 8. The plots of ln (C/C_0)

against time for atrazine, paraquat and bentazon are straight lines (Fig. 6.9), implying that the photo-degradation of the three herbicides fitted as pseudo-first-order kinetics (Yola *et al.,* 2014; Sorolla *et al.,* 2012; Pourata *et al.,* 2009).

Table 8: Type of pollutant, linear correlation coefficient (R^2) value and rate constant

Type of membrane	Type of pollutant	R^2	Rate constant (min^{-1})
3%N-TiO_2-PMAA-g-PVDF/ PAN	Bentazon	0.9717	1.49×10^{-2}
	Atrazine	0.9668	9.09×10^{-4}
	Paraquat	0.9522	3.38×10^{-3}

The high coefficients of determination (R^2>0.95) (Table 8) yielded from the semi-logarithmic plots of the concentration data for the photo-degradation of bentazon, paraquat and atrazine signified a good fit to pseudo-first-order rate kinetics.

6.3. Removal of organic pollutants via ozonolysis

The removal of the herbicides bentazon, paraquat and atrazine were also investigated using ozonolysis. Aliquots that were collected were immediately treated with 0.005 M sodium thiosulphate to quench any remaining ozone and prevent further reaction after sampling.

6.3.1. Effect of initial pollutant concentration

The degradation profiles obtained for the degradation of bentazon using ozone (O_3) are shown in Figures 6.10. The ozone was supplied at a constant rate while the concentration of

bentazon was varied from 5 ppm to 15 ppm. The effectiveness of ozone degradation was evaluated with an increasing concentration of bentazon. Initially the removal rate of bentazon was very fast, but subsequently became slow. When the initial concentration of bentazon was increased from 5 ppm to 10 ppm, a significant decrease in the removal efficiency of the pollutant by ozone is observed (Fig. 6.10).

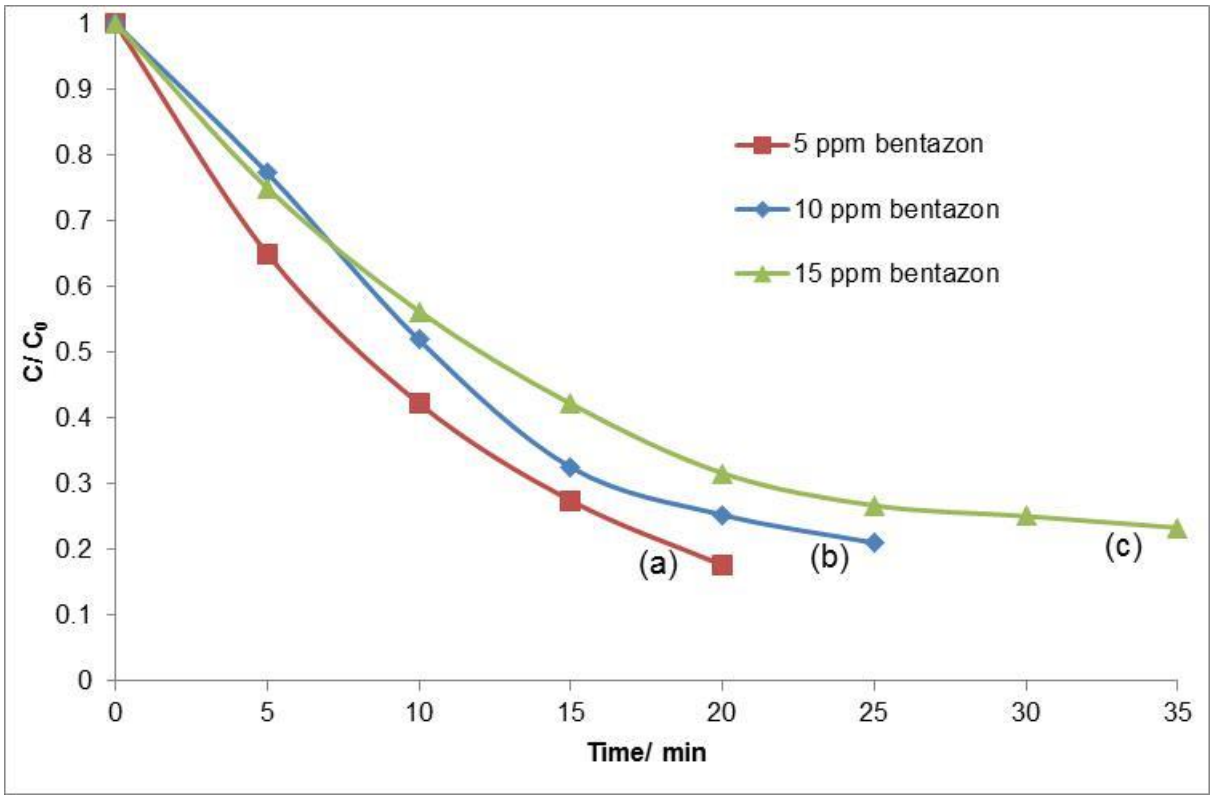

Figure 6.10: Ozone degradation of bentazon (a) 5 ppm, (b) 10 ppm and (c) 15 ppm at ozone flow rate of 25 L/ min and concentration of 4 g/ hr.

The degradation profiles clearly showed that when the initial concentration of bentazon was further to 15 ppm, there is a decrease in the removal efficiency. At an initial bentazon concentration of 5 ppm, a removal efficiency of 96.5 % was achieved in 20 minutes of treatment with ozone. At initial bentazon concentrations of 10 ppm and 15 ppm, removal efficiencies of 90.9 % and 86.7 % were achieved in 25 and 35 minutes respectively. It is

expected that at constant ozone concentration degradation of an increasing amount of bentazon results in an increased amount of reaction time. The results obtained revealed that bentazon removal efficiency decreases with increasing pollutant concentration.

The effect of increasing initial organic pollutant removal via ozone degradation was further investigated using two other herbicides (paraquat and atrazine). The degradation profiles obtained are shown in figures 6.11 and 6.12. The degradation profiles of paraquat showed that the initial degradation of paraquat by ozone is very rapid, but gradually slows down. Increasing the initial paraquat concentration to 10 ppm and 15 ppm was observed to reduce the removal efficiency of the pollutant via ozone degradation. The removal efficiencies achieved with initial paraquat concentrations of 5 ppm, 10 ppm and 15 ppm were 70 % in 30 minutes, 38.9 % in 60 minutes and 30.3 % in 80 minutes.

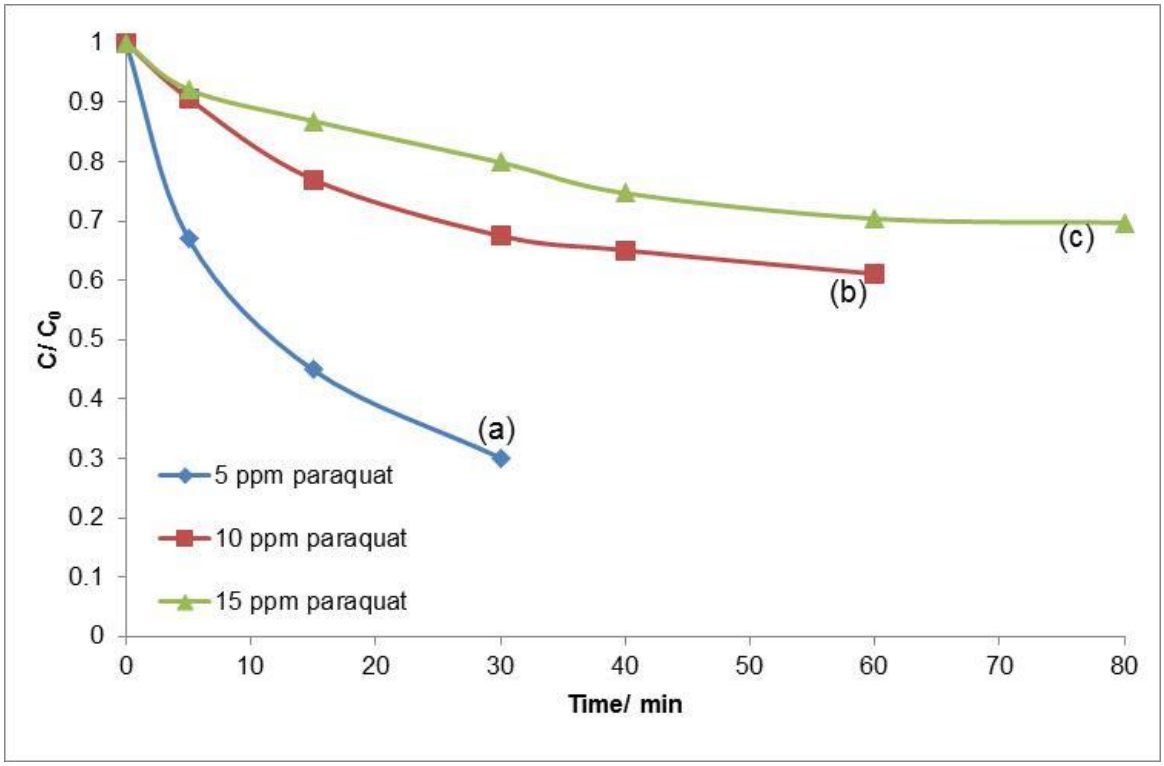

Figure 6.11: Ozone degradation of paraquat (a) 5 ppm, (b) 10 ppm and (c) 15 ppm at ozone flow rate of 25 L/ min and concentration of 4 g/ hr.

The profiles obtained for the degradation of atrazine using ozone are shown in figure 6.12. As observed for the degradation of bentazon and paraquat, the removal efficiency of atrazine also decreases with increasing initial concentration of the pollutant.

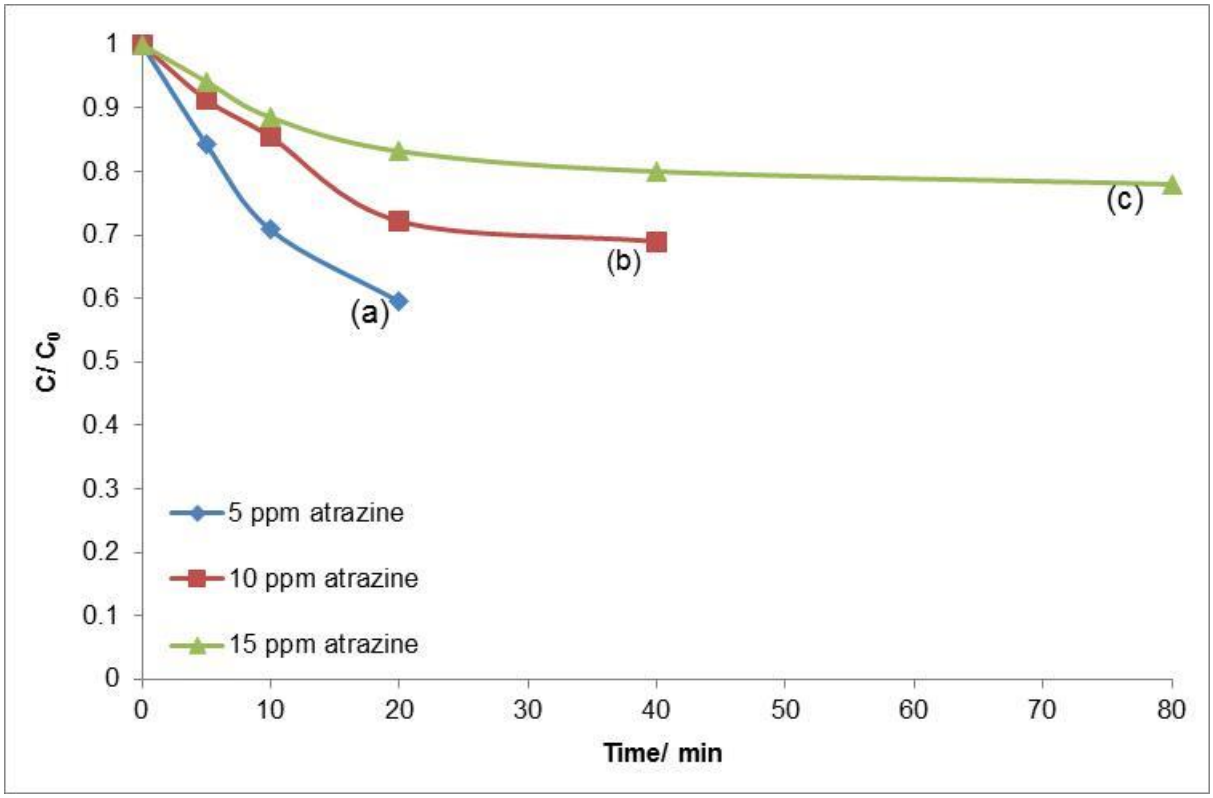

Figure 6.12: Ozone degradation of atrazine (a) 5 ppm, (b) 10 ppm and (c) 15 ppm at ozone flow rate of 25 L/ min and concentration of 4 g/ hr

The removal efficiencies obtained for the ozone degradation of 5 ppm, 10 ppm and 15 ppm atrazine were 40.6 % in 20 minutes, 31.1 % in 40 minutes and 22.1 % in 80. Findings of this study indicated that for all the three herbicide pollutants, increasing the initial pollutant concentration results in decreased removal efficiency. Complete degradation of paraquat and atrazine could not be achieved even after longer periods if treatment. This indicates that paraquat and atrazine are resistant to ozonation possibly due to the electron withdrawing effect of the nitrogen atoms, which make the molecules stable since the N atoms resist the

removal of electrons. In the case of atrazine, the electron withdrawing property of the chloride atom also adds stability to the molecule. The electron density on the ring is reduced by the electron-withdrawing chlorine atom hence deactivating it, such that ozone attack is nucleophilic which is generally slow.

6.3.2. Removal of organic pollutants using O_3/ N-TiO_2-PMAA-g-PVDF/ PAN system

The effectiveness of the O_3/ N-TiO_2-PMAA-g-PVDF/ PAN system was evaluated on the degradation of the herbicides bentazon, paraquat and atrazine in water. Figure 6.13 shows the degradation profiles obtained for the degradation of bentazon.

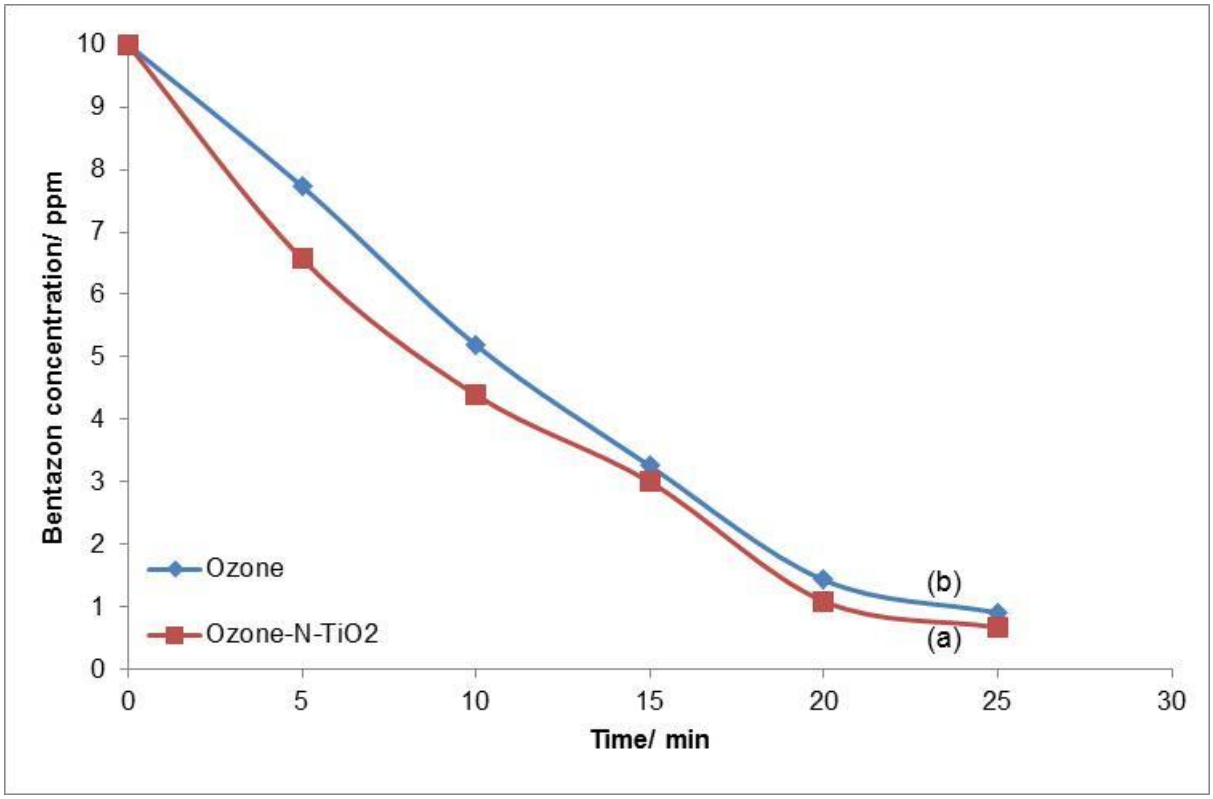

Figure 6.13: Degradation of bentazon with (a) O_3/ 3 % N-TiO_2-PMAA-g-PVDF/ PAN and (b) O_3 at ozone flow rate of 25 L/ min and concentration of 4 g/ hr

The degradation of bentazon was carried out under solar irradiation using O_3/ 3 % N-TiO_2-PMAA-g-PVDF/ PAN system. The results obtained were compared to those for bentazon degradation using ozone (flow rate of 25 L/ min and concentration of 4000 mg/ hr) alone. The degradation of bentazon with ozone is very rapid achieving a removal efficiency of 90.9 %. The combination of ozone with 3 % N-TiO_2 was observed to improve the degradation of bentazon, attaining a removal efficiency of 93.3 %.

The degradation of paraquat using the O_3/ 3 % N-TiO_2-PMAA-g-PVDF/ PAN system (45.2 % removal efficiency) and ozone (33.9 % removal efficiency) alone also yielded similar trends as observed in the degradation of bentazon. However, the degradation of paraquat is much slower compared to bentazon.

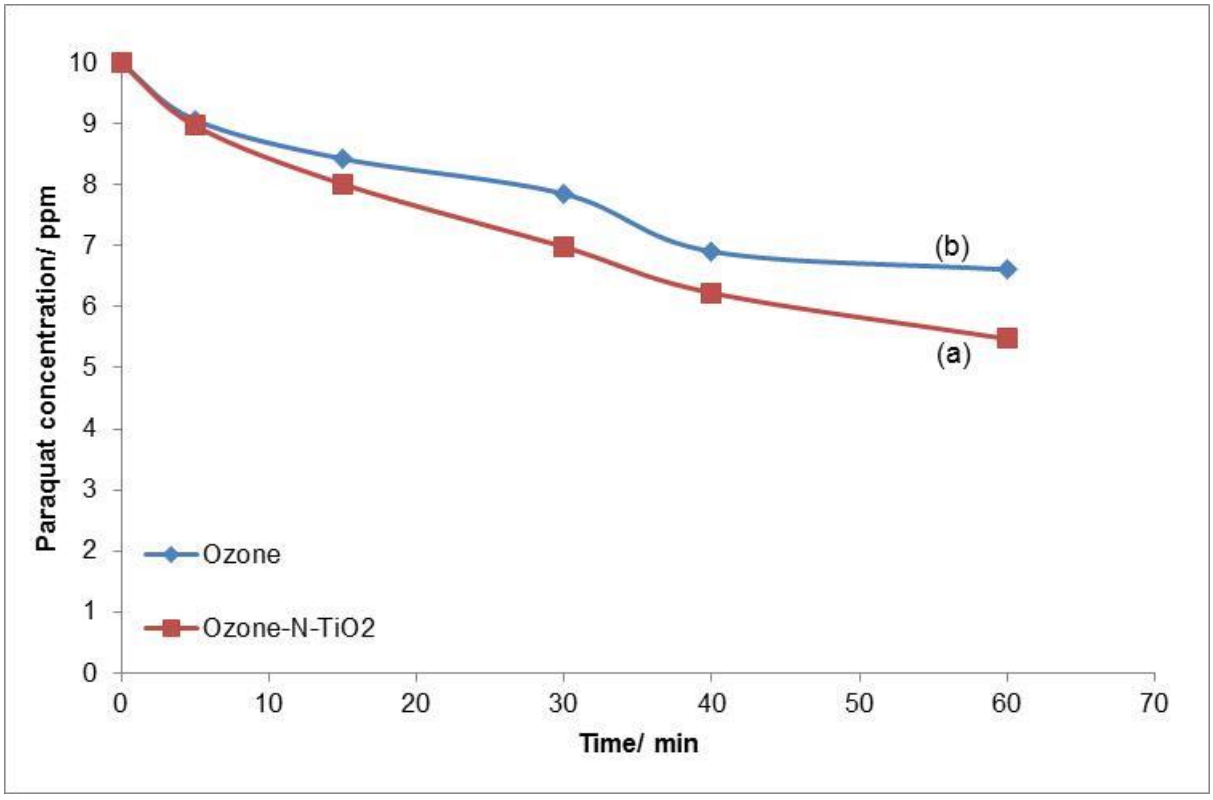

Figure 6.14: Degradation of paraquat with (a) O_3/ 3 % N-TiO_2-PMAA-g-PVDF/ PAN and (b) O_3 at ozone flow rate of 25 L/ min and concentration of 4 g/ hr

The degradation profiles obtained for atrazine are shown in figure 6.15. The degradation process is quite slow, nevertheless combination of ozone with 3 % N-TiO_2 was observed to increase the degradation rate of atrazine. The removal efficiency of atrazine increased by 7.98 % when the O_3/ 3 % N-TiO_2-PMAA-g-PVDF/ PAN system were employed compared to using ozone alone.

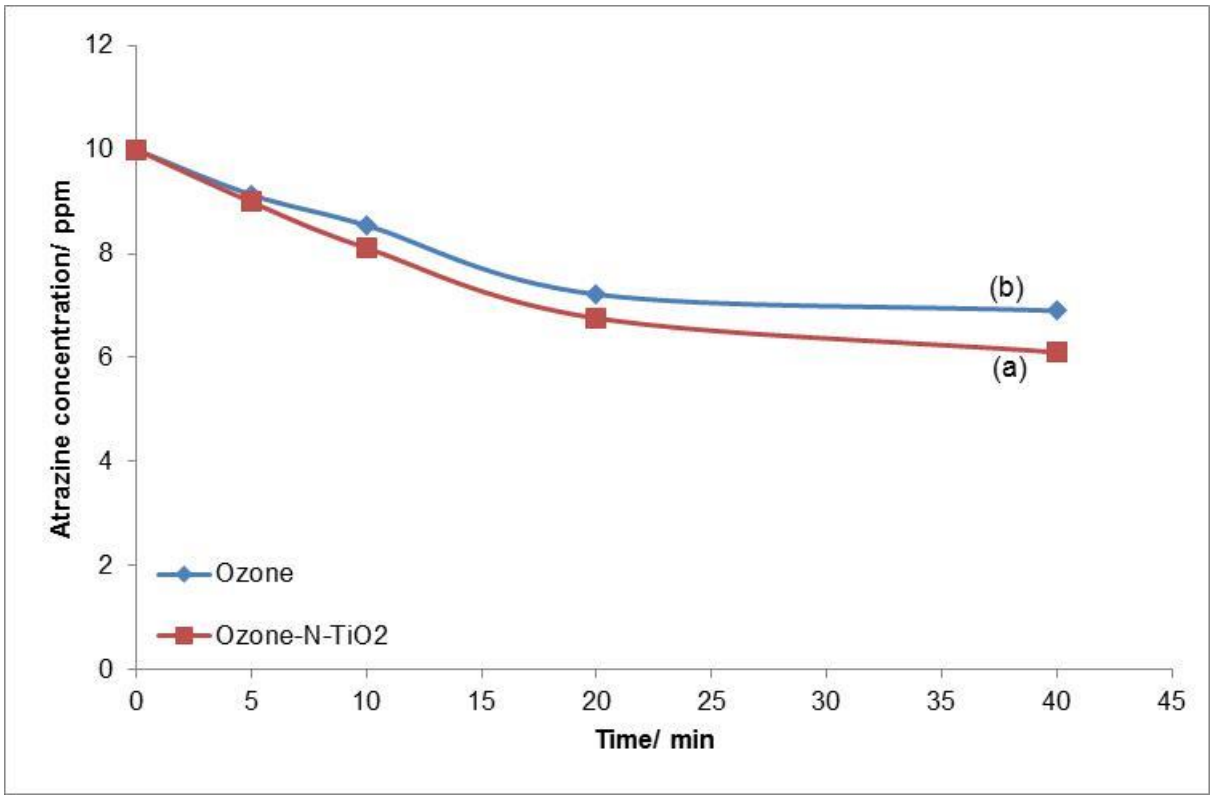

Figure 6.15: Degradation of atrazine with (a) O_3/ 3 % N-TiO_2-PMAA-g-PVDF/ PAN and (b) O_3 at 25 ˚C, natural pH, with ozone flow rate of 25 L/ min and concentration of 4 g/ hr

The combination of TiO_2 photo-catalysis with inorganic oxidants is known to lead to synergic effects (Černigoj *et al.*, 2010). Several reports mention that ozone is more easily reduced by a photo-generated conduction band electron from TiO_2 compared to oxygen, hence improving hydroxyl radical production through prevention of generated electron/ hole pair

recombination as it scavenges electrons resulting in the formation of super-oxides (Ye *et al.,* 2009; Tizaoui *et al.,* 2008; Gogate and Pandit, 2004; Pera-Titus *et al.,* 2004; Vogelpohl *et al.,* 2004; Akawat *et al.,* 1999). Ye and co-workers used the TiO_2/ UV/ O_3 system in the removal of 4-chloronitrobenzene (4-CNB) from water. The researchers observed that combination of TiO_2/ UV and O_3 greatly enhanced the rate of 4-chloronitrobenzene removal (Ye *et al.,* 2009). Kim and co-workers developed a TiO_2 assisted reactor with improved with UV light penetration. They also observed an improved rate of isopropyl alcohol (IPA) photo-oxidation when they charged the solution with ozone micro-bubbles. Recently some researchers investigated the degradation of formic acid using ozonation and photo-degradation. They discovered that the combination of ozonation and photo-catalysis synergistically enhanced the removal efficiency of the pollutant (Parrino *et al.,* 2014). Černigoj and co-workers 2010 studied the effect of dissolved ozone or ferric ions on the photo-degradation of thiacloprid in the presence of different TiO_2 catalysts. They observed that higher TiO_2 surface area leads to increased synergic effect. However, increasing the photo-catalyst loading did not have a bearing on the degree of synergy. It was deduced that their findings supported the theory that the synergy was a consequence of adsorption of ozone on the surface of TiO_2.

6.4. LC-MS analysis of bentazon degradation

The photo-degradation of bentazon using 3 % N-TiO_2-PMAA-g-PVDF/ PAN was followed by LC-MS analysis to identify the by-products involved and also to get an understanding of the overall degradation process. UV-Vis spectroscopy gave an indication of how many by-products can be expected from the photo-degradation of bentazon (Fig. 6.16). The UV-Vis spectra show the changes in the absorption of the compounds present over time which gave an idea of the disappearance of the herbicide bentazon during the photo-degradation process using N-TiO_2 photo-catalyst.

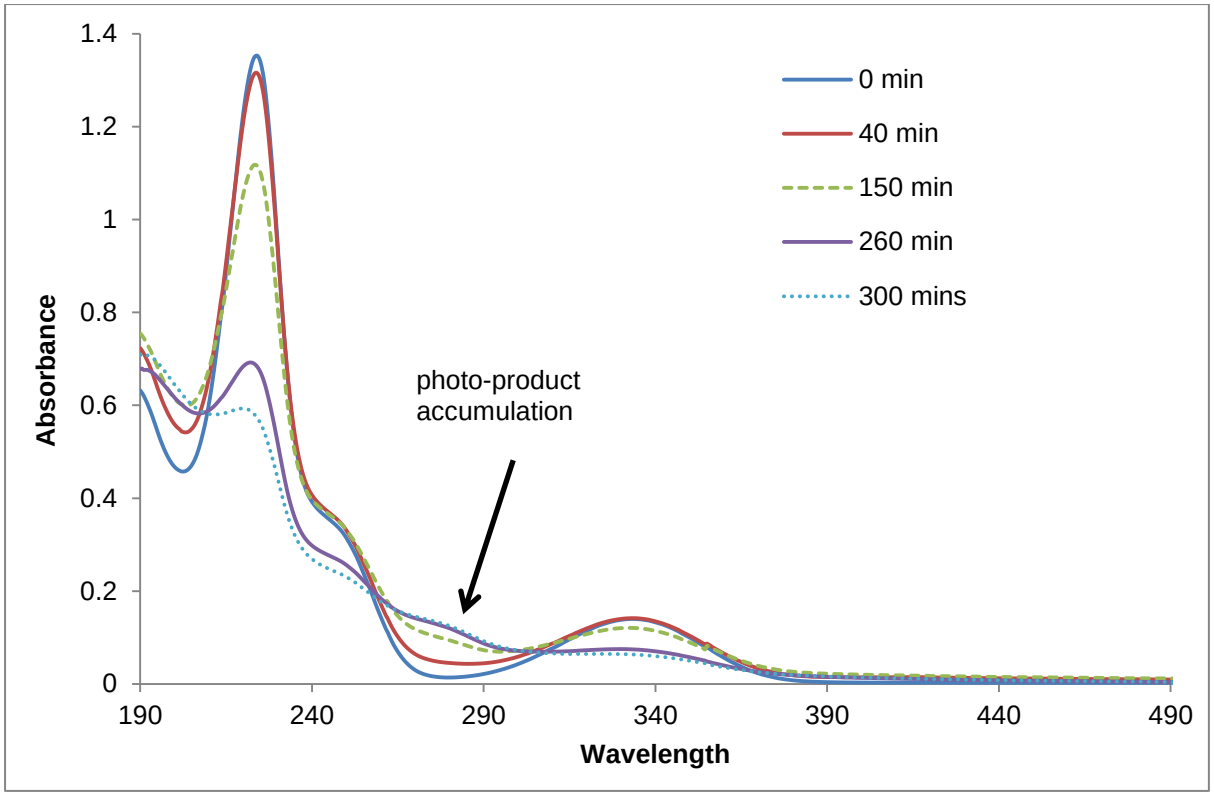

Figure 6.16: UV-Vis Absorption spectra for the photo-degradation of the herbicide bentazon using 3 % N-TiO_2-PMAA-g-PVDF/ PAN

Figure 6.17 shows the LC-MS spectra obtained for the degradation of bentazon. The first elution spectrum (0 minutes) is for bentazon before treatment with N-TiO_2 photo-catalyst and the second one is for bentazon (240 minutes) after treatment with N-TiO_2 photo-catalyst. Comparison of the two spectra shows that there is a new component eluting at 7.10 minutes, and the fact that the M+1 peak eluting at 20.40 minutes kept on diminishing in size indicating continuous breakdown of the herbicide bentazon. Figure 6.18 shows the elution spectra of the six aliquots collected at fixed intervals during the photo-degradation of bentazon. The spectra are overlaid for comparison purpose to show the changes in intensities of certain peaks over time. The component that was eluted at 7.10 minutes had a mass-to-charge ratio of 226.1285, suggesting bentazon parent molecule that has lost a nitrogen atom. Table 9 shows the photo-products obtained, retention times and spectral patterns.

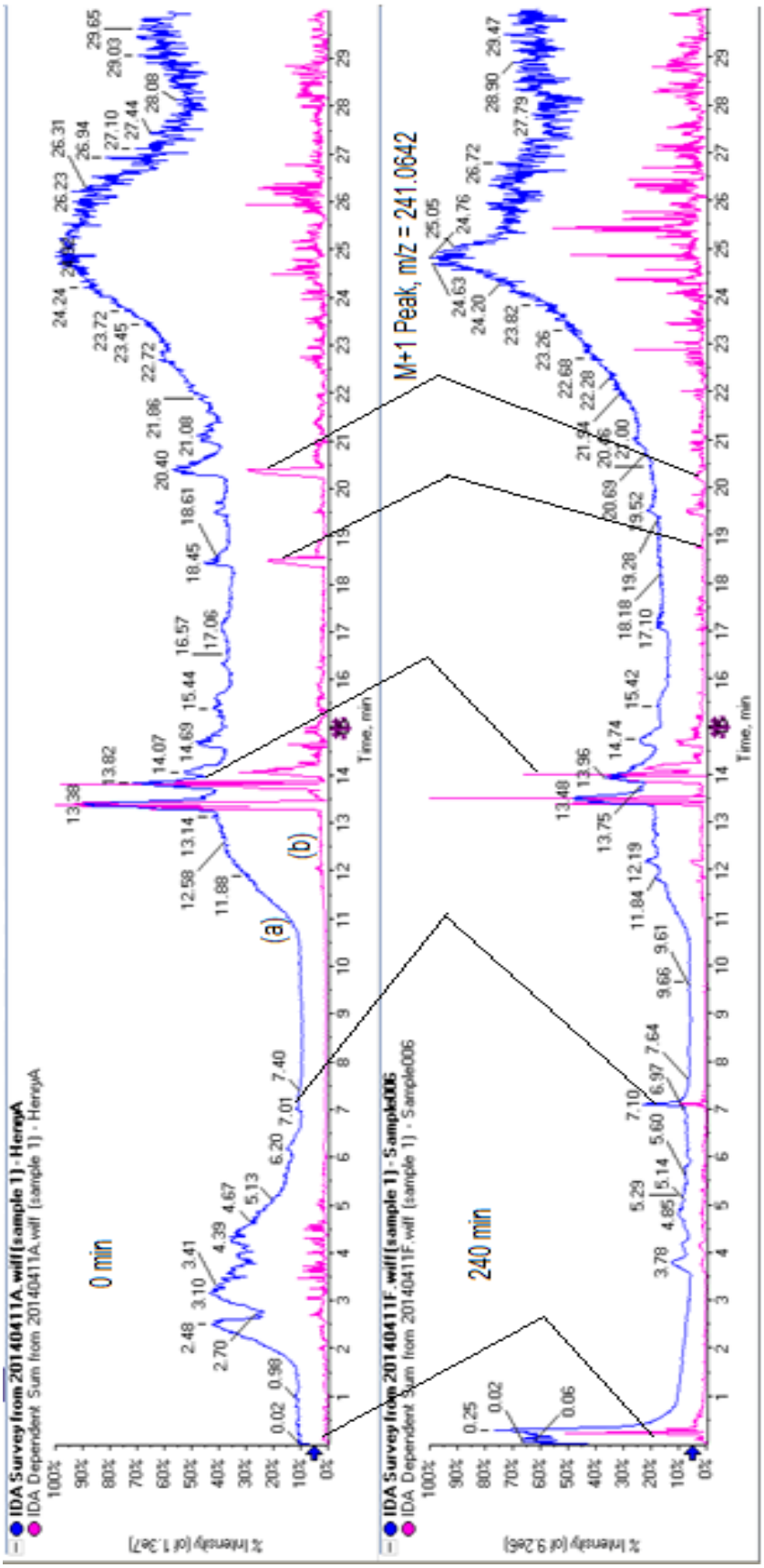

Figure 6.17: LC-MS spectra showing (a) elution time, and (b) intensities of components eluted at specific elution times from the degradation of bentazon under sunlight irradiation

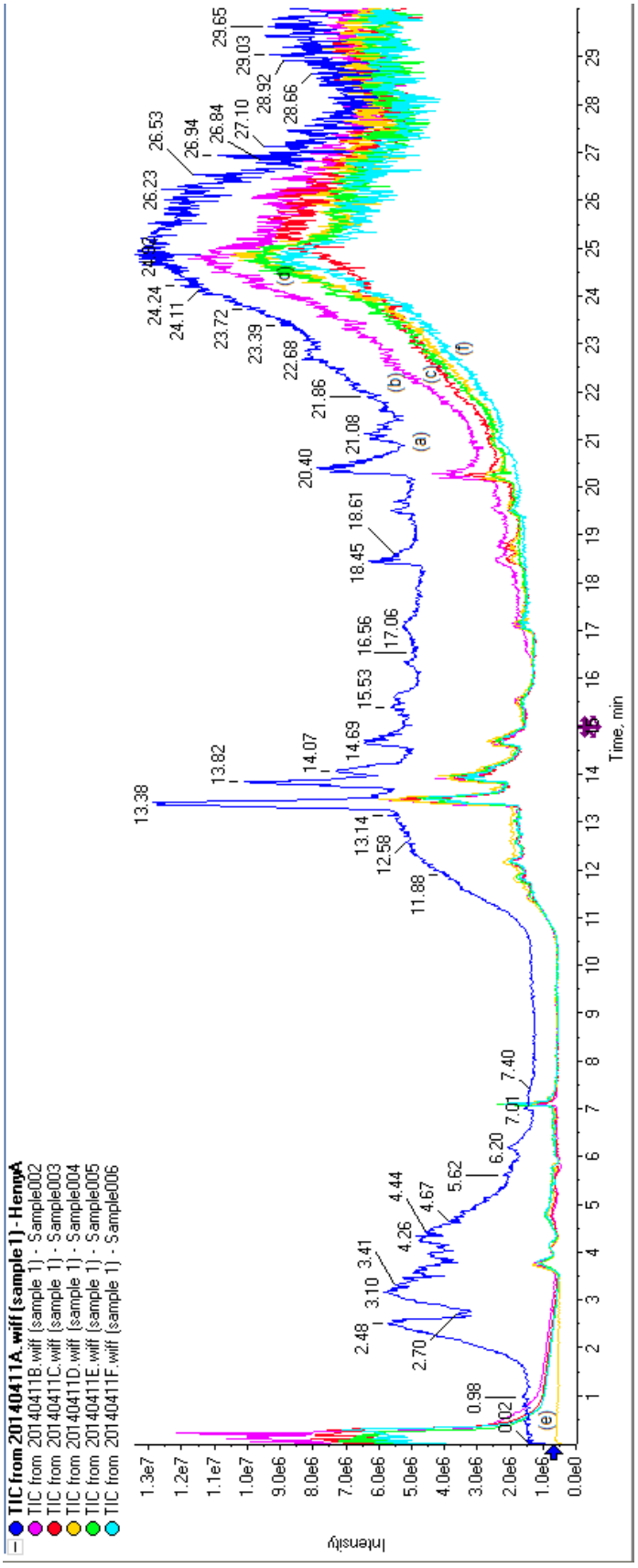

Figure 6.18: Elution time spectra of bentazon photo-degradation products with increasing time of treatment using 3 % N-TiO_2-PMAA-g-PVDF/ PAN

Table 9: Intermediate products formed during the photo-degradation of bentazon using 3 % N-TiO_2-PMAA-g-PVDF/ PAN at 25 ˚C under sunlight

m/z	Possible structure	Retention time (min)	Fragment ions
226.1285	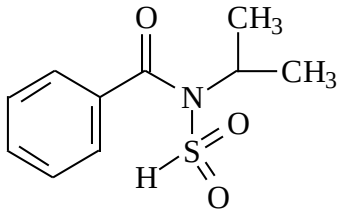	7.10	194.3, 176.1, 178.1

The peak at retention time 20.40 minutes was used to monitor the presence of bentazon during the photo-degradation process (Fig. 6.19). The peak at m/z 241 had an initial intensity of 1.8×10^5, which was observed to decrease in intensity with progression of reaction signifying the photo-degradation of bentazon by the N-TiO_2 photo-catalyst. LC-MS data is in agreement with UV-Vis absorption spectra which showed the accumulation of a single photo-product/ intermediate with the progression of the photo-degradation reaction.

Other researchers investigated the photo-degradation of bentazon using sol gel prepared TiO_2 and commercial TiO_2 (Degussa P25). LC-MS studies revealed the presence of three possible transient intermediates with a mass-to-charge ratio of 255. The value was higher than that of the parent molecule (m/z 241), but consistent with the hypothesis that suggested the formation of mono-hydroxylated products. Nevertheless, the fragmentation pattern of these three molecules permitted them to accurately determine the different position of the hydroxyl group (Seck *et al.*, 2012). However, in this study only a single photo-product was identified, and was observed to accumulate with time.

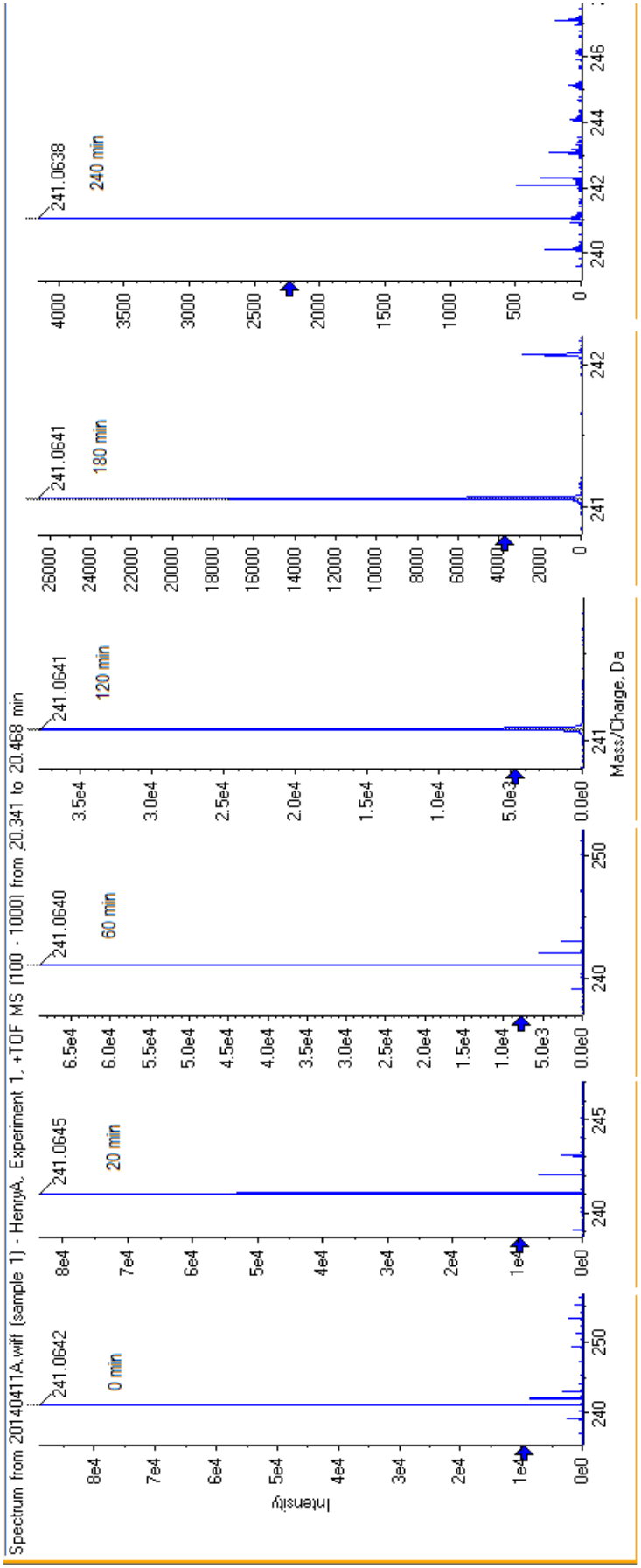

Figure 6.19: LC-MS spectra of bentazon degradation followed through the peak at m/z 241

6.5. Removal of heavy metals from water

The effect of N-TiO_2 photo-catalyst loading was evaluated on the removal of the heavy metals lead (Pb^{2+}) and iron (Fe^{3+}) from water. The photo-catalyst loading was varied between 1 % N-TiO_2 and 3 % N-TiO_2. The support materials investigated were PAN, PMAA-g-PVDF/ PAN and PVDF and the experiments were carried out under solar irradiation. Experimental details are given in chapter 3, sub-section 3.5.3.

6.5.1. Effect of photo-catalyst loading and support material on the removal of iron (Fe^{3+})

The removal efficiencies obtained for the removal of Fe^{3+} from synthetic water are shown in Figure 6.20 (i-iii). Using 1 % N-TiO_2-PAN photo-catalyst, 37.7 % removal efficiency of Fe^{3+} was achieved (Fig 6.20 (i)).

(i)

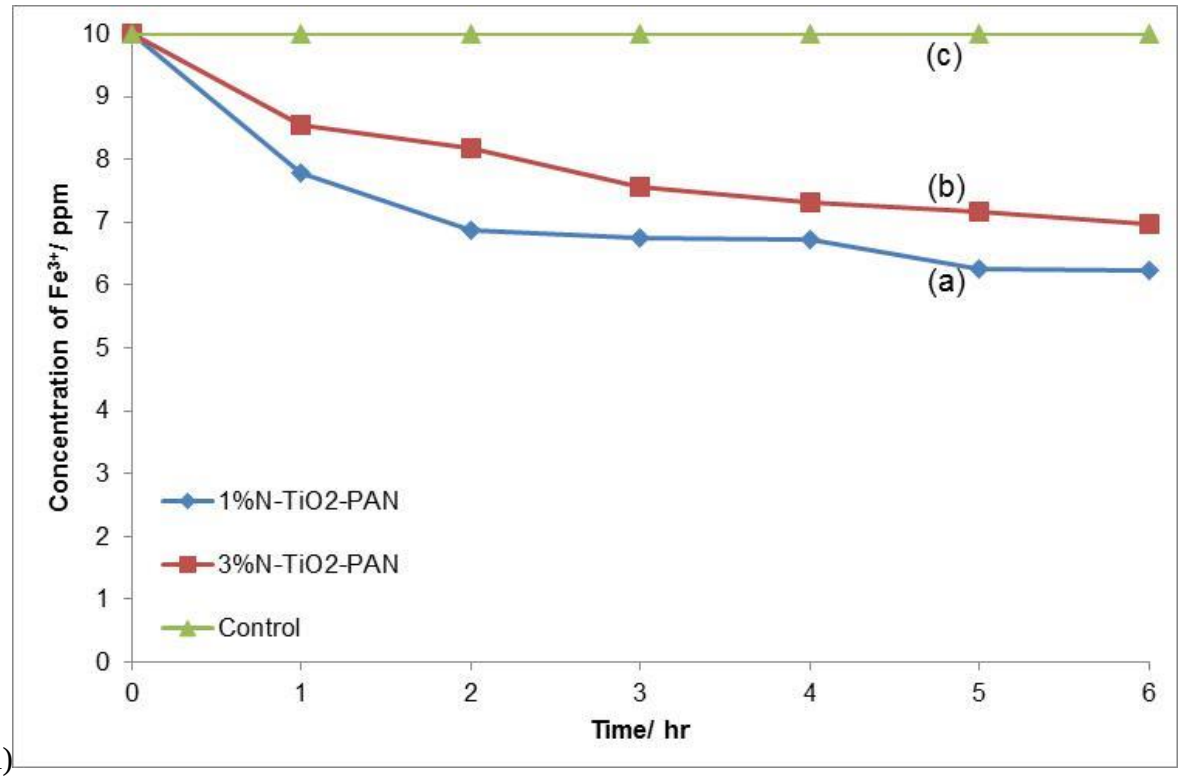

(ii)

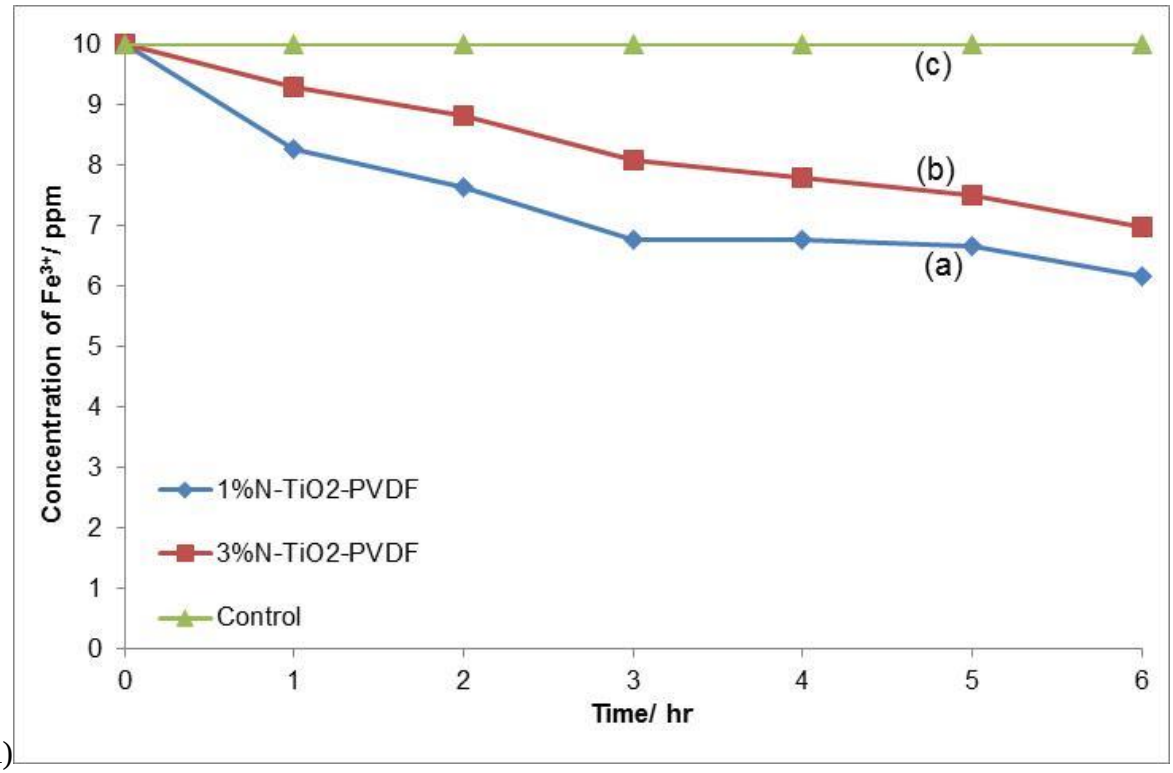

(iii)

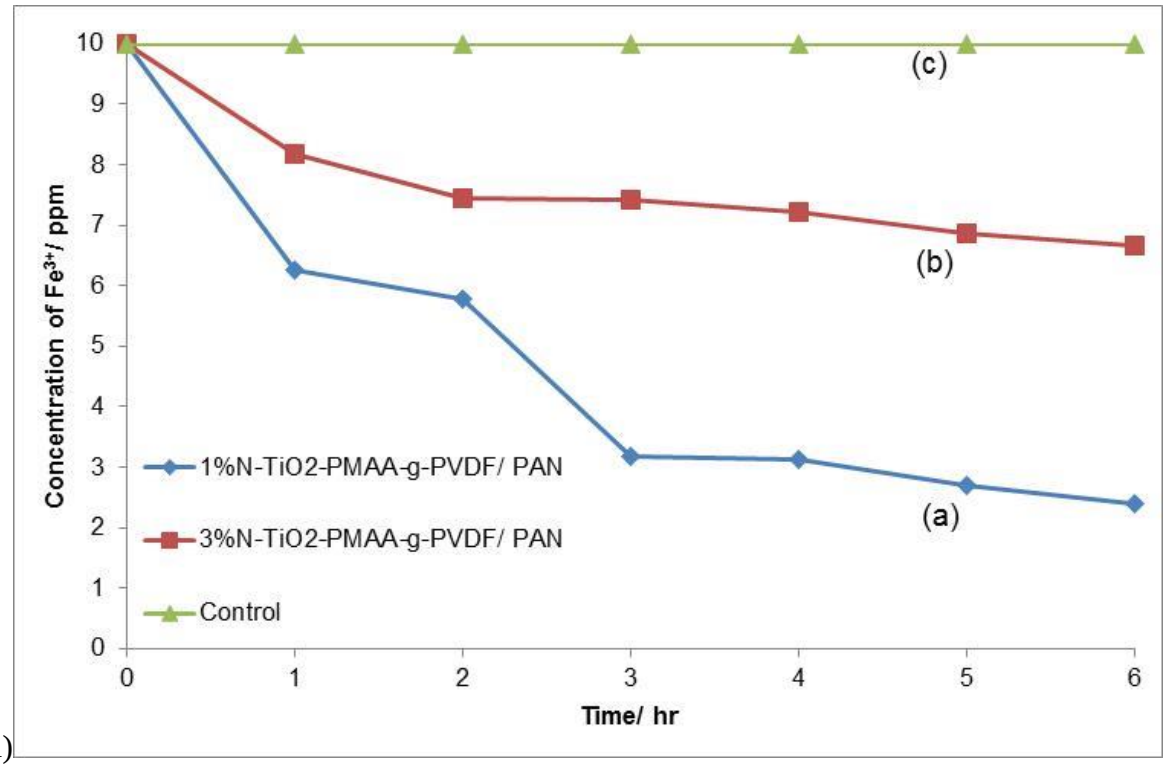

Figure 6.20: Removal of Fe^{3+} from water using (i) N-TiO_2-PAN, (ii) N-TiO_2-PVDF, and (iii) N-TiO_2-PMAA-g-PVDF/ PAN at 25 ˚C, natural pH, under sunlight

The heavy metal pollutant was removed via N-TiO_2 assisted reduction. No precipitate was observed at the bottom of the reaction vessel over time which is also another indication that removal of heavy metal did not proceed via precipitation. The 1 % N-TiO_2-PVDF photo-catalyst achieved a slightly higher Fe^{3+} removal efficiency (38.3 %) compared 1 % N-TiO_2-PAN (37.7 %). However, the highest removal efficiency was observed for 1 % N-TiO_2-PMAA-g-PVDF/ PAN photo-catalyst (76.2 %). The findings of this study indicated that PMAA-g-PVDF/ PAN membranes were the best support material for the photo-catalyst N-TiO_2. The most likely reason was increased adsorption of Fe^{3+} on the surface of the PMAA-g-PVDF/ PAN through interaction with the carboxylic acid moieties of the PMAA chains.

When the photo-catalyst loading (N-TiO_2) was increased on all three membrane support material (PAN, PVDF, and PMAA-g-PVDF/ PAN), a sharp decrease in the removal efficiencies of Fe^{3+} was observed. A 7.3 % decrease in Fe^{3+} removal efficiency was observed for 3 % N-TiO_2-PAN, 7.9 % for 3 % N-TiO_2-PVDF and 42.8 % for 3 % N-TiO_2-PMAA-g-PVDF/ PAN. The findings of this study indicated that increasing the concentration of the photo-catalyst negatively impacted the removal efficiencies of Fe^{3+}. Most likely when the amount of photo-catalyst loading on the membranes is increased, it interacts with more binding sites on the polymer membranes hence reducing the binding sites that can interact with the Fe^{3+} ions. This in turn leads to a reduced removal efficiency of the pollutant from water. However, this study is not completely alluding to the fact that reduction in removal efficiency of Fe^{3+} ions from water with increasing photo-catalyst loading is solely due to reduction in binding sites, as other factors could also come into play. Increasing the photo-catalyst loading may lead to the agglomeration of N-TiO_2 photo-catalyst, hence reducing the surface area that is available for reaction, which may have contributed to reduced removal efficiency for Fe^{3+} ions from water.

6.5.2. Effect of photo-catalyst loading and support material on the removal of iron (Pb^{2+})

The removal of Pb^{2+} from water was also investigated using N-TiO_2 supported on PAN, PVDF, and PMAA-g-PVDF/ PAN membranes. The profiles obtained on the removal of Pb^{2+} are shown in Figure 6.21 (i-iii). High removal efficiencies were achieved for the removal of Pb^{2+} ions from water. The profiles obtained for the removal Pb^{2+} ions from synthetic water illustrated that the process is initially very rapid, but gradually slows down with progression of reaction for all three photo-catalyst-support material combinations. The 1 % N-TiO_2-PAN photo-catalyst attained a Pb^{2+} removal efficiency of 90.5 % within 6 hours of treatment, while 1 % N-TiO_2-PMAA-g-PVDF/ PAN had a removal efficiency of 88.9 %, lastly 1 % N-TiO_2-PVDF with a removal efficiency of 86.9 %.

(i)

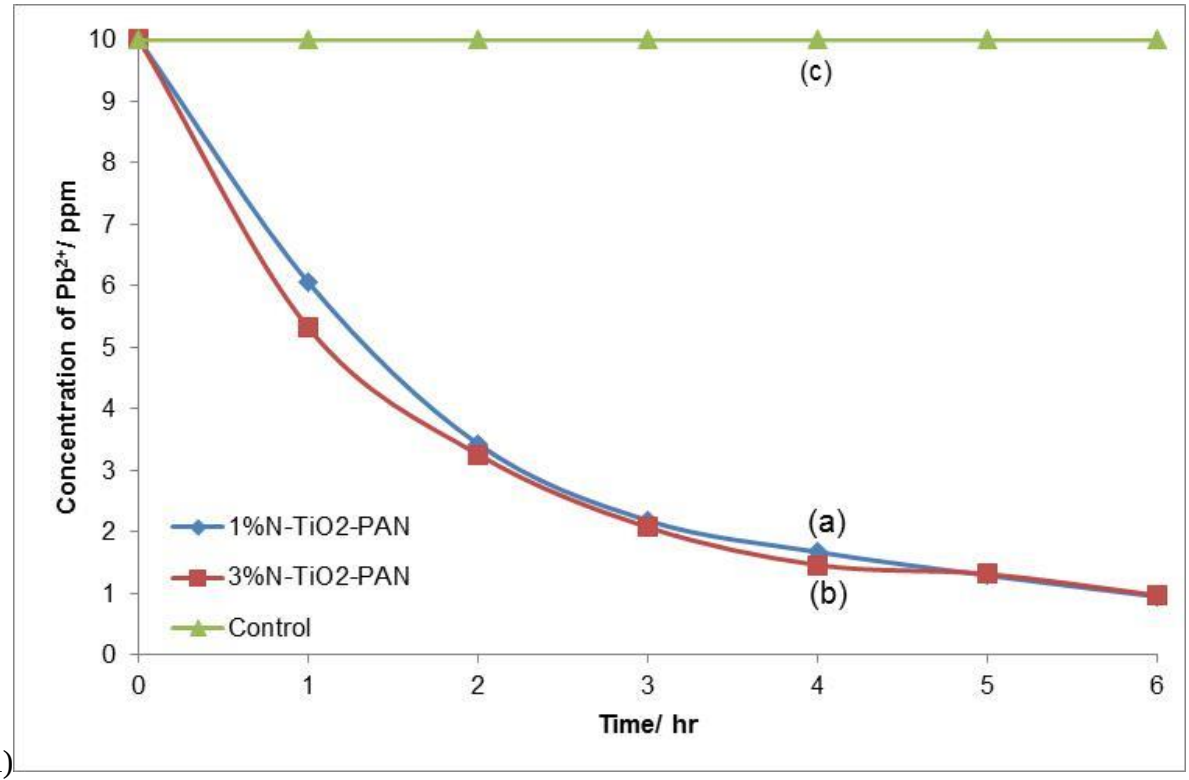

(ii)

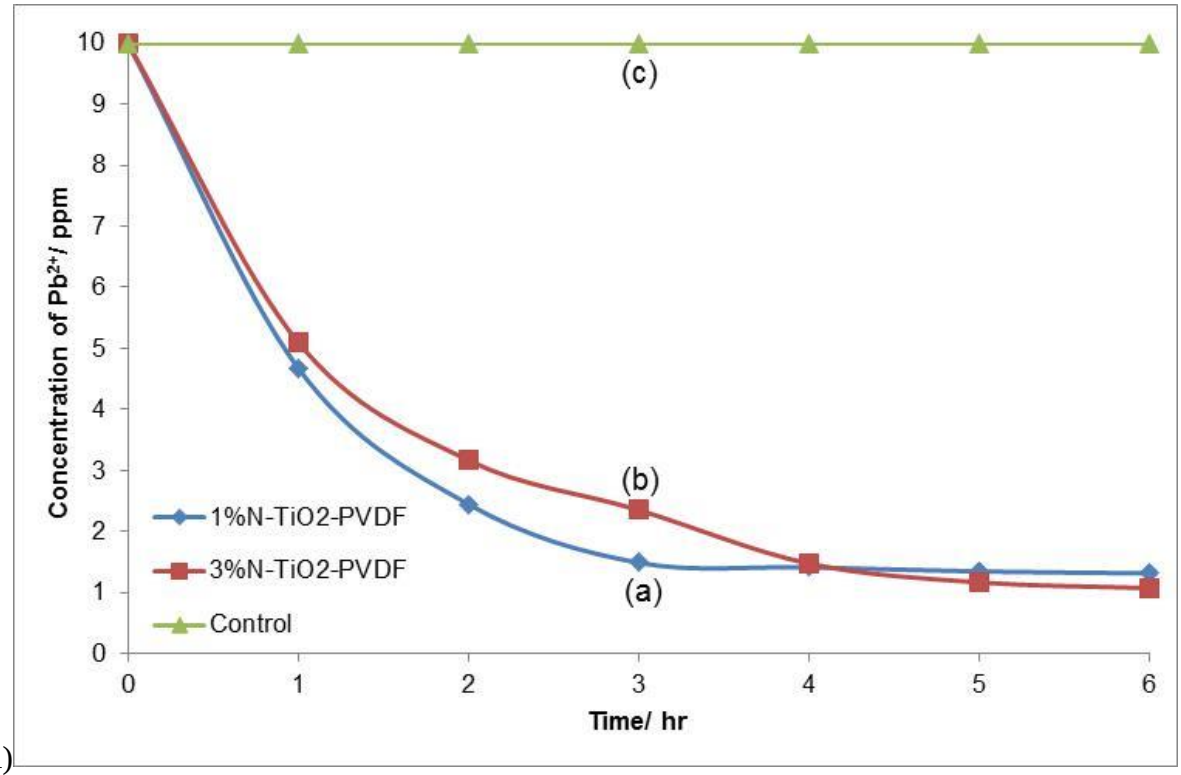

(iii)

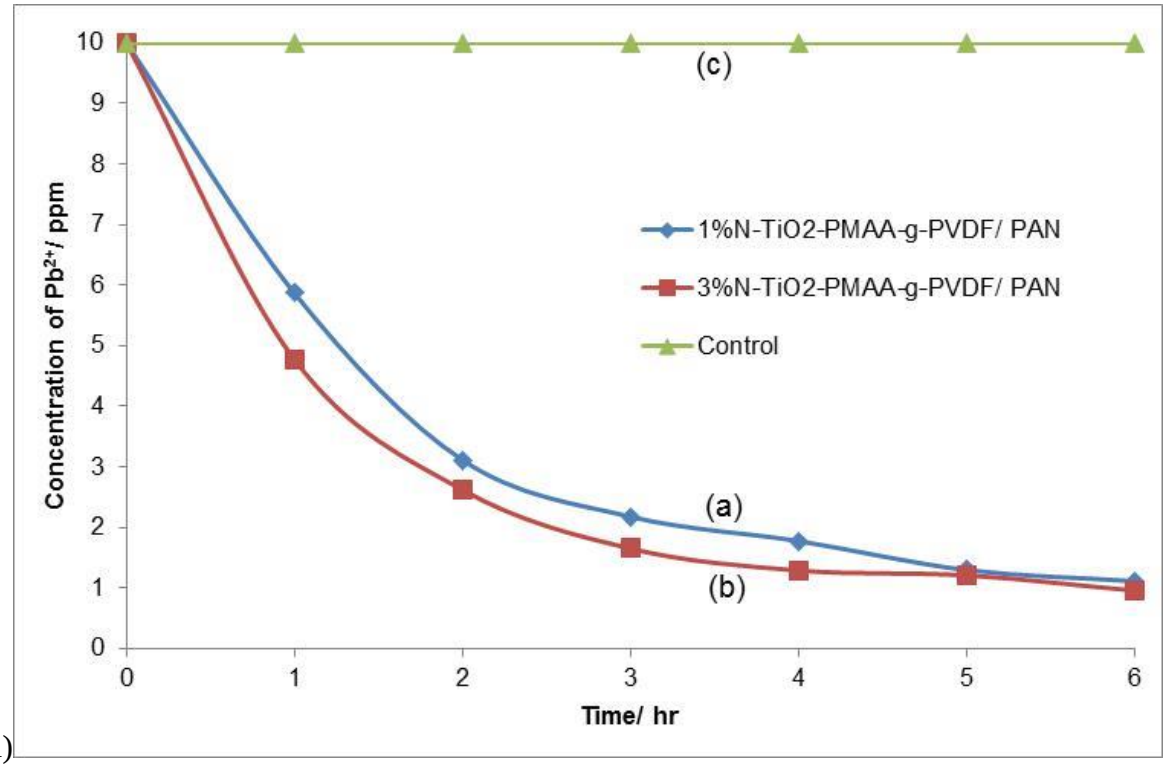

Figure 6.21: Removal of Pb^{2+} from water using (i) N-TiO_2-PAN, (ii) N-TiO_2-PVDF, and (iii) N-TiO_2-PMAA-g-PVDF/ PAN at 25 ˚C, natural pH, under sunlight

Fairly high removal efficiencies were attained on the removal of Pb^{2+} ions from water as compared to Fe^{3+} ions removal (Section 6.5.1). The performance of the three support materials (PAN, PVDF and PMAA-g-PVDF/ PAN) on the removal Pb^{2+} ions from synthetic water was closely matched. However, PAN support material performed slightly better as compared to PMAA-g-PVDF/ PAN, unlike in the case of Fe^{3+} ions removal from synthetic water where PMAA-g-PVDF/ PAN supported attained the highest removal efficiency.

The effect of N-TiO_2 photo-catalyst loading was also investigated on the removal of Pb^{2+} from synthetic water. The PAN, PVDF, and PMAA-g-PVDF/ PAN membranes were loaded with 3 % N-TiO_2 photo-catalyst and evaluated on their Pb^{2+} ion removal efficiencies. No significant change in Pb^{2+} removal efficiency was observed for 3 % N-TiO_2-PAN since it remained around 90.3 %. Nevertheless, 3 % N-TiO_2-PVDF and 3 % N-TiO_2-PMAA-g-PVDF/ PAN achieved 2.4 % and 1.55 % increase in Pb^{2+} removal efficiencies respectively. The findings of this study indicated that increasing the amount N-TiO_2 on the membrane support material resulted in an increased Pb^{2+} removal efficiency, unlike in the case of Fe^{3+} (Section 6.5.1) where increasing the photo-catalyst loading negatively impacted on the removal efficiency. The optimum amount of photo-catalyst for the removal of Pb^{2+} ions from synthetic water was 1 % N-TiO_2 on PAN membrane support. Another deduction from the findings of this study was that efficiency of a support material on the removal of the studied inorganic pollutants was dependent on the type of heavy metal species in question; for Fe^{3+} removal 1 % N-TiO_2-PMAA-g-PVDF/ PAN was the most effective, while for Pb^{2+} removal 1 % N-TiO_2-PAN was the most effective photo-catalyst-support material combination.

6.5.3. Effect of pH on the removal of Fe^{3+} and Pb^{2+}

The effect of pH was investigated on the removal of heavy metals Pb^{2+} and Fe^{3+} from synthetic water. The pH was adjusted from low pH to high pH through the addition of acid or base in order to establish the optimum pH for the removal of the two heavy metal ions from synthetic water. Figure 6.22 shows the removal efficiencies obtained for Pb^{2+} and Fe^{3+} ions. The most suitable photo-catalyst-support material combination was used for the removal of either heavy metal ion; 1 % N-TiO_2-PAN for Pb^{2+} ions and 1 % N-TiO_2-PMAA-g-PVDF/ PAN for Fe^{3+} ions.

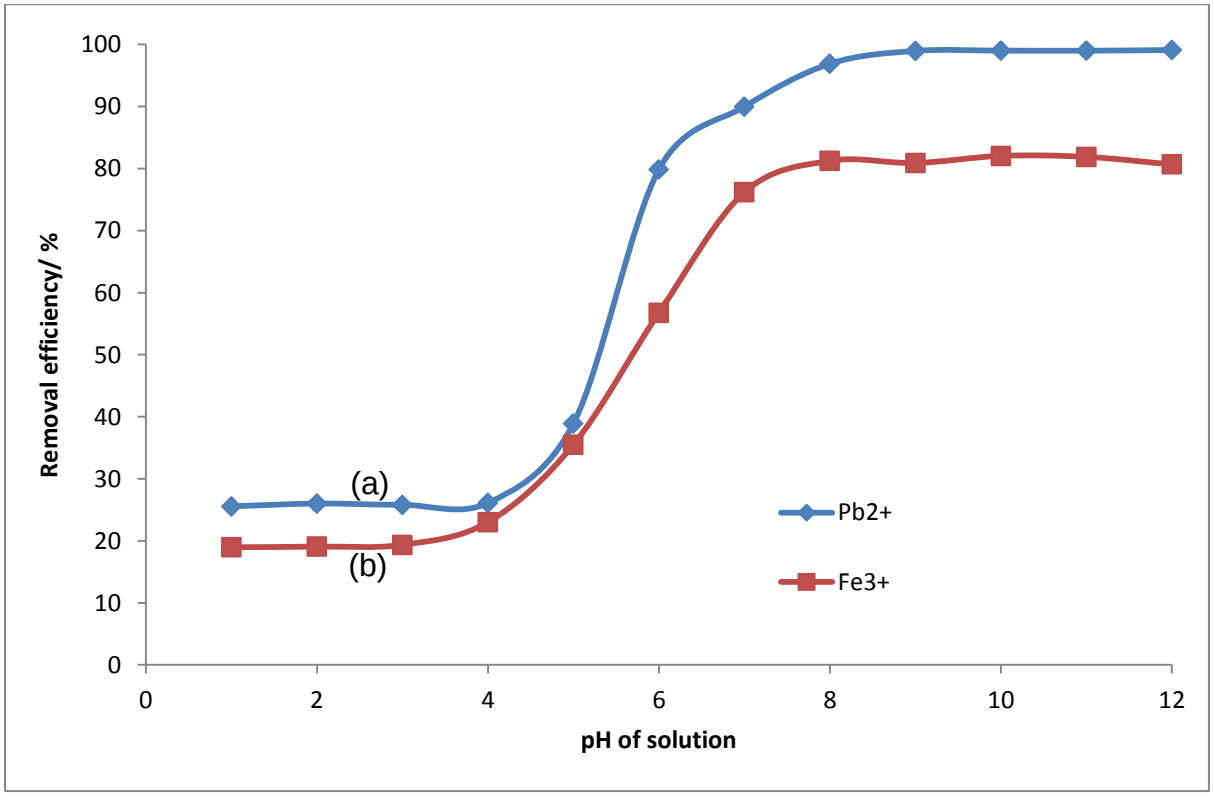

Figure 6.22: Removal efficiencies for (a) Pb^{2+} and (b) Fe^{3+} at various pH, under sunlight, at 25 ˚C

At low pH, the removal efficiencies of both Pb^{2+} and Fe^{3+} were very low; Pb^{2+} had an initial removal efficiency of 25.6 % while Fe^{3+} had an initial removal efficiency of 18.9 %. The

removal efficiencies of Pb^{2+} and Fe^{3+} ions from synthetic water gradually increased with increasing pH. Around pH 6, a rapid increase in Pb^{2+} and Fe^{3+} removal efficiencies was observed; 79.9 % removal for Pb^{2+} and 56.8 % removal for Fe^{3+}. The removal efficiencies reached a peak at pH 8 where no further increase in the removal efficiencies was observed. At the optimum pH 8, 98.9 % removal efficiency was attained for Pb^{2+} ions and 81.8 % for Fe^{3+} ions. The findings of this study indicated that the pH of the solution is very important as it determines how much of the heavy metal ions can be removed from the aqueous solution. A more basic solution allowed the removal of a higher percentage of the heavy metal ions while acid conditions hampered the removal of these heavy metal ions from water.

It was reported in literature that titanium dioxide photo-catalysis is capable of simultaneously converting toxic heavy metals into non-toxic ionic states and further reducing them into their corresponding elemental form for metal recovery (Chong *et al.,* 2010). It was been reported that metals of Ag(I), Cr(IV), Hg(II) and Pt(II) were easily treated with TiO_2 of 0.1wt% whereas it was not possible to remove Cd(II), Cu(II) and Ni(II) (Prairie *et al.,* 1994). The level of conversion for such metals and their recovery process are greatly dependent on the standard reduction potential of the metals for the reduction reactions. An efficient removal of the metals is achievable with a positive potential that is greater than 0.4 V or a TiO_2 flat band potential (Kabra et.al., 2004; Herrmann, 1999).

6.6. Conclusion

The investigation was carried out to identify the most suitable support material for N-TiO_2 photo-catalyst and this revealed that PMAA-g-PVDF/ PAN membranes were the most appropriate matrix, since they were observed to allow higher rates of pollutant photo-degradation compared to PVDF and PAN membranes. The investigation carried out on the

effect of photo-catalyst loading on the photo-degradation of the herbicide bentazon in water indicated that the optimum amount of N-TiO_2 that could be successfully immobilized on the membranes investigated was 3 %. Increasing the amount of N-TiO_2 to 5 % was observed to effect any significant change in the rate of pollutant photo-degradation. Accumulation of the N-TiO_2 within the membrane matrix could have resulted in the agglomeration of the nano-powders resulting in reduction of surface area that could be presented for photo-catalysis. The investigation carried out on the photo-degradation of three herbicides (bentazon, paraquat, and atrazine) revealed that atrazine and paraquat were more recalcitrant, since they were very slow to degrade when exposed to 3 % N-TiO_2-PMAA-g-PVDF/ PAN. Findings of this study also indicated that solution pH played a very important role on the photo-degradation of organic pollutants in water. High removal efficiencies were achieved for bentazon and atrazine between pH 3 and 7, whereas high pH (9.0) promoted higher removal efficiencies for paraquat. The plots of ln (C/ C_0) against time for atrazine, paraquat and bentazon were straight lines (Fig. 6.9), implying that the photo-degradation of the three herbicides fitted as pseudo-first-order kinetics. Studies carried out on the ozonolysis of bentazon showed a decrease in the rate of degradation with increasing pollutant concentration at a fixed concentration of ozone supply. The use of the O_3/ 3 % N-TiO_2-PMAA-g-PVDF/ PAN system was observed to enhance organic pollutant removal efficiency. LC-MS studies of bentazon degradation indicated that there was accumulation of a single photo-product/ intermediate with m/z 226 over time.

Heavy metals Pb^{2+} and Fe^{3+} were removed from water via N-TiO_2 assisted reduction. The highest removal efficiency for Fe^{3+} was achieved with 1 % N-TiO_2-PMAA-g-PVDF/ PAN photo-catalyst (76.2 %), while for Pb^{2+} removal 1 % N-TiO_2-PAN was the most effective

photo-catalyst (90.5 %). An increasingly basic environment promotes high removal efficiencies for Pb^{2+} and Fe^{3+}.

Bibliography

Akawat S., Charles G., Hill J., and Marc A. *Catalysis Today*: 54 **(1999)** 159-164.

Athanasekou C.P., Romanos G.E., Katsaros F.K., Kordatos K., Likodimos V., and Falaras P. *Journal of Membrane Science*: 392-393 **(2012)** 192-203.

Bosc F., Ayral A., and Guizard C. *Journal of Membrane Science*: 265 (1–2) **(2005)** 13-19.

Cantavenera M.J., Catanzaro I., Loddo V., Palmisano L., and Sciandrello G. *Journal of Photochemistry and Photobiology A: Chemistry*: 185 **(2007)** 277-282.

Castro A.L., Nunes M.R., Carvalho M.D., Ferreira L.P., Jumas J.-C., Costa F.M., and Florêncio M.H. *Journal of Solid State Chemistry*: 182 **(2009)** 1838-1845.

Chong M.N., Jin B., Chow C.W.K., and Saint C. *Water Research*: 44 **(2010)** 2997-3027.

Cernigoj U., Stranger U.L., and Jirkovsky J. *Journal of Material Science*: 177 (1-3) **(2010)** 399-406.

Doong R.-A., Chen C.-H., Maithreepala R.A., and Chang S.-M. *Water Research*: 35 (12) **(2001)** 2873-2880.

Furman O.S., Yu M., Teel A.L., and Watts R.J. *Chemosphere*: 93 (9) **(2013)** 1734-1741.

Gogate P.R., and Pandit A.B. *Advances in Environmental Research*: 8 (3-4) **(2004)** 501-551.

Haque M.M., Muneer M., and Bahnemann D.W. *Environmental Science & Technology*: 40 **(2006)** 4765-4770.

Herrmann J.M. *Catalysis Today*: 53 (1999) 115-129.

Hintsho N., Petrik L., Nechaev A., Titinchi S., and Ndungu P. *Applied Catalysis B: Environmental*: 156-157 **(2014)** 273-283.

Hu A., Zhang X., Oakes K.D., Peng P., Zhou Y.N., and Servos M.R. *Journal of Hazardous Materials*: 189 **(2011)** 278-285.

Jiaguo Y., Zhou M., Cheng B., and Zhao X. *Journal of Molecular Catalysis A*: 246 **(2006)** 176-184.

Kabra K., Chaudhary R., and Sawhney R.L. 2004. *Industrial and Engineering Chemistry Research*: 43 **(2004)** 7683-7696.

Khan H., and Berk D. *Journal of Photochemistry and Photobiology A*: *Chemistry*: **(2014)** 4.

Kobayakawa Y., Murakami Y., and Sato Y. *Journal of Photochemistry and Photobiology A: Chemistry*: 170 **(2005)** 177-179.

Ksibi M., Rossignol S., Tatibouët J.-M., and Trapalis C. *Materials Letters*: 62 **(2008)** 4204-4206.

Liao J., Lin S., Pan N., Li S., Cao X., and Cao Y. *Materials Characterization*: 66 **(2012)** 24-29.

Lin Y.-F., Tung K.-L., Tzeng Y.-S., Chen J.-H., and Chang K.-S. *Journal of Membrane Science*: 389 **(2012)** 83-90.

Liu L., Chen F., and Yang F. *Separation and Purification Technology*: 70 **(2009)** 173-178.

Liu L., Liu Z., Bai H., and Sun D.D. *Water Research*: 46 **(2012)** 1101-1112.

Liu P., Liu H., Liu G., Yao K., and Lv W. *Applied Surface Science*: 258 **(2012)** 9593-9598.

Morris R.E., Krikanova E., and Shadman F. *Clean Technologies and Environmental Policy*: 6 **(2004)** 96-104.

Mungondori H., and Tichagwa L. *Materials Science Forum*: 734 **(2013)** 226-236.

Nyamukamba P., Tichagwa L., and Greying C. *Materials Science Forum*: 712 **(2012)** 49-63.

Parrino F., Camera-Roda G., Loddo V., Palmisano G., and Augugliaro V. *Water Research*: 50 **(2014)** 189-199.

Pera-Titus M., Garcia-Molina V., Banos M.A., Gimenez J., and Esplugas S. *Applied Catalysis B: Environmental*: 47(4) **(2004)** 219-256.

Pourata R., Khataee A.R., Aber S., and Daneshvar N. *Desalination*: 249 **(2009)** 301-307.

Prairie M.R., Evans L.R., and Martinez S.L. Destruction of organics and removal of heavy metals in water via TiO_2 photo-catalysis. In: Eckenfelder W.W., Roth J.A., Bowers A.R. (Eds.), *Chemical Oxidation*: *Technologies for the Nineties*, vol. 2. Technomic Publishing Company Inc, Pennsylvania US, (1994) 428-441.

Quan F., Hu Y., Zhang X., and Wei C. *Applied Surface Science*: **(2014)** 4.

Romanos G.E., Athanasekou C.P., Katsaros F.R., Kanellopoulos N.K., Dionysiou D.D., Likodimos V., and Falaras P. *Journal of Hazardous Materials*: 211-212 **(2012)** 304-316.

Seck E.I., Doña-Rodríguez J.M., Fernández-Rodríguez C., González-Díaz O.M., Araña J., and Pérez-Peña J. *Chemical Engineering Journal*: 203 **(2012)** 52-62.

Singh H.K., Saquib M., Haque M., Munueer M., and Bahnemann D. *Journal of Molecular Catalysis A: Chemical*: 264 **(2007)** 66-72.

Sorolla M.G., Dalida M.L., Khemthong P., and Grisdanurak N. *Journal of Environmental Sciences*: 24 (6) **(2012)** 1125-1132.

Tizaoui C., Bickley R.I., Slater M.J., Wang W-J., Ward D.B., and Al-Jaberi A. *Desalination*: 227 **(2008)** 57–71.

Vogelpohl A., and Kim S.M. *Journal of Industrial and Engineering Chemistry*: 10(1) **(2004)** 33-40.

Ye M., Chen Z., Liu X., Ben Y., and Shen J. *Journal of Hazardous Materials*: 167 **(2009)** 1021-1027.

Yola M.L., Eren T., and Atar N. *Chemical Engineering Journal*: 250 **(2014)** 288-294.

You S.-J., Semblante G.U., Luc S.-C., Damodar R.A., and Wei T.-C. *Journal of Hazardous Materials*: 237–238 **(2012)** 10-19.

Yuan J., Chen M., Shi J., and Shangguan W. *International Journal of Hydrogen Energy*: 31 **(2006)** 1326-1331.

CHAPTER 7

7. Evaluation of antimicrobial properties of N-TiO_2-PMAA-g-PVDF/ PAN membranes

7.1. Introduction

This chapter is on the evaluation of antimicrobial properties of membrane (PVDF, PMAA-g-PVDF/ PAN, and PAN) supported N-TiO_2 photo-catalyst. The optimum amount of N-TiO_2 that can be incorporated into the membranes was determined in Chapter 6. Hence evaluation was carried out using membranes loaded with 1 % and 3 % nitrogen doped titanium dioxide (N-TiO_2). The antimicrobial studies were carried out on the removal or inactivation of *Escherichia coli* ATCC 8739 in water. The study focused on evaluating the effectiveness of N-TiO_2 immobilized on different polymer support material with regard to microbial agent removal.

7.2. Experimental procedure

7.2.1. Materials

The following materials were employed in the evaluation of antimicrobial properties of membrane supported N-TiO_2: Nutrient agar (Merck, biolab), Nutrient broth (Merck, biolab), sterile inoculating loops (Lasec, SA), 90 mm sterilized petri dishes (Yacheng Huida Medical Instruments Co. LTD), Distilled water, and *Escherichia coli* ATCC 8739.

7.2.2 Preparation of a McFarland turbidity standard

A McFarland 0.5 turbidity standard was used for all the antimicrobial experiments carried out. The standard was prepared by mixing 0.10 mL of a 1 % solution (w/v) of $BaCl_2$ with 19.90 mL of a 1 % solution (v/v) of H_2SO_4 (McFarland, 1907; Murray *et al.*, 2007). The standard gave an absorbance of 0.08 abs units at a wavelength of 625 nm. The prepared standard was then used to estimate bacterial densities of *E. Coli* ATCC 8739 in saline solution by comparing absorbance. Table 10 shows the approximate densities of organisms for each McFarland standard.

Table 10: McFarland standards for visual/ spectrophotometric comparisons of bacterial densities in saline or liquid growth medium

Standard	0.5	1	2	3	4
Approximate bacterial density × 10^8/ mL	1.5	3	6	9	12

7.2.3. Preparation of nutrient agar

The nutrient agar that was used in all the antimicrobial experiments carried out was prepared by dissolving 31g of agar in one litre of distilled water. After dissolution, the solution was sterilized by autoclaving at 121 ˚C. The nutrient agar was then poured into agar plates and allowed to set. All the plates were then stored in a refrigerator at 4 ˚C ready for use.

7.2.4. Preparation of nutrient broth

Nutrient broth was prepared by dissolving 16 g of the nutrient broth powder in one litre of distilled water. After homogenizing, the solution is sterilized in an autoclave at 121 ˚C for 15 minutes. All the experiments were carried out using the sterilized nutrient broth.

7.2.5. Culturing of Escherichia coli ATCC 8739

Escherichia coli ATCC 8739 were transferred onto freshly prepared nutrient agar using a sterile inoculating loop. The bacterial cells were spread by gently rubbing the inoculating loop onto the surface of the nutrient agar material. The plate was then incubated at 37 ˚C for 24 hours. After the incubation period the *Escherichia coli* were transferred into a saline solution (0.85 % NaCl) using a sterilized loop to make up the 0.5 McFarland standard containing approximately 1.5×10^8 organisms. The standardized saline solution containing the *Escherichia coli* ATCC 8739 was then used in all the antimicrobial experiments carried out.

7.2.6. Antimicrobial experiments

All antimicrobial experiments were carried out under visible light irradiation. The evaluation of antimicrobial activity was carried out using sterilized 90 mm petri dishes. Evaluation was carried out on (1 % and 3 % N-TiO_2) nitrogen doped titanium dioxide supported on PVDF, PMAA-g-PVDF/ PAN and PAN membranes. A total of six membranes were evaluated. Each membrane was cut into a disc (Area = 28.3 cm^2) and placed into a sterilized 90 mm petri dish. Twenty millilitres of autoclaved nutrient broth were added to each of the petri dishes holding the membranes. *E. coli* ATCC 8739 (0.1 mL) were then inoculated into each petri while stirring to homogenize. All the petri dishes were covered and then exposed to sunlight to allow activation of the nitrogen doped titanium dioxide (N-TiO_2). The control of the

experiment involved the use of the three membranes without any N-TiO_2 on them. These three vessels were also inoculated with 0.1 mL of *E. coli* ATCC 8739 and exposed to the same conditions as the other petri dishes. Every 30 minutes swabs were taken from each reaction vessel and placed on the freshly prepared nutrient agar plates. The set up was left for 3 hours and results collected in duplicate. All the plates were labelled and then placed in a Cocono incubator operating at 37 ˚C for 24 hours.

7.3. Results and discussion

This section presents the results obtained from the antimicrobial evaluation of polymeric membrane supported nitrogen doped titanium dioxide.

7.3.1. Inactivation of *E. coli* ATCC 8739

The profiles obtained for the photo-catalytic inactivation of *E. coli* ATCC 8739 using poly (acrylonitrile) supported nitrogen doped titanium dioxide (N-TiO_2-PAN) are shown Figure 7.1. The essence of this work was to evaluate the effect of support material as well as the photo-catalyst loading on the bacterial inactivation (*E. coli* ATCC 8739). The investigation involved three sets of membranes (PAN, 1 % N-TiO_2-PAN and 3 % N-TiO_2-PAN). The control {PAN membrane (c)} of the experiment clearly indicates that in the absence of N-TiO_2 there is no inhibition of *E. coli* ATCC 8739. Hence a steady increase in the number of *E. coli* ATCC 8739 colony forming units (CFU) was observed over time. A sharp decline in the number *E. coli* ATCC 8739 colony forming units was observed in the case of 1 % N-TiO_2-PAN membrane. Initial CFU count after 30 minutes of exposure indicates a CFU of 214. However, when exposure time was increased to 60 minutes, the number CFU was reduced to approximately half (103 CFU). After 90 minutes of exposure to N-TiO_2-PAN

under solar irradiation the number *E. coli* ATCC 8739 CFU had decreased to 23. Total inactivation of *E. coli* ATCC 8739 bacterial cells was achieved with an exposure period of 120 minutes.

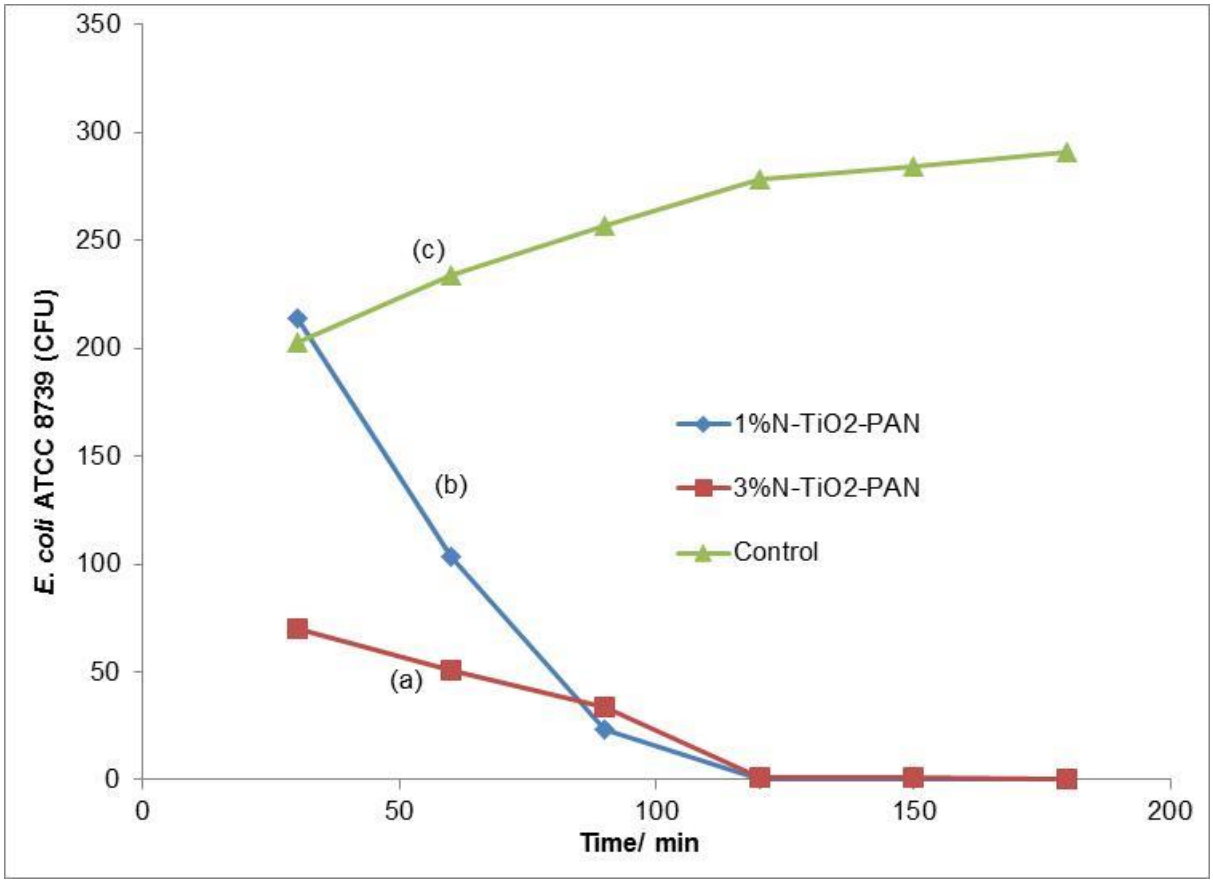

Figure 7.1: Photo-catalytic inactivation of *E. coli* ATCC 8739 under visible light using (a) 3%N-TiO_2-PAN, (b) 1%N-TiO_2-PAN and (c) control

The effect of increasing the N-TiO_2 photo-catalyst loading can be seen from the inactivation profile of 3 % N-TiO_2-PAN (a) on *E. coli* ATCC 8739. The growth rate of *E. coli* ATCC 8739 is very low under a higher dose of the photo-catalyst as witnessed from the initial CFU count of 70. Exposure for 60 minutes further reduces the CFU count to 51. After 90 minutes of the *E. coli* ATCC 8739 had been reduced to 34 CFU, a value slightly higher than that

obtained for 1 % N-TiO_2-PAN after the same period of exposure. Beyond 120 minutes almost all of the E. coli ATCC 8739 bacterial cells had been inactivated.

The inactivation profiles of *E. coli* ATCC 8739 obtained using N-TiO_2 supported on poly (vinylidene difluoride) (PVDF) are shown in figure 7.2.

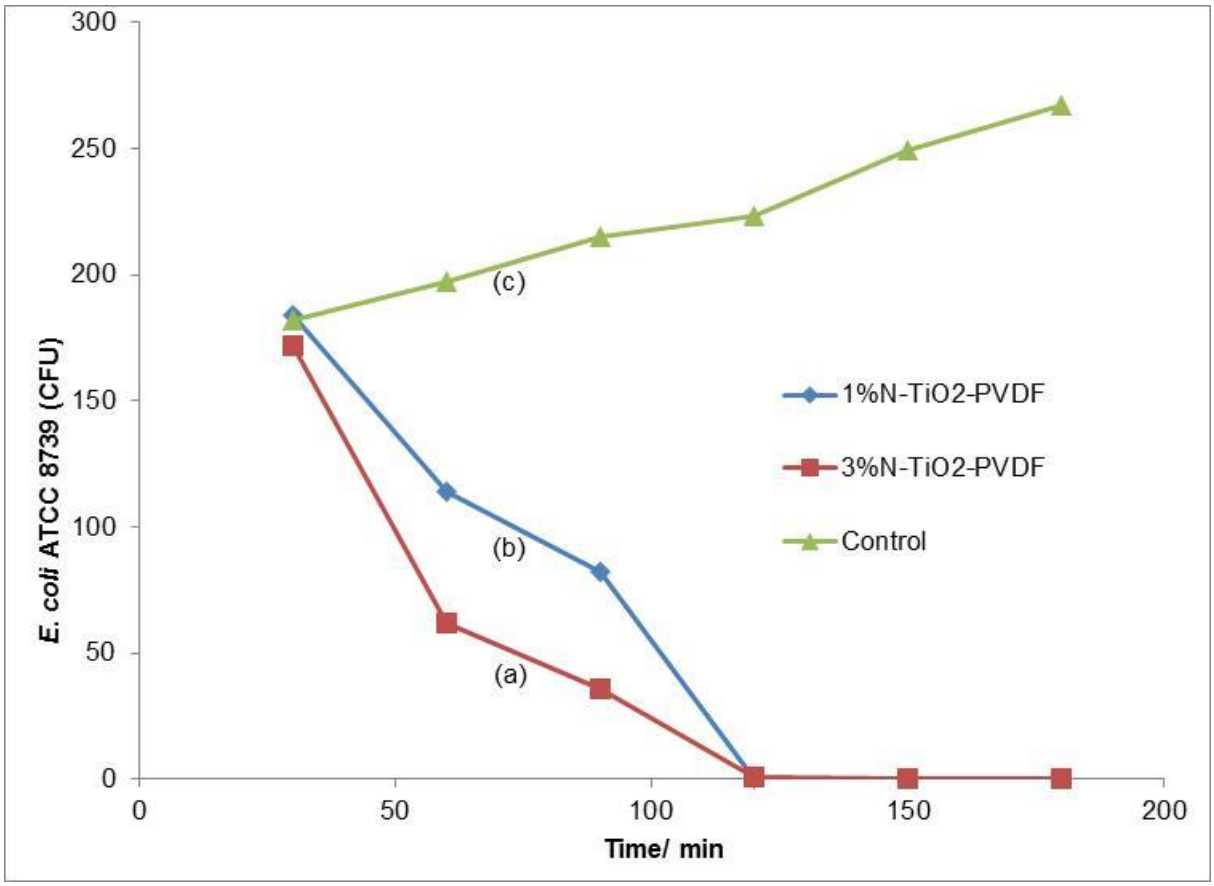

Figure 7.2: Photo-catalytic inactivation of *E. coli* ATCC 8739 under visible light using (a) 3%N-TiO_2-PVDF, (b) 1%N-TiO_2-PVDF and (c) control

Increasing the photo-catalyst loading from 1 % N-TiO_2 to 3 % N-TiO_2 noticeably has a profound effect on the inactivation of *E. coli* ATCC 8739 in water. Using 3 % N-TiO_2 allowed the reduction of *E. coli* ATCC 8739 colonies by 64 % within 60 minutes of exposure as opposed to 38 % reduction of colonies when using 1 % N-TiO_2 for the same period of

exposure. Nevertheless, all the *E. coli* ATCC 8739 bacterial cells had been inactivated beyond 120 minutes of exposure to N-TiO_2-PVDF under solar irradiation.

Figure 7.3 shows the inactivation profiles of *E. coli* ATCC 8739 using N-TiO_2 supported on poly (methacrylic acid) grafted onto poly (vinylidene difluoride) and blended with poly (acrylonitrile).

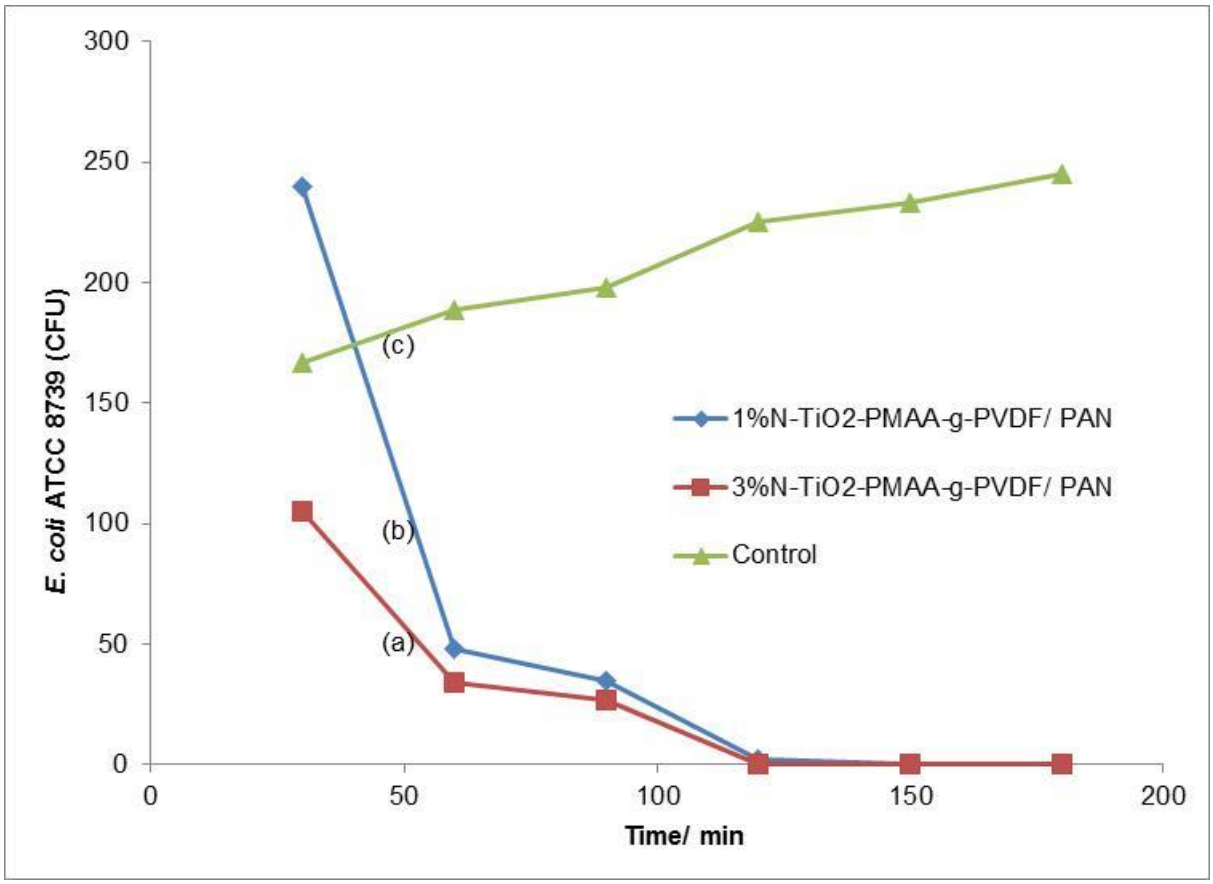

Figure 7.3: Photo-catalytic inactivation of *E. coli* ATCC 8739 under visible light using (a) 3%N-TiO_2-PMAA-g-PVDF/ PAN, (b) 1%N-TiO_2-PMAA-g-PVDF/ PAN and (c) control

Increasing the amount of N-TiO_2 photo-catalyst on the support material (that is PMAA-g-PVDF/ PAN) definitely increases the rate of bacterial inactivation as observed in the case of N-TiO_2-PAN and N-TiO_2-PVDF. This study established that for all three different polymeric

membrane support material for N-TiO_2, increasing the amount of photo-catalyst translates to increased rate of bacterial inactivation. However, studies in section 5.4.4 indicated that increasing the amount of N-TiO_2 reduces the tensile strength, elongation at break and the young's modulus which compromises the integrity of the membrane and durability. Findings of this study revealed that inactivation of *E. coli* ATCC 8739 occurs fastest when using N-TiO_2 supported on the novel PMAA-g-PVDF/ PAN membranes prepared (Fig. 7.4), followed by N-TiO_2-PAN and lastly N-TiO_2-PVDF.

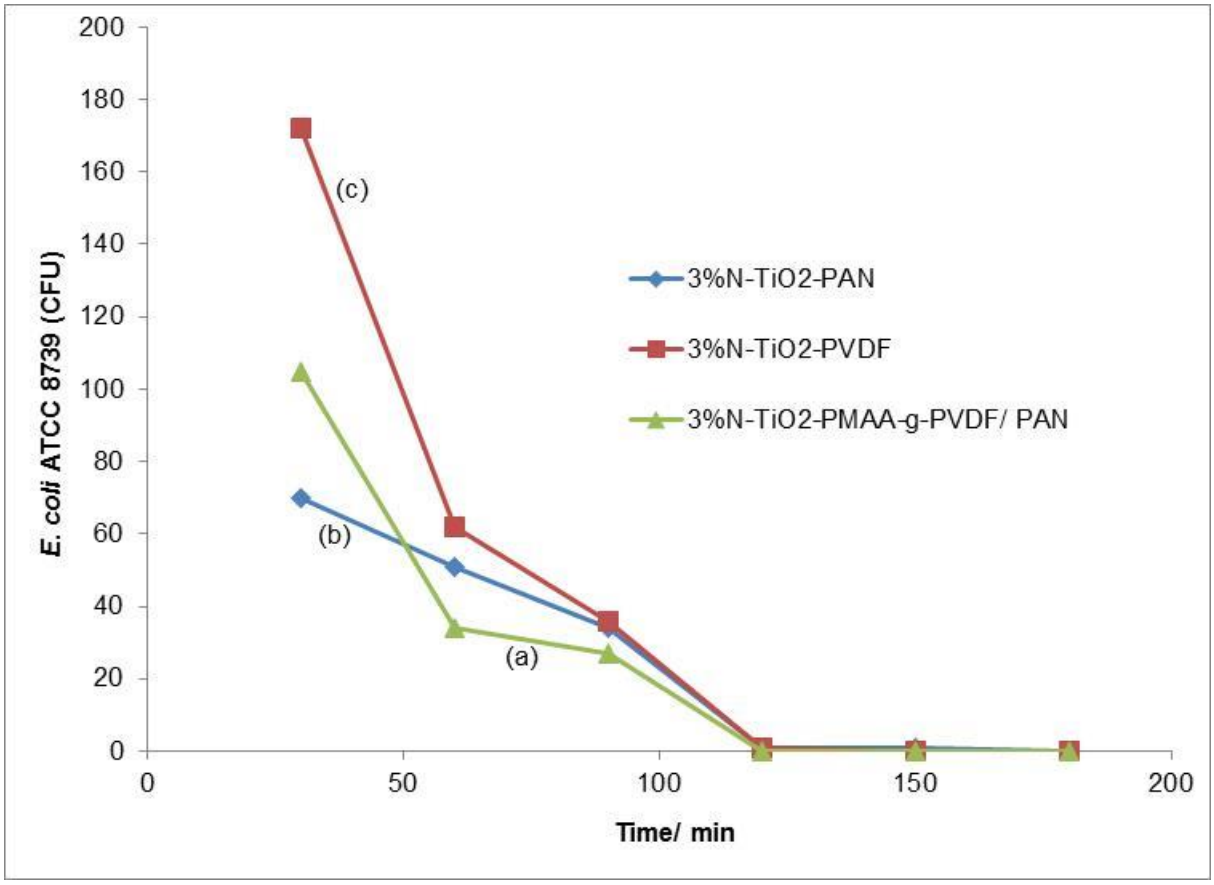

Figure 7.4: Photo-catalytic inactivation of *E. coli* ATCC 8739 under visible light using (a) 3%N-TiO_2-PMAA-g-PVDF/ PAN, (b) 3%N-TiO_2-PAN, and (c) 3%N-TiO_2-PVDF

Figures 7.5, 7.6 and 7.7 show the images of *E. coli* ATCC 8739 growing on nutrient agar plates after exposure to 1 % and 3 % N-TiO_2 supported on PAN, PVDF and PMAA-g-PVDF/

PAN membranes. These images all complement the information provided by the inactivation profiles of *E. coli* ATCC 8739 (Fig. 7.1-7.3).

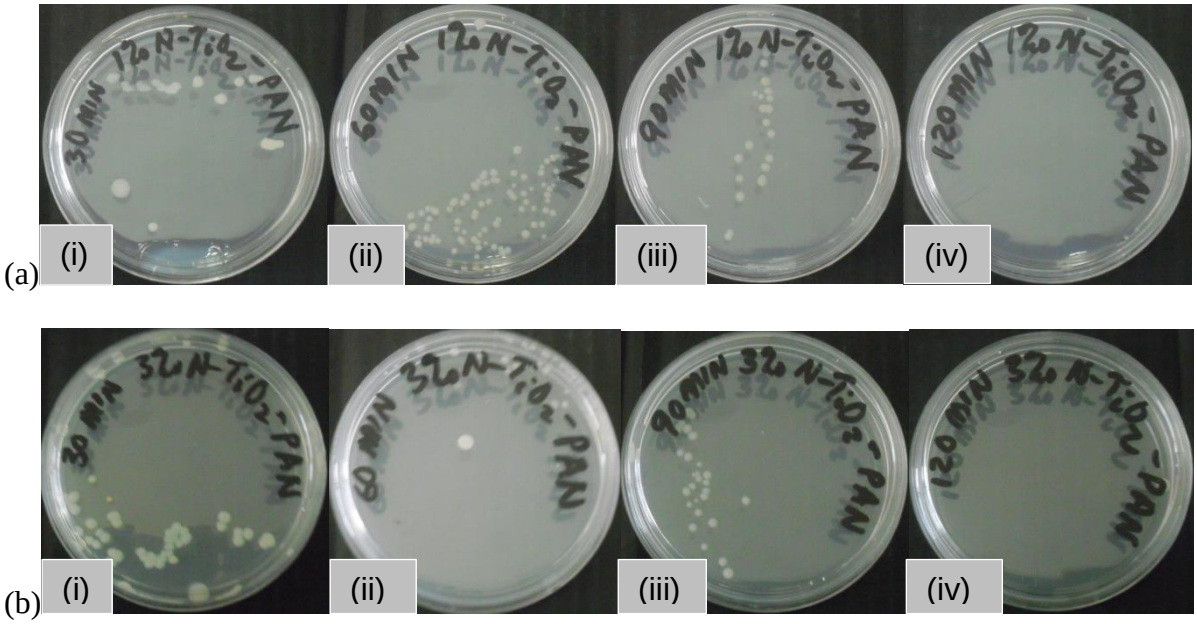

Figure 7.5: Images of *E. coli* ATCC 8739 treated with (a) 1%N-TiO_2-PAN, and (b) 3%N-TiO_2-PAN, (i) 30 minutes, (ii) 60 minutes, (iii) 90 minutes, and (iv) 120 minutes

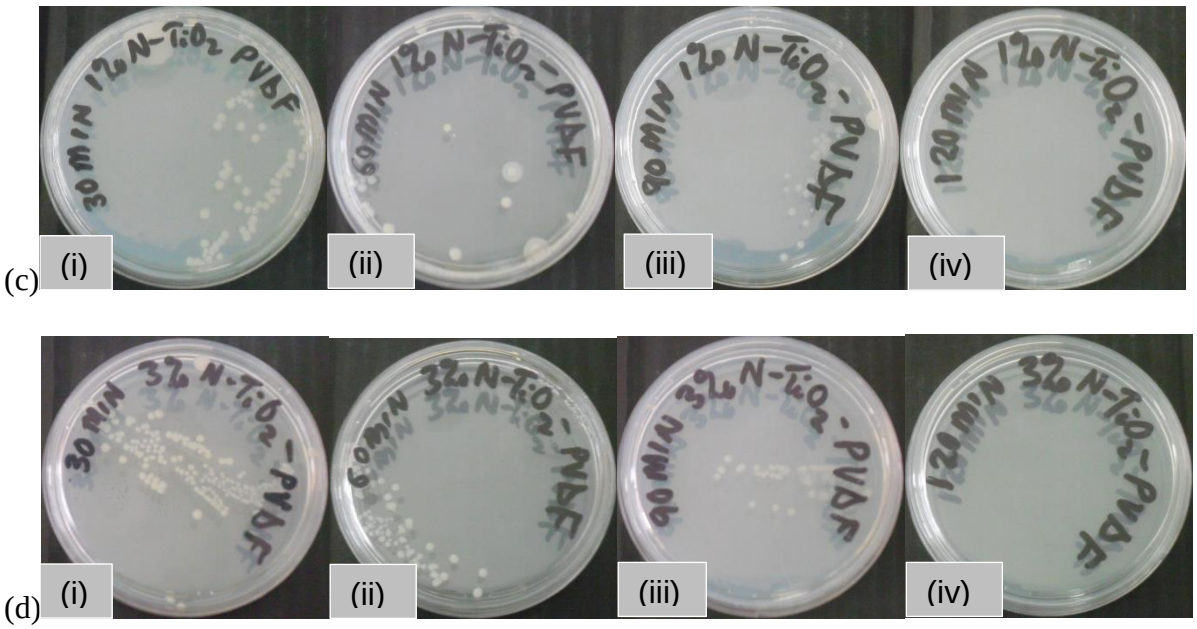

Figure 7.6: Images of *E. coli* ATCC 8739 treated with (c) 1%N-TiO_2-PVDF, and (d) 3%N-TiO_2-PVDF, (i) 30 minutes, (ii) 60 minutes, (iii) 90 minutes, and (iv) 120 minutes

(e) 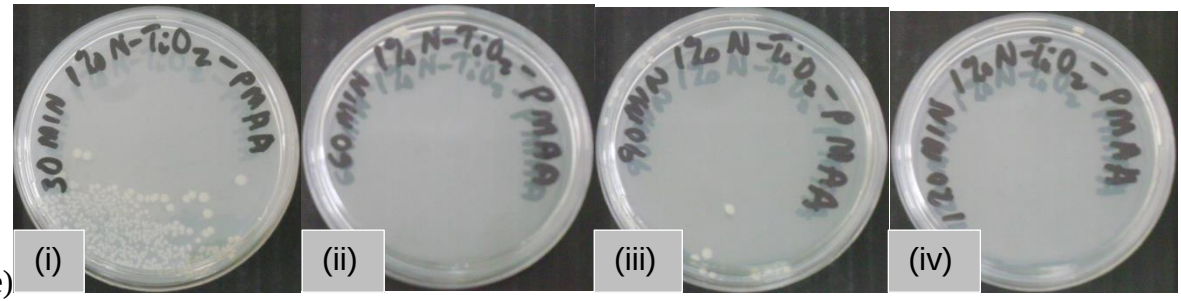

(f) 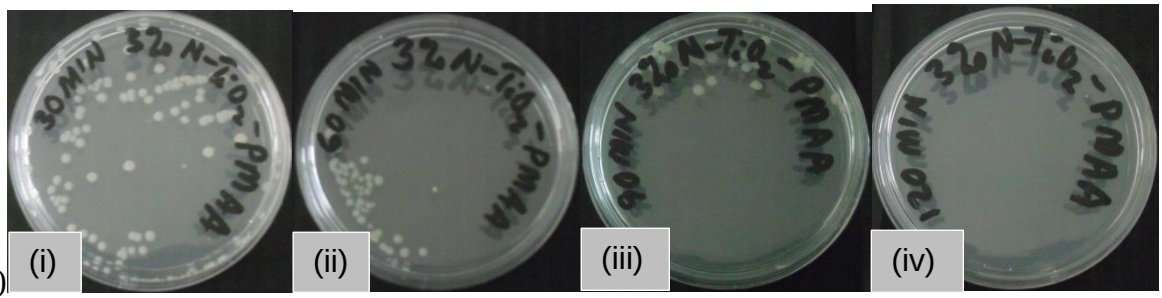

Figure 7.7: Images of *E. coli* ATCC 8739 treated with (c) 1%N-TiO_2-PMAA-g-PVDF/ PAN, and (d) 3%N-TiO_2-PMAA-g-PVDF/ PAN, (i) 30 minutes, (ii) 60 minutes, (iii) 90 minutes, and (iv) 120 minutes

All the sets of images show a decrease in the number of colonies of *E. coli* ATCC 8739 with the progression of time from 30 minutes of exposure to 120 minutes. In other studies, the effectiveness of platinum, carbon and nitrogen doped commercial powders were investigated on the inactivation of *E. coli* ATCC 8739. These experiments were carried out under visible light and UV-light. They noticed a reduction in bacterial colony count to 3.3±0.1 log with a photo-catalyst load of 4.2 gm^{-2} Pt-TiO_2 within a period of two hours of fluorescent light exposure. However, their C-TiO_2 showed lower antimicrobial activity towards *E. coli* ATCC 8739 inactivation (1.2±0.2 log) (Caballero *et al.,* 2014). In literature other researchers investigated the antimicrobial properties of apatite coated titanium dioxide photo-catalyst on the inactivation of bacteria (*Staphylococcus aureus, Escherichia coli,* Methicillin-resistant *Staphylococcus aureus, and Micrococcus luteus*) using black light (ultra-violet light), visible light and dark conditions. They observed a decrease in the number of viable bacteria with

increasing irradiation time up to 24 hours. They found black light irradiation to be more effective on bacterial cell inactivation as opposed to visible light and dark conditions. Their findings suggested that apatite coated titanium dioxide possesses antimicrobial activity under both black and visible light irradiation (Kangwansupamonkon *et al.*, 2009).

7.4. Conclusion

The results obtained from this investigation indicated that increasing the photo-catalyst loading (N-TiO_2) translates to an increased rate of *E. coli* ATCC 8739 inactivation. As observed for all three sets of membranes (PAN, PVDF and PMAA-g-PVDF/ PAN) incorporated with N-TiO_2 photo-catalyst, when the catalyst loading was increased from 1 % N-TiO_2 to 3 % N-TiO_2 the rate of bacterial cell inactivation also increased. The three polymer materials allowed inactivation of *E. coli* ATCC 8739 in a reasonable amount of time (120 minutes) that is the antimicrobial capabilities of N-TiO_2 were not hindered by its incorporation into support material. However, there was an indication from the results obtained that N-TiO_2 supported on PMAA-g-PVDF/ PAN showed higher inactivation rate of *E. coli* ATCC 8739 compared to N-TiO_2-PAN and N-TiO_2-PVDF membranes.

Bibliography

Caballero L., Whitehead K.A., Allen N.S., and Verran J. *Journal of Photochemistry and Photobiology A*: *Chemistry*: 276 **(2014)** 50-57.

Kangwansupamonkon W., Lauruengtana V., Surassmo S., and Ruktanonchai U. *Nano-medicine: Nanotechnology, Biology and Medicine*: 5 **(2009)** 240-249.

McFarland J. *Nephelometer*: 14 **(1907)** 1176-1178.

Murray P.R., Baron E.J., Jorgensen J.H., Landry M.L., and Pfaller M.A. *Manual of Clinical Microbiology* 9th edition ASM Press, Washington DC, **(2007)**.

CHAPTER 8

8. Evaluation of antifouling properties of N-TiO_2-PMAA-g-PVDF/ PAN membranes

8.1. Introduction

This chapter is on the evaluation of the filtration capacity of asymmetric membranes (PVDF, PMAA-g-PVDF/ PAN, and PAN) loaded with (1 %, 3 %, and 5 %) nitrogen doped titanium dioxide (N-TiO_2) as well as their antifouling properties. The objective of this part of the experiments was to assess the performance of the modified membranes on protein fouling. The filtration studies were carried on the filtration of bovine serum albumin (Met-U-Ed, M_w 67 000) solution in order to compare the protein fouling on the unmodified and modified membranes.

8.2. Experimental

8.2.1. Materials

The following materials were employed for this part of the study: Bovine serum albumin (BSA) (Met-U-Ed, M_w 67 000), Sodium dihydrogen phosphate (NaH_2PO_4), disodium hydrogen phosphate (Na_2HPO_4), and deionized water.

8.2.2. Protein static adsorption tests

Protein static adsorption tests were carried out to investigate the protein resistant property of N-TiO_2 modified asymmetric membranes of PAN, PVDF, and PMAA-g-PVDF/ PAN. The concentration of the BSA solution used in the investigation was 1 mg/ mL, which was

prepared by dissolving BSA flakes in 0.1 M phosphate buffer solution (PBS) at pH 7.4. Each of the membranes was cut into a 3 cm × 3 cm piece, which was immersed into a bath containing 1 mg/ mL BSA solution for a period of 6 hours. Changes in concentration of the BSA solution were measured at a wavelength of 280 nm using a Perkin Elmer Lambda 25 UV/ Vis spectrophotometer. The static saturated adsorption capacities were calculated from the resulting data using equation (8.1):

$$\eta = \frac{(c_b - c_a)}{A} \quad \text{..... (8.1)}$$

Where η is the static adsorption capacity (mg/ cm^2), c_b and c_a are the BSA concentrations before and after equilibrium respectively, and A is the membrane surface area.

8.2.3. Filtration studies

The protein adsorption resistance of the N-TiO_2 modified asymmetric membranes of PAN, PVDF, and PMAA-g-PVDF/ PAN was investigated by carrying out pure water filtration tests as well BSA filtration tests. The filtration experiments were carried out using a home-made set-up consisting of a filtration cell with a perforated surface that supports a disc shaped membrane (6 cm diameter) with area 28.3 cm^2, a pressure gauge, and a vacuum pump. The filtration cell used was a dead end filtration cell, with graduations to allow measurement of permeate volume. The feed solution was continuously stirred, with a constant temperature of 25 ˚C. The filtration pressure was maintained at 96 KPa for all the experiments carried out. The membrane was fixed in place and reservoir filled with deionized water. The flux of pure water Jw was then determined using equation 8.2:

$$J_w = \frac{Q}{A\Delta t} \quad \text{.....} \quad (8.2)$$

Where J_W is the pure water flux (L/ m^2h), Q is the permeate volume (L), A is the surface area of the membrane (m^2), Δt is the time (hr). Protein filtration experiments were then carried out using 1 mg/ mL BSA solutions, and the protein solution flux (J_P) determined. The BSA rejection ratio was then calculated using equation 8.3:

$$\mathrm{R} = \left(1 - \frac{c_p}{c_f}\right) \times 100\% \quad \text{.....} \quad (8.3)$$

Where R is the rejection ratio (%), C_f and C_p are the concentrations (mg/ mL) of BSA in the feed and permeate respectively. After protein filtration experiments the membranes were washed with deionized water and then pure water filtration experiments carried out again to determine the pure water flux (J_R). The water flux recovery was investigated through comparison of the values of J_W, J_P, and J_R. The relative flux reduction (RFR) and the flux recovery ratio (FRR) were calculated using the following equations (8.4 and 8.5):

$$\mathrm{RFR} = \left(1 - \frac{J_P}{J_W}\right) \times 100\% \quad \text{.....} \quad (8.4)$$

$$\mathrm{FRR} = \left(\frac{J_R}{J_W}\right) \times 100\% \quad \text{.....} \quad (8.5)$$

(Cruz *et al.,* 2014; Morihama and Mierzwa, 2014; Zhang *et al.,* 2012; Fan *et al.,* 2012; You *et al.,* 2012; Hu *et al.,* 2011; Yi *et al.,* 2011; Zhang *et al.,* 2008; Bosc *et al.,* 2005; Khay *et al.,* 2002)

8.3. Results and discussion

8.3.1. Protein static adsorption tests

The effect of the amount of inorganic filler (N-TiO_2) on the resistance of PAN, PVDF, and PMAA-g-PVDF/ PAN membranes to adsorb BSA on their surfaces was investigated. The amount of inorganic filler was increased from 1 % up to 5 % and the trends in BSA adsorption monitored (Fig. 8.1).

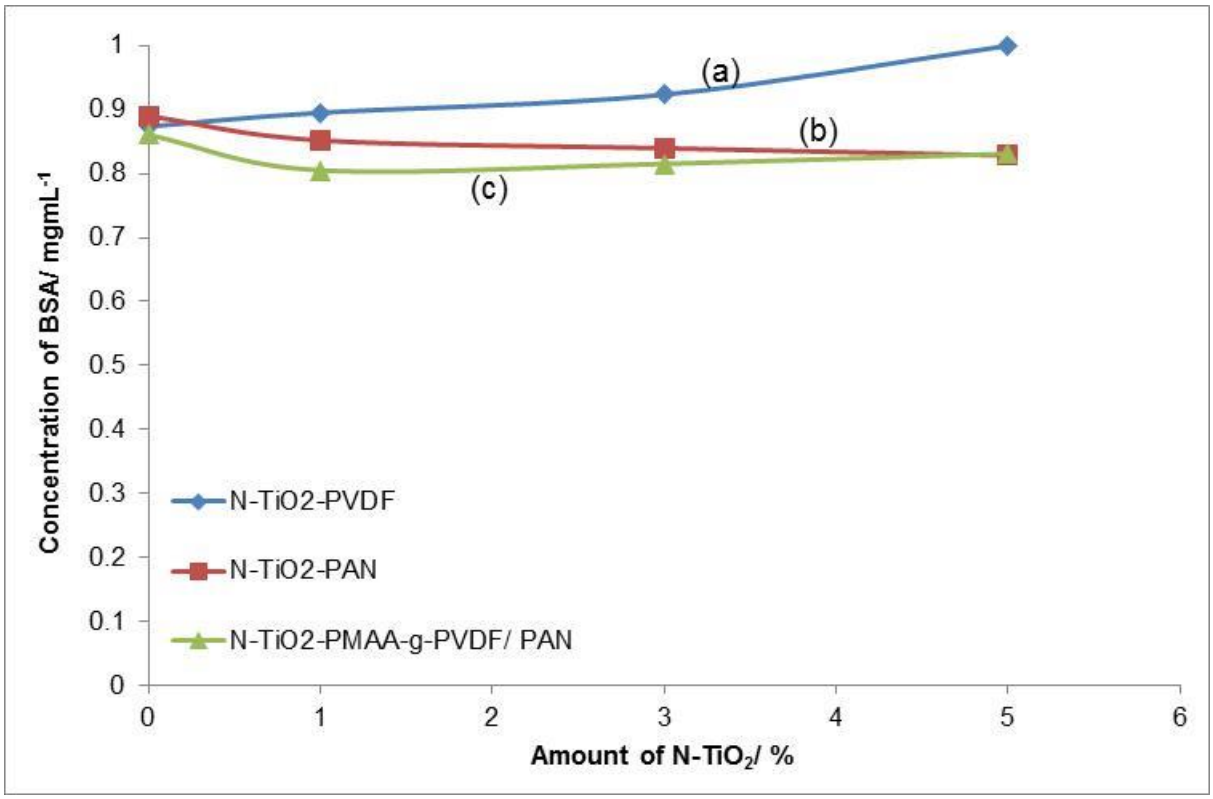

Figure 8.1: BSA adsorption Vs. N-TiO_2 inorganic filler loading for (a) PVDF, (b) PAN, and (c) PMAA-g-PVDF/ PAN membranes

The amount of BSA adsorbed by pristine PVDF membranes was 0.14 mg/ mL in a period of 6 hours, however, a decrease in the amount of protein adsorbed is observed with the addition of incremental amounts of N-TiO_2 nano-powders. With 5 % N-TiO_2, no BSA adsorption

occurred on the surface of PVDF membranes. Pristine PAN membranes had an initial BSA adsorption of 0.11 mg/ mL, and this value was lower than that obtained for pristine PVDF membranes. Nevertheless, an opposite effect is observed for BSA adsorption onto the surface of PAN membranes with the addition of N-TiO_2. A gradual increase in the amount of BSA adsorbed onto PAN membrane surface was observed for the PAN membranes, unlike in the case of PVDF membrane where BSA adsorption was reduced with increasing N-TiO_2. PMAA-g-PVDF/ PAN membranes had an initial BSA adsorption of 0.14 mg/ mL which compares to that of PVDF membranes. However, an increase in the amount of BSA adsorbed was observed with the addition of 1 % N-TiO_2. Further increase in the amount of N-TiO_2 up to 3 % and 5 % brings about a gradual decrease in the amount of BSA adsorbed as can be seen from Figure 8.1.

The protein static saturated adsorption capacities obtained for the membranes PAN, PVDF, and PMAA-g-PVDF/ PAN are shown in table 11.

Table 11: Protein static saturation adsorption capacities for PAN, PVDF, and PMAA-g-PVDF/ PAN membranes blended with 1 % to 5 % N-TiO_2

	η (mg/ cm^2)			
Membrane	0 % N-TiO_2	1 % N-TiO_2	3 % N-TiO_2	5 % N-TiO_2
PVDF	0.014	0.011	0.00085	0.000
PAN	0.012	0.016	0.018	0.019
PMAA-g-PVDF/ PAN	0.016	0.022	0.021	0.019

The data gives an indication of how much BSA was adsorbed by the PAN, PVDF, and PMAA-g-PVDF/ PAN membranes per square centimeter of membrane surface. The findings from literature indicated that protein static adsorption is highly dependent on the surface chemistry of the membrane. It was observed that hydroxyl groups form a large hydration layer through hydrogen and polar interactions which contributes to a high hydrophobicity (Leong *et al.,* 2014; Fan *et al.,* 2012; Li *et al.,* 2009; Zhang *et al.,* 2008). Zhang and co-workers reported that the content of TiO_2 had significant effects on the performance of hybrid membranes, through promotion of hydrophilicity and permeability, thus enhancing the antifouling ability of the hybrid membranes (Zhang *et al.,* 2012). Pristine PVDF membranes are highly hydrophobic (You *et al.,* 2012), hence they exhibited a very high protein static adsorption capacity (0.014 mg/ cm^2). Modifying PVDF with N-TiO_2 imparts hydrophilicity onto the membrane surface, hence the realized continuous decrease in protein static adsorption capacity with increasing amount of N-TiO_2 (Table 9). Grafting PMAA onto PVDF known to bring about hydrophilicity, however, the protein static adsorption capacity for N-TiO_2-PMAA-g-PVDF/ PAN initially increased, then started decreasing gradually (Table 9). The protein static adsorption capacity of PAN membranes was also observed to increase with increasing amount of N-TiO_2; nevertheless it was much lower than that of PMAA-g-PVDF/ PAN.

8.3.2. Filtration tests

Filtration experiments were carried out on N-TiO_2 entrapped PAN, PVDF, and PMAA-g-PVDF/ PAN asymmetric membranes to assess their antifouling properties. Table 12 summarizes the filtration data obtained for PAN membranes modified with N-TiO_2 nano-powders in a bid to improve water flux through enhancing hydrophilicity and also to minimize membrane surface fouling.

Table 12: Flux, protein rejection ratio, relative flux reduction and flux recovery ratio for PAN, 1 % N-TiO_2-PAN, and 3 % N-TiO_2-PAN asymmetric membranes

	L/m^2h			%		
Membrane	J_W	J_P	J_R	R	RFR	FRR
PAN	73.85	17.94	49.01	64.0	75.7	66.4
1 % N-TiO_2-PAN	239.05	28.47	238.95	73.1	88.1	99.9
3 % N-TiO_2-PAN	183.65	18.66	140.93	69.7	89.8	76.7

Pristine PAN membranes had an initial water flux of 73.85 L/m^2h which is quite low. PAN membranes are relatively hydrophilic and stable (Scharnagl and Buschatz, 2001), though they still suffer from significant fouling which calls for modification to improve their fouling resistance (Asatekin *et al.,* 2007; Hilal *et al.,* 2005; Goosen *et al.,* 2004; Marshall *et al.,* 1993). When PAN membranes were modified with 1 % N-TiO_2, the pure water flux increased three fold (239.05 L/m^2h). Nevertheless, further increase in the amount of inorganic filler to 3 % did not realize further increase in pure water flux, but a decrease to 183.66 L/m^2h. However, the pure water flux for 3 % N-TiO_2-PAN was still higher than that obtained for pristine PAN membranes (Table 12). Addition of excessive amounts of inorganic filler is believed to cause clogging of membrane pores hence ultimately reducing the pure water flux (Cruz *et al.,* 2014). The PAN membrane had a very low flux (17.94 L/m^2h) for 1 mg/ mL BSA solution filtration, which increased to 28.47 L/m^2h after modification with 1 % N-TiO_2 powders. The trends in protein rejection (BSA) also follow those obtained for pure water flux in that a higher BSA rejection (73.1 %) was realized after modification of PAN membranes with 1 % N-TiO_2 and that further increase in N-TiO_2 to 3 % did not translate to a further increase in BSA rejection (Table 12). After BSA solution filtration, membranes were

thoroughly washed with pure water which resulted in a pure water flux recoveries of 66.4 %, 99.9 %, and 76.7 % for PAN, 1 % N-TiO_2-PAN, and 3 % N-TiO_2-PAN membranes respectively. However, 3 % N-TiO_2-PAN membrane had the highest relative flux reduction (Table 12). Filtration experiments were also carried out on PMAA-g-PVDF/ PAN membranes and the results are shown in Table 13.

Table 13: Flux, protein rejection ratio, relative flux reduction and flux recovery ratio for PMAA-g-PVDF/ PAN, 1 % N-TiO_2-PMAA-g-PVDF/ PAN, and 3 % N-TiO_2-PMAA-g-PVDF/ PAN asymmetric membranes

	L/m^2h			%		
Membrane	J_W	J_P	J_R	R	RFR	FRR
PMAA-g-PVDF/ PAN	95.85	36.26	85.45	71.4	62.2	89.2
1 % N-TiO_2-PMAA-g-PVDF/ PAN	421.83	44.89	263.66	76.5	89.4	62.5
3 % N-TiO_2-PMAA-g-PVDF/ PAN	170.55	41.08	96.39	78.0	75.9	56.5

The initial pure water flux for PMAA-g-PVDF/ PAN was higher than that obtained for PAN (Table 12) and PVDF (Table 14) membranes. The high flux can be attributed to grafting of PMAA chains to the PVDF backbone to impart hydrophilicity into the membranes. Fan and co-worker prepared δ-gluconolactone modified poly (sulfone) membranes (PSF-Gle) to impart hydrophilicity. Findings from protein adsorption and filtration studies revealed that the modified PSF membranes had improved hydrophilicity and anti-protein adsorption properties (Fan *et al.,* 2012). The PMAA chains do not only enhance the hydrophilicity of the PVDF

membranes, but also steric hindrance suppresses protein adsorption on the membrane surface (He *et al.,* 2010; Wei *et al.,* 2000). The blending of PMAA-g-PVDF/ PAN membranes with 1 % N-TiO_2 further increased the membrane hydrophilicity resulting in a 4 fold increase in the pure water flux. However, increasing the amount of entrapped N-TiO_2 resulted in a decrease in the pure water flux (170.55 L/m^2h) of the PMAA-g-PVDF/ PAN membranes. This could have resulted from the clogging of the membrane pores by N-TiO_2 nano-particles. The highest BSA rejection was observed for 3 % N-TiO_2-PMAA-g-PVDF/ PAN membranes (78.0 %). This was in agreement with protein static adsorption results which showed a gradual decrease in BSA fouling with increasing amount of N-TiO_2. During 1 mg/ mL BSA solution filtration, the water flux for PMAA-g-PVDF/ PAN membranes dropped to 36.26 L/m^2h due to fouling. However, after thorough washing of the membranes with pure water, an 89.2 % pure water flux recovery was observed for the same membrane. The relative flux reduction was a bit high for 1 % N-TiO_2-PMAA-g-PVDF/ PAN membranes (89.4 %).

Table 14 shows the data obtained from the filtration studies carried out on N-TiO_2 modified PVDF asymmetric membranes. Generally PVDF membranes presented very low fluxes during pure water filtration. The explanation can be found in the structure of the membrane's supporting porous sub-layer which is sponge-like, as opposed to that of PAN and PMAA-g-PVDF/ PAN membranes which exhibit finger-like micro-voids which perhaps allow much higher water flux. Blending of PVDF membranes with 1 % N-TiO_2 was observed to bring about a 24.8 % improvement in pure water flux. Further increase in the amount of N-TiO_2 entrapped in the PVDF membrane matrix was observed to reduce the pure water flux by 15.9 %. Calculations carried out indicated that N-TiO_2-PVDF membranes however maintained considerably higher BSA rejection ratios (Table 14) compared to PAN (Table 12) and

PMAA-g-PVDF/ PAN (Table 13) membranes, owing to the fine structure of the thin selective layer of the membrane.

Table 14: Flux, Protein rejection ratio, Relative flux reduction and flux recovery ratio for PVDF, 1 % N-TiO_2-PVDF, and 3 % N-TiO_2-PVDF asymmetric membranes

	L/m^2h			%		
Membrane	J_W	J_P	J_R	R	RFR	FRR
PVDF	30.50	16.10	26.01	49.6	47.2	85.3
1 % N-TiO_2-PVDF	38.07	17.69	33.35	81.6	53.5	87.6
3 % N-TiO_2-PVDF	25.64	14.35	25.64	77.7	46.3	95.9

Protein static adsorption tests (Table 11) also support the high BSA rejection observed for N-TiO_2 modified PVDF membranes.

8.4. Conclusion

It is desired for a membrane to have high fouling resistance; however optimization of membrane properties is of utmost importance for superior performance and durability. The 1 % N-TiO_2-PMAA-g-PVDF/ PAN membranes gave the highest pure water flux (421.83 L/m^2h). This increase in pure water flux is owed to PMAA grafting as well as addition of N-TiO_2. These modifications resulted in an increased membrane surface hydrophilicity, which promoted permeation of pure water through the membrane structure. The high BSA rejection (76.5 %) can be attributed to steric hindrance brought about by PMAA side chains which

prevented the bulky BSA molecules from attaching to the membrane surface. However, the supporting porous sub-layer of an asymmetric membrane plays a very important role in the overall permeability of a membrane, as observed in the case of PVDF membranes. PVDF membranes have a sponge-like supporting porous sub-layer as opposed to PAN and PMAA-g-PVDF/ PAN membranes which presented finger-like micro-voids in the porous sub-layer. The sponge-like sub-layer of PVDF membranes caused resistance to pure water flow resulted in the observed low pure water fluxes. The essence of modifying membranes was to optimise their overall performance which water achieved through grafting and addition of inorganic powders. The 1 % N-TiO_2-PAN membranes performed better than the PVDF membranes, presenting a pure water flux of 239.05 L/m^2h as opposed to 38.07 L/m^2h for 1 % N-TiO_2-PVDF membranes.

Bibliography

Asatekin A., Kang S., Elimelech M., and Mayes A.M. *Journal of Membrane Science*: 298 **(2007)** 136-146.

Bosc F., Ayral A., and Guizard. *Journal of Membrane Science*: 265 **(2005)** 13-19.

Cruz N.K.O., Semblante G.U., Senoro D.B., You S-J., and Lu S-J. *Journal of the Taiwan Institute of Chemical Engineers*: 45 **(2014)** 192-201.

Fan H., Wang C., Li Y., and Wei Y. *Journal of Membrane Science*: 415-416 **(2012)** 161-167.

Goosen M.F.A., Sablani S.S., Ai-Hinai H., Ai-Obeidani S., Al-Belushi R., and Jackson D. *Separation Science Technology*: 39 **(2004)** 2261-2297.

He Y., Wei Y., Zheng X., and Zheng J. *Electrophoresis*: 31 **(2010)** 630-633.

Hilal N., Ogumbiyi O.O., Miles N.J., and Nigmatullin R. *Separation Science Technology*: 40 **(2005)** 1957-2005.

Hu A., Zhang X., Oakes K.D., Peng P., Zhou Y.N., and Servos M.R. *Journal of Hazardous Materials*: 189 **(2011)** 278-285.

Leong S., Razmjou A., Wang K., Hapgood K., Zhang X., and Wang H. *Journal of Membrane Science*: 472 **(2014)** 167-184.

Li J-H., Xu Y-X., Zhu L-P., Wang J-H., and Du C-H. *Journal of Membrane Science*: 326 **(2009)** 659-666.

Marshall A.D., Munro P.A., and Tragardh G. *Desalination*: 91 **(1993)** 65-108.

Morihama A.C.D., and Mierzwa J.C. *Brazilian Journal of Chemical Engineering*: 31 **(2014)** 205-210.

Scharnagl N., and Buschatz H. *Desalination*: 139 **(2001)** 191-198.

Wei Y., Chen Q., Jiang B., Geng X. *Ion Exchange Adsorption*: I6 (5) **(2000)** 441-448.

You S-J., Semblante G.U., Lu S-C., Damodar R.A., and Wei T-C. *Journal of Hazardous Materials*: 237-238 **(2012)** 10-19.

Zhang X., Du A.J., Lee P., Sun D.D., and Leckie J.O. *Journal of Membrane Science*: 313 **(2008)** 44-51.

Zhang X., Wang Y., You Y., Meng H., Zhang J., and Xu X. *Applied Surface Science*: **(2012)** 1-28.

CHAPTER 9

9. Conclusions and recommendations

9.1. Conclusions

Nitrogen doped titanium dioxide nano-particles were successfully prepared via sol gel synthesis. Ammonia was used as the source of nitrogen. FT-IR, SXPS, and XRD analyses confirmed that the prepared nano-powders were anatase phase nitrogen doped titanium dioxide. The product was capable of absorbing visible light as confirmed by diffuse reflectance spectroscopy.

The essence of the study was to prepare a suitable support membrane material with high photo-catalytic properties which also served as an ultrafiltration media. Poly (acrylonitrile) and poly (vinylidene difluoride) membranes have been prepared and studied. A novel asymmetric membrane which combined the properties of both PAN and PVDF was prepared. The membrane was prepared via the dry-wet phase inversion technique. The membrane was constituted of PVDF backbone with poly (methacrylic acid) side chains that were grafted on through RAFT polymerization. This membrane was then blended with PAN, and varying amounts of the N-TiO_2 photo-catalyst powder. FT-IR, NMR, and SEM analysis confirmed successful preparation of PMAA-g-PVDF/ PAN asymmetric membranes. Tensile strength measurements showed that there was a decrease in tensile strength with increasing amounts of N-TiO_2 powders entrapped within the membrane matrix. However, PMAA-g-PVDF/ PAN membranes were least affected as compared to PVDF and PAN membranes.

The prepared photo-catalytic asymmetric membranes of PAN, PMAA-g-PVDF/ PAN, and PVDF were evaluated on the photo-degradation of the herbicides bentazon, paraquat, and atrazine in synthetic water. Findings of the photo-degradation study showed that 3 % N-TiO_2 was the optimum amount that could be immobilized on the membranes. The PMAA-g-PVDF/ PAN asymmetric membranes were the most suitable support material and they allowed high removal efficiencies for organic pollutants. Atrazine and paraquat were more recalcitrant, hence required longer treatment periods as compared to bentazon. Solution pH is a very important parameter on the photo-degradation of organic pollutants in water. High removal efficiencies were achieved for bentazon and atrazine between pH 3 and 7, whereas high pH (9.0) promoted higher removal efficiencies for paraquat. The plots of ln (C_0/ C) against time for atrazine, paraquat and bentazon were straight lines, implying that the photo-degradation of the three herbicides fitted as pseudo-first-order kinetics. The R^2 values were also greater than 0.90 for the three herbicides.

Another advanced oxidation technology (ozonolysis) was also evaluated on the degradation of bentazon, paraquat and atrazine. Ozonolysis is very effective on the degradation of organic pollutants. However, in some cases it results in the formation of undesirable by-products that cannot be further degraded. Trends observed in the ozone degradation of the herbicides in water were similar to those observed for N-TiO_2 photo-degradation except that ozonation occurred at a much faster rate. An O_3/ 3 % N-TiO_2-PMAA-g-PVDF/ PAN system was also investigated. Findings from the study revealed that there was significant enhancement in the removal efficiencies for the three herbicides investigated.

The photo-catalytic removal of heavy metal ions from water was also investigated using the prepared photo-catalytic asymmetric membranes. Heavy metals Pb^{2+} and Fe^{3+} were removed

from water via N-TiO_2 assisted reduction. The highest removal efficiency for Fe^{3+} was achieved with 1 % N-TiO_2-PMAA-g-PVDF/ PAN photo-catalyst (76.2 %), while for Pb^{2+} removal 1 % N-TiO_2-PAN was the most effective photo-catalyst (90.5 %). An increasingly basic environment promotes high removal efficiencies for Pb^{2+} and Fe^{3+}.

The antimicrobial properties of N-TiO_2 entrapped PAN, PMAA-g-PVDF/ PAN, and PVDF asymmetric membranes were evaluated on the inactivation of Escherichia coli ATCC 8739. All three types of membrane were capable of inactivating *E. coli* ATCC 8739. The findings of the study also indicated that increasing the N-TiO_2 photo-catalyst load translated to an increased rate of *E. coli* ATCC 8739 inactivation. The most effective photo-catalyst-support material combination on the inactivation of E. coli ATCC 8739 was 3 % N-TiO_2-PMAA-g-PVDF/ PAN.

The antifouling properties of N-TiO_2 entrapped PAN, PMAA-g-PVDF/ PAN, and PVDF membranes were evaluated through protein static adsorption and BSA filtration experiments. The grafting of PMAA chains onto the PVDF backbone imparted hydrophilicity into the PMAA-g-PVDF/ PAN membranes. This was evident through their high pure water fluxes observed as well as protein fouling resistance. The blending of N-TiO_2 with the membranes also imparted the hydrophilic character into the asymmetric polymeric membranes. Comparison of pristine and N-TiO_2 modified membranes revealed that the modified membranes achieved higher pure water fluxes and better BSA fouling resistance. It is believed that PMAA-g-PVDF/ PAN membranes avoid BSA adsorption onto the membrane surface through steric hindrance brought about by the PMAA side chains.

9.2. Recommendations

Polymeric membrane immobilized nitrogen doped titanium dioxide photo-catalyst can be used several times on the photo-degradation of organic pollutants in water without any significant loss in photo-catalytic power because the catalyst is photo-stable and regenerates at the end of photo-catalytic cycles. In this study N-TiO_2 entrapped PMAA-g-PVDF/ PAN membranes were used over four degradation cycles without any loss in photo-degradation capacity. Further studies can be carried out to investigate the performance of the N-TiO_2 PMAA-g-PVDF/ PAN photo-catalytic asymmetric membranes under continuous flow conditions, since they achieved considerably high organic and inorganic pollutant removal efficiencies under batch studies. These N-TiO_2-PMAA-g-PVDF/ PAN membranes proved capable of inactivating *E. coli* 8739 within short period of treatment even with low photo-catalyst loading (1 % N-TiO_2). The membrane could be used in a continuous flow flat-bed reactor, where the reactor design would allow these photo-catalytic membranes to be employed as photo-catalyst as well as ultrafiltration media for the removal of pollutants which fall within the ultrafiltration range. However, further studies need to be carried out to establish such conditions and conceptualize such reactor design.

Extensive work needs be carried out in the case of PVDF membranes since they performed poorly as ultrafiltration media. There are also several problems encountered in the preparation of PVDF membranes and they also have a tendency to shrink as soon as they are placed in a non-solvent bath, which hinders the production of smooth flawless membranes. PAN asymmetric membranes performed fairly well and could perform better with further modification. Although N-TiO_2-PMAA-g-PVDF/ PAN membranes possessed antimicrobial activity, further modification could also be beneficial to enhance performance when it comes

to continuous flow treatment to allow very large flow rates. For instance nano-silver and nitrogen co-doped TiO_2 could be prepared, since nano-silver possesses antimicrobial power.